FINITE ELEMENT METHODS FOR LINEARLY PERTURBED SINGLE- AND TWO-PHASE FLOWS

A thesis submitted to the University of Manchester
for the degree of Doctor of Philosophy
in the Faculty of Engineering and Physical Sciences

2014

Patrick Hurley
School of Mathematics

Contents

Word count 33076

List of Tables

List of Figures

The University of Manchester

Patrick Hurley
Doctor of Philosophy
Finite element methods for linearly perturbed single- and two-phase flows
June 10, 2014

This thesis is concerned with the development of a general numerical framework that allows the computation of the evolution of non-axisymmetric perturbations to arbitrary axisymmetric base flows. Both single- and two-phase flows are considered. This framework is developed within `oomph-lib`, a finite element library for the simulation of multi-physics problems.

Following the introduction of the core concepts of the finite element method via the example of a two-phase viscous flow problem in a Cartesian coordinate system, we begin our discussion of the Navier–Stokes equations in cylindrical polar coordinates by deriving the finite element formulation of the equations governing an axisymmetric flow and the conditions to be applied at a free surface. We apply this formulation to two problems involving the relaxation of a free surface in a cylindrical geometry, and validate the numerical results against analytical predictions for the frequency and decay rate obtained from linearised analyses of the respective problems. We then linearise the weak form of the governing equations for a fully three-dimensional flow written in terms of a cylindrical polar coordinate system to obtain the finite element formulation for a linear perturbation to a nonlinear base flow. The solution to the linear problem depends on the base flow and is periodic in the azimuthal direction. We exploit this periodicity by performing a Fourier decomposition in the azimuthal direction, transforming the three-dimensional problem into a series of two-dimensional problems in which the azimuthal mode number appears as a parameter. We implement these equations in `oomph-lib` and apply this newly-developed methodology to two representative single-phase flow problems. In both cases we demonstrate that our computations match previously published results generated using different numerical methods.

Having validated our implementation of the equations governing the perturbation of a (time-dependent) axisymmetric base flow by a linear, non-axisymmetric disturbance, we extend this formulation to include problems containing two immiscible fluids separated by an interface. We derive the equations which need to be applied at the free boundary in such a problem, and augment `oomph-lib`'s existing moving-domain 'machinery' to allow the computation of arbitrary perturbations to a 'base' free surface position, which is itself an unknown in the problem. We validate this methodology for the case of an axisymmetric disturbance to an axisymmetric base flow, and demonstrate the use of the newly-developed functionality by applying it to a non-axisymmetric relaxing interface problem. We demonstrate that, for all stably stratified configurations of this system, all disturbances to the interface position decay. For an unstably stratified configuration, however, we observe the growth of certain non-axisymmetric modes.

Declaration

No portion of the work referred to in the thesis has been submitted in support of an application for another degree or qualification of this or any other university or other institute of learning.

Copyright Statement

Acknowledgements

This PhD project (and the thesis presented here) would not have been possible without the unwavering enthusiasm, encouragement, guidance and good humour of my supervisors, Prof Matthias Heil and Dr Andrew Hazel. I am exceptionally grateful for their continual support and supervision over the course of my studies.

I also wish to thank Prof Anne Juel and Dr Chris Johnson for many helpful conversations over the course of my PhD, and to acknowledge the generous financial support provided by both the school of Mathematics and the Engineering and Physical Sciences Research Council.

I am indebted to my parents, who have always supported me throughout my education (and beyond), and to Christine, who more than anyone understands what it means to me to be able to present this work.

Finally, it is impossible to overstate my gratitude towards the many people, both within the school of Mathematics and the university as a whole, who have helped to make my time in Manchester so rewarding. While it is impossible to mention everyone, I am especially grateful to Alice, Andrew, Ben, Bev, Draga, Hannah, Matt, Phil, Richard, Ruth, Stephen, Tom and Vicki for countless cups of tea and for keeping me laughing over many years. I would not have made it to this point without you all.

Chapter 1

Introduction

1.1 Background and motivation

In many practically important fluid mechanical problems, the domain occupied by the fluid and the boundary conditions to be satisfied by the flow are such that the problem admits axisymmetric solutions, i.e. flow fields in which the velocity and the pressure are independent of the azimuthal coordinate, measured about some symmetry axis. Probably the best-known example is that of Hagen–Poiseuille flow in a circular cylindrical pipe, in which (for sufficiently small flow rates, or Reynolds numbers) the flow is not only axisymmetric but also unidirectional, with a parabolic axial velocity profile in which the axial velocity is a function of the radius only. Other fluid mechanical problems that admit axisymmetric solutions include jets emerging from circular nozzles [Batchelor and Gill, 1962]; the flow in a cylindrical cavity either above a rotating disk [Batchelor, 1951] or between two parallel, rotating disks [Zandbergen and Dijkstra, 1987]; and the flow past spheres [Payne and Pell, 1960], to name but a few.

A key question that arises in the study of such flows is the following: what is the effect of introducing a (small) perturbation[1] to these simple solutions? There are three outcomes: either

(i) the perturbation decays over time, and the flow eventually returns to the state it was in before it was disturbed, or

(ii) the perturbation grows over time, and the flow gradually evolves away from its

[1] We will address the issue of precisely what we mean by a 'small perturbation' in some detail in section 1.2.

initial state, or

(iii) the perturbation neither grows nor decays, and remains at the same amplitude indefinitely.

Famously, Osborne Reynolds studied this question in the context of Hagen–Poiseuille flow in 1883 [Reynolds, 1883]. He observed that the steady, unidirectional axisymmetric flows mentioned above are only observed at sufficiently small flow rates (low Reynolds number). As the flow rate (or the Reynolds number) is increased, the simple axisymmetric solution disappears, and the flow becomes increasingly complex and ultimately fully turbulent [Mullin, 2011].

Similar scenarios arise, e.g., in the flow in an annular region between two concentric, rotating cylinders. At low Reynolds numbers this flow (known as 'circular Couette flow') is steady and, in the limit where the cylinders are of infinite length, the only non-zero velocity component is in the azimuthal direction. In 1923, G .I. Taylor demonstrated that as the angular velocity of the inner cylinder is increased above a particular threshold, axisymmetric perturbations to this base flow no longer decay: instead they give rise to a secondary steady state characterised by toroidal vortices [Taylor, 1923]. As the angular velocity is increased further still, this flow is eventually subject to three-dimensional disturbances, causing it to lose its regular spatial structure.

The same type of instability also arises in boundary layers in flow past a concave wall, as discovered by Görtler in 1940 [Görtler, 1940]. For boundary layer thicknesses that are small compared to the radius of curvature of the wall and sufficiently low flow speeds, a unidirectional flow along the wall is observed. When a critical velocity is exceeded, however, this simple unidirectional flow (in boundary layer coordinates) becomes unstable, leading to the formation of so-called 'Görtler vortices' [Saric, 1994]. The onset of this instability in the boundary layer is characterised by the 'Görtler number', which can be interpreted as the ratio of the centrifugal force (which acts to destabilise the flow) to the viscous frictional force (which acts to stabilise the flow). This dimensionless parameter is analogous to the 'Taylor number' which characterises the onset of Taylor vortices in circular Couette flow (as discussed above) [Oertel and Prandtl, 2004].

Another example is that of an axisymmetric jet emerging from a circular orifice into an ambient fluid with the same properties. The axisymmetric solution of the governing equations is only observed for sufficiently low Reynolds numbers: outside of this regime, small disturbances in the flow field grow quickly and cause this laminar, axisymmetric 'base state' to break down [Tritton, 1988].

The presence of free surfaces (defined as interfaces between two fluids) introduces further complications. The surface tension forces acting at such interfaces generally act to decrease the interfacial area. Many free surface flows therefore adopt axisymmetric configurations, so long as the geometry admits them. However, even such flows can become unstable. A famous example of this was first studied by Joseph Plateau in 1873, who observed the break up of a vertically falling jet of water into a series of droplets [Plateau, 1873]. Here surface tension destabilises an axisymmetric, axially uniform flow. The perturbations retain the axial symmetry of the jet but make the flow axially non-uniform. A few years later, Lord Rayleigh presented an analysis of this problem for an inviscid fluid [Rayleigh, 1878], and predicted that (in this limiting case) all non-axisymmetric perturbations would neither grow nor decay, as would all axisymmetric perturbations with wavelength smaller than the circumference of the jet. For axisymmetric perturbations with sufficiently high wavelength, however, the dominance of azimuthal curvature over longitudinal curvature promotes a pressure gradient that amplifies the original disturbance: this leads to the fluid stream 'pinching off' at this point. This effect is known as the 'Plateau–Rayleigh instability'. Rayleigh's 1878 paper is also notable for first suggesting that the mode that one would observe in experiments would correspond to the fastest-growing perturbation [Drazin and Reid, 2004]. An analysis of the viscous problem was subsequently presented by Weber, who provided a prediction for the most rapidly growing axisymmetric mode in terms of the fluid viscosity, density and surface tension and the radius of the jet [Weber, 1931]. There has been considerable further study of this and many other related problems, including (but certainly not limited to) the interaction of viscous and capillary forces acting at the interface between a cylinder of viscous fluid surrounded by another viscous fluid [Tomotika, 1935]; the stability of annular jets of viscous fluid moving in an inviscid medium [Meyer and Weihs, 1987]; and the stability of an annular coating of viscous fluid on a wire (or on the inside of a small tube) subject to capillary forces

at its free surface [Goren, 1962].

It important to note that the presence of surface tension does not necessarily suppress all non-axisymmetric perturbations. In a study of fluid jets which are in a state of solid rotation, Ponstein found that, in certain cases, non-axisymmetric perturbations grew more rapidly than those disturbances that were axially symmetric, a feature that does not occur in non-rotating jets [Ponstein, 1959]. Another interesting example is the system studied by Shyh and Munson in 1986, where a cylindrical vessel containing two stably stratified fluids with large viscosity contrast was subjected to sinusoidal oscillations about its axis of rotational symmetry [Shyh and Munson, 1986]. At low forcing amplitudes and frequencies an unsteady axisymmetric flow was observed, but as either the amplitude or frequency was increased the interface was found to become unstable to non-axisymmetric perturbations as a result of large velocity contrasts at either side of the free surface. This instability manifested itself as a set of regularly-spaced 'fingers' of the high-viscosity fluid.

A final example is that of two superposed fluids contained within a vertical cylinder [Batchelor and Nitsche, 1993]. If the fluids are stably stratified (so that the lower layer is that which has the greater density) then surface tension and gravitational acceleration both act to restore any perturbation of the interface to its flat, undeformed configuration. If the system is set up so that the more dense fluid is the upper layer, however, then the force of gravitational acceleration acts to destabilise the interface. For low density contrasts, disturbances to the interface position will still decay due to the restoring force driven by surface tension. As the ratio of the densities of the two layers is increased, however, gravitational forces will dominate and perturbations to the interface position will grow, eventually causing the fluid system to 'overturn'. This is an example of the 'Rayleigh–Taylor' instability, first observed by Rayleigh in 1883 [Rayleigh, 1883].

1.2 Introduction to linear stability theory

Having introduced a range of classical problems in which it is useful to be able to determine the time-evolution of perturbations to various fluid dynamical systems, we

will now define what we mean by 'small amplitude perturbations' in a more mathematical sense. In this thesis we are only concerned with computing *linear* or 'first order' perturbations to flows, and to put this into context we will summarise the key concepts of linear stability theory in the following section.

Let us suppose that we have a physical system that can be described in terms of a system of nonlinear partial differential equations. Since we are concerned with fluid dynamical problems in this work, we shall assume here that the governing equations are the Navier–Stokes equations and that the field variables are the velocity, $\mathbf{u}(\mathbf{x}, t)$, and the pressure, $p(\mathbf{x}, t)$. The governing equations are augmented by boundary conditions appropriate for the problem geometry.

Let us now suppose that we have a velocity field $\bar{\mathbf{u}}$ and a pressure field $\bar{p}$ that form a solution

$$\mathbf{N}\left\{\bar{\mathbf{u}}, \bar{p}\right\} = 0 \tag{1.1}$$

to this system of nonlinear equations and boundary conditions. This solution, which we call the 'base state', is typically chosen to be 'simpler' in some way: for example, the solution may be independent of a particular coordinate direction, and/or independent of time. In the Reynolds pipe experiment described in section 1.1, a sensible choice of base state would be Hagen–Poiseuille flow, which is steady and in which the velocity is uniaxial and depends on the radial coordinate only. Similarly, circular Couette flow admits a steady solution in which the only non-zero component of the velocity is in the azimuthal direction, and is a function of the radial coordinate only. Base flows are not necessarily required to be steady, however: an appropriate base state for the problem studied by Shyh and Munson[2], in which a cylindrical vessel containing two fluids is oscillated sinusoidally with period T about its axis of rotational symmetry, would be one in which the solution was independent of the azimuthal coordinate θ and periodic in time, so that

$$\bar{\mathbf{u}}(r, z, t) = \bar{\mathbf{u}}(r, z, t + T) \qquad \text{and} \qquad \bar{p}(r, z, t) = \bar{p}(r, z, t + T). \tag{1.2}$$

Whatever the base state, the key requirement is that we must be able to clearly define what we mean by a growing or decaying perturbation to that state. Having defined the base flow, we next introduce a small perturbation of the form $(\hat{\mathbf{u}}, \hat{p})$, so

[2]See the previous section (1.1) for an overview of this problem.

that the solution of the nonlinear system of equations is now given by

$$\mathbf{u} = \bar{\mathbf{u}} + \epsilon\,\hat{\mathbf{u}} \qquad \text{and} \qquad p = \bar{p} + \epsilon\,\hat{p}, \tag{1.3}$$

where $\epsilon \ll 1$ is the 'perturbation amplitude'. The perturbation quantities $\hat{\mathbf{u}}$ and $\hat{p}$ typically depend on more variables than the underlying base flow: for example, to assess the stability of fully-developed Hagen–Poiseuille flow to linear, time-dependent perturbations in the azimuthal direction we would let

$$\begin{aligned} \mathbf{u}(r,z,t) &= \bar{\mathbf{u}}(r) + \epsilon\,\hat{\mathbf{u}}(r,z,t) \quad \text{and} \\ p(r,z,t) &= \bar{p}(z) + \epsilon\,\hat{p}(r,z,t). \end{aligned} \tag{1.4}$$

The same decomposition would be used, for example, to investigate the stability of steady circular Couette flow to axisymmetric perturbations, such as the ones which lead to the onset of Taylor vortices. In the case of the problem studied by Shyh and Munson, we would assess the stability of the periodic, axisymmetric base flow to time-dependent, non-axisymmetric perturbations by letting

$$\begin{aligned} \mathbf{u}(r,z,\theta,t) &= \bar{\mathbf{u}}(r,z,t) + \epsilon\,\hat{\mathbf{u}}(r,z,\theta,t) \quad \text{and} \\ p(r,z,\theta,t) &= \bar{p}(r,z,t) + \epsilon\,\hat{p}(r,z,\theta,t). \end{aligned} \tag{1.5}$$

By substituting (1.3) into the governing equations and expanding in the small parameter ϵ we obtain a system of equations which we can group into powers of the perturbation amplitude. Terms of order one correspond to the governing equations for the base flow, while terms of order ϵ correspond to a linearised set of equations governing the dynamics of the perturbations $\hat{\mathbf{u}}(\mathbf{x},t)$ and $\hat{p}(\mathbf{x},t)$. In general these 'linear perturbation equations' contain coefficients which depend on the solution of the base flow problem. For a known base flow, therefore, the time-evolution of a linear perturbation to this flow can be computed simply by time-evolving these perturbation equations, and there are three possible outcomes as $t \to \infty$:

(i) The perturbation decays: in this case, we consider the base flow to be *linearly stable*.

(ii) The perturbation grows: in this case, we consider the base flow to be *linearly unstable*.

(iii) The perturbation neither grows nor decays, and thus the amplitude remains the same for all time: in this case, we consider the base flow to be *neutrally stable*.

Just because linear stability theory predicts that a particular solution is stable does not necessarily mean that the corresponding physical state would be observed in an experiment. A famous example of this is the very first example discussed in section 1.1, that of Hagen–Poiseuille flow in a circular pipe. The results of a linear stability analysis about this base state suggest that this flow is stable for all flow rates (or values of the Reynolds number) [Mullin, 2011]. In reality, however, the basic laminar flow is observed to undergo a transition to turbulence for Reynolds numbers greater than a certain critical value. This value has been observed experimentally to range between ~ 2000 and ~ 40000, depending on the smoothness of the pipe walls and the regularity of the flow at the inlet [Davey and Drazin, 1969]. The reason behind this apparent inconsistency is that Hagen–Poiseuille flow, while stable to infinitesimal perturbations, is unstable to perturbations of a finite size at sufficiently high flow rates. More recent research suggests that a possible mechanism for this transition might be by initially small disturbances growing in a transient phase, which can arise as a consequence of the non-normality of the linearised Navier–Stokes operator [Schmid and Henningson, 1994, O'Sullivan and Breuer, 1994]. The initial linear growth (which subsequently decays exponentially) can enable small disturbances to a linearly stable flow to reach sufficiently high amplitude that nonlinear effects become important, and this highlights one of the failings of a linear stability analysis of this type. By disregarding terms of order ϵ^2 and above we are restricted to a regime in which the amplitude of the perturbations remains very small, as we are neglecting the effects of the interaction of the perturbations with themselves. Consequently, in the case of an unstable flow we cannot ascertain the long-term evolution of a perturbation since the amplitude is no longer sufficiently small for the linearised equations to be valid. Despite these limitations, however, the analysis of a linear perturbation to a given base flow remains a very useful tool in a range of stability problems.

1.3 The aim and structure of this thesis

The aim of this project is to develop a general numerical framework that allows the computation of the evolution of linear, non-axisymmetric perturbations for arbitrary nonlinear, axisymmetric base flows, both with and without free surfaces. This was achieved by systematically deriving the equations governing (i) the (possibly time-dependent) axisymmetric base state and (ii) the linearised non-axisymmetric perturbations to such flows. The equations were implemented in `oomph-lib`, the open-source, object-oriented finite element library developed by Matthias Heil and Andrew Hazel [Heil and Hazel, 2006], and validated/applied to representative test problems.

The outline of the thesis is as follows. In chapter 2 we introduce `oomph-lib` and provide a brief overview of its data structures. We then introduce the Navier–Stokes equations in chapter 3 and discuss the conditions which must be applied at an interface between two fluids. We introduce the concept of a 'weak solution' and go on to derive the weak form of the governing equations and boundary conditions. From here we provide an overview of the finite element method, and discuss its primary features via the example of the Navier–Stokes equations. For compactness (and clarity) the equations presented throughout this chapter are formulated with respect to a Cartesian coordinate system. In chapter 4 we then go on to apply this formulation to two free surface problems: (i) the relaxation of a (two-dimensional) fluid layer due to surface tension and gravitational forces, and (ii) the relaxation of an interface between two fluids of differing material properties.

With this introduction to the finite element formulation of free surface Navier–Stokes problems complete, we will begin to discuss the formulation of these equations in terms of cylindrical polar coordinates. We begin chapter 5 by deriving the weak form of the governing equations in a general orthogonal coordinate system, before specialising to cylindrical polar coordinates. We follow the same process for the free surface boundary conditions, before considering the governing equations and boundary conditions for the special case of an axisymmetric flow. Once we have written down the full set of residual equations for such a problem, we consider two applications of these in chapter 6. These two problems mirror those discussed in chapter 4.

Chapter 7 marks the start of our discussion of non-axisymmetric perturbations

to axisymmetric flows. Here we consider just the bulk terms: we begin with the three-dimensional Navier–Stokes equations in cylindrical polar coordinates and linearise them about an axisymmetric base flow. We then exploit the fact that they are periodic in the azimuthal direction in order to perform a Fourier decomposition: in this way we transform a single three-dimensional problem into a series of two-dimensional problems in which the azimuthal mode number appears as a parameter. The application of the resulting equations is then illustrated in chapter 8, where we discuss two specific problems: (i) the flow between two counter-rotating disks, and (ii) the flow between two concentric cylinders, where the inner cylinder rotates at constant angular velocity and the outer cylinder is driven sinusoidally in time. Both of these problems admit axisymmetric solutions, and we use the methodology developed in chapter 7 to assess the stability of these to both axisymmetric and non-axisymmetric perturbations.

The two problems discussed in chapter 8 both consider a single-fluid system only. To complete the discussion we began in chapter 7, we present the derivation of the free boundary conditions corresponding to linear, non-axisymmetric perturbations of an otherwise axisymmetric surface in chapter 9. Finally, we combine the methodology formulated in both of these chapters and apply them it to two problems involving perturbations to a two-phase axisymmetric flow: these are discussed in chapter 10. We conclude in chapter 11 with a brief summary of the functionality developed over the course of this project, and its inclusion within the overall `oomph-lib` framework.

Chapter 2

Introduction to `oomph-lib`

All of the code development and numerical simulations performed as part of this project took place within the general framework of `oomph-lib` [Heil and Hazel, 2006], an object-oriented, open-source finite element library developed by Matthias Heil and Andrew Hazel for the simulation of multi-physics problems. The library is written in `C++`, with particular emphasis placed on maximising code re-use, in order to provide an infrastructure in which it is possible to formulate a 'new' problem by combining pre-existing elements, meshes, timesteppers and solvers. It also provides a consistent framework in which to develop new functionality, such as the 'machinery' which will be discussed throughout the course of the current work.

The basic principle at the heart of `oomph-lib`'s design is that, in principle, 'any' problem can be discretised both spatially and temporally to yield a system of nonlinear algebraic equations[1], which can then be solved monolithically by Newton's method [Press et al., 2007, sec 9.6]. Let us suppose that we have a system of residual equations $\mathcal{R}_l(V_1, \ldots, V_M) = 0$, where M is the number of degrees of freedom in the problem and l ranges from 1 to M. Each of the M residual equations is a function of the M unknowns V_j, where $j = 1, \ldots, M$. The solution to this system of equations is computed by application of the following algorithm:

1. Set the iteration counter k to zero and provide an initial approximation for the unknowns,

$$V_j^{(0)} = V_j \qquad \text{for} \quad j = 1, \ldots, M. \tag{2.1}$$

[1] `oomph-lib` assumes that all problems are nonlinear by default, and treats linear problems as a special case.

2. Evaluate the residuals

$$\mathcal{R}_l^{(k)} = \mathcal{R}_l\left(V_1^{(k)}, \ldots, V_M^{(k)}\right) \tag{2.2}$$

for $l = 1, \ldots, M$.

3. Find the maximum entry in the global residual vector $\mathcal{R}_l^{(k)}$. If this is less than some prescribed tolerance, **stop** and accept $V_j^{(k)}$ as the solution.

4. Compute the Jacobian matrix

$$\mathcal{J}_{lj} = \left.\frac{\partial \mathcal{R}_l}{\partial V_j}\right|_{\left(V_1^{(k)},\ldots,V_M^{(k)}\right)} \tag{2.3}$$

for $j, l = 1, \ldots, M$.

5. Solve the linear system

$$\sum_{j=1}^{M} \mathcal{J}_{lj}\, \delta V_j = -\mathcal{R}_l^{(k)}, \tag{2.4}$$

where $l = 1, \ldots, M$, for δV_j.

6. Compute an improved approximation for the solution using

$$V_j^{(i+1)} = V_j^{(i)} + \delta V_j \tag{2.5}$$

for $j = 1, \ldots, M$.

7. Update the iteration counter $k \to k + 1$ and go to step (2).

Provided that a 'good enough' initial guess $V_j^{(0)}$ has been provided in step (1) (and that the Jacobian matrix $\mathcal{J}_{lj}$ is sufficiently well-conditioned) the Newton method converges quadratically towards the exact solution. In the special case in which we have a linear system of equations, the method provides the exact solution in a single iteration.

The majority of the 'machinery' in `oomph-lib` is concerned with the task of formulating physical problems in terms of a system of algebraic equations which can then be solved in the manner described above. This discretisation is achieved through a finite element framework in which the equations which are to be solved are specified via (and implemented within) the individual elements themselves. This concept is key to the overall design: every element e computes its local residual vector $\mathcal{R}^{(e)}$ and Jacobian matrix $\mathcal{J}^{(e)}$, and the global residual vector $\mathcal{R}$ and Jacobian matrix $\mathcal{J}$ are

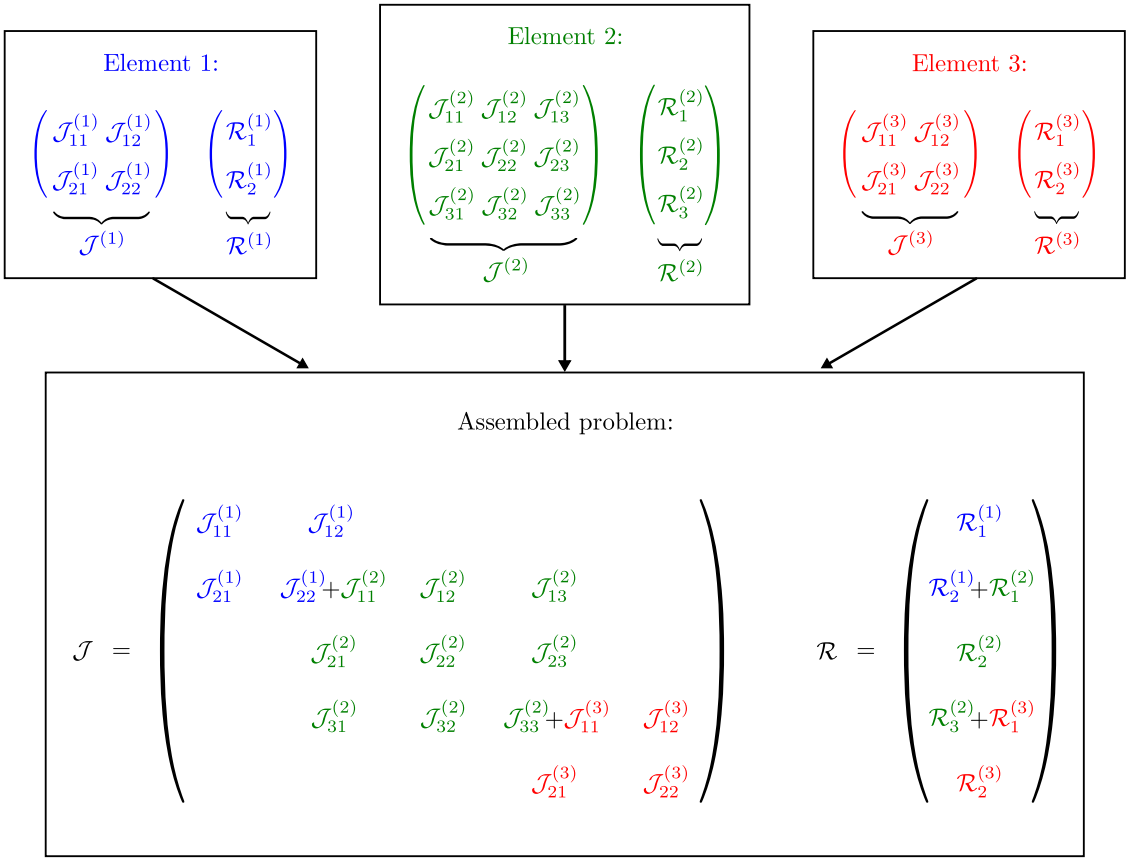

Figure 2.1: Sketch illustrating the assembly of the global Jacobian matrix $\mathcal{J}$ and residual vector $\mathcal{R}$ from the individual elemental contributions. This diagram is based on a similar schematic originally presented in [Heil and Hazel, 2006].

then constructed via element-by-element assembly. This process is sketched in figure 2.1. Once $\mathcal{R}$ and $\mathcal{J}$ have been assembled we apply the Newton method, which requires the solution of a series of large linear systems (arising from the application of step (5) of the above algorithm). In all of the problems considered in this work, these linear systems were solved using the `SuperLU` code [Demmel et al., 1999], a library specialising in the direct solution of large systems of linear equations by LU decomposition methods. `oomph-lib` contains wrappers to several other state-of-the-art linear solvers, however, such as the `HSL` frontal solvers [HSL2004, 2004] and `MUMPS` [Amestoy et al., 2000], as well as the iterative solvers implemented by the `Hypre` [Falgout and Yang, 2002] and `Trilinos` [Heroux et al., 2003] projects. Although these iterative solvers come with their own 'black-box' preconditioning strategies, `oomph-lib` also provides a range of problem-specific `Preconditioner` classes.

Central to the design of `oomph-lib` is the ability to construct a range of single- and multi-physics problems by combining more basic functionality in as flexible as possible a way. This ability to constantly 'recycle' code is facilitated via heavy use of object-orientation, which provides both

(i) **encapsulation**: the combining of data into small logical units known as 'objects' which can be interacted with by well-defined interfaces, and

(ii) **inheritance**: the construction of more complex objects by adding new functionality to already existing simpler ones.

Designing the library in this way leads to a hierarchical data structure, in which derived classes 'inherit' existing functionality before adding to it. In certain cases it is also useful for derived classes to 'overload' the more general functionality inherited from the base class with new, more specific functionality tailored to the more specialised function of the derived class.

2.1 Overview of the data structure

Figure 2.2 presents a simplified, general overview of the relationship between the basic data structures within `oomph-lib`. The most fundamental of these is the `Data` class, which provides storage for one or more 'values', or double precision numbers. By default `oomph-lib` treats every value as an 'unknown' (or 'degree of freedom') in the overall problem, and therefore each individual value has a global equation number associated with it. The `Data` class provides an interface to 'pin' a value: this operation is used when the user wishes to prescribe the value of the solution at a particular point, for example on a domain boundary. 'Pinned' values are not treated as degrees of freedom, and as such are not included in the global system of equations. By contrast, 'unpinned' values represent unknowns and will be determined by the solution of the problem. In addition to this functionality, the `Data` class also stores an arbitrary number of 'history values' corresponding to each value: these are required by timestepping schemes and are therefore necessary for the solution of time-dependent problems.

There are many occasions when we wish to associate a given set of values with an Eulerian position within the problem domain. The `Node` class inherits from the `Data`

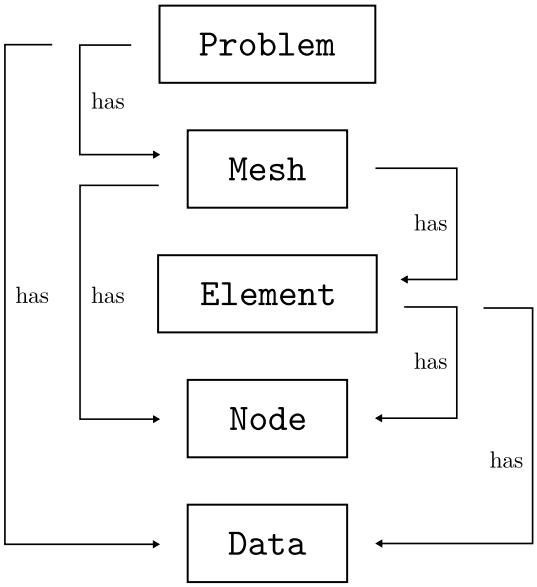

Figure 2.2: Overview of the relationship between the fundamental objects in `oomph-lib`. This diagram is based on a similar sketch originally presented in [Heil and Hazel, 2006].

class and adds storage for the position (in an arbitrary number of spatial dimensions), and is used to represent the discrete nodal points in the finite element method at which the solution is represented by discrete coefficients. The details of this formulation will be discussed in the following chapter, but we note here that in problems with a moving mesh the nodal positions will evolve over time. In order to accomodate this the `Node` class stores the required number of history values associated with each Eulerian position, thus facilitating the computation of the nodal velocities. Moreover, in certain problems the actual nodal positions may themselves be unknowns in the problem. The `SolidNode` class inherits from the base `Node` class and provides the extra functionality to allow the position to be an unknown which is then represented by `Data`.

All `Nodes` are associated with one or more `Elements`. Each `Element` is responsible for computing its own residual vector and Jacobian matrix. The `Elements` (and their associated `Nodes`) are then stored in a `Mesh`, which represents the physical geometry of the problem. The `Mesh` class stores information such as which `Nodes` lie on which domain boundaries, and provides interfaces through which this information may be accessed in an ordered manner. The `Mesh` is also responsible for setting up the connectivity of the elements and nodes based on the geometry of the domain.

The 'highest level' class in the oomph-lib hierarchy is known as a Problem. Each Problem object is meant to represent a discrete physical problem, and is responsible for implementing the problem formulation. The Problem class provides interfaces for standard tasks such as setting up the Mesh, defining boundary conditions, setting up timesteppers and defining the various non-dimensional parameters that feature in the equations. The Problem object is also responsible for assembling the global residual vector and Jacobian matrix from the individual elemental contributions, and in order to do so must provide routines to set up the overall equation numbering schemes.

It is often convenient to formulate more complex physical problems by representing them as two or more 'simpler' Problem objects, which are coupled together in some way. This is particularly useful in multi-physics problems, since it allows for maximum code re-use. We will refer back to this concept in chapter 8 of this work when we discuss the implementation of the linearised perturbation equations about a base flow: in these applications the base flow is represented by a single Problem object and the perturbation equations by a second, with a one-way coupling between the two.

2.2 Developing new functionality

When designing a large library of this kind, care must be taken to ensure that new functionality can easily be inserted at the 'correct' level of the data structure, with minimum disruption in terms of interface changes and alterations to pre-existing classes. As previously discussed, oomph-lib's design philosophy is to avoid code duplication wherever possible, and to this end the library employs a rich inheritance structure for its classes. So-called 'base' classes establish common functionality that will be required for all objects derived from this type, and many of these base classes have the property that they are 'virtual': this means that specific implementations of generic tasks can be delayed to derived classes. We will expand on this concept via the example of the AxisymmetricQCrouzeixRaviartElement, an oomph-lib class that implements a quadratic Crouzeix–Raviart[2] finite element for the solution of axisymmetric Navier–Stokes problems. Figure 2.3 shows the (simplified) inheritance diagram for this class, and we notice that in this case the base class is a GeneralisedElement. We recall

[2]We will introduce Crouzeix–Raviart elements properly in section 3.3.2.

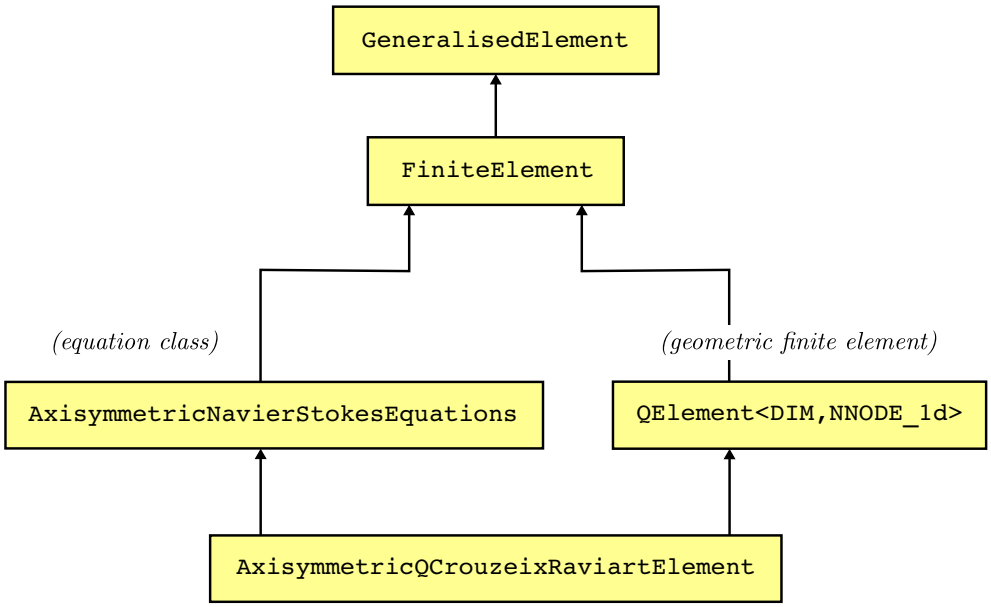

Figure 2.3: Simplified inheritance diagram for the `AxisymmetricQCrouzeix-RaviartElement` class.

that it is a requirement that every element computes its contribution to the global residual vector and Jacobian matrix, and therefore the interfaces to these functions are *defined* in this base class:

```
GeneralisedElement::get_residual(...)
GeneralisedElement::get_jacobian(...)
```

Crucially, however, the actually *implementation* of these elements will be delayed until the `AxisymmetricQCrouzeixRaviartElement` class, which is sufficiently specialist that the functions can be specified in a 'concrete', rather than an 'abstract', sense.

The `GeneralisedElement` class is also responsible for implementing other generic tasks which are common to *all* elements, such as returning the number of degrees of freedom and setting up the lookup scheme that stores the correspondence between local and global equation numbers. The `FiniteElement` class then inherits from this class and adds the additional functionality that must be shared by all finite elements: this includes storage for (pointers to) the element's nodes and a spatial integration scheme, interfaces which specify the spatial dimension of the element, interfaces to specify the local shape functions (and their derivatives) and functions to calculate the

mapping between the local and global coordinates, amongst many other tasks. Any functions which cannot be implemented in complete generality are defined as virtual interfaces so that their specific implementation can be 'overloaded' in derived classes. One example of this is the definition of the shape functions: since all finite elements must have these, a common interface is defined here, but their actual implementation must be delayed until the specific geometry of the element has been established.

Note from figure 2.3 that at the next layer of abstraction the definition of the geometry has been isolated from the definition of the equations. The `QElement` class inherits from `FiniteElement` and provides all of the functionality common to quadrilateral elements. This element makes use of 'templating', which allows this single class to implement an entire family of geometric elements. The two template parameters are the spatial dimension of the element, `DIM`, and the number of nodes along one edge, `NNODE_1D`. In this way this one class can provide the specific implementation of, for example:

- `QElement<1,4>`: a four-node 'line' element, or
- `QElement<3,3>`: a twenty-seven-node 'brick' element.

The `AxisymmetricNavierStokesEquations` class implements the actual axisymmetric Navier–Stokes equations themselves, and its principal task is to overload the virtual `get_residual(...)` and `get_jacobian(...)` functions defined in the base class with concrete implementations specific to this particular equation class. It also stores (pointers to) any source functions or parameters that occur in the governing equations.

The final class in figure 2.3 is of type `AxisymmetricQCrouzeixRaviartElement`, and is termed the 'specific element'. It inherits from both the `AxisymmetricNavier-StokesEquations` and `QElement<2,3>` classes[3] to form a 'specific element' which implements the axisymmetric Navier–Stokes equations in a nine-noded quadrilateral element. These 'specific element' classes are often (and deliberately) fairly 'lightweight', since it is desirable that as much generic 'machinery' as possible is abstracted away.

Separating the geometry from the equation class in the manner described above provides just one example of the power of object-orientation. Let us suppose that

[3]This is known as 'multiple inheritance'. `oomph-lib` regularly makes use of the 'diamond' multiple inheritance structure, where a specific class inherits from one or more classes which themselves inherit from the *same* base class(es). To avoid any ambiguity in the implementation of specific functions arising from such a structure, `oomph-lib` generally employs 'virtual' inheritance by default.

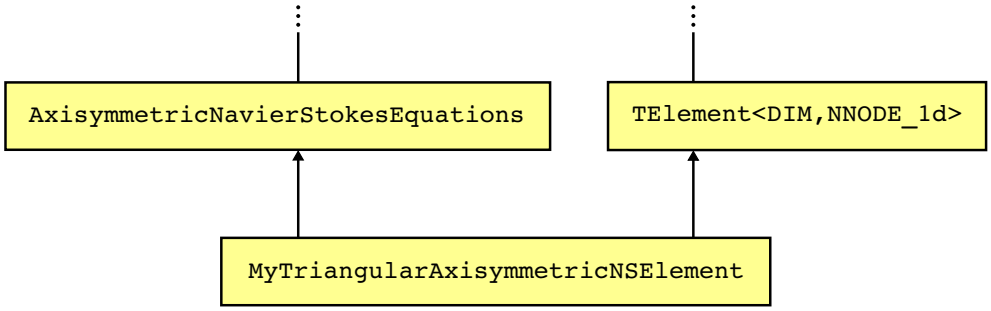

Figure 2.4: Illustration of the manner in which the underlying geometry of a finite element can be changed by simply 'dropping' in a new geometric element class: in this case, the `TElements` class has been substituted for the `QElements` class.

we wish to solve the axisymmetric Navier–Stokes equations using six-noded triangular elements. To do this we would simply 'drop' these new elements into the overall framework by defining a new specific element class, `MyTriangularAxisymmetricNSElement`, which inherits from both the `AxisymmetricNavierStokesEquations` and `oomph-lib`'s generic triangular elements class, `TElement<DIM,NNODE_1D>`, as shown in figure 2.4. The existing axisymmetric Navier–Stokes equations, as well as all the generic functionality implemented in the various base classes, have all been 'recycled'. The same would be true if we wanted to develop a new set of equations, and solve them using quadratic finite elements. By way of an example, let us imagine that we have developed a class, `LinearisedAxisymNavierStokesEquations`, which implement a linearised version of the axisymmetric Navier–Stokes equations. In order to begin using this new equation class within our finite element framework all we need to do is 'swap' the existing `AxisymmetricNavierStokesEquations` class with our new class, and write a new specific element to combine these new equations with our existing quadratic geometric elements, as illustrated in figure 2.5. In this way we have again 'recycled' almost all of the existing functionality which is not specific to our equation class.

Most of the development carried out throughout this project was performed at the element level, in developing new classes of equations to study generic non-axisymmetric perturbations to otherwise axisymmetric flows. Throughout this document we will (briefly) discuss the classes which were implemented, but we note here that their inclusion into the overall framework took place (broadly speaking) in the manner

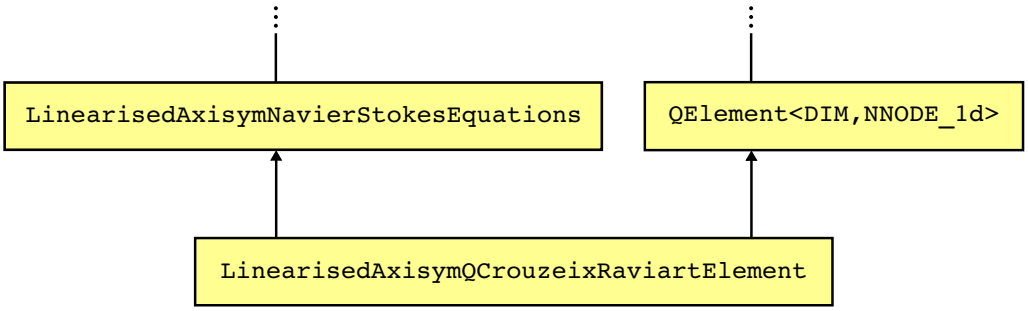

Figure 2.5: Illustration to demonstrate how new equation classes can easily be 'slotted into' `oomph-lib`'s overall finite element framework. In this example, a 'new' class of equations, the `LinearisedAxisymNavierStokesEquations`, have been inserted in the place of the 'standard' `AxisymmetricNavierStokesEquations`. All of the existing generic functionality has been retained, however, thanks to the inheritance structure in place.

described above.

Chapter 3

The free surface Navier–Stokes equations and the Finite Element Method

3.1 Governing equations

In dimensional form the Navier–Stokes equations (in Cartesian coordinates x_i^*) for a Newtonian fluid with constant density, ρ, and dynamic viscosity, μ, are given by the momentum equations

$$\rho\left(\frac{\partial u_i^*}{\partial t^*} + u_j^*\frac{\partial u_i^*}{\partial x_j^*}\right) = -\frac{\partial p^*}{\partial x_i^*} + B_i^* + \rho\, G_i^* + \frac{\partial}{\partial x_j^*}\left[\mu\left(\frac{\partial u_i^*}{\partial x_j^*} + \frac{\partial u_j^*}{\partial x_i^*}\right)\right] \tag{3.1}$$

and the continuity equation

$$\frac{\partial u_j^*}{\partial x_j^*} = Q^*, \tag{3.2}$$

where we have used index notation and the summation convention. The velocity components are denoted by u_i^*, the pressure by p^* and time by t^*, and the free index i runs over the spatial dimension. The body force has been split into two components: a constant vector $\rho\, G_i^*$ which typically represents gravitational forces, and a variable body force, $B_i^*(x_j^*, t^*)$. $Q^*(x_j^*, t^*)$ is a volumetric source term for the continuity equation and is typically equal to zero. The stress-divergence form of the viscous terms has been used as it will be required for the formulation of free surface problems.

We non-dimensionalise the equations, using problem-specific reference quantities for the velocity, $\mathcal{U}$, length, $\mathcal{L}$, and time, $\mathcal{T}$, and scale the constant body force vector

on the gravitational acceleration, g, so that

$$\begin{aligned} u_i^* &= \mathcal{U}\, u_i, \qquad x_i^* = \mathcal{L}\, x_i, \qquad t^* = \mathcal{T}\, t, \\ G_i^* &= g\, G_i, \qquad B_i^* = \frac{\mathcal{U}\,\mu_{\text{ref}}}{\mathcal{L}^2}\, B_i, \\ p^* &= \frac{\mathcal{U}\,\mu_{\text{ref}}}{\mathcal{L}}\, p, \qquad Q^* = \frac{\mathcal{U}}{\mathcal{L}}\, Q, \end{aligned} \tag{3.3}$$

where we note that the pressure and the variable body force have been non-dimensionalised on the viscous scale. μ_{ref} and ρ_{ref} are reference values for the fluid's dynamic viscosity and density, respectively, and in single-fluid problems are identical to the viscosity μ and density ρ of the (one and only) fluid in the problem. In problems involving multiple fluids, however, we use the ratios $R_\mu = \mu/\mu_{\text{ref}}$ and $R_\rho = \rho/\rho_{\text{ref}}$ to describe a particular fluid's viscosity and density relative to the reference values used to form the non-dimensional parameters.

The non-dimensional form of the Navier–Stokes equations is then given by

$$R_\rho \,\text{Re}\left(\text{St}\,\frac{\partial u_i}{\partial t} + u_j \frac{\partial u_i}{\partial x_j}\right) = -\frac{\partial p}{\partial x_i} + B_i + R_\rho\,\frac{\text{Re}}{\text{Fr}} G_i + \frac{\partial}{\partial x_j}\left[R_\mu\left(\frac{\partial u_i}{\partial x_j} + \frac{\partial u_j}{\partial x_i}\right)\right] \tag{3.4}$$

and

$$\frac{\partial u_j}{\partial x_j} = Q, \tag{3.5}$$

where the dimensionless parameters

$$\text{Re} = \frac{\mathcal{U}\mathcal{L}\rho_{\text{ref}}}{\mu_{\text{ref}}}, \qquad \text{St} = \frac{\mathcal{L}}{\mathcal{U}\mathcal{T}} \qquad \text{and} \qquad \text{Fr} = \frac{\mathcal{U}^2}{g\mathcal{L}} \tag{3.6}$$

are the Reynolds number, Strouhal number and Froude number respectively.

The (non-dimensional) stress tensor is given by

$$\tau_{ij} = -p\,\delta_{ij} + R_\mu\left(\frac{\partial u_i}{\partial x_j} + \frac{\partial u_j}{\partial x_i}\right), \tag{3.7}$$

and we can use this to rewrite (3.4) as

$$R_\rho \,\text{Re}\left(\text{St}\,\frac{\partial u_i}{\partial t} + u_j \frac{\partial u_i}{\partial x_j}\right) = B_i + R_\rho\,\frac{\text{Re}}{\text{Fr}} G_i + \frac{\partial \tau_{ij}}{\partial x_j}. \tag{3.8}$$

These governing equations determine the velocity u_i and pressure p within a domain D. They must be augmented by conditions applied at the boundary ∂D. The simplest of these is the Dirichlet condition, in which the values of one or more velocity components are prescribed on (a subsection of) the boundary:

$$u_i = u_i^{[\text{prescribed}]} \qquad \text{for some } i. \tag{3.9}$$

For example, where fluid meets an (axis-aligned) solid boundary the normal velocity component must be prescribed to be zero so that there is no penetration of the boundary by the fluid. Similarly, any tangential velocity components are required to be identical to the velocity of the boundary in the corresponding coordinate direction, so that there is no movement (or 'slip') of the fluid along the boundary. This set of conditions, in which every component is prescribed to be identical to the boundary motion, are known as the 'no slip' boundary conditions. Another common case, which will feature in many of the problems discussed in this work, are so-called 'non-penetration' conditions in which the normal component of the fluid velocity is prescribed to be zero but the values of the components tangential to the boundary remain unconstrained[1]. These often arise on symmetry boundaries.

Another typical boundary condition which can be applied is a Neumann condition, in which the flow on (a subsection of) the boundary is driven by an applied traction, $\mathbf{t}^{[\text{prescribed}]}$, which balances the fluid stress so that

$$\mathbf{t}_i \;=\; \tau_{ij}\, n_j \;=\; \mathbf{t}_i^{[\text{prescribed}]} \qquad \text{for some } i, \tag{3.10}$$

where $\mathbf{n}$ is a unit normal to the boundary pointing out of the fluid. Note that we cannot directly prescribe the pressure field at a boundary: we can only impose the normal component of the applied traction, $\mathbf{t} \cdot \mathbf{n}$. From (3.10) and (3.7) it can be seen that this applied traction is then distributed between the pressure and the viscous normal stresses.

3.1.1 Boundary conditions at a free surface

At the interface between two fluids, two boundary conditions must be applied:

(i) a dynamic condition which is concerned with the force balance at the free surface, and

(ii) a kinematic condition which relates the motion of the free surface to the fluid velocities at the surface.

[1] We note that although the current work will only ever consider domains in which the boundaries are axis-aligned, it is straightforward to generalise the concepts described here to boundaries which are not parallel to any particular coordinate axis.

The dynamic condition

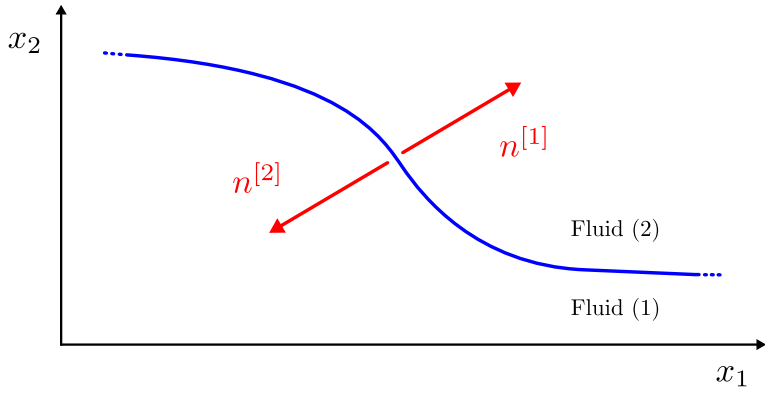

Figure 3.1: Sketch of the interface between two fluids.

The dynamic boundary condition requires the stress to be continuous across a flat interface between two fluids. Referring to figure 3.1, we define the lower fluid to be fluid 1 and the upper fluid to be fluid 2. The traction exerted by fluid 1 onto fluid 2, $\mathbf{t}^{[1]*}$, is equal and opposite to that exerted by fluid 2 onto fluid 1, $\mathbf{t}^{[2]*}$, and therefore $\mathbf{t}^{[1]*} = -\mathbf{t}^{[2]*}$. The traction in fluid β ($\beta = 1, 2$) is given by

$$t_i^{[\beta]*} = \tau_{ij}^{[\beta]*} n_j^{[\beta]}, \tag{3.11}$$

where $\boldsymbol{\tau}^{[\beta]*}$ is the stress tensor in fluid β and $\mathbf{n}^{[\beta]}$ is the outer unit normal to fluid β. Since $\mathbf{n}^{[2]}$ must equal $-\mathbf{n}^{[1]}$, we have

$$\tau_{ij}^{[1]*} n_j^{[1]} = \tau_{ij}^{[2]*} n_j^{[1]}, \tag{3.12}$$

where we have arbitrarily chosen to use $\mathbf{n}^{[1]}$ as the unit normal.

On curved surfaces, surface tension creates a pressure jump $\Delta p^* = \sigma\kappa^*$ across the interface, where σ is the surface tension and κ^* is equal to twice the mean curvature of the surface, and can be computed via

$$\kappa^* = -\nabla \cdot \mathbf{n}^{[1]}. \tag{3.13}$$

The dynamic boundary condition is therefore given by

$$\tau_{ij}^{[1]*} n_j^{[1]} = \tau_{ij}^{[2]*} n_j^{[1]} + \sigma\, \kappa^*\, n_i^{[1]}, \tag{3.14}$$

where $\kappa^* < 0$ if the centre of curvature lies inside fluid 1. In this work we shall always assume that the surface tension is constant along the interface (and so any Marangoni

stresses vanish). Again using the reference quantities (3.3) we have

$$\tau_{ij}^* = \frac{\mathcal{U}\mu_{\text{ref}}}{\mathcal{L}}\,\tau_{ij} \qquad \text{and} \qquad \kappa^* = \frac{1}{\mathcal{L}}\,\kappa, \tag{3.15}$$

and the non-dimensional form of the dynamic boundary condition is therefore given by

$$\tau_{ij}^{[1]}\,n_j^{[1]} = \tau_{ij}^{[2]}\,n_j^{[1]} + \frac{1}{\text{Ca}}\kappa\,n_i^{[1]}, \tag{3.16}$$

where the Capillary number is

$$\text{Ca} = \frac{\mathcal{U}\mu_{\text{ref}}}{\sigma}. \tag{3.17}$$

In certain problems we wish to model the fluid above the interface as totally inviscid, and in these cases the stress tensor in fluid 2 reduces to $\tau_{ij}^{[2]} = -\delta_{ij}\,p_{\text{ext}}$, where p_{ext} is the (non-dimensional) constant pressure above the free surface. The dynamic boundary condition therefore becomes

$$\tau_{ij}\,n_j = \frac{1}{\text{Ca}}\,\kappa\,n_i - p_{\text{ext}}\,n_i, \tag{3.18}$$

where we have dropped the explicit references to fluid 1 since it is understood that the stress tensor and unit normals refer to those of the (one and only) viscous fluid in the problem.

The kinematic condition

The kinematic condition states that any fluid particles at the surface remain on the surface for all times. If the surface is parameterised by intrinsic coordinates ζ_α^*, where α runs over the spatial dimension of the surface, then the Eulerian position vector which describes the surface at a given time t^* can be written as $\mathbf{X}^* = \mathbf{X}^*(\zeta_\alpha^*, t^*)$. The kinematic condition is then given by

$$\left(u_i^* - \frac{\partial X_i^*}{\partial t^*}\right) n_i = 0, \tag{3.19}$$

where n_i are the components of the outer unit normal to the free surface. Using the same problem-specific reference quantities (3.3) we scale the dimensional quantities such that

$$u_i^* = \mathcal{U}\,u_i, \qquad X_i^* = \mathcal{L}\,X_i \qquad \text{and} \qquad t^* = \mathcal{T}\,t, \tag{3.20}$$

and the non-dimensional form of the kinematic boundary condition is then given by

$$\left(u_i - \text{St}\,\frac{\partial X_i}{\partial t}\right) n_i = 0. \tag{3.21}$$

3.2 Weak form of the governing equations

Let us write the governing equations (3.8) and (3.5) in residual form, so that the momentum equations are given by

$$R_\rho \,\mathrm{Re}\left(\mathrm{St}\,\frac{\partial u_i}{\partial t} + u_j \frac{\partial u_i}{\partial x_j}\right) - B_i - R_\rho \,\frac{\mathrm{Re}}{\mathrm{Fr}} G_i - \frac{\partial \tau_{ij}}{\partial x_j} = 0 \tag{3.22}$$

and the continuity equation is given by

$$\frac{\partial u_j}{\partial x_j} - Q = 0. \tag{3.23}$$

Let us also assume from this point onwards that we are solving these equations in a two-dimensional domain. This is simply to make the following discussion clearer; the results below can easily be generalised to three spatial dimensions.

A classical, or 'strong', solution of these equations is one in which $u_i(x_j)$ and $p(x_j)$ satisfy (3.22) and (3.23), as well as the appropriate boundary conditions, at every point in the domain D. To facilitate the subsequent solution of the equations by the method of finite elements we shall now introduce the concept of a 'weak' solution: one which satisfies the Dirichlet boundary conditions, and for which the 'weighted residuals'[2],

$$\mathcal{R}_i^{[\mathrm{f}]} = \iint_D \left\{ R_\rho \,\mathrm{Re}\left(\mathrm{St}\,\frac{\partial u_{(i)}}{\partial t} + u_j \frac{\partial u_{(i)}}{\partial x_j}\right) - B_{(i)} - R_\rho \,\frac{\mathrm{Re}}{\mathrm{Fr}} G_{(i)} - \frac{\partial \tau_{(i)j}}{\partial x_j} \right\} \phi_{(i)}^{[\mathrm{f}]}(x_k)\; \mathrm{d}x_1\, \mathrm{d}x_2 \tag{3.24}$$

and

$$\mathcal{R}^{[\mathrm{p}]} = \iint_D \left(\frac{\partial u_j}{\partial x_j} - Q\right) \phi^{[\mathrm{p}]}(x_k)\; \mathrm{d}x_1\, \mathrm{d}x_2, \tag{3.25}$$

vanish for *any* 'test functions' $\phi_i^{[\mathrm{f}]}(x_k)$ and $\phi^{[\mathrm{p}]}(x_k)$. Each of these three (as $i = 1, 2$ in two spatial dimensions) test functions correspond to the three scalar fields $u_1(x_1, x_2)$, $u_2(x_1, x_2)$ and $p(x_1, x_2)$, and have the property that they must evaluate to zero on any boundaries for which the corresponding scalar quantity is subject to Dirichlet boundary conditions. Since (as discussed in section 3.1) we never have any pressure boundary conditions, the previous statement can be simplified in the following way: we insist that any test function $\phi_i^{[\mathrm{f}]}$ vanishes on boundaries at which the i-th velocity component is prescribed by Dirichlet conditions. The choice of the specific forms of

[2]Note that from (3.24) onwards we shall adopt the usual convention where we do not perform a sum over any repeated indices in parentheses.

$\phi_i^{[\mathrm{f}]}$ and $\phi^{[\mathrm{p}]}$ is important and will be discussed in detail in section 3.3.2. While the weak form may appear to considerably relax the concept of a solution, we note that the insistence that the integral vanishes for *any* test function implies that the weak solution does, in fact, satisfy the strong (original) equations point-wise rather than just in an average sense.

Note that (3.24) involves second derivatives of u (in the $\partial\tau_{ij}/\partial x_j$ term) and zero-th derivatives of the test function $\phi^{[\mathrm{f}]}$. A 'symmetric' form, which will turn out to be useful for the practical implementation of the method of finite elements (section 3.3.2), can be obtained using the divergence theorem,

$$\iint_D \frac{\partial \tau_{(i)j}}{\partial x_j}\,\phi_{(i)}^{[\mathrm{f}]}\;\mathrm{d}x_1\,\mathrm{d}x_2 = \oint_{\partial D} \tau_{(i)j}\,\phi_{(i)}^{[\mathrm{f}]}\,n_j\;\mathrm{d}\zeta - \iint_D \tau_{(i)j}\frac{\partial \phi_{(i)}^{[\mathrm{f}]}}{\partial x_j}\;\mathrm{d}x_1\,\mathrm{d}x_2, \tag{3.26}$$

where the line integral is evaluated over the entire domain boundary ∂D. The parameter ζ is the arc length along ∂D, and so $\oint_{\partial D}\mathrm{d}\zeta$ evaluates to the perimeter of the domain. Substituting (3.26) into (3.24) yields

$$\begin{aligned}\mathcal{R}_i^{[\mathrm{f}]} = \iint_D \left\{ R_\rho\,\mathrm{Re}\left[\mathrm{St}\,\frac{\partial u_{(i)}}{\partial t} + u_j\frac{\partial u_{(i)}}{\partial x_j}\right] - B_{(i)} - R_\rho\,\frac{\mathrm{Re}}{\mathrm{Fr}}G_{(i)}\right\}\phi_{(i)}^{[\mathrm{f}]}\;\mathrm{d}x_1\,\mathrm{d}x_2 \\ + \iint_D \tau_{(i)j}\frac{\partial \phi_{(i)}^{[\mathrm{f}]}}{\partial x_j}\;\mathrm{d}x_1\,\mathrm{d}x_2 - \oint_{\partial D}\tau_{(i)j}\,n_j\,\phi_{(i)}^{[\mathrm{f}]}\;\mathrm{d}\zeta,\end{aligned} \tag{3.27}$$

and finally we use the definition of the stress tensor (3.7) to rewrite the second term in (3.27):

$$\begin{aligned}\mathcal{R}_i^{[\mathrm{f}]} = \iint_D \left\{ R_\rho\,\mathrm{Re}\left[\mathrm{St}\,\frac{\partial u_{(i)}}{\partial t} + u_j\frac{\partial u_{(i)}}{\partial x_j}\right] - B_{(i)} - R_\rho\,\frac{\mathrm{Re}}{\mathrm{Fr}}G_{(i)}\right\}\phi_{(i)}^{[\mathrm{f}]}\;\mathrm{d}x_1\,\mathrm{d}x_2 \\ - \iint_D p\,\frac{\partial \phi_{(i)}^{[\mathrm{f}]}}{\partial x_{(i)}}\;\mathrm{d}x_1\,\mathrm{d}x_2 + \iint_D R_\mu\left(\frac{\partial u_{(i)}}{\partial x_j} + \frac{\partial u_j}{\partial x_{(i)}}\right)\frac{\partial \phi_{(i)}^{[\mathrm{f}]}}{\partial x_j}\;\mathrm{d}x_1\,\mathrm{d}x_2 \\ - \oint_{\partial D}\tau_{(i)j}\,n_j\,\phi_{(i)}^{[\mathrm{f}]}\;\mathrm{d}\zeta.\end{aligned} \tag{3.28}$$

Equation (3.28) now simply involves first derivatives of both u_i and the test function $\phi_i^{[\mathrm{f}]}$, and using the definition of the traction (3.11) we can replace the line integral term with

$$-\oint_{\partial D}\mathfrak{t}_{(i)}\,\phi_{(i)}^{[\mathrm{f}]}\;\mathrm{d}\zeta. \tag{3.29}$$

This line integral must be evaluated over the entire domain boundary. However, since the test function $\phi_i^{[\mathrm{f}]}$ evaluates to zero on Dirichlet boundaries for u_i, the integral (3.29) vanishes there and the only contribution is made on non-Dirichlet boundaries, where

the applied traction $\mathfrak{t}_i$ must be specified. It follows that leaving out the line integral term in (3.28) on these boundaries is equivalent to prescribing the applied traction to be zero: this is the 'natural boundary condition'. We note that the use of the divergence theorem implies certain differentiability requirements on the test functions and the solution: these requirements will be discussed in detail in section 3.3.1.

3.2.1 Weak form of the free surface boundary conditions

The dynamic condition

The free surface is a non-Dirichlet boundary, but one on which we are not prescribing the traction explicitly. Let us consider the case in which we are describing a single viscous fluid layer: the traction on the free surface is given by the dynamic boundary condition (3.18),

$$\mathfrak{t}_i = \frac{1}{\mathrm{Ca}}\,\kappa\, n_i - p_{\mathrm{ext}}\, n_i, \tag{3.30}$$

and therefore the contribution to the line integral term (3.29) from the free surface boundary Ω is given by

$$\int_\Omega \frac{\kappa}{\mathrm{Ca}}\, n_{(i)}\, \phi^{[\mathrm{f}]}_{(i)}\, \mathrm{d}\zeta - \int_\Omega p_{\mathrm{ext}}\, n_{(i)}\, \phi^{[\mathrm{f}]}_{(i)}\, \mathrm{d}\zeta. \tag{3.31}$$

The above expression implicitly contains second derivatives of the position vector to the surface (in the κ term) and zero-th derivatives of the test function $\phi^{[\mathrm{f}]}$. Once again we wish to obtain a symmetric form, and employ the surface divergence theorem [Weatherburn, 1955, Article 122]:

$$\iint_S \nabla_S \cdot \mathbf{v}\, \mathrm{d}S = \oint_C (\mathbf{v}\cdot\mathbf{m})\, \mathrm{d}C - \iint_S \kappa\,(\mathbf{v}\cdot\mathbf{n})\, \mathrm{d}S, \tag{3.32}$$

where $\mathbf{v}$ is an arbitrary vector field on the surface and $\mathbf{m}$ is the outward-pointing unit vector which is tangent to the surface and normal to the contour bounding the free surface, C. This contour will in future be referred to as the 'contact line'. $\nabla_S = (\mathbf{I}-\mathbf{nn})\cdot\nabla$ is the surface gradient. Since in our two-dimensional example the free surface is one-dimensional, we reduce (3.32) appropriately,

$$\int_\Omega \nabla_S \cdot \mathbf{v}\, \mathrm{d}\zeta = \mathbf{v}\cdot\mathbf{m}\big|_{C_1} + \mathbf{v}\cdot\mathbf{m}\big|_{C_2} - \int_\Omega \kappa\,(\mathbf{v}\cdot\mathbf{n})\, \mathrm{d}\zeta, \tag{3.33}$$

and note that the contact 'line' reduces to two contact 'points', C_1 and C_2. These are located at either side of the portion of the domain boundary corresponding to the free

surface, and hence the integral over C in (3.33) has reduced to two point contributions. Additionally, we use the fact that in one dimension the action of ∇_S acting on a scalar field $\phi(x_i)$ can be rewritten in the following way:

$$\nabla_S \phi \;=\; (\mathbf{I} - \mathbf{nn}) \cdot \nabla\phi \;=\; \mathbf{I} \cdot \nabla\phi - \mathbf{n}\,(\mathbf{n} \cdot \nabla\phi) \;=\; \nabla\phi - \mathbf{n}\frac{\partial\phi}{\partial n}. \tag{3.34}$$

We can then resolve $\nabla\phi$ into two orthogonal components which are normal and tangential to the free surface such that

$$\nabla\phi = \mathbf{n}\frac{\partial\phi}{\partial n} + \mathbf{t_1}\frac{\partial\phi}{\partial\zeta}, \tag{3.35}$$

where ζ is the arc length along the free surface (as before) and $\mathbf{n}$ and $\mathbf{t_1}$ are unit normal and tangent vectors to the free surface respectively. Substituting (3.35) into (3.34) gives

$$\nabla_S \phi = \mathbf{t_1}\frac{\partial\phi}{\partial\zeta} \qquad \text{or} \qquad \nabla_S = \mathbf{t_1}\frac{\partial}{\partial\zeta}, \tag{3.36}$$

which enables us to rewrite (3.33) as

$$\int_\Omega \mathbf{t_1} \cdot \frac{\partial\mathbf{v}}{\partial\zeta}\;\mathrm{d}\zeta = \mathbf{v}\cdot\mathbf{m}\big|_{C_1} + \mathbf{v}\cdot\mathbf{m}\big|_{C_2} - \int_\Omega \kappa\,(\mathbf{v}\cdot\mathbf{n})\;\mathrm{d}\zeta. \tag{3.37}$$

We apply this one-dimensional form of the surface divergence theorem by first letting $\mathbf{v} = \frac{1}{Ca}\,\phi^{[\mathrm{f}]}_{(i)}\,\mathbf{e}_{(i)}$, where $\mathbf{e}_i$ $(i = 1, 2)$ is the Cartesian basis vector in the i-th coordinate direction, to obtain

$$\int_\Omega \frac{1}{Ca}\,(t_1)_{(i)}\,\frac{\mathrm{d}\phi^{[\mathrm{f}]}_{(i)}}{\mathrm{d}\zeta}\;\mathrm{d}\zeta = \frac{1}{Ca}\,\phi^{[\mathrm{f}]}_{(i)}\,m_{(i)}\bigg|_{C_1} + \frac{1}{Ca}\,\phi^{[\mathrm{f}]}_{(i)}\,m_{(i)}\bigg|_{C_2} - \int_\Omega \frac{\kappa}{Ca}\,n_{(i)}\,\phi^{[\mathrm{f}]}_{(i)}\;\mathrm{d}\zeta, \tag{3.38}$$

which can be substituted into the first term of the dynamic boundary condition (3.31) to give

$$\int_\Omega t_{(i)}\,\phi^{[\mathrm{f}]}_{(i)}\;\mathrm{d}\zeta = -\int_\Omega p_{\mathrm{ext}}\,n_{(i)}\,\phi^{[\mathrm{f}]}_{(i)}\;\mathrm{d}\zeta - \int_\Omega \frac{1}{Ca}\,(t_1)_{(i)}\,\frac{\mathrm{d}\phi^{[\mathrm{f}]}_{(i)}}{\mathrm{d}\zeta}\;\mathrm{d}\zeta + \frac{1}{Ca}\,\phi^{[\mathrm{f}]}_{(i)}\,m_{(i)}\bigg|_{C_1} + \frac{1}{Ca}\,\phi^{[\mathrm{f}]}_{(i)}\,m_{(i)}\bigg|_{C_2}. \tag{3.39}$$

The complete weak form of the Navier–Stokes momentum equations are thus obtained

by substituting the above into (3.28) to give

$$\begin{aligned}\mathcal{R}_i^{[\mathrm{f}]} = \iint_D \left\{ R_\rho \,\mathrm{Re}\left[\mathrm{St}\,\frac{\partial u_{(i)}}{\partial t} + u_j \frac{\partial u_{(i)}}{\partial x_j}\right] - B_{(i)} - R_\rho \,\frac{\mathrm{Re}}{\mathrm{Fr}} G_{(i)} \right\} \phi_{(i)}^{[\mathrm{f}]} \,\mathrm{d}x_1\,\mathrm{d}x_2 \\ - \iint_D p\,\frac{\partial \phi_{(i)}^{[\mathrm{f}]}}{\partial x_{(i)}}\,\mathrm{d}x_1\,\mathrm{d}x_2 + \iint_D R_\mu \left(\frac{\partial u_{(i)}}{\partial x_j} + \frac{\partial u_j}{\partial x_{(i)}}\right)\frac{\partial \phi_{(i)}^{[\mathrm{f}]}}{\partial x_j}\,\mathrm{d}x_1\,\mathrm{d}x_2 \\ - \int_{\partial D/\Omega} \tau_{(i)j}\, n_j\, \phi_{(i)}^{[\mathrm{f}]}\,\mathrm{d}\zeta + \int_\Omega p_{\mathrm{ext}}\, n_{(i)}\, \phi_{(i)}^{[\mathrm{f}]}\,\mathrm{d}\zeta \\ + \int_\Omega \frac{1}{Ca}\,(t_1)_{(i)}\,\frac{\mathrm{d}\phi_{(i)}^{[\mathrm{f}]}}{\mathrm{d}\zeta}\,\mathrm{d}\zeta - \frac{1}{Ca}\,\phi_{(i)}^{[\mathrm{f}]}\, m_{(i)}\Big|_{C_1} - \frac{1}{Ca}\,\phi_{(i)}^{[\mathrm{f}]}\, m_{(i)}\Big|_{C_2}, \end{aligned} \tag{3.40}$$

where $\partial D/\Omega$ represents the portion of ∂D which is not the free boundary Ω. Note that if the contact points C_1 or C_2 are located on Dirichlet boundaries then the test function evaluates to zero at this point and these contributions vanish. Alternatively, the contributions are added by specifying the tangent to the surface, m_i, at each of the contact points, which is equivalent to prescribing the contact angle that the free surface makes with the neighbouring domain boundary. Neglecting these contributions is equivalent to implicitly prescribing a 90^o contact angle, which is the 'natural' condition. This condition is appropriate at symmetry boundaries. Additionally, we note that we have to prescribe the external pressure p_{ext}, and that not doing so is equivalent to setting it to zero (the natural condition).

The kinematic condition

By solving $\mathcal{R}_i^{[\mathrm{f}]} = 0$ (for the two spatial dimensions $i = 1, 2$) and $\mathcal{R}^{[\mathrm{p}]} = 0$ we can determine the fluid velocities and pressure. However, we have a further unknown in a free surface problem: the position of the surface itself. To account for this extra degree of freedom we must also solve the weak form of the kinematic boundary condition (3.21), $\mathcal{R}^{[\mathrm{h}]} = 0$, where the weighted residual $\mathcal{R}^{[\mathrm{h}]}$ is given by

$$\mathcal{R}^{[\mathrm{h}]} = \int_\Omega \left(u_i - \mathrm{St}\,\frac{\partial X_i}{\partial t}\right) n_i\, \phi^{[\mathrm{h}]}(\zeta)\,\mathrm{d}\zeta \tag{3.41}$$

where $\phi^{[\mathrm{h}]}$ is any test function (subject to the usual requirement that it vanishes at points where the position of the free surface is fixed).

3.3 Discretisation of the equations and the finite element method

3.3.1 Discretisation of the bulk equations

In the previous section we derived the weak form of a two-dimensional Cartesian free surface Navier–Stokes problem. Let us for the moment just consider the 'bulk' equations: that is, the terms in the governing equations (3.40) and (3.25) that perform an integral over the two-dimensional domain D. To facilitate this we shall express the weak form of the momentum equations $\mathcal{R}_i^{[\mathrm{f}]}$ (3.40) as a sum of bulk terms, $\mathcal{R}_i^{[\mathrm{f,bulk}]}$, and terms arising from integrals over the domain boundary, $\mathcal{R}_i^{[\mathrm{f,boundary}]}$, (including the point contributions), so that

$$\mathcal{R}_i^{[\mathrm{f}]} = \mathcal{R}_i^{[\mathrm{f,bulk}]} + \mathcal{R}_i^{[\mathrm{f,boundary}]}. \tag{3.42}$$

Additionally, we will assume (for now) that the problem domain is fixed. The 'bulk' problem that we are considering for the time being is therefore given by

$$\begin{aligned}\mathcal{R}_i^{[\mathrm{f,bulk}]} = \iint_D \left\{ R_\rho \,\mathrm{Re}\left[\mathrm{St}\,\frac{\partial u_{(i)}}{\partial t} + u_j \frac{\partial u_{(i)}}{\partial x_j}\right] - B_{(i)} - R_\rho \,\frac{\mathrm{Re}}{\mathrm{Fr}} G_{(i)} \right\} \phi_{(i)}^{[\mathrm{f}]} \,\mathrm{d}x_1\,\mathrm{d}x_2 \\ - \iint_D p\,\frac{\partial \phi_{(i)}^{[\mathrm{f}]}}{\partial x_{(i)}}\,\mathrm{d}x_1\,\mathrm{d}x_2 + \iint_D R_\mu \left(\frac{\partial u_{(i)}}{\partial x_j} + \frac{\partial u_j}{\partial x_{(i)}}\right)\frac{\partial \phi_{(i)}^{[\mathrm{f}]}}{\partial x_j}\,\mathrm{d}x_1\,\mathrm{d}x_2\end{aligned} \tag{3.43}$$

and

$$\mathcal{R}^{[\mathrm{p}]} = \iint_D \left(\frac{\partial u_j}{\partial x_j} - Q\right)\phi^{[\mathrm{p}]}\,\mathrm{d}x_1\,\mathrm{d}x_2. \tag{3.44}$$

In order to discretise these equations we expand u_i in the following way,

$$u_i(x_k) \;=\; u_i^{[\mathrm{Dirichlet}]}(x_k) \;+\; \sum_{j=1}^{\infty} U_{(i)j}\,\psi_{(i)j}^{[\mathrm{f}]}(x_k), \tag{3.45}$$

where $u_i^{[\mathrm{Dirichlet}]}$ is a function which satisfies the Dirichlet boundary conditions and the $\psi_{ij}^{[\mathrm{f}]}$, for a particular i, are a (given) infinite set of basis functions ($j = 1, \ldots, \infty$). A consequence of this construction is that the basis functions $\psi_{ij}^{[\mathrm{f}]}$ are required to vanish on any boundaries where the i-th velocity component is subject to Dirichlet boundary conditions. Because there are no Dirichlet conditions for the pressure we can simply expand this field as

$$p(x_k) = \sum_{j=1}^{\infty} P_j\,\psi_j^{[\mathrm{p}]}(x_k), \tag{3.46}$$

where $\psi_j^{[\mathrm{p}]}$ are another (given) infinite set of basis functions. The basis sets $\psi_{ij}^{[\mathrm{f}]}$ and $\psi_j^{[\mathrm{p}]}$ must be chosen such that:

(i) they form a complete basis for the function space containing the velocities and pressures, respectively, and

(ii) they are sufficiently well-behaved that the integrals in (3.43) and (3.44) are 'well defined'.

The solution is now determined by the (unknown) discrete coefficients U_{ij} ($i = 1, 2$ and $j = 1, \ldots, \infty$) and P_j ($j = 1, \ldots, \infty$). Substituting (3.45) and (3.46) into (3.43) and (3.44) yields expressions of the form

$$\mathcal{R}_i^{[\mathrm{f,bulk}]}\left(U_{11}, U_{12}, \ldots; U_{21}, U_{22}, \ldots; P_1, P_2, \ldots\right) = \iint_D \Big\{ \ldots \Big\} \phi_{(i)}^{[\mathrm{f}]} \, \mathrm{d}x_1 \, \mathrm{d}x_2 - \iint_D \Big\{ \ldots \Big\} \frac{\partial \phi_{(i)}^{[\mathrm{f}]}}{\partial x_{(i)}} \, \mathrm{d}x_1 \, \mathrm{d}x_2 \quad (3.47)$$

and

$$\mathcal{R}^{[\mathrm{p}]}\left(U_{11}, U_{12}, \ldots; U_{21}, U_{22}, \ldots\right) = \iint_D \Big\{ \ldots \Big\} \phi^{[\mathrm{p}]} \, \mathrm{d}x_1 \, \mathrm{d}x_2, \quad (3.48)$$

and we now employ the Galerkin method by expanding the test functions in terms of the same basis functions $\psi_{ij}^{[\mathrm{f}]}$ and $\psi_j^{[\mathrm{p}]}$ with which we represent the solution,

$$\phi_i^{[\mathrm{f}]} = \sum_{l=1}^{\infty} \Phi_{(i)l}^{[\mathrm{f}]} \, \psi_{(i)l}^{[\mathrm{f}]} \quad (3.49)$$

and

$$\phi^{[\mathrm{p}]} = \sum_{l=1}^{\infty} \Phi_l^{[\mathrm{p}]} \, \psi_l^{[\mathrm{p}]}. \quad (3.50)$$

Inserting these into the weak solution, (3.47) and (3.48), and exploiting the fact that the solution is linear in $\phi_i^{[\mathrm{f}]}$ and $\phi^{[\mathrm{p}]}$, yields

$$\mathcal{R}_i^{[\mathrm{f,bulk}]} = \sum_{l=1}^{\infty} \Phi_{(i)l}^{[\mathrm{f}]} \, \mathcal{R}_{(i)l}^{[\mathrm{f,bulk}]}\left(U_{11}, U_{12}, \ldots; U_{21}, U_{22}, \ldots; P_1, P_2, \ldots\right) \quad (3.51)$$

and

$$\mathcal{R}^{[\mathrm{p}]} = \sum_{l=1}^{\infty} \Phi_l^{[\mathrm{p}]} \, \mathcal{R}_l^{[\mathrm{p}]}\left(U_{11}, U_{12}, \ldots; U_{21}, U_{22}, \ldots\right), \quad (3.52)$$

where

$$\mathcal{R}_{il}^{[\mathrm{f,bulk}]} = \iint_D \left\{ R_\rho \, \mathrm{Re} \left[\mathrm{St} \, \frac{\partial u_{(i)}}{\partial t} + u_j \frac{\partial u_{(i)}}{\partial x_j} \right] - B_{(i)} - R_\rho \, \frac{\mathrm{Re}}{\mathrm{Fr}} G_{(i)} \right\} \psi_{(i)l}^{[\mathrm{f}]} \, \mathrm{d}x_1 \, \mathrm{d}x_2 - \iint_D p \, \frac{\partial \psi_{(i)l}^{[\mathrm{f}]}}{\partial x_{(i)}} \, \mathrm{d}x_1 \, \mathrm{d}x_2 + \iint_D R_\mu \left(\frac{\partial u_{(i)}}{\partial x_j} + \frac{\partial u_j}{\partial x_{(i)}} \right) \frac{\partial \psi_{(i)l}^{[\mathrm{f}]}}{\partial x_j} \, \mathrm{d}x_1 \, \mathrm{d}x_2 \quad (3.53)$$

and

$$\mathcal{R}_l^{[\mathrm{p}]} = \iint_D \left(\frac{\partial u_j}{\partial x_j} - Q \right) \psi_l^{[\mathrm{p}]} \, \mathrm{d}x_1 \, \mathrm{d}x_2. \tag{3.54}$$

We recall from section 3.2 that the equations (3.47) and (3.48) are obliged to hold for *any* test functions $\phi_i^{[\mathrm{f}]}$ and $\phi^{[\mathrm{p}]}$. In order to ensure this, therefore, we must impose the condition that (3.51) and (3.52) hold for *any* value of the coefficients $\Phi_{il}^{[\mathrm{f}]}$ and $\Phi_l^{[\mathrm{p}]}$. Hence U_{ij} and P_j must satisfy

$$\mathcal{R}_{il}^{[\mathrm{f,bulk}]} \left(U_{11}, U_{12}, \ldots ; U_{21}, U_{22}, \ldots ; P_1, P_2, \ldots \right) = 0 \qquad \text{for } l = 1, \ldots, \infty \tag{3.55}$$

and

$$\mathcal{R}_l^{[\mathrm{p}]} \left(U_{11}, U_{12}, \ldots ; U_{21}, U_{22}, \ldots \right) = 0 \qquad \text{for } l = 1, \ldots, \infty. \tag{3.56}$$

By examination of the discrete momentum equation (3.53) we observe that the velocity basis functions $\psi_{ij}^{[\mathrm{f}]}$ and their derivatives both appear in squares inside the integral, and hence the minimum requirements on $\psi_{ij}^{[\mathrm{f}]}$ are that both the functions themselves and their first derivatives can be square-integrated over the problem domain. Examination of the discrete continuity equation (3.54), on the other hand, reveals that there are no derivatives of the pressure basis functions $\psi_j^{[\mathrm{p}]}$ and hence the only requirement is that they are themselves square-integrable over the domain. Note that a consequence of this construction is that while the velocity solution is required to be continuous, discontinuities in the pressure solution are permitted. If $H^0(D)$ denotes the Sobolev space containing all functions which are square-integrable over D, then we require $\psi_j^{[\mathrm{p}]} \in H_0^0(D)$, a subset of this space containing only those members of $H^0(D)$ which vanish on the domain boundary $\partial D_{[\mathrm{Dirichlet}]}$. Similarly, we require $\psi_{ij}^{[\mathrm{f}]} \in H_0^1(D)$, a further subset containing only those members of $H_0^0(D)$ for which their first derivatives are also square-integrable over D. In order for us to expand the solution variables and the test functions in the manner described above, (3.45)–(3.46) and (3.49)–(3.50), we require $\psi_{ij}^{[\mathrm{f}]}$ and $\psi_j^{[\mathrm{p}]}$ to form complete bases for $H_0^1(D)$ and $H_0^0(D)$ respectively.

So far we have been solving for the exact solution u_i and p, but in practice we must truncate the expansions (3.45), (3.46), (3.49) and (3.50) after a finite number of terms. We are therefore solving for the approximate solutions

$$\widetilde{u}_i = \sum_{j=1}^{M_u} U_{(i)j} \, \psi_{(i)j}^{[\mathrm{f}]} \tag{3.57}$$

and

$$\widetilde{p} = \sum_{j=1}^{M_p} P_j \, \psi_j^{[\mathrm{p}]}, \tag{3.58}$$

and determine the $2M_u + M_p$ unknowns from the $2M_u$ equations

$$\mathcal{R}_{il}^{[\mathrm{f,bulk}]} \left(U_{11}, \ldots, U_{1M_u}, U_{21}, \ldots, U_{2M_u}, P_1, \ldots, P_{M_p} \right) = 0 \tag{3.59}$$

for $i = 1, 2$ and $l = 1, \ldots, M_u$, and the M_p equations

$$\mathcal{R}_{l}^{[\mathrm{p}]} \left(U_{11}, \ldots, U_{1M_u}, U_{21}, \ldots, U_{2M_u} \right) = 0 \tag{3.60}$$

for $l = 1, \ldots, M_p$. Note that (as a consequence of employing the Galerkin method) we obtain precisely the same number of equations as there are degrees of freedom in the problem. Having obtained the discrete residual equations (3.59) and (3.60), we must now choose a specific form for the various basis functions $\psi_{ij}^{[\mathrm{f}]}$ and $\psi_j^{[\mathrm{p}]}$.

3.3.2 Overview of the finite element method

Central to the method of finite elements is the decomposition of the problem domain D into a number of subdomains, or 'elements', as sketched in figure 3.2. The key feature is that the basis functions $\psi_{ij}^{[\mathrm{f}]}$ and $\psi_j^{[\mathrm{p}]}$ are chosen to have finite support. The approximation of the solution (3.57) and (3.58) is performed within each element, and then the finite element solution for the entire domain is assembled from the individual elemental contributions.

In order to represent the finite element solution of a problem over a particular element, it is assumed that the value of the solution is known at a certain number of points in that element. At each of these so-called 'nodal points' the value of the field in question is precisely the value of the corresponding coefficient U_{ij} or P_j. Note that from this point onwards we take the index j to mean the j-th *local* unknown of any particular field, where we are using the word 'local' to refer to any elemental-level quantity. The range of j is therefore from 1 to the number of degrees of freedom of the field in question represented in the element. In general, the number of velocity degrees of freedom in an element is not equal to the number of pressure degrees of freedom. We note that since nodes located on element boundaries are 'shared' with neighbouring elements, continuity of the solution between elements is guaranteed.

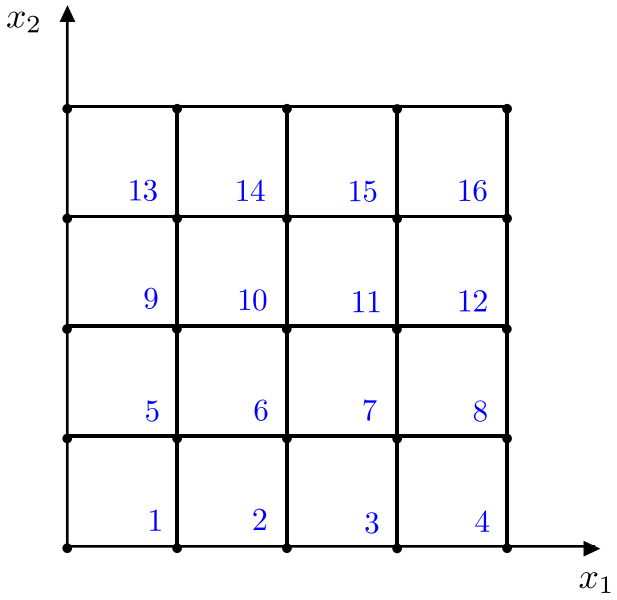

Figure 3.2: Sketch representing the subdivision of a typical problem domain into a number of finite elements.

Between these nodal points, or 'nodes', the solution is interpolated using a set of local basis functions, or 'shape functions', which are usually chosen to be simple polynomials. It is convenient to express these as functions of a set of local coordinates ($s_1 \in [-1,1]$, $s_2 \in [-1,1]$) which are intrinsic to the element, as illustrated in figure 3.3 for a quadrilateral element.

The finite element solution within a particular element e is then represented in the following way:

$$u_i(s_1,s_2) = \sum_{j=1}^{n_u} U_{(i)j}\, \psi^{[\mathrm{f}]}_{(i)j}(s_1,s_2) \tag{3.61}$$

and

$$p(s_1,s_2) = \sum_{j=1}^{n_p} P_j\, \psi^{[\mathrm{p}]}_{j}(s_1,s_2), \tag{3.62}$$

where n_u and n_p are the number of velocity and pressure degrees of freedom in e respectively. We can now incorporate the Dirichlet boundary conditions into this representation by treating some of the nodal velocity values U_{ij} as 'pinned'. In a finite element context, 'pinning' a value means that we no longer treat it as an unknown: instead, it becomes a prescribed quantity. With the Dirichlet conditions incorporated in this manner we no longer require a separate set of shape functions for each of the velocity components, and can instead interpolate each velocity field using the *same* set of shape functions. The representation of the i-th velocity field within each element is

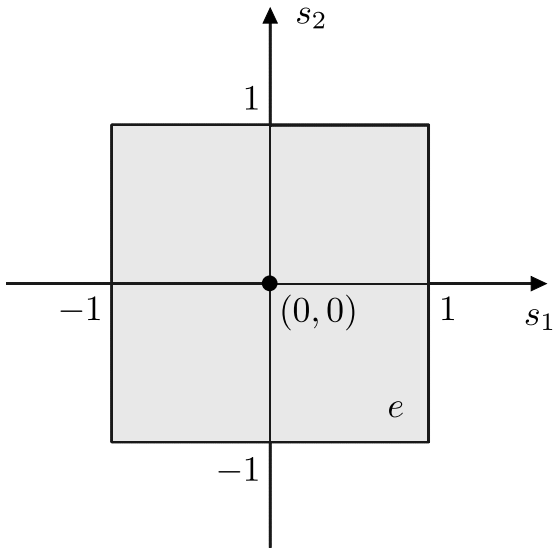

Figure 3.3: A sketch of a quadrilateral finite element, parametrised by the local coordinates $s_1 \in [-1,1]$ and $s_2 \in [-1,1]$. In the case of a four-noded element the nodes would be located at local coordinates (-1,-1), (-1,1), (1,-1) and (1,1).

therefore simply given by

$$u_i(s_1,s_2) = \sum_{j=1}^{n_u} U_{ij}\,\psi_j^{[\mathrm{f}]}(s_1,s_2). \tag{3.63}$$

The exact forms of $\psi^{[\mathrm{f}]}$ and $\psi^{[\mathrm{p}]}$ will be discussed below, but it is clear that in order for the solution to be equal to the value of the coefficients U_{ij} and P_j at the j-th node, the j-th local shape function must evaluate to one at the j-th node and zero at all other nodes. This is known as the 'interpolation condition',

$$\psi_j^{[\mathrm{f}]}(s_{k1},s_{k2}) = \delta_{jk} \qquad \text{and} \qquad \psi_j^{[\mathrm{p}]}(s_{k1},s_{k2}) = \delta_{jk}, \tag{3.64}$$

where in both expressions (s_{k1},s_{k2}) represents the local coordinates (s_1,s_2) of the k-th local node corresponding to either a velocity or pressure degree of freedom.

From (3.61) and (3.62) we observe that the finite element solution is now represented exclusively in terms of quantities which are intrinsic to the element. However, the integrals in $\mathcal{R}_{il}^{[\mathrm{f,bulk}]}$ and $\mathcal{R}_{l}^{[\mathrm{p}]}$ require the evaluation of quantities such as $B_i(x_k)$ rather than $B_i(s_k)$, and we therefore have to specify the mapping $x_i(s_k)$ between the local and global coordinates. We choose an 'isoparametric mapping' where the global coordinates are interpolated using the same shape functions $\psi^{[\mathrm{f}]}$ as are used to interpolate the unknown velocity fields. The i-th component of the global coordinate of

the j-th local node in element e is thus given by

$$x_i(s_1, s_2) = \sum_{j=1}^{n} X_{ij}\, \psi_j^{[\mathrm{f}]}(s_1, s_2), \tag{3.65}$$

where n is the number of nodes in e. The Jacobian of this mapping between local and global coordinates is given by

$$\mathcal{J}_{ij} = \frac{\partial x_j}{\partial s_i} = \sum_{k=1}^{n} X_{jk}\, \frac{\partial \psi_k^{[\mathrm{f}]}}{\partial s_i}, \tag{3.66}$$

and its inverse, $(\mathcal{J}^{-1})_{ij}$, can be used to evaluate derivatives with respect to the global coordinates of any particular variable v in the following way:

$$\frac{\partial v}{\partial x_i} = \left(\mathcal{J}^{-1}\right)_{ij} \frac{\partial v}{\partial s_j}. \tag{3.67}$$

If we let $\mathcal{J} = \det \mathcal{J}_{ij}$ then the integration over the element e can be performed in local coordinates,

$$\iint_e \Big\{ \ldots \Big\}\, \mathrm{d}x_1\, \mathrm{d}x_2 = \int_{-1}^{1}\int_{-1}^{1} \Big\{ \ldots \Big\}\, \mathcal{J}\, \mathrm{d}s_1\, \mathrm{d}s_2, \tag{3.68}$$

and the elemental residual equations (3.53) and (3.54) are therefore given by

$$\begin{aligned}
\mathcal{R}_{il}^{[\mathrm{f,bulk}]} = &\int_{-1}^{1}\int_{-1}^{1} R_\rho \,\mathrm{Re}\,\mathrm{St}\, \frac{\partial u_i}{\partial t}\, \psi_l^{[\mathrm{f}]}\, \mathcal{J}\, \mathrm{d}s_1\, \mathrm{d}s_2 \\
&+ \int_{-1}^{1}\int_{-1}^{1} R_\rho \,\mathrm{Re}\, u_j \frac{\partial u_i}{\partial x_j}\, \psi_l^{[\mathrm{f}]}\, \mathcal{J}\, \mathrm{d}s_1\, \mathrm{d}s_2 - \int_{-1}^{1}\int_{-1}^{1} B_i\, \psi_l^{[\mathrm{f}]}\, \mathcal{J}\, \mathrm{d}s_1\, \mathrm{d}s_2 \\
&- \int_{-1}^{1}\int_{-1}^{1} R_\rho \,\frac{\mathrm{Re}}{\mathrm{Fr}} G_i\, \psi_l^{[\mathrm{f}]}\, \mathcal{J}\, \mathrm{d}s_1\, \mathrm{d}s_2 - \int_{-1}^{1}\int_{-1}^{1} p\, \frac{\partial \psi_l^{[\mathrm{f}]}}{\partial x_i}\, \mathcal{J}\, \mathrm{d}s_1\, \mathrm{d}s_2 \\
&+ \int_{-1}^{1}\int_{-1}^{1} R_\mu \left(\frac{\partial u_i}{\partial x_j} + \frac{\partial u_j}{\partial x_i}\right) \frac{\partial \psi_l^{[\mathrm{f}]}}{\partial x_j}\, \mathcal{J}\, \mathrm{d}s_1\, \mathrm{d}s_2
\end{aligned} \tag{3.69}$$

and

$$\mathcal{R}_l^{[\mathrm{p}]} = \int_{-1}^{1}\int_{-1}^{1} \left(\frac{\partial u_j}{\partial x_j} - Q\right) \psi_l^{[\mathrm{p}]}\, \mathcal{J}\, \mathrm{d}s_1\, \mathrm{d}s_2. \tag{3.70}$$

These integrals, which are now functions of the local coordinates exclusively, can be evaluated numerically by Gauss quadrature rules. The integrand is evaluated at N_{int} 'integration points' within the element, located at a series of known positions (S_{i1}, S_{i2}), where $i = 1, \ldots, N_{\mathrm{int}}$. Each integration point has a (known) associated 'weight' W_i, and the integral is approximated by summing the products of the evaluated integrands and their corresponding weights,

$$\int_{-1}^{1}\int_{-1}^{1} \mathcal{F}(s_1, s_2)\, \mathrm{d}s_1\, \mathrm{d}s_2 \approx \sum_{i=1}^{N_{\mathrm{int}}} \mathcal{F}(S_{i1}, S_{i2})\, W_i. \tag{3.71}$$

Taylor–Hood and Crouzeix–Raviart elements

Having subdivided the problem domain into a number of 'elements', each of which are responsible for making their own contributions to the overall problem, we turn our attention to the matter of the *choice* of element. The geometry of the problems we will consider in this work lend themselves well to quadrilateral rather than triangular elements, and choosing these allows us to build straightforward structured meshes of the problem domain. Out of the many choices for two-dimensional quadrilateral elements we will restrict ourselves to two: the so-called 'Taylor–Hood' (Q_2Q_1) and 'Crouzeix–Raviart' (Q_2P_{-1}) elements. Both contain nine nodes, located at the points $(-1,-1)$, $(0,-1)$, $(1,-1)$, $(-1,0)$, $(0,0)$, $(1,0)$, $(-1,1)$, $(0,1)$ and $(1,1)$, and the mapping between local and global coordinates is given by

$$x_i(s_1,s_2) = \sum_{j=1}^{9} X_{ij}\,\psi_j^{[\mathrm{f}]}(s_1,s_2), \tag{3.72}$$

where X_{ij} is the i-th Eulerian coordinate of the j-th local node. If the nodes are labelled in the manner specified by the blue characters in figure 3.4, then the associated shape functions are given by

$$\begin{aligned}
\psi_1^{[\mathrm{f}]} &= \frac{s_1 s_2}{4}(s_1-1)(s_2-1),\\
\psi_2^{[\mathrm{f}]} &= \frac{s_2}{2}(1-s_1^2)(s_2-1),\\
\psi_3^{[\mathrm{f}]} &= \frac{s_1 s_2}{4}(s_1+1)(s_2-1),\\
\psi_4^{[\mathrm{f}]} &= \frac{s_1}{2}(s_1-1)(1-s_2^2),\\
\psi_5^{[\mathrm{f}]} &= (1-s_1^2)(1-s_2^2),\\
\psi_6^{[\mathrm{f}]} &= \frac{s_1}{2}(s_1+1)(1-s_2^2),\\
\psi_7^{[\mathrm{f}]} &= \frac{s_1 s_2}{4}(s_1-1)(s_2+1),\\
\psi_8^{[\mathrm{f}]} &= \frac{s_2}{2}(1-s_1^2)(s_2+1),\\
\psi_9^{[\mathrm{f}]} &= \frac{s_1 s_2}{4}(s_1+1)(s_2+1).
\end{aligned} \tag{3.73}$$

The velocity components u_i are stored as nodal values and are represented by the same bi-quadratic interpolation as the nodal coordinates,

$$u_i(s_1,s_2) = \sum_{j=1}^{9} U_{ij}\,\psi_j^{[\mathrm{f}]}(s_1,s_2), \tag{3.74}$$

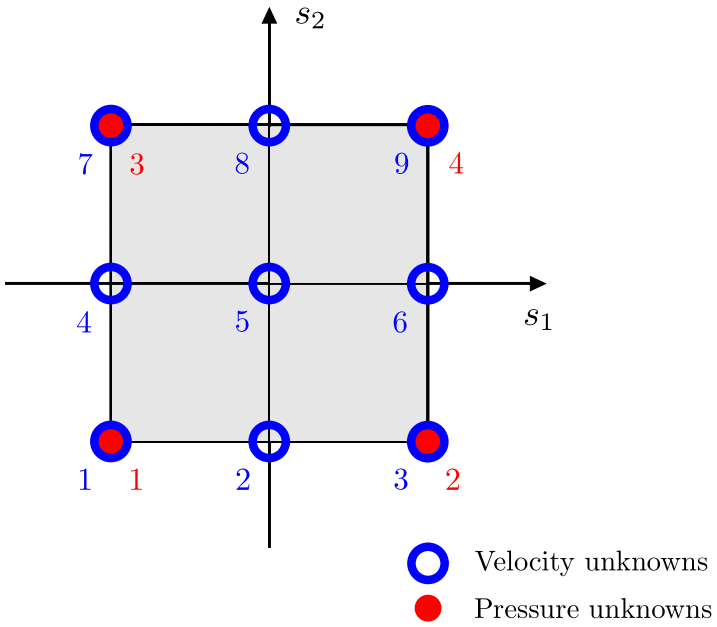

Figure 3.4: Sketch illustrating the node numbering scheme in a Taylor–Hood element. This type of element contains nine nodes, each of which stores n unknowns U_{ij} $(i = 1, \ldots, n)$ corresponding to the value of the i-th velocity field at the particular local node j. The four 'corner nodes' each store an additional unknown P_j corresponding to the value of the pressure field at local node j.

where U_{ij} is the i-th component of the velocity at the j-th local node.

The difference between the two elements is the way in which the pressure is represented. In Taylor–Hood elements the pressure is represented by a globally-continuous, piecewise bilinear interpolation between the unknowns P_j that are stored at the element's four corner nodes,

$$p(s_1, s_2) = \sum_{j=1}^{4} P_j \, \psi_j^{[\mathrm{p}]}(s_1, s_2), \tag{3.75}$$

where the pressure shape functions are given by

$$\begin{aligned}
\psi_1^{[\mathrm{p}]} &= \frac{1}{4}(1 - s_1)(1 - s_2), \\
\psi_2^{[\mathrm{p}]} &= \frac{1}{4}(1 + s_1)(1 - s_2), \\
\psi_3^{[\mathrm{p}]} &= \frac{1}{4}(1 - s_1)(1 + s_2), \\
\psi_4^{[\mathrm{p}]} &= \frac{1}{4}(1 + s_1)(1 + s_2),
\end{aligned} \tag{3.76}$$

and we note that P_1, P_2, P_3 and P_4 are the pressure values stored at nodes 1, 3, 7 and 9 respectively (as labelled on figure 3.4). In Crouzeix–Raviart elements, however, the

pressure is given by

$$p(s_1, s_2) = P_1 + P_2\, s_1 + P_3\, s_2, \tag{3.77}$$

which provides a discontinuous, piecewise bilinear representation in terms of three degrees of freedom per element. Unlike Taylor–Hood elements, Crouzeix–Raviart elements ensure that the continuity equation is satisfied in an average sense within each element. This can be clearly seen from (3.77), where we observe that in each element one of the basis functions used to represent the pressure is 1, and therefore when testing against this we have one equation satisfying the condition that the integral of the continuity equation itself over the element must vanish. Taylor–Hood elements, on the other hand, only ensure that the continuity equation is satisfied in a weak sense over the entire domain. Crouzeix–Raviart elements are a convenient choice for problems containing two fluids and finite surface tension, since their discontinuous pressure representation allows them to accommodate pressure jumps across the interface.

As a final note, we point out that both Taylor–Hood and Crouzeix–Raviart elements are 'LBB-stable' [Gresho and Sani, 2000, pp. 551-9], which means that they are guaranteed to converge at the optimal rate under mesh refinement. Although it is possible to perform finite element computations using elements which do not satisfy the conditions for LBB stability, we shall not consider any such elements in this work.

3.3.3 Temporal discretisation

Having discussed the manner in which the domain is spatially discretised, we will now briefly introduce the concept of temporal discretisation and timestepping. In time-dependent problems we accommodate time dependence in the nodal values so that

$$u_i(s_k, t) = \sum_{j=1}^{n_u} U_{ij}(t)\, \psi_j^{[\mathrm{f}]}(s_k) \tag{3.78}$$

and

$$p(s_k, t) = \sum_{j=1}^{n_p} P_j(t)\, \psi_j^{[\mathrm{p}]}(s_k). \tag{3.79}$$

This turns the nonlinear algebraic equations into systems of coupled nonlinear ordinary differential equations, where the time derivative of the i-th velocity component in (3.69)

is represented by

$$\frac{\partial u_i}{\partial t} = \sum_{j=1}^{n_u} \frac{\mathrm{d}U_{ij}}{\mathrm{d}t}\, \psi_j^{[\mathrm{f}]}. \tag{3.80}$$

Note that no time derivatives of the pressure field ever appear in the governing equations. We discretise the functions $U_{ij}(t)$ and $P_j(t)$ in time using an implicit timestepping method, and we choose the second-order 'Backward Differentiation Formula' (or 'BDF2') scheme [Gresho and Sani, 2000, pp. 805-6] for the majority of the problems in this work. Terms of the form (3.80) are then approximated by

$$\frac{dU_{ij}}{dt} \approx \sum_{\tau=0}^{N_{\mathrm{history}}} (U_{ij})_\tau\, \omega_\tau, \tag{3.81}$$

where N_{history} is the number of history values required by the scheme ($N_{\mathrm{history}} = 2$ in the case of BDF2) and ω_τ (for $\tau = 0, \ldots, N_{\mathrm{history}}$) are a set of (known) weights. Quantities with the index $\tau = 0$ denote the solution at the 'current' time, with indices > 0 representing 'previous' timesteps.

3.3.4 Moving domains

In section 3.3.1 we considered the solution of the bulk equations in a stationary domain. Throughout this work, however, we will (at times) be considering problems in which the domain is moving. We will always discretise the domain using a boundary-fitted mesh, which is then required to deform in response to changes in the problem's geometry. In order to accommodate this we use the arbitrary Lagrangian-Eulerian (ALE) formulation of the Navier–Stokes equations [Donea et al., 1982], which involves adding an extra term to the (discretised weak form of the) momentum equations in the bulk of the fluid (3.69).

If we consider the continuous momentum equations (3.40) briefly, we note that the $\partial u_i/\partial t$ term describes the time-derivative of the i-th velocity component at a fixed Eulerian position. By discretising the equations as outlined in section 3.3.1, this term is actually evaluated by computing (a sum of) the time-derivatives of the nodal values U_{ij}, which is appropriate when solving the equations on a stationary mesh. In a problem where the nodal positions vary as a function of time, however, the time-derivatives of the nodal values $\mathrm{d}U_{ij}/\,\mathrm{d}t$ actually represent the rate-of-change of u_i at the *moving node*. In order to compensate for this, we note that this quantity can also

be expressed by the material derivative,

$$\left.\frac{Du_i}{Dt}\right|_{\text{node } j} = \left.\frac{\partial u_i}{\partial t}\right|_{\text{node } j} + \sum_{a=1}^{d} v_{aj}\,\frac{\partial u_i}{\partial x_a}, \tag{3.82}$$

where d is the spatial dimension and the quantity

$$v_{aj} = \frac{dX_{aj}}{dt} \tag{3.83}$$

is the a-th velocity component of local node j and is described as the 'mesh velocity'. The rate of change of u_i as experienced at the (fixed) Eulerian position that coincides with the current position of node j is therefore given by

$$\left.\frac{\partial u_i}{\partial t}\right|_{\text{node } j} = \frac{dU_{ij}}{dt} - \sum_{a=1}^{d}\left(\frac{dX_{aj}}{dt}\sum_{k=1}^{N_{\text{node}}} U_{ik}\,\frac{\partial \psi_k^{[\text{f}]}}{\partial x_a}\right), \tag{3.84}$$

and hence the rate of change of u_i at any point in the domain is evaluated using

$$\frac{\partial u_i}{\partial t} = \sum_{j=1}^{N_{\text{node}}} \frac{dU_{ij}}{dt}\psi_j^{[\text{f}]} - \sum_{a=1}^{d}\left[\sum_{j=1}^{N_{\text{node}}}\left(\frac{dX_{aj}}{dt}\sum_{k=1}^{N_{\text{node}}} U_{ik}\,\frac{\partial \psi_k^{[\text{f}]}}{\partial x_a}\right)\psi_j^{[\text{f}]}\right]. \tag{3.85}$$

We note that from this point forward we are implying (3.85) whenever we write terms of the form $\partial u_i/\partial t$. When we linearise the governing equations in section 7.1 it will be useful, however, to explicitly show contributions from the mesh velocity terms. In order to do this, we rewrite (3.85) as

$$\frac{\partial u_i}{\partial t} = \frac{\delta u_i}{\delta t} - \sum_{a=1}^{d} u_a^{[\text{M}]}\frac{\partial u_i}{\partial x_a}, \tag{3.86}$$

where

$$\frac{\delta u_i}{\delta t} = \sum_{j=1}^{N_{\text{node}}} \frac{dU_{ij}}{dt}\,\psi_j^{[\text{f}]} \tag{3.87}$$

is the rate of change of u_i at a *fixed set of local coordinates* and

$$u_a^{[\text{M}]} = \sum_{j=1}^{N_{\text{node}}} v_{aj}\,\psi_j^{[\text{f}]} \tag{3.88}$$

is the a-th component of the interpolated mesh velocity.

In the moving-domain problems that we shall be considering, the change in geometry of the mesh is driven by changes in the shape of the free surface. As the position of the free surface $\mathbf{X}$ is unknown, this introduces additional degrees of freedom into the problem, and the 'extra equation' that is required in order to accommodate for this is

the kinematic boundary condition. Once $\mathbf{X}$ has been established for a given timestep, the positions of the 'bulk' nodes must be updated accordingly, and we shall consider two distinct approaches to this problem here: a pseudo-solid meshing strategy and a scheme based on the method of spines.

The method of spines

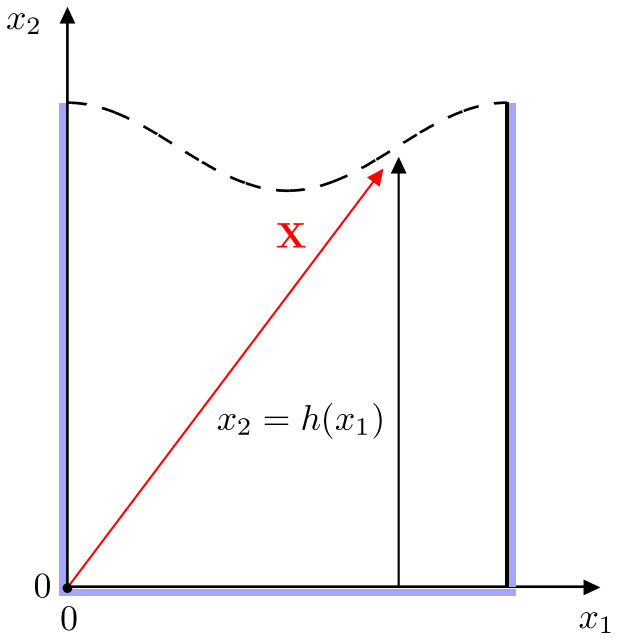

Figure 3.5: Sketch of a typical free surface problem in two dimensions, in which (at any given time t) it is possible to describe the 'height' of the surface as a scalar function $x_2 = h(x_1)$. Solid boundaries are displayed as solid lines with blue shading, and the dashed line denotes the free surface. The position vector to this surface is labelled in red.

The 'method of spines' was originally proposed by Kistler and Scriven for the computation of coating flows [Kistler and Scriven, 1983]. We demonstrate the technique (as utilised in this current work) by first considering the sketch in figure 3.5, which displays a typical free surface problem in the $x_1 - x_2$ plane with three solid boundaries (solid lines, blue shading) and a free surface boundary (dashed line). For the interface shape shown in this sketch there exists a unique x_2 value associated with each x_1 value. It is therefore possible to describe the 'height' of the free surface as a (continuous) scalar function $x_2 = h(x_1, t)$, and so the position vector to the surface can be expressed as

$$\mathbf{X} = x_1\,\mathbf{i} + h(x_1, t)\,\mathbf{j}, \tag{3.89}$$

where **i** and **j** are the Cartesian unit basis vectors in the x_1 and x_2 directions respectively. The function $h(x_1, t)$ is unknown and needs to be determined as part of the solution, and we therefore discretise it in a similar manner to that described in section 3.3.1,

$$h(s,t) = \sum_{j=1}^{N_{\text{node}}} H_j(t)\, \psi_j^{[\text{f}]}(s), \tag{3.90}$$

where s is the local coordinate that parametrises the free surface. Note that we are choosing to represent the height using the same shape functions $\psi^{[\text{f}]}$ as are used to interpolate the Eulerian positions of the nodal coordinates, but evaluated on the boundary. This choice is motivated by the requirement that the 'height' shape functions are the trace of the 'coordinate' shape functions $\psi^{[\text{f}]}$ in order to ensure that the geometries are consistent.

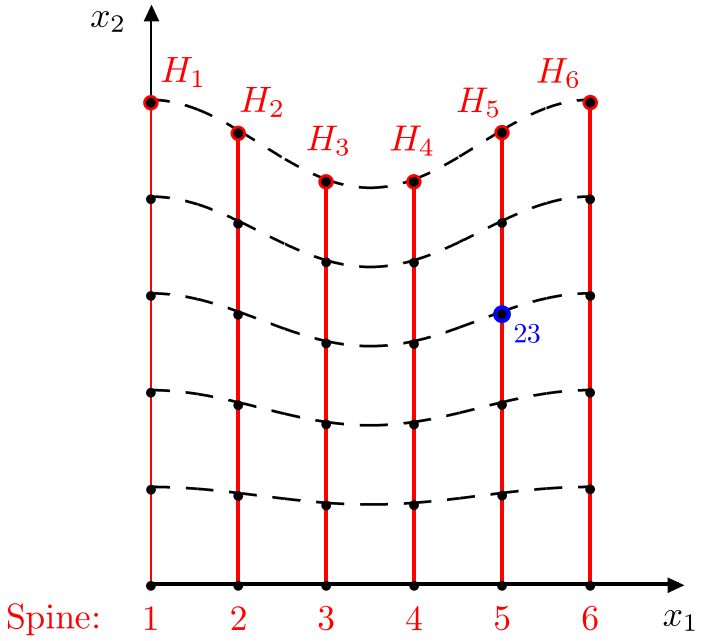

Figure 3.6: Sketch illustrating the manner in which the position each node (represented by black dots) is defined by the fraction at which it is located along the spine (represented by red lines) with which it is associated. Here, global node 23 is located on spine $s_{23} = 5$, and at a fraction $w_{23} = 0.6$ along its length. Each spine s has a variable associated with it that defines its 'height' H_s. The axial position of global node 23 is therefore given by $0.6 \times H_5$.

Figure 3.6 shows a body-fitted finite element mesh that discretises the domain, and we note that as a result of discretising $h(x_1, t)$ we have an unknown value H associated with each node on the free surface (at any given time t). Let us now assume that the mesh has been constructed in such a way that its N_{node} nodes are distributed along

N_{spine} lines that are (topologically) orthogonal to the free surface boundary. We call these lines 'spines' and note that they each have an associated unknown coefficient H_s ($s = 1, \ldots, N_{\text{spine}}$) which determines the 'height' of the domain in a direction parallel to that spine: these will be referred to as the 'spine heights'. We then set the mesh up in such a way that each node j is located at a fixed fraction w_j along a particular spine s_j, so that its position is prescribed by

$$\mathbf{x}_j = \mathbf{B}_{s_j} + w_j \, H_{s_j} \, \mathbf{S}_{s_j}, \tag{3.91}$$

where $\mathbf{B}_s$ is the vector to the 'base' of spine s and $\mathbf{S}_s$ the unit vector along that spine (as shown in figure 3.6). In all of the problems considered in the following work we will use spines which are orientated such that they are parallel to the vertical axis. Moreover, the bases of the spines will always be located along the horizontal axis, so that the j-th node's position (3.91) simplifies to

$$\mathbf{x}_j = x_1 \, \mathbf{i} + w_j \, H_{s_j} \, \mathbf{j}. \tag{3.92}$$

The key feature of this method is that the only additional unknowns which are introduced into the problem are the N_{spine} spine heights H_{s_j} that correspond to the position of the free surface boundary. The positions of the nodes in the bulk of the domain are 'enslaved variables' which simply update themselves algebraically once the values of H_{s_j} have been determined. This is known as a 'sparse' node-update strategy and is computationally inexpensive. However, the formulation is dependent on the ability to express the 'height' of the surface as a one-to-one function in the horizontal coordinate, and as a result cannot be used to simulate problems involving 'overturning' of the free boundary. The second, pseudo-solid-based approach (which we shall consider now) does not suffer from this issue.

The pseudo-solid node-update procedure

In the spine-based method described above, the position of the free surface is determined as part of the solution, and the positions of the bulk nodes are then updated based on this result. By contrast, the pseudo-solid approach discussed here treats the interior of the mesh as a fictitious elastic solid, and a solid mechanics problem is solved at every timestep for the (unknown) nodal positions. The deformation of the

free surface boundary is imposed by applying a suitable line traction $v\,\mathbf{n}$ along the free surface, which is discretised in the usual way,

$$v(s) = \sum_{j=1}^{N_{\text{node}}} \Upsilon_j \, \psi_j^{[\text{f}]}(s), \tag{3.93}$$

and the nodal values Υ_j of the line traction are then determined by the solution of the kinematic boundary condition.

In addition to being able to accommodate a wider range of interface shapes (than a spine-based method), this approach benefits from being able to take advantage of the existing refineable element framework which has already been developed within `oomph-lib`. It is, however, far more costly in a computational sense than the spine method since it introduces two additional unknowns for every node in the mesh and requires the solution of a solid mechanics problem at each timestep on top of the fluid problem that we are actually interested in. Moreover, while it is (in principle) able to accommodate any change in shape of the interface, as individual elements get increasingly stretched there will be a point at which the domain will require 're-meshing'. Problems of this nature are outside the scope of this work, however.

3.3.5 Discretisation of the free surface boundary conditions

The dynamic condition

In section 3.3.1 we split the contributions to the momentum equations into those arising from integrals over the bulk of the domain and those arising from integrals over its boundary, and wrote down the terms in the il-th elemental residual momentum equations corresponding to the bulk contributions $\mathcal{R}_{il}^{[\text{f,bulk}]}$ (3.69). We turn our attention now to the remaining terms in (3.40),

$$\mathcal{R}_i^{[\text{f,boundary}]} = -\int_{\partial D/\Omega} \tau_{ij}\, n_j\, \phi^{[\text{f}]}\, \mathrm{d}\zeta + \int_{\Omega} p_{\text{ext}}\, n_i\, \phi^{[\text{f}]}\, \mathrm{d}\zeta + \int_{\Omega} \frac{1}{Ca}(t_1)_i \frac{\mathrm{d}\phi^{[\text{f}]}}{\mathrm{d}\zeta}\, \mathrm{d}\zeta - \frac{1}{Ca}\phi^{[\text{f}]}\, m_i\Big|_{C_1} - \frac{1}{Ca}\phi^{[\text{f}]}\, m_i\Big|_{C_2}, \tag{3.94}$$

and recall that from (3.49) we have

$$\mathcal{R}_i^{[\text{f,boundary}]} = \sum_{l=1}^{\infty} \Phi_l^{[\text{f}]}\, \mathcal{R}_{il}^{[\text{f,boundary}]}\left(U_{k1}, U_{k2}, \ldots; P_1, P_2, \ldots; X_{k1}, X_{k2}, \ldots\right), \tag{3.95}$$

where $k = 1, 2$ and

$$\mathcal{R}_{il}^{[\mathrm{f,boundary}]} = -\int_{\partial D/\Omega} \tau_{ij}\, n_j\, \psi_l^{[\mathrm{f}]}\, \mathrm{d}\zeta + \int_{\Omega} p_{\mathrm{ext}}\, n_i\, \psi_l^{[\mathrm{f}]}\, \mathrm{d}\zeta + \int_{\Omega} \frac{1}{Ca}\,(t_1)_i\, \frac{\mathrm{d}\psi_l^{[\mathrm{f}]}}{\mathrm{d}\zeta}\, \mathrm{d}\zeta - \left.\frac{1}{Ca}\,\psi_l^{[\mathrm{f}]}\, m_i\right|_{C_1} - \left.\frac{1}{Ca}\,\psi_l^{[\mathrm{f}]}\, m_i\right|_{C_2}. \quad (3.96)$$

The line integrals in (3.96) are computed by one-dimensional 'face' elements which are 'attached' to the appropriate faces of those bulk elements adjacent to the boundary over which the integral is to be performed. Within these elements the Jacobian of the mapping between local and global coordinates is given by $\mathcal{J} = \mathrm{d}\zeta/\,\mathrm{d}s$, where s is the (one and only) local coordinate, and the contributions to the elemental residual momentum equations arising from the boundary integral terms are therefore given by

$$\mathcal{R}_{il}^{[\mathrm{f,boundary}]} = -\int_{-1}^{1} \mathfrak{t}_i\, \psi_l^{[\mathrm{f}]}\, \mathcal{J}\, \mathrm{d}s \quad (3.97)$$

on non-Dirichlet, non-free surface boundaries[3], and

$$\mathcal{R}_{il}^{[\mathrm{f,boundary}]} = \int_{-1}^{1} p_{\mathrm{ext}}\, n_i\, \psi_l^{[\mathrm{f}]}\, \mathcal{J}\, \mathrm{d}s + \int_{-1}^{1} \frac{1}{Ca}\,(t_1)_i\, \frac{\mathrm{d}\psi_l^{[\mathrm{f}]}}{\mathrm{d}s}\, \mathrm{d}s \quad (3.98)$$

on free surface boundaries. Additionally, the two point contributions

$$\mathcal{R}_{il}^{[\mathrm{f,boundary}]} = -\left.\frac{1}{Ca}\psi_l^{[\mathrm{f}]}\, m_i\right|_{C_1} - \left.\frac{1}{Ca}\psi_l^{[\mathrm{f}]}\, m_i\right|_{C_2} \quad (3.99)$$

need to be added at the two contact points at either side of the free surface.

The kinematic condition

Finally, we require the elemental residual equation for the kinematic boundary condition. From section (3.2.1) we have that the (continuous) weak form is given by

$$\mathcal{R}^{[\mathrm{h}]} = \int_{\Omega} \left(u_i - \mathrm{St}\,\frac{\partial X_i}{\partial t}\right) n_i\, \phi^{[\mathrm{f}]}\, \mathrm{d}\zeta, \quad (3.100)$$

and we shall assume from this point onwards that we are using the method of spines as described in section 3.3.4 to update the bulk nodal positions. We can express the rate of change of the position vector to the surface (3.89) as

$$\frac{\partial \mathbf{X}}{\partial t} = \frac{\partial h}{\partial t}\,\mathbf{j}, \quad (3.101)$$

[3]Note that we have used (3.11) to write (3.97) in terms of the traction $\mathfrak{t}_i$.

and from (3.49) we have

$$\mathcal{R}^{[\mathrm{h}]} = \sum_{l=1}^{\infty} \Phi_l^{[\mathrm{f}]}\, \mathcal{R}_l^{[\mathrm{h}]}\left(U_{k1}, U_{k2}, \ldots; H_1, H_2, \ldots\right), \tag{3.102}$$

where

$$\mathcal{R}_l^{[\mathrm{h}]} = \int_{\Omega} \left(u_i\, n_i - \mathrm{St}\, \frac{\partial h}{\partial t}\, n_2 \right) \psi_l^{[\mathrm{f}]}\, \mathrm{d}\zeta. \tag{3.103}$$

Finally, using the same mapping from local to global coordinates, $\mathcal{J} = \mathrm{d}\zeta/\,\mathrm{d}s$, the elemental residual kinematic equation is given by

$$\mathcal{R}_l^{[\mathrm{h}]} = \int_{-1}^{1} \left(u_i\, n_i - \mathrm{St}\, \frac{\partial h}{\partial t}\, n_2 \right) \psi_l^{[\mathrm{f}]}\, \mathcal{J}\, \mathrm{d}s. \tag{3.104}$$

3.3.6 Implementation

In `oomph-lib` the `get_residual(...)` and `get_jacobian(...)` functions for the Navier–Stokes equations are implemented in the `NavierStokesEquations<DIM>` class, which is templated by the spatial dimension of the problem. As discussed in section 2.2[4], this class implements the governing equations but contains no specific geometrical information: the concrete implementations of the (quadrilateral) Taylor–Hood and Crouzeix–Raviart elements are therefore defined in `QTaylorHoodElement<DIM>` and `QCrouzeixRaviartElement<DIM>` respectively[5]. Both of these classes inherit from the `NavierStokesEquations<DIM>` and `QElement<DIM,3>` classes[6], and are again templated by the spatial dimension. The triangular counterparts of these elements, `TTaylorHoodElement<DIM>` and `TCrouzeixRaviartElement<DIM>`, are also available. From this point forward, however, we will *only* consider quadrilateral elements when discussing implementation details since no triangular elements were used for any of the computations presented in the current work.

The common interfaces and functions for all interface elements are implemented in the `FluidInterfaceElement` base class. This class inherits from `FaceElement`, a class which provides the generic functionality common to all elements which are in some way 'attached' to the faces of higher-dimensional 'bulk' elements, and adds functionality specific to fluid interface elements. Because the implementation of the boundary conditions differs considerably depending on the spatial dimension of the

[4] In particular, see figure 2.3 on page 28 (and surrounding discussion).
[5] See section 3.3.2 for a discussion of these element types and the differences between them.
[6] Both of these elements are quadratic elements and hence have 3×3 nodes.

interface element, the kinematic condition and contributions made to the momentum equations by the dynamic condition are implemented in classes that are derived from `FluidInterfaceElement`. For two-dimensional Navier–Stokes problems (as discussed for the majority of this chapter) the corresponding interface element is implemented in the `LineFluidInterfaceElement` class.

Node-update methodology

Since the 'bulk' elements described above are to be used in free surface problems, they require additional functionality which enables their nodal positions to be adjusted in accordance with the motion of the interface. In section 3.3.4 we discussed two different node-update strategies: (i) the method of spines, and (ii) a pseudo-solid technique, and `oomph-lib` provides a straightforward approach to allow existing 'standard' elements to be augmented with the appropriate capabilities through the use of templated 'wrapper' classes. The `SpineElement<BASIC_ELEMENT>` class takes an existing element as a template parameter and adds the necessary functionality to allow the element to be updated using the method of spines. This includes adding storage for a vector of (pointers to) spines and a lookup scheme to establish which local equation numbers are associated with each spine. The pseudo-solid counterpart to this element is defined in the `PseudoSolidNodeUpdateElement<BASIC_ELEMENT,PSEUDOSOLID_ELEMENT>` class, which takes two template parameters: the 'basic' existing element, as well as an element which will be used to solve the solid mechanics equations on which this node-update method is based.

The interface elements also require additional functionality that differs depending on the chosen node-update strategy: `oomph-lib` therefore supplies the `SpineLineFluidInterfaceElement` and `ElasticLineFluidInterfaceElement` classes, both of which inherit from the 'standard' `LineFluidInterfaceElement` class. It is the responsibility of these classes to overload the function that determines the equation number of the kinematic boundary condition associated with each local node depending on the node-update strategy which has been employed.

Chapter 4

Applications of the two-dimensional free surface Navier–Stokes equations

Having formulated the weak forms of the governing equations and boundary conditions for an arbitrary free surface Navier–Stokes problem in Cartesian coordinates, we shall apply the newly-developed methodology to two specific applications:

(i) the relaxation of a fluid layer due to surface tension and gravitational forces, and

(ii) the relaxation of an interface between two fluids of differing material properties.

These particular problems are chosen in part because they can (in the limit of small amplitudes) be validated against analytical predictions.

4.1 Relaxation oscillations of a fluid layer

We consider the problem sketched in figure 4.1, in which we have a single, incompressible, viscous fluid layer governed by the Navier–Stokes equations

$$\mathrm{Re}\,\mathrm{St}\,\frac{\partial u_i}{\partial t} + \mathrm{Re}\,u_j\frac{\partial u_i}{\partial x_j} = -\frac{\partial p}{\partial x_i} + \frac{\mathrm{Re}}{\mathrm{Fr}}G_i + \frac{\partial}{\partial x_j}\left(\frac{\partial u_i}{\partial x_j} + \frac{\partial u_j}{\partial x_i}\right) \tag{4.1}$$

and

$$\frac{\partial u_j}{\partial x_j} = 0, \tag{4.2}$$

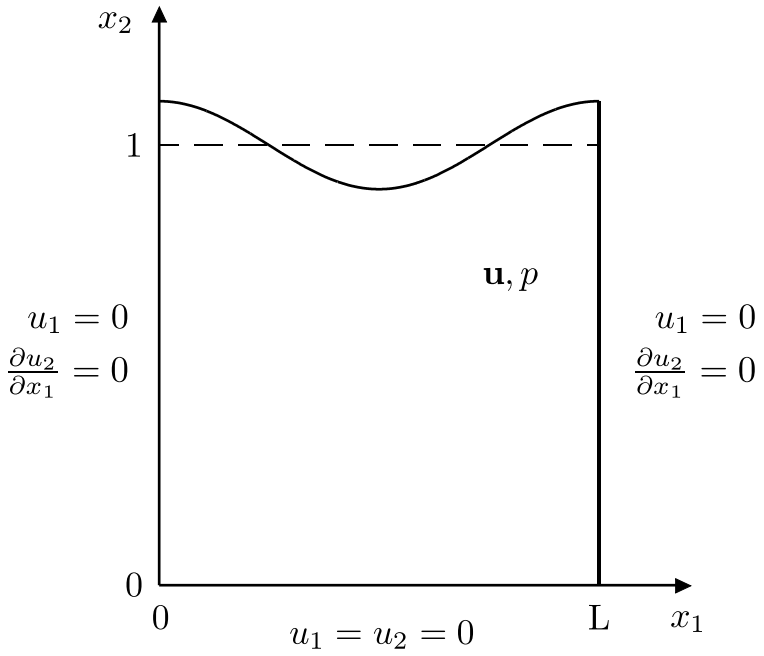

Figure 4.1: Sketch of a single layer free surface problem in two dimensions. The equilibrium position of the interface corresponds to $x_2 = 1$ and is represented by the dashed line.

with gravity acting in the negative x_2 direction. In order to facilitate the validation of this problem against a corresponding analytical problem (which we will do in section 4.1.1) we wish to solve 4.1 and 4.2 in a truncated domain with boundary conditions chosen so that this domain represents a 'periodic box'. This is advantageous since it allows the problem to be set up in such a way that (in the limit of small perturbations away from the equilibrium position) we can solve for a single linearised separable eigenmode of the system. With this in mind, we choose to solve the governing equations in the domain $x_1 \in [0, L]$, $x_2 \in [0, 1]$ and apply non-penetration boundary conditions, $u_1 = 0$, on the left and right boundaries and the no-slip condition, $u_1 = u_2 = 0$, on the bottom (solid) boundary. The free surface is located at $\mathbf{X}$ and is subject to the kinematic condition,

$$\left(u_i - \mathrm{St}\,\frac{\partial X_i}{\partial t}\right) n_i = 0, \tag{4.3}$$

and the dynamic condition,

$$\tau_{ij}\, n_j = \frac{1}{\mathrm{Ca}}\,\kappa\, n_i - p_{\mathrm{ext}}\, n_i, \tag{4.4}$$

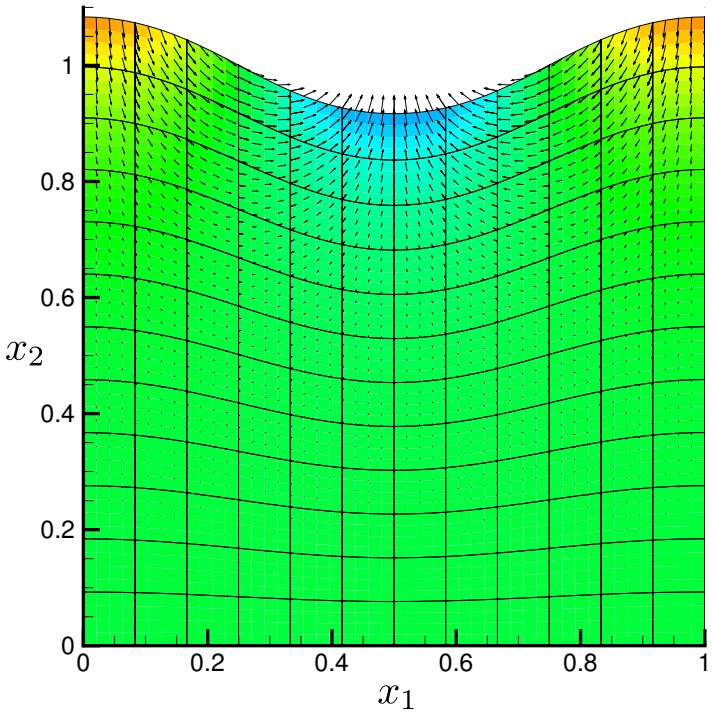

Figure 4.2: Pressure contour plot for the relaxing interface problem at time $t = 0.01$, with superimposed velocity vectors. A mesh of 12×12 Crouzeix–Raviart elements and a second-order-accurate BDF timestepping scheme with a non-dimensionalised timestep of 0.0025 were used, for the parameters $\mathrm{Re} = \mathrm{Re}\,\mathrm{St} = \mathrm{Re}/\mathrm{Fr} = 5.0$, $\mathrm{Ca} = 0.01$, $L = 1$ and $\epsilon = 0.1$. The (non-dimensional) pressure ranges from -244 to 281, with areas of highest and lowest pressure shown in red and blue respectively. Note that although the usual hydrostatic pressure variation is present, it cannot be seen here since its contribution to the pressure field is sufficiently small in comparison to the fluctuations close to the surface.

where the stress tensor is defined to be

$$\tau_{ij} = -p\,\delta_{ij} + \left(\frac{\partial u_i}{\partial x_j} + \frac{\partial u_j}{\partial x_i}\right). \tag{4.5}$$

This problem was solved numerically in `oomph-lib` using both Taylor–Hood and Crouzeix–Raviart elements, using the methodology described in section 3.3.2. The problem domain was discretised into a 12×12 element mesh whose deformation in response to the motion of the free surface boundary was implemented by a spine-based node update strategy (section 3.3.4). The time-derivatives were discretised using a second-order-accurate BDF scheme with a (non-dimensionalised) timestep of 0.0025.

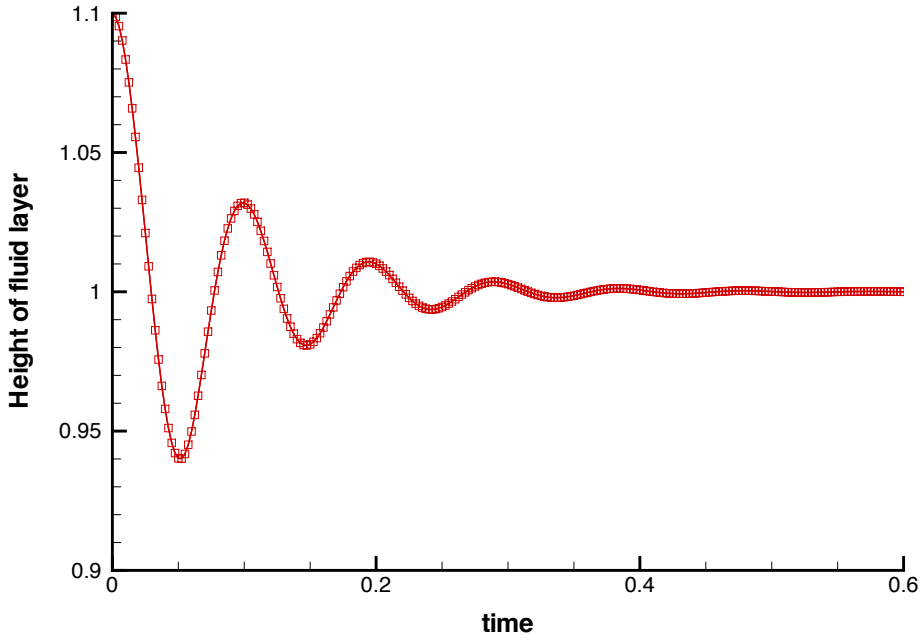

Figure 4.3: Time-trace of the height of the fluid layer at the edge of the domain for the parameters $\mathrm{Re} = \mathrm{Re}\,\mathrm{St} = \mathrm{Re}/\mathrm{Fr} = 5.0$, $\mathrm{Ca} = 0.01$ and $\epsilon = 0.1$. A mesh of 12×12 Crouzeix–Raviart elements and a second-order-accurate BDF timestepping scheme with a non-dimensionalised timestep of 0.0025 were used.

The free-surface boundary conditions (4.3 and 4.4) were implemented by attaching one-dimensional face elements to the upper boundaries of the bulk elements adjacent to the free boundary, as described in section 3.3.5. The initial configuration of the system was such that the velocity everywhere was zero and the free surface was deformed by

$$\mathbf{X} = x_1\,\mathbf{i} + [1.0 + \epsilon\cos(2\pi x_1/L)]\,\mathbf{j}, \tag{4.6}$$

where ϵ is a (small) parameter controlling the amplitude of the deflection away from the equilibrium position. The simulation ran for 240 timesteps after being started 'impulsively': by this we mean that we assume that for all previous timesteps $t < 0$ the interface was 'held' in this initial static configuration. Figure 4.2 shows a contour plot of the pressure distribution with superimposed velocity vectors at the fourth timestep ($t = 0.01$), for the parameters $\mathrm{Re} = \mathrm{Re}\,\mathrm{St} = \mathrm{Re}/\mathrm{Fr} = 5.0$, $\mathrm{Ca} = 0.01$ and $L = 1$. The initial amplitude of the free surface perturbation was 10% of the domain width ($\epsilon = 0.1$).

At time $t \leq 0$ the free surface is fixed in its deformed shape, but as the simulation

begins the restoring forces of surface tension and gravitational acceleration act to revert it to its undeformed flat state. The surface oscillates up and down, but the motion is damped as the energy in the system is dissipated through viscous forces. Eventually the interface settles down to its equilibrium position. This viscous damping effect can be seen in the time-trace of the height of the fluid layer at the edge of the domain shown in figure 4.3.

4.1.1 Validation against an analytical dispersion relation

In order to validate the numerical simulations described above we shall compare them to analytical predictions for the frequency and decay rate obtained from a linearised analysis of the problem (valid for small amplitudes). We begin by considering the problem sketched in figure 4.4, in which we are solving the Navier–Stokes equations (4.1) and (4.2) in a domain chosen so that the equilibrium position of the free surface corresponds to the line $x_2 = 0$. The position of the free boundary is described by defining its 'height', h, as a function of the horizontal coordinate, and the position vector to the surface can therefore be expressed as

$$\mathbf{X}(x_1, t) = x_1\,\mathbf{i} + h(x_1, t)\,\mathbf{j}. \tag{4.7}$$

A unit vector normal to a line specified by $x_2 = h(x_1, t)$ is given by

$$\mathbf{n} = \left[1 + \left(\frac{\partial h}{\partial x_1}\right)^2\right]^{-\frac{1}{2}} \left(-\frac{\partial h}{\partial x_1}\,\mathbf{i} + \mathbf{j}\right), \tag{4.8}$$

and the curvature can be expressed as

$$\kappa = \frac{\partial^2 h}{\partial {x_1}^2}\left[1 + \left(\frac{\partial h}{\partial x_1}\right)^2\right]^{-\frac{3}{2}}. \tag{4.9}$$

Using (4.7) and (4.8) the kinematic condition (4.3) then becomes

$$-u_1\frac{\partial h}{\partial x_1} + u_2 - \mathrm{St}\,\frac{\partial h}{\partial t} = 0, \tag{4.10}$$

and using (4.8) and (4.9) the dynamic condition (4.4) is given by

$$-\frac{\partial h}{\partial x_1}\tau_{11} + \tau_{12} = -\frac{1}{\mathrm{Ca}}\frac{\partial h}{\partial x_1}\frac{\partial^2 h}{\partial {x_1}^2}\left[1 + \left(\frac{\partial h}{\partial x_1}\right)^2\right]^{-\frac{3}{2}} \tag{4.11}$$

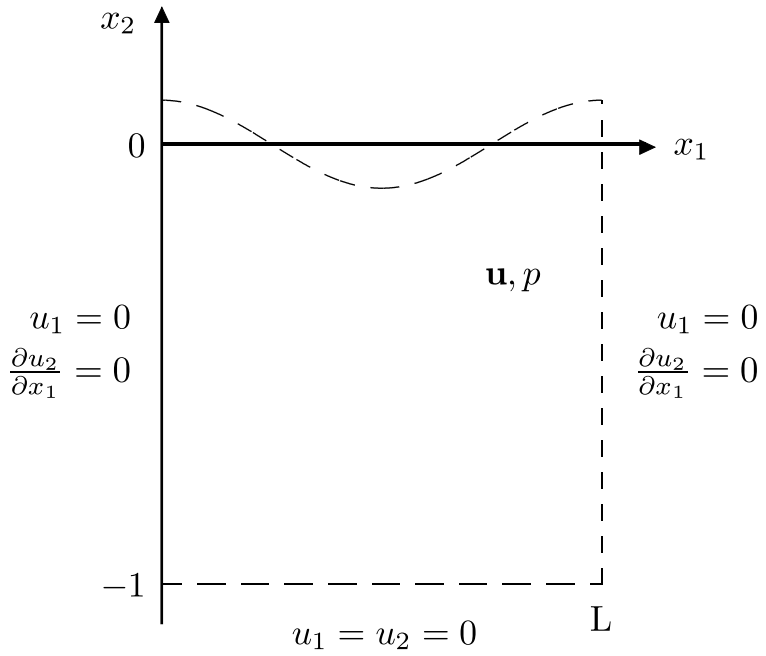

Figure 4.4: Sketch of the problem domain used to derive the dispersion relation for a single-layer free surface problem. The problem is very similar to that described in figure 4.1, except that in this case it is convenient to set the problem up so that the equilibrium position of the interface corresponds to the line $x_2 = 0$.

and

$$-\frac{\partial h}{\partial x_1}\tau_{21} + \tau_{22} = \frac{1}{\mathrm{Ca}}\frac{\partial^2 h}{\partial {x_1}^2}\left[1 + \left(\frac{\partial h}{\partial x_1}\right)^2\right]^{-\frac{3}{2}}, \tag{4.12}$$

where the external pressure has been set to zero. The definition of the stress tensor (4.5) can now be used to write these conditions in the form

$$\frac{\partial h}{\partial x_1}p - 2\frac{\partial h}{\partial x_1}\frac{\partial u_1}{\partial x_1} + \frac{\partial u_1}{\partial x_2} + \frac{\partial u_2}{\partial x_1} = -\frac{1}{\mathrm{Ca}}\frac{\partial h}{\partial x_1}\frac{\partial^2 h}{\partial {x_1}^2}\left[1 + \left(\frac{\partial h}{\partial x_1}\right)^2\right]^{-\frac{3}{2}} \tag{4.13}$$

and

$$-\frac{\partial h}{\partial x_1}\left(\frac{\partial u_2}{\partial x_1} + \frac{\partial u_1}{\partial x_2}\right) - p + 2\frac{\partial u_2}{\partial x_2} = \frac{1}{\mathrm{Ca}}\frac{\partial^2 h}{\partial {x_1}^2}\left[1 + \left(\frac{\partial h}{\partial x_1}\right)^2\right]^{-\frac{3}{2}}. \tag{4.14}$$

A trivial solution to the governing equations and associated boundary conditions described above is one in which the interface is undeformed, the velocity is zero everywhere and there is a hydrostatic pressure gradient. We shall call this the 'base state', and define it to be

$$\bar{h} = 0, \qquad \bar{u}_1 = \bar{u}_2 = 0 \qquad \text{and} \qquad \bar{p} = -\frac{\mathrm{Re}}{\mathrm{Fr}}\, x_2. \tag{4.15}$$

Note that this is a steady solution of the governing equations. We then consider an infinitesimal perturbation to this base state, so that the solution is given by

$$h = \bar{h} + \epsilon\,\hat{h}, \qquad u_i = \bar{u}_i + \epsilon\,\hat{u}_i \qquad \text{and} \qquad p = \bar{p} + \epsilon\,\hat{p}, \tag{4.16}$$

where $\epsilon \ll 1$. Substituting (4.16) into the governing equations and neglecting orders of ϵ^2 and higher yields

$$\mathrm{Re}\,\mathrm{St}\,\frac{\partial \hat{u}_i}{\partial t} = -\frac{\partial \hat{p}}{\partial x_i} + \frac{\partial}{\partial x_j}\left(\frac{\partial \hat{u}_i}{\partial x_j} + \frac{\partial \hat{u}_j}{\partial x_i}\right) \tag{4.17}$$

and

$$\frac{\partial \hat{u}_j}{\partial x_j} = 0, \tag{4.18}$$

and we note that using (4.18) we can rewrite (4.17) as

$$\mathrm{Re}\,\mathrm{St}\,\frac{\partial \hat{u}_i}{\partial t} = -\frac{\partial \hat{p}}{\partial x_i} + \frac{\partial^2 \hat{u}_i}{\partial {x_j}^2}. \tag{4.19}$$

The kinematic condition (4.10) is evaluated at the interface, $h = \epsilon\,\hat{h}$, which gives

$$\epsilon\,\hat{u}_2\big|_{x_2=\epsilon\hat{h}} = \epsilon\,\mathrm{St}\,\frac{\partial \hat{h}}{\partial t} + \mathrm{O}(\epsilon^2), \tag{4.20}$$

and we use Taylor's theorem to express u_2 as a power series about $x_2 = 0$,

$$\hat{u}_2\big|_{x_2=\epsilon\hat{h}} = \hat{u}_2\big|_{x_2=0} + \epsilon\,\hat{h}\,\left.\frac{\partial \hat{u}_2}{\partial x_2}\right|_{x_2=0} + \mathrm{O}(\epsilon^2). \tag{4.21}$$

This allows us to evaluate the kinematic condition at the *undeformed* position of the free boundary,

$$\hat{u}_2\big|_{x_2=0} = \mathrm{St}\,\frac{\partial \hat{h}}{\partial t}, \tag{4.22}$$

where we have neglected terms of order ϵ^2 and higher. The dynamic conditions (4.13) and (4.14) contain terms raised to negative powers, and we expand these using the binomial theorem,

$$\left[1 + \left(\frac{\partial h}{\partial x_1}\right)^2\right]^{-\frac{3}{2}} = \left[1 + \epsilon^2\left(\frac{\partial \hat{h}}{\partial x_1}\right)^2\right]^{-\frac{3}{2}} = 1 + \mathrm{O}(\epsilon^2), \tag{4.23}$$

before using (4.16) and (4.15) to give

$$\epsilon\left[\left.\frac{\partial \hat{u}_1}{\partial x_2}\right|_{x_2=\epsilon\hat{h}} + \left.\frac{\partial \hat{u}_2}{\partial x_1}\right|_{x_2=\epsilon\hat{h}}\right] = \mathrm{O}(\epsilon^2) \tag{4.24}$$

and

$$\epsilon\left[-\hat{p}|_{x_2=\epsilon\hat{h}}+2\left.\frac{\partial\hat{u}_2}{\partial x_2}\right|_{x_2=\epsilon\hat{h}}+\frac{\mathrm{Re}}{\mathrm{Fr}}\hat{h}\right]=\frac{\epsilon}{\mathrm{Ca}}\frac{\partial^2\hat{h}}{\partial {x_1}^2}+\mathrm{O}(\epsilon^2). \tag{4.25}$$

As before we wish to evaluate these conditions at the undeformed interface position, and therefore use Taylor's theorem to give

$$\left.\frac{\partial\hat{u}_1}{\partial x_2}\right|_{x_2=0}+\left.\frac{\partial\hat{u}_2}{\partial x_1}\right|_{x_2=0}=0 \tag{4.26}$$

and

$$-\hat{p}|_{x_2=0}+2\left.\frac{\partial\hat{u}_2}{\partial x_2}\right|_{x_2=0}+\frac{\mathrm{Re}}{\mathrm{Fr}}\hat{h}=\frac{1}{\mathrm{Ca}}\frac{\partial^2\hat{h}}{\partial {x_1}^2}, \tag{4.27}$$

where we have again neglected terms of order ϵ^2 and higher. Finally, we have the following Dirichlet boundary conditions:

$$\begin{aligned}
\hat{u}_1|_{x_2=-1} &= 0, && (4.28)\\
\hat{u}_2|_{x_2=-1} &= 0, && (4.29)\\
\hat{u}_1|_{x_1=0} &= 0 \quad \text{and} && (4.30)\\
\hat{u}_1|_{x_1=L} &= 0. && (4.31)
\end{aligned}$$

The governing equations (4.18 and 4.19) and boundary conditions (4.22 and 4.26–4.31) have now been linearised and we propose a separable solution of the form

$$\begin{aligned}
\hat{h}(x_1,t) &= H\,\cos(2\pi k x_1)\,e^{\lambda t},\\
\hat{u}_1(x_1,x_2,t) &= U(x_2)\sin(2\pi k x_1)\,e^{\lambda t},\\
\hat{u}_2(x_1,x_2,t) &= V(x_2)\cos(2\pi k x_1)\,e^{\lambda t} \quad \text{and}\\
\hat{p}(x_1,x_2,t) &= P(x_2)\,\cos(2\pi k x_1)\,e^{\lambda t}, && (4.32)
\end{aligned}$$

where $k=1/L$ is the wavenumber. We note that this ansatz automatically satisfies the conditions (4.30) and (4.31). Substituting (4.32) into the governing equations yields

$$\begin{aligned}
\mathrm{Re}\,\mathrm{St}\,\lambda\,U &= 2\pi k\,P-4\pi^2k^2\,U+\frac{\mathrm{d}^2U}{\mathrm{d}{x_2}^2}, && (4.33)\\
\mathrm{Re}\,\mathrm{St}\,\lambda\,V &= -\frac{\mathrm{d}P}{\mathrm{d}x_2}-4\pi^2k^2\,V+\frac{\mathrm{d}^2V}{\mathrm{d}{x_2}^2} && (4.34)
\end{aligned}$$

and

$$2\pi k\,U+\frac{\mathrm{d}V}{\mathrm{d}x_2}=0. \tag{4.35}$$

Rearranging (4.35) for U and substituting into (4.33) gives

$$P = \frac{1}{4\pi^2 k^2}\frac{\mathrm{d}^3 V}{\mathrm{d}{x_2}^3} - \left(1 + \frac{\mathrm{Re}\,\mathrm{St}\,\lambda}{4\pi^2 k^2}\right)\frac{\mathrm{d}V}{\mathrm{d}x_2}, \tag{4.36}$$

where we have rearranged for P. We then differentiate this expression with respect to x_2 and substitute it into (4.34) to obtain a fourth-order ODE in V,

$$\frac{\mathrm{d}^4 V}{\mathrm{d}{x_2}^4} - \left(\mathrm{Re}\,\mathrm{St}\,\lambda + 8\pi^2 k^2\right)\frac{\mathrm{d}^2 V}{\mathrm{d}{x_2}^2} + 4\pi^2 k^2\left(\mathrm{Re}\,\mathrm{St}\,\lambda + 4\pi^2 k^2\right) V = 0. \tag{4.37}$$

As all the coefficients are constant we can find a general solution for $V(x_2)$ by assuming a solution of the form $V(x_2) = Ae^{mx_2}$, which gives rise to the following auxiliary equation:

$$m^4 - \left(\mathrm{Re}\,\mathrm{St}\,\lambda + 8\pi^2 k^2\right) m^2 + 4\pi^2 k^2\left(\mathrm{Re}\,\mathrm{St}\,\lambda + 4\pi^2 k^2\right) = 0. \tag{4.38}$$

Provided that both the Reynolds and Strouhal numbers are non-zero the solutions of (4.38) are $m = \pm 2\pi k,\ \pm\sqrt{\mathrm{Re}\,\mathrm{St}\,\lambda + 4\pi^2 k^2}$, and hence the general solution of $V(x_2)$ is given by

$$V(x_2) = Ae^{2\pi k x_2} + Be^{-2\pi k x_2} + Ce^{\beta x_2} + De^{-\beta x_2}, \tag{4.39}$$

where $\beta = \sqrt{\mathrm{Re}\,\mathrm{St}\,\lambda + 4\pi^2 k^2}$. Using (4.35) and (4.36) we can also obtain general solutions for $U(x_2)$,

$$U(x_2) = -Ae^{2\pi k x_2} + Be^{-2\pi k x_2} - \frac{\beta}{2\pi k}Ce^{\beta x_2} + \frac{\beta}{2\pi k}De^{-\beta x_2}, \tag{4.40}$$

and $P(x_2)$,

$$P(x_2) = -\frac{\mathrm{Re}\,\mathrm{St}\,\lambda}{2\pi k}Ae^{2\pi k x_2} + \frac{\mathrm{Re}\,\mathrm{St}\,\lambda}{2\pi k}Be^{-2\pi k x_2}. \tag{4.41}$$

A, B, C and D are constant coefficients to be determined from the boundary conditions, and we therefore substitute the same ansatz (4.32) into (4.22), (4.26), (4.27), (4.28) and (4.29) to obtain the separated forms of the kinematic,

$$V(0) = \mathrm{St}\,H\,\lambda, \tag{4.42}$$

dynamic,

$$\left.\frac{\mathrm{d}U}{\mathrm{d}x_2}\right|_{x_2=0} - 2\pi k\,V(0) = 0, \tag{4.43}$$

$$-P(0) + 2\left.\frac{\mathrm{d}V}{\mathrm{d}x_2}\right|_{x_2=0} + \left(\frac{4\pi^2 k^2}{\mathrm{Ca}} + \frac{\mathrm{Re}}{\mathrm{Fr}}\right)H = 0, \tag{4.44}$$

and Dirichlet conditions,

$$U(-1) = 0 \qquad \text{and} \qquad V(-1) = 0. \tag{4.45}$$

We can now use the general solutions of $U(x_2)$, $V(x_2)$ and $P(x_2)$ in (4.42)–(4.45) to obtain the following homogeneous linear system,

$$\begin{aligned}
A + B + C + D - \mathrm{St}\,\lambda H &= 0, \\
8\pi^2 k^2 (A + B) + \left(\mathrm{Re}\,\mathrm{St}\,\lambda + 8\pi^2 k^2\right)(C + D) &= 0, \\
\frac{\mathrm{Re}\,\mathrm{St}\,\lambda + 8\pi^2 k^2}{2\pi k}(A - B) + 2\,\beta\,(C - D) + \left(\frac{4\pi^2 k^2}{\mathrm{Ca}} + \frac{\mathrm{Re}}{\mathrm{Fr}}\right) H &= 0, \\
-Ae^{-2\pi k} + Be^{2\pi k} - \frac{\beta}{2\pi k} Ce^{-\beta} + \frac{\beta}{2\pi k} De^{\beta} &= 0, \\
Ae^{-2\pi k} + Be^{2\pi k} + Ce^{-\beta} + De^{\beta} &= 0.
\end{aligned} \tag{4.46}$$

This system of five equations in the five unknowns A, B, C, D and H can be written in the form

$$\mathbf{M} \begin{bmatrix} A \\ B \\ C \\ D \\ H \end{bmatrix} = \begin{bmatrix} 0 \\ 0 \\ 0 \\ 0 \\ 0 \end{bmatrix}, \tag{4.47}$$

where $\mathbf{M}$ is a 5×5 matrix whose entries are the coefficients of the unknowns. This system only has a non-trivial solution if $|\mathbf{M}| = 0$, and we solve this equation numerically to obtain a dispersion relation $\lambda(k)$. $\Re(\lambda)$ is the growth rate of the wave and $\Im(\lambda)$ is its frequency, and this analytical result can now be compared to `oomph-lib`'s computations for given values of the wavenumber k. An initial deflection amplitude of 1% of the domain width was chosen to be 'sufficiently small' that the nonlinear terms would be negligible, and the growth rate and frequency of the oscillation was determined from a time-trace of the left-hand edge of the interface (such as the one plotted in figure 4.3) using a Levenberg–Marquardt fitting technique [Press et al., 2007, sec 15.5.2]. The comparison is shown in figure 4.5, where the real and imaginary parts of λ are plotted as lines and the points represent the results generated using `oomph-lib`. The figure shows excellent agreement between the numerics and the linear theory. We

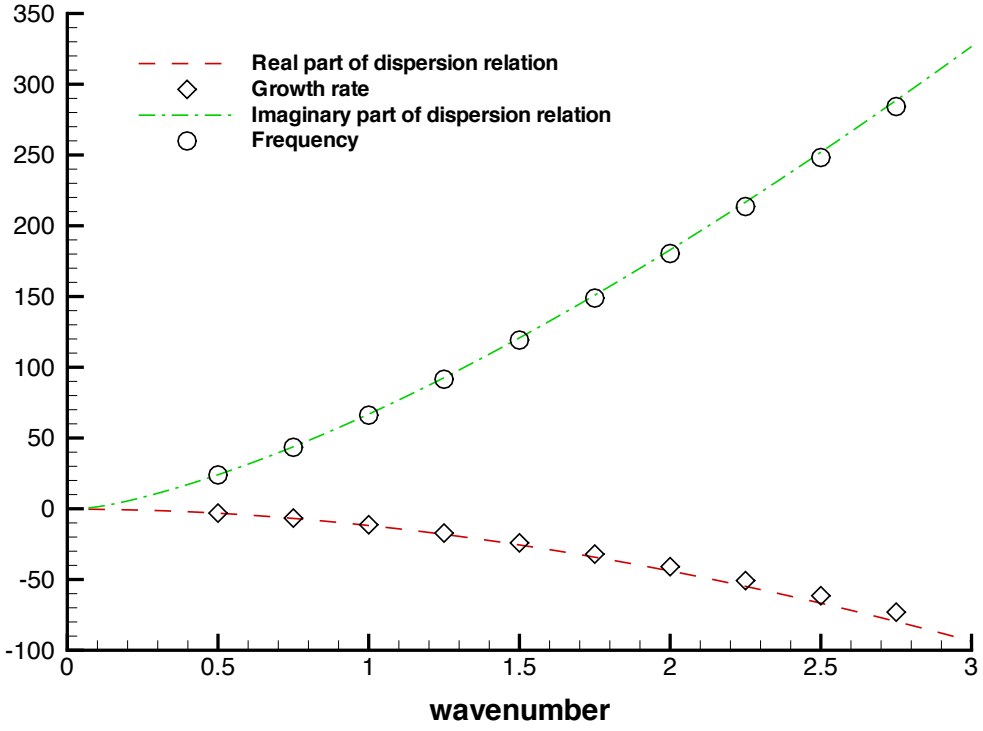

Figure 4.5: Validation of the `oomph-lib` code (points) by comparison with an analytical dispersion relation (lines) for the two-dimensional single-layer interface problem. The `oomph-lib` simulations employ a 12×12 element mesh and a second-order BDF timestepper with a (non-dimensionalised) timestep of 0.0025, for the parameters $\mathrm{Re} = \mathrm{Re}\,\mathrm{St} = \mathrm{Re}/\mathrm{Fr} = 5.0$, $\mathrm{Ca} = 0.01$ and $\epsilon = 0.01$.

note that at higher wavenumbers the results generated by `oomph-lib` slightly drift away from the analytical result: this is due to the fact that as we reduce the width of the problem domain, but keep the amplitude of the initial perturbation constant, we 'steepen' the free surface. Hence we would not expect the linear analysis to provide quite as good an approximation to the numerical solutions as the domain width decreases.

4.1.2 Implementation

The problem discussed above was implemented as a demonstration code in `oomph-lib`, and as such forms part of its range of self-test routines. The source file,

```
spine_single_layer.cc,
```

is located in the

`demo_drivers/navier_stokes/single_layer_free_surface/`

directory. The same problem was also implemented using a pseudo-solid node-update strategy, and its source file,

`elastic_single_layer.cc`,

is located in the same directory. This latter code takes advantage of `oomph-lib`'s refineable element framework to (automatically) refine the mesh in regions where there are steep velocity gradients. We note that there is excellent agreement between the results generated by the two implementations of this problem. The pseudo-solid version of this driver code was also comprehensively documented in an `oomph-lib` tutorial, which can be found in the

`doc/navier_stokes/single_layer_free_surface/`

directory.

4.2 Relaxation oscillations of an interface between two viscous fluids

Let us now extend the problem discussed above to one involving two immiscible, incompressible viscous fluids separated by an interface, as sketched in figure 4.6. The governing equations in the lower fluid are the same as before (4.1 and 4.2), but the momentum equation in the upper fluid must be modified to include the ratios R_ρ and R_μ which describe the density and dynamic viscosity of this layer relative to that of the lower layer:

$$R_\rho \,\mathrm{Re}\,\mathrm{St}\,\frac{\partial u_i}{\partial t} + R_\rho \,\mathrm{Re}\,u_j\frac{\partial u_i}{\partial x_j} = -\frac{\partial p}{\partial x_i} + R_\rho\,\frac{\mathrm{Re}}{\mathrm{Fr}}G_i + R_\mu\frac{\partial}{\partial x_j}\left(\frac{\partial u_i}{\partial x_j} + \frac{\partial u_j}{\partial x_i}\right). \qquad (4.48)$$

As for the single-layer example, we wish to set up this problem in such a way that it can be compared to analytical results which we will derive in section 4.2.1. We facilitate this by choosing the domain to be that sketched in figure 4.6, and subject the governing equations to the no-slip boundary conditions $u_1 = u_2 = 0$ on the top and bottom solid boundaries and the non-penetration conditions $u_1 = \partial u_2/\partial x_1 = 0$ on the left and right boundaries. Gravity again acts in the negative x_2 direction. The

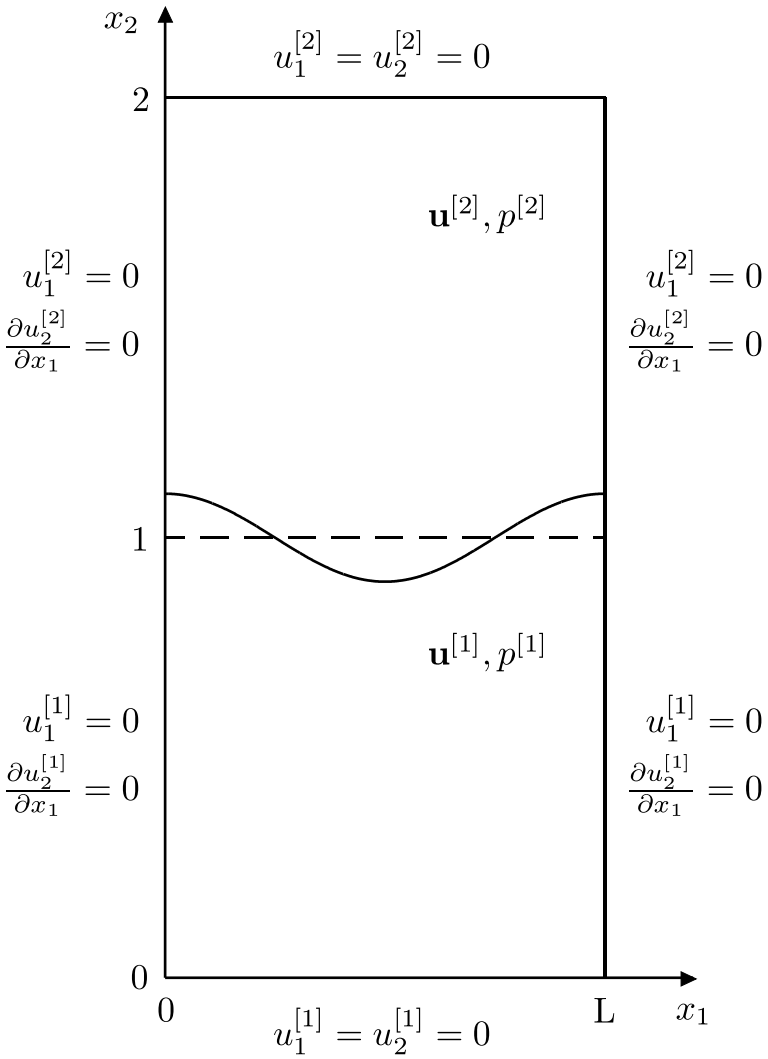

Figure 4.6: Sketch of a two layer interface problem in two dimensions. The equilibrium position of the interface is located at $x_2 = 1$ and is represented by the dashed line.

interface, located at $\mathbf{X}$, is subject to the kinematic condition (4.3) and the dynamic condition,

$$\tau_{ij}^{[1]} n_j^{[1]} = \tau_{ij}^{[2]} n_j^{[1]} + \frac{1}{\mathrm{Ca}} \kappa \, n_i^{[1]}, \tag{4.49}$$

where the lower and upper fluids are denoted by [1] and [2] respectively, and the stress tensor is defined as before (3.7).

This problem was solved numerically in `oomph-lib` using a very similar approach to the previous example (discussed in section 4.1). The problem domain was discretised into a 12×24 mesh of Crouzeix–Raviart elements. Taylor–Hood elements were not used for this problem since they cannot accomodate the pressure jump at the interface. A spine-based node update strategy was again used to deform the mesh in response

to the motion of the interface, and the time-derivatives were again discretised using a second-order-accurate BDF scheme with a (non-dimensionalised) timestep of 0.0025.

The simulation was started impulsively from the initial conditions of zero velocity everywhere and an interfacial deformation as before (4.6), and ran for 240 timesteps. The amplitude of the perturbation was again chosen to be 10% of the domain width, and figure 4.7 shows a time-trace of the height of the fluid layer at the edge of the domain for the parameters $\mathrm{Re} = \mathrm{Re}\,\mathrm{St} = \mathrm{Re}/\mathrm{Fr} = 5.0$, $\mathrm{Ca} = 0.01$, $R_\rho = 0.5$, $R_\mu = 0.1$ and $L = 1$. The mechanics of the relaxation of the interface are the same as in the single-layer example: surface tension and gravitational forces act to restore it to its equilibrium position, with the energy in the system being damped by viscous forces in the two layers.

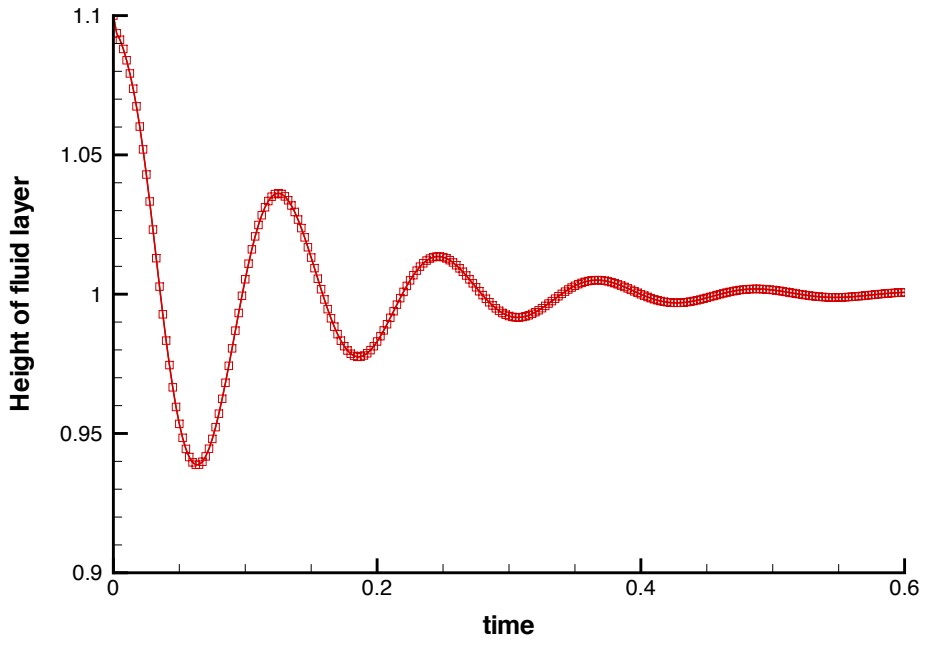

Figure 4.7: Time-trace of the height of the interface at the point $x_1 = 0$ for the parameters $\mathrm{Re} = \mathrm{Re}\,\mathrm{St} = \mathrm{Re}/\mathrm{Fr} = 5.0$, $\mathrm{Ca} = 0.01$, $R_\rho = 0.5$, $R_\mu = 0.1$, $L = 1$ and $\epsilon = 0.1$. A mesh of 12×24 Crouzeix–Raviart elements and a second-order-accurate BDF timestepping scheme with a non-dimensionalised timestep of 0.0025 were used.

4.2.1 Validation against an analytical dispersion relation

The simulations described above were again validated against an analytical test case in a similar manner to those discussed in section 4.1. We consider a domain $x_1 \in [0, L]$, $x_2 \in [-1, 1]$, with gravity acting in the negative x_2 direction, in which we have an interface corresponding to the line $x_2 = 0$. We are solving the Navier–Stokes equations in both regions of the domain, and for sufficiently small amplitudes, $\epsilon \ll 1$, these can be linearised about the trivial steady base state

$$\bar{h} = 0, \qquad \bar{u}_1^{[1]} = \bar{u}_2^{[1]} = \bar{u}_1^{[2]} = \bar{u}_2^{[2]} = 0,$$

$$\bar{p}^{[1]} = -R_\rho^{[1]} \frac{\mathrm{Re}}{\mathrm{Fr}} (x_2 + 1) \qquad \text{and} \qquad \bar{p}^{[2]} = -\frac{\mathrm{Re}}{\mathrm{Fr}} \left(R_\rho^{[1]} + R_\rho^{[2]} x_2 \right) \tag{4.50}$$

to give

$$R_\rho^{[\beta]} \mathrm{Re}\, \mathrm{St}\, \frac{\partial \hat{u}_i^{[\beta]}}{\partial t} = -\frac{\partial \hat{p}^{[\beta]}}{\partial x_i} + R_\mu^{[\beta]} \frac{\partial^2 \hat{u}_i^{[\beta]}}{\partial {x_j}^2} \tag{4.51}$$

and

$$\frac{\partial \hat{u}_j^{[\beta]}}{\partial x_j} = 0, \tag{4.52}$$

where $\beta = 1, 2$ and we note that $R_\rho^{[1]} = R_\mu^{[1]} = 1$. The linearised form of the kinematic boundary condition is as before,

$$\hat{u}_2^{[\beta]}\Big|_{x_2=0} = \mathrm{St}\, \frac{\partial \hat{h}}{\partial t}, \tag{4.53}$$

and the two components of the linearised dynamic condition are

$$R_\mu^{[1]} \left.\frac{\partial \hat{u}_1^{[1]}}{\partial x_2}\right|_{x_2=0} + R_\mu^{[1]} \left.\frac{\partial \hat{u}_2^{[1]}}{\partial x_1}\right|_{x_2=0} = R_\mu^{[2]} \left.\frac{\partial \hat{u}_1^{[2]}}{\partial x_2}\right|_{x_2=0} + R_\mu^{[2]} \left.\frac{\partial \hat{u}_2^{[2]}}{\partial x_1}\right|_{x_2=0} \tag{4.54}$$

and

$$\begin{aligned} -\hat{p}^{[1]}\big|_{x_2=0} + 2R_\mu^{[1]} \left.\frac{\partial \hat{u}_2^{[1]}}{\partial x_2}\right|_{x_2=0} &= -\hat{p}^{[2]}\big|_{x_2=0} + 2R_\mu^{[2]} \left.\frac{\partial \hat{u}_2^{[2]}}{\partial x_2}\right|_{x_2=0} \\ &\quad + \frac{1}{\mathrm{Ca}} \frac{\partial^2 \hat{h}}{\partial {x_1}^2} - \frac{\mathrm{Re}}{\mathrm{Fr}} \left(R_\rho^{[1]} - R_\rho^{[2]} \right) \hat{h}. \end{aligned} \tag{4.55}$$

Additionally we have the following Dirichlet conditions at the top and bottom solid boundaries,

$$\hat{u}_1^{[1]}\Big|_{x_2=-1} = \hat{u}_2^{[1]}\Big|_{x_2=-1} = \hat{u}_1^{[2]}\Big|_{x_2=1} = \hat{u}_2^{[2]}\Big|_{x_2=1} = 0, \tag{4.56}$$

and we note that the horizontal component of the velocity must be continuous across the interface:

$$\hat{u}_1^{[1]}\Big|_{x_2=0} = \hat{u}_1^{[2]}\Big|_{x_2=0}. \tag{4.57}$$

This requirement is automatically satisfied by ensuring that the kinematic condition (4.53) is evaluated for both fluids. Substitution of the ansatz

$$\begin{aligned}
\hat{h}(x_1,t) &= H\,\cos(2\pi k x_1)\,e^{\lambda t},\\
\hat{u}_1^{[\beta]}(x_1,x_2,t) &= U^{[\beta]}(x_2)\sin(2\pi k x_1)\,e^{\lambda t},\\
\hat{u}_2^{[\beta]}(x_1,x_2,t) &= V^{[\beta]}(x_2)\cos(2\pi k x_1)\,e^{\lambda t} \quad \text{and}\\
\hat{p}^{[\beta]}(x_1,x_2,t) &= P^{[\beta]}(x_2)\,\cos(2\pi k x_1)\,e^{\lambda t}
\end{aligned} \tag{4.58}$$

into the linearised governing equations and boundary conditions yields the following linear system,

$$
\begin{aligned}
A^{[1]} + B^{[1]} + C^{[1]} + D^{[1]} - \mathrm{St}\,\lambda H &= 0, \\
A^{[2]} + B^{[2]} + C^{[2]} + D^{[2]} - \mathrm{St}\,\lambda H &= 0, \\
R_\mu^{[1]} A^{[1]} + R_\mu^{[1]} B^{[1]} + \left(\frac{R_\rho^{[1]} \mathrm{Re}\,\mathrm{St}\,\lambda}{8\pi^2 k^2} + R_\mu^{[1]} \right) \left(C^{[1]} + D^{[1]} \right) & \\
- R_\mu^{[2]} A^{[2]} - R_\mu^{[2]} B^{[2]} - \left(\frac{R_\rho^{[2]} \mathrm{Re}\,\mathrm{St}\,\lambda}{8\pi^2 k^2} + R_\mu^{[2]} \right) \left(C^{[2]} + D^{[2]} \right) &= 0, \\
\left(\frac{R_\rho^{[1]} \mathrm{Re}\,\mathrm{St}\,\lambda}{2\pi k} + 4\pi R_\mu^{[1]} k \right) \left(A^{[1]} - B^{[1]} \right) + 2R_\mu^{[1]} a_1 \left(C^{[1]} - D^{[1]} \right) & \\
- \left(\frac{R_\rho^{[2]} \mathrm{Re}\,\mathrm{St}\,\lambda}{2\pi k} + 4\pi R_\mu^{[2]} k \right) \left(A^{[2]} - B^{[2]} \right) - 2R_\mu^{[2]} a_2 \left(C^{[2]} - D^{[2]} \right) & \\
+ \left(\frac{4\pi^2 k^2}{\mathrm{Ca}} + \frac{\mathrm{Re}}{\mathrm{Fr}} \left(R_\rho^{[1]} - R_\rho^{[2]} \right) \right) H &= 0, \\
- A^{[1]} e^{-2\pi k} + B^{[1]} e^{2\pi k} - \frac{a_1}{2\pi k} C^{[1]} e^{-a_1} + \frac{a_1}{2\pi k} D^{[1]} e^{a_1} &= 0, \\
A^{[1]} e^{-2\pi k} + B^{[1]} e^{2\pi k} + C^{[1]} e^{-a_1} + D^{[1]} e^{a_1} &= 0, \\
- A^{[2]} e^{2\pi k} + B^{[2]} e^{-2\pi k} - \frac{a_2}{2\pi k} C^{[2]} e^{a_2} + \frac{a_2}{2\pi k} D^{[2]} e^{-a_2} &= 0, \\
A^{[2]} e^{2\pi k} + B^{[2]} e^{-2\pi k} + C^{[2]} e^{a_2} + D^{[2]} e^{-a_2} &= 0, \\
- A^{[1]} + B^{[1]} - \frac{a_1}{2\pi k} C^{[1]} + \frac{a_1}{2\pi k} D^{[1]} + A^{[2]} - B^{[2]} + \frac{a_2}{2\pi k} C^{[2]} - \frac{a_2}{2\pi k} D^{[2]} &= 0,
\end{aligned}
$$

where $a_\beta = \left[\left(R_\rho^{[\beta]} \mathrm{Re}\,\mathrm{St}\,\lambda / R_\mu^{[\beta]} \right) + 4\pi^2 k^2 \right]^{1/2}$. The dispersion relation $\lambda(k)$ can then be obtained using the same procedure as before (section 4.1.1), and figure 4.8 shows a comparison between the real and imaginary parts of λ and the growth rate and frequency of the oscillating interface as computed by `oomph-lib` for a range of wavenumbers k. An initial deflection amplitude of 1% of the domain width was again chosen for this validation exercise, and we note that, as in the single-layer example, there is excellent agreement between the numerical results and those predicted by the linear theory.

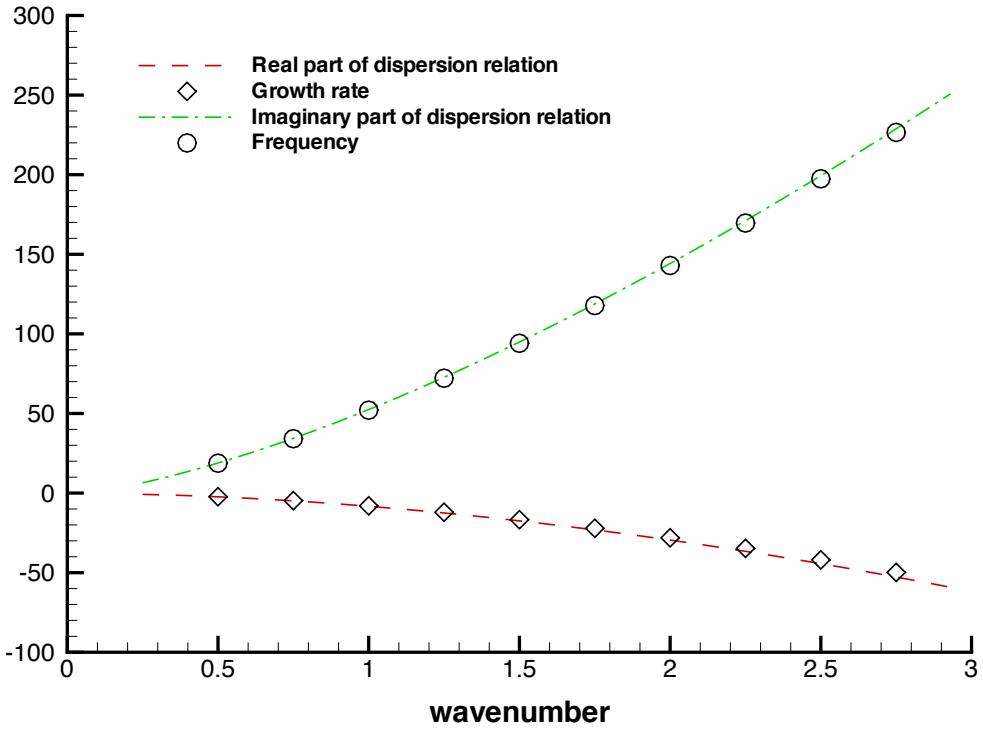

Figure 4.8: Validation of the `oomph-lib` code (points) by comparison with an analytical dispersion relation (lines) for the two-dimensional two-layer interface problem. The `oomph-lib` simulations employ a 12×24 element mesh and a second-order BDF timestepper with a (non-dimensionalised) timestep of 0.0025, for the parameters $\mathrm{Re} = \mathrm{Re}\,\mathrm{St} = \mathrm{Re}/\mathrm{Fr} = 5.0$, $\mathrm{Ca} = 0.01$, $R_\rho = 0.5$, $R_\mu = 0.1$ and $\epsilon = 0.01$.

4.2.2 Implementation

As in the case of the single-layer example, the problem discussed above was also implemented as two separate demonstration codes in `oomph-lib`, employing the two different node-update strategies discussed earlier in this work. The source for the spine-based implementation is located in

```
spine_two_layer_interface.cc,
```

and that for the pseudo-solid implementation is located in

```
elastic_two_layer_interface.cc.
```

Both of these codes are located in the

```
demo_drivers/navier_stokes/two_layer_interface/
```

directory, and once again there is excellent agreement of the results generated by the two implementations. The pseudo-solid version of this driver code was comprehensively documented in an `oomph-lib` tutorial, which can be found in the

```
doc/navier_stokes/two_layer_interface/
```

directory.

Chapter 5

The free surface Navier–Stokes equations in cylindrical geometries

At this point we will cease to consider problems formulated in Cartesian coordinate systems, and instead take the principles introduced in the past two chapters and apply them to problems formulated in cylindrical geometries. We begin our discussion by examining the (strong) form of the governing equations and boundary conditions in cylindrical polar coordinates in section 5.1. In order to solve problems governed by these equations using the finite element method we must first derive their weak form, and we present this formulation in the following way: first, we consider the weak form of the Navier–Stokes equations in a general orthogonal coordinate system in section 5.2, before specialising to cylindrical geometries in section 5.3. We then derive the weak form of the free boundary conditions in a general orthogonal coordinate system in section 5.4. Finally, in section 5.5 we consider the special case of flows in cylindrical coordinates which are independent of the azimuthal coordinate. We write down the weak form of the governing equations (section 5.5.1) and the boundary conditions at a free surface (section 5.5.2), before combining these in section 5.5.3. The complete set of elemental residual equations for the finite element formulation of an axisymmetric free surface Navier–Stokes problem is then presented in section 5.5.4.

5.1 Governing equations

In a cylindrical polar coordinate system (r^*, z^*, θ^*) the Navier–Stokes equations (in dimensional form) are given by the momentum equations

$$\rho\left[\frac{\partial u_r^*}{\partial t^*} + u_r^*\frac{\partial u_r^*}{\partial r^*} + \frac{u_\theta^*}{r^*}\frac{\partial u_r^*}{\partial \theta} - \frac{u_\theta^{*2}}{r^*} + u_z^*\frac{\partial u_r^*}{\partial z^*}\right]$$
$$= -\frac{\partial p^*}{\partial r^*} + B_r^* + \rho\, G_r^* + \mu\left[\frac{\partial^2 u_r^*}{\partial r^{*2}} + \frac{1}{r^*}\frac{\partial u_r^*}{\partial r^*} - \frac{u_r^*}{r^{*2}} + \frac{1}{r^{*2}}\frac{\partial^2 u_r^*}{\partial \theta^2} + \frac{\partial^2 u_r^*}{\partial z^{*2}} - \frac{2}{r^{*2}}\frac{\partial u_\theta^*}{\partial \theta}\right],$$

$$\rho\left[\frac{\partial u_z^*}{\partial t^*} + u_r^*\frac{\partial u_z^*}{\partial r^*} + \frac{u_\theta^*}{r^*}\frac{\partial u_z^*}{\partial \theta} + u_z^*\frac{\partial u_z^*}{\partial z^*}\right]$$
$$= -\frac{\partial p^*}{\partial z^*} + B_z^* + \rho\, G_z^* + \mu\left[\frac{\partial^2 u_z^*}{\partial r^{*2}} + \frac{1}{r^*}\frac{\partial u_z^*}{\partial r^*} + \frac{1}{r^{*2}}\frac{\partial^2 u_z^*}{\partial \theta^2} + \frac{\partial^2 u_z^*}{\partial z^{*2}}\right],$$

$$\rho\left[\frac{\partial u_\theta^*}{\partial t^*} + u_r^*\frac{\partial u_\theta^*}{\partial r^*} + \frac{u_\theta^*}{r^*}\frac{\partial u_\theta^*}{\partial \theta} + \frac{u_r^* u_\theta^*}{r^*} + u_z^*\frac{\partial u_\theta^*}{\partial z^*}\right]$$
$$= -\frac{1}{r^*}\frac{\partial p^*}{\partial \theta} + B_\theta^* + \rho\, G_\theta^* + \mu\left[\frac{\partial^2 u_\theta^*}{\partial r^{*2}} + \frac{1}{r^*}\frac{\partial u_\theta^*}{\partial r^*} - \frac{u_\theta^*}{r^{*2}} + \frac{1}{r^{*2}}\frac{\partial^2 u_\theta^*}{\partial \theta^2} + \frac{\partial^2 u_\theta^*}{\partial z^{*2}} + \frac{2}{r^{*2}}\frac{\partial u_r^*}{\partial \theta}\right], \tag{5.1}$$

and the continuity equation

$$\frac{\partial u_r^*}{\partial r^*} + \frac{u_r^*}{r^*} + \frac{1}{r^*}\frac{\partial u_\theta^*}{\partial \theta} + \frac{\partial u_z^*}{\partial z^*} = Q^*, \tag{5.2}$$

where u_r^*, u_z^* and u_θ^* are the radial, axial and azimuthal velocity components respectively [Panton, 2005, pp. 781-5], and all other quantities are as defined in section 3.1. These equations can be non-dimensionalised using the same scalings as in the Cartesian example (3.3) to give

$$R_\rho\,\mathrm{Re}\left[\mathrm{St}\,\frac{\partial u_r}{\partial t} + u_r\frac{\partial u_r}{\partial r} + \frac{u_\theta}{r}\frac{\partial u_r}{\partial \theta} - \frac{u_\theta^2}{r} + u_z\frac{\partial u_r}{\partial z}\right]$$
$$= -\frac{\partial p}{\partial r} + B_r + R_\rho\frac{\mathrm{Re}}{\mathrm{Fr}}G_r + R_\mu\left[\frac{\partial^2 u_r}{\partial r^2} + \frac{1}{r}\frac{\partial u_r}{\partial r} - \frac{u_r}{r^2} + \frac{1}{r^2}\frac{\partial^2 u_r}{\partial \theta^2} + \frac{\partial^2 u_r}{\partial z^2} - \frac{2}{r^2}\frac{\partial u_\theta}{\partial \theta}\right],$$

$$R_\rho\,\mathrm{Re}\left[\mathrm{St}\,\frac{\partial u_z}{\partial t} + u_r\frac{\partial u_z}{\partial r} + \frac{u_\theta}{r}\frac{\partial u_z}{\partial \theta} + u_z\frac{\partial u_z}{\partial z}\right]$$
$$= -\frac{\partial p}{\partial z} + B_z + R_\rho\frac{\mathrm{Re}}{\mathrm{Fr}}G_z + R_\mu\left[\frac{\partial^2 u_z}{\partial r^2} + \frac{1}{r}\frac{\partial u_z}{\partial r} + \frac{1}{r^2}\frac{\partial^2 u_z}{\partial \theta^2} + \frac{\partial^2 u_z}{\partial z^2}\right],$$

$$R_\rho \,\mathrm{Re}\left[\mathrm{St}\,\frac{\partial u_\theta}{\partial t} + u_r\frac{\partial u_\theta}{\partial r} + \frac{u_\theta}{r}\frac{\partial u_\theta}{\partial \theta} + \frac{u_r u_\theta}{r} + u_z\frac{\partial u_\theta}{\partial z}\right]$$
$$= -\frac{1}{r}\frac{\partial p}{\partial \theta} + B_\theta + R_\rho\frac{\mathrm{Re}}{\mathrm{Fr}}G_\theta + R_\mu\left[\frac{\partial^2 u_\theta}{\partial r^2} + \frac{1}{r}\frac{\partial u_\theta}{\partial r} - \frac{u_\theta}{r^2} + \frac{1}{r^2}\frac{\partial^2 u_\theta}{\partial \theta^2} + \frac{\partial^2 u_\theta}{\partial z^2} + \frac{2}{r^2}\frac{\partial u_r}{\partial \theta}\right] \tag{5.3}$$

and

$$\frac{\partial u_r}{\partial r} + \frac{u_r}{r} + \frac{1}{r}\frac{\partial u_\theta}{\partial \theta} + \frac{\partial u_z}{\partial z} = Q, \tag{5.4}$$

where the Reynolds (Re), Strouhal (St) and Froude (Fr) numbers are as defined in (3.6). The components of the (non-dimensional) stress tensor are

$$\begin{aligned}
\tau_{rr} &= -p + 2R_\mu\frac{\partial u_r}{\partial r}, \qquad \tau_{zz} = -p + 2R_\mu\frac{\partial u_z}{\partial z},\\
\tau_{\theta\theta} &= -p + 2R_\mu\left(\frac{1}{r}\frac{\partial u_\theta}{\partial \theta} + \frac{u_r}{r}\right), \qquad \tau_{rz} = \tau_{zr} = R_\mu\left(\frac{\partial u_r}{\partial z} + \frac{\partial u_z}{\partial r}\right),\\
\tau_{r\theta} &= \tau_{\theta r} = R_\mu\left(\frac{\partial u_\theta}{\partial r} - \frac{u_\theta}{r} + \frac{1}{r}\frac{\partial u_r}{\partial \theta}\right), \qquad \tau_{z\theta} = \tau_{\theta z} = R_\mu\left(\frac{1}{r}\frac{\partial u_z}{\partial \theta} + \frac{\partial u_\theta}{\partial z}\right),
\end{aligned} \tag{5.5}$$

and we can use this to rewrite (5.3) as

$$R_\rho \,\mathrm{Re}\left[\mathrm{St}\,\frac{\partial u_r}{\partial t} + u_r\frac{\partial u_r}{\partial r} + \frac{u_\theta}{r}\frac{\partial u_r}{\partial \theta} - \frac{u_\theta^2}{r} + u_z\frac{\partial u_r}{\partial z}\right]$$
$$= B_r + R_\rho\frac{\mathrm{Re}}{\mathrm{Fr}}G_r + \frac{\tau_{rr}}{r} + \frac{\partial \tau_{rr}}{\partial r} + \frac{\partial \tau_{zr}}{\partial z} + \frac{1}{r}\frac{\partial \tau_{\theta r}}{\partial \theta} - \frac{\tau_{\theta\theta}}{r},$$

$$R_\rho \,\mathrm{Re}\left[\mathrm{St}\,\frac{\partial u_z}{\partial t} + u_r\frac{\partial u_z}{\partial r} + \frac{u_\theta}{r}\frac{\partial u_z}{\partial \theta} + u_z\frac{\partial u_z}{\partial z}\right]$$
$$= B_z + R_\rho\frac{\mathrm{Re}}{\mathrm{Fr}}G_z + \frac{\tau_{rz}}{r} + \frac{\partial \tau_{rz}}{\partial r} + \frac{\partial \tau_{zz}}{\partial z} + \frac{1}{r}\frac{\partial \tau_{\theta z}}{\partial \theta}$$

and

$$R_\rho \,\mathrm{Re}\left[\mathrm{St}\,\frac{\partial u_\theta}{\partial t} + u_r\frac{\partial u_\theta}{\partial r} + \frac{u_\theta}{r}\frac{\partial u_\theta}{\partial \theta} + \frac{u_r u_\theta}{r} + u_z\frac{\partial u_\theta}{\partial z}\right]$$
$$= B_\theta + R_\rho\frac{\mathrm{Re}}{\mathrm{Fr}}G_\theta + 2\frac{\tau_{r\theta}}{r} + \frac{\partial \tau_{r\theta}}{\partial r} + \frac{\partial \tau_{z\theta}}{\partial z} + \frac{1}{r}\frac{\partial \tau_{\theta\theta}}{\partial \theta}. \tag{5.6}$$

As usual these equations will be augmented by Dirichlet boundary conditions for some (or all) of the velocity components. In cases where there is a free boundary between two fluids located at position $\mathbf{X}$, we must (as before) apply both the dynamic and kinematic conditions,

$$\tau_{ij}^{[1]}\,n_j^{[1]} = \tau_{ij}^{[2]}\,n_j^{[1]} + \frac{1}{\mathrm{Ca}}\kappa\,n_i^{[1]} \tag{5.7}$$

and

$$\left(u_i - \mathrm{St}\,\frac{\partial X_i}{\partial t}\right)n_i = 0. \tag{5.8}$$

5.2 Weak form of the Navier–Stokes equations in a general orthogonal coordinate system

To derive the weak form of equations (5.4) and (5.6), it turns out to be convenient to first derive the weak form of the Navier–Stokes equations in a general orthogonal coordinate system in which the (unit) basis vectors are $\mathbf{e}_1$, $\mathbf{e}_2$ and $\mathbf{e}_3$. If $\mathbf{a} = a_1\,\mathbf{e}_1 + a_2\,\mathbf{e}_2 + a_3\,\mathbf{e}_3$ and $\mathbf{b} = b_1\,\mathbf{e}_1 + b_2\,\mathbf{e}_2 + b_3\,\mathbf{e}_3$ are two arbitrary vectors, then the tensor product (or 'dyad') of $\mathbf{a}$ and $\mathbf{b}$ is written as $\mathbf{a} \otimes \mathbf{b}$ and evaluated in the following way [Lebedev and Cloud, 2003, p. 23]:

$$\mathbf{a} \otimes \mathbf{b} = (a_i\,\mathbf{e}_i) \otimes (b_j\,\mathbf{e}_j) = a_i\,b_j\,(\mathbf{e}_i \otimes \mathbf{e}_j)\,. \tag{5.9}$$

Written in dyadic form, the momentum and continuity equations are given by

$$R_\rho\,\mathrm{Re}\,\mathrm{St}\,\frac{\partial \mathbf{u}}{\partial t} + R_\rho\,\mathrm{Re}\,[\mathbf{u} \cdot (\nabla \otimes \mathbf{u})] = \mathbf{B} + R_\rho\,\frac{\mathrm{Re}}{\mathrm{Fr}}\mathbf{G} + \nabla \cdot \boldsymbol{\tau} \tag{5.10}$$

and

$$\nabla \cdot \mathbf{u} = Q \tag{5.11}$$

respectively, where the velocity is given by $\mathbf{u} = u_1\,\mathbf{e}_1 + u_2\,\mathbf{e}_2 + u_3\,\mathbf{e}_3$ and the variable and gravitational body forces are given by $\mathbf{B} = B_1\,\mathbf{e}_1 + B_2\,\mathbf{e}_2 + B_3\,\mathbf{e}_3$ and $\mathbf{G} = G_1\,\mathbf{e}_1 + G_2\,\mathbf{e}_2 + G_3\,\mathbf{e}_3$. The stress tensor is defined by

$$\boldsymbol{\tau} = -p\,\mathbf{I} + R_\mu\left[(\nabla \otimes \mathbf{u}) + (\nabla \otimes \mathbf{u})^T\right], \tag{5.12}$$

where $\mathbf{I}$ is the identity matrix, and we note that the $\nabla \otimes \mathbf{u}$ terms in (5.10) and (5.12) are non-trivial due to the fact that in general the coordinate vectors $\mathbf{e}_i$ depend on position.

In preparation for the following discussion we shall define the product (from the right) of a dyad $\mathbf{a} \otimes \mathbf{b}$ by a vector $\mathbf{c}$ to be

$$(\mathbf{a} \otimes \mathbf{b}) \cdot \mathbf{c} = (\mathbf{b} \cdot \mathbf{c})\,\mathbf{a}, \tag{5.13}$$

and the product from the left to be

$$\mathbf{c} \cdot (\mathbf{a} \otimes \mathbf{b}) = (\mathbf{c} \cdot \mathbf{a})\,\mathbf{b}. \tag{5.14}$$

It will also be useful to define the following product of two dyads $\mathbf{a}\otimes\mathbf{b}$ and $\mathbf{c}\otimes\mathbf{d}$ to be

$$(\mathbf{a}\otimes\mathbf{b}) : (\mathbf{c}\otimes\mathbf{d}) = (\mathbf{a}\cdot\mathbf{d})\,(\mathbf{b}\cdot\mathbf{c})\,. \tag{5.15}$$

To find the weak form of the momentum equations we first write (5.10) in residual form before taking the dot product (on the right) with a vector test function $\boldsymbol{\phi}^{[\mathrm{f}]}$. Integrating over the entire domain then gives the weighted residual

$$\mathcal{R}^{[\mathrm{f}]} = \iiint_V \left\{ R_\rho \,\mathrm{Re}\,\mathrm{St}\,\frac{\partial \mathbf{u}}{\partial t}\cdot\boldsymbol{\phi}^{[\mathrm{f}]} + R_\rho\,\mathrm{Re}\,\left[\mathbf{u}\cdot(\nabla\otimes\mathbf{u})\right]\cdot\boldsymbol{\phi}^{[\mathrm{f}]} \right.$$
$$\left. -\mathbf{B}\cdot\boldsymbol{\phi}^{[\mathrm{f}]} - R_\rho\,\frac{\mathrm{Re}}{\mathrm{Fr}}\mathbf{G}\cdot\boldsymbol{\phi}^{[\mathrm{f}]} - (\nabla\cdot\boldsymbol{\tau})\cdot\boldsymbol{\phi}^{[\mathrm{f}]} \right\}\,\mathrm{d}V, \tag{5.16}$$

and we recall from section 3.2 that we require $\mathcal{R}^{[\mathrm{f}]}$ to vanish for any choice of test function. We now make use of the product rule for tensors to rewrite the stress tensor term. The divergence of $\boldsymbol{\tau}\cdot\boldsymbol{\phi}^{[\mathrm{f}]}$ can be written as

$$\nabla\cdot\left(\boldsymbol{\tau}\cdot\boldsymbol{\phi}^{[\mathrm{f}]}\right) = \left[(\nabla\cdot\boldsymbol{\tau})\cdot\boldsymbol{\phi}^{[\mathrm{f}]}\right] + \left[\boldsymbol{\tau} : \left(\nabla\otimes\boldsymbol{\phi}^{[\mathrm{f}]}\right)\right], \tag{5.17}$$

and therefore

$$\iiint_V (\nabla\cdot\boldsymbol{\tau})\cdot\boldsymbol{\phi}^{[\mathrm{f}]}\,\mathrm{d}V = \iiint_V \left\{\nabla\cdot\left(\boldsymbol{\tau}\cdot\boldsymbol{\phi}^{[\mathrm{f}]}\right) - \boldsymbol{\tau} : \left(\nabla\otimes\boldsymbol{\phi}^{[\mathrm{f}]}\right)\right\}\,\mathrm{d}V. \tag{5.18}$$

The divergence theorem states that for any tensor field $\mathbf{T}$,

$$\iiint_V \nabla\cdot\mathbf{T}\,\mathrm{d}V = \iint_S \mathbf{T}\cdot\mathbf{n}\,\mathrm{d}S, \tag{5.19}$$

where S is the surface enclosing the volume V and $\mathbf{n}$ is an outward-pointing unit normal to S [Riley et al., 2002, p. 803], and applying this to the second term in (5.18) gives

$$\iiint_V (\nabla\cdot\boldsymbol{\tau})\cdot\boldsymbol{\phi}^{[\mathrm{f}]}\,\mathrm{d}V = \iint_S \left(\boldsymbol{\tau}\cdot\boldsymbol{\phi}^{[\mathrm{f}]}\right)\cdot\mathbf{n}\,\mathrm{d}S - \iiint_V \boldsymbol{\tau} : \left(\nabla\otimes\boldsymbol{\phi}^{[\mathrm{f}]}\right)\,\mathrm{d}V. \tag{5.20}$$

Substituting (5.20) into (5.16) yields the weak form of the momentum equations in a general orthogonal coordinate system:

$$\mathcal{R}^{[\mathrm{f}]} = \iiint_V \left\{ R_\rho \,\mathrm{Re}\,\mathrm{St}\,\frac{\partial \mathbf{u}}{\partial t}\cdot\boldsymbol{\phi}^{[\mathrm{f}]} + R_\rho\,\mathrm{Re}\,\left[\mathbf{u}\cdot(\nabla\otimes\mathbf{u})\right]\cdot\boldsymbol{\phi}^{[\mathrm{f}]} \right.$$
$$\left. -\mathbf{B}\cdot\boldsymbol{\phi}^{[\mathrm{f}]} - R_\rho\,\frac{\mathrm{Re}}{\mathrm{Fr}}\mathbf{G}\cdot\boldsymbol{\phi}^{[\mathrm{f}]} + \left[\boldsymbol{\tau} : \left(\nabla\otimes\boldsymbol{\phi}^{[\mathrm{f}]}\right)\right] \right\}\,\mathrm{d}V$$
$$- \iint_S \left(\boldsymbol{\tau}\cdot\boldsymbol{\phi}^{[\mathrm{f}]}\right)\cdot\mathbf{n}\,\mathrm{d}S = 0. \tag{5.21}$$

The three momentum equations are obtained by taking the three test functions $\boldsymbol{\phi}^{[\mathrm{f}]} = \phi^{[\mathrm{f}]}\,\mathbf{e}_1$, $\boldsymbol{\phi}^{[\mathrm{f}]} = \phi^{[\mathrm{f}]}\,\mathbf{e}_2$ and $\boldsymbol{\phi}^{[\mathrm{f}]} = \phi^{[\mathrm{f}]}\,\mathbf{e}_3$ and resolving (5.21) into components. We note that if we choose a Cartesian basis where $\mathbf{e}_1 = \mathbf{i}$, $\mathbf{e}_2 = \mathbf{j}$, $\mathbf{e}_3 = \mathbf{k}$ and the gradient operator is therefore defined to be

$$\mathbf{e}_j \frac{\partial}{\partial x_j}, \tag{5.22}$$

then by choosing a test function of the form $\boldsymbol{\phi}^{[\mathrm{f}]} = \phi^{[\mathrm{f}]}\,\mathbf{e}_i$ we recover the form of the momentum equations given in (3.27):

$$\begin{aligned}\mathcal{R}_i^{[\mathrm{f}]} = \iiint_V \Bigg\{ & R_\rho \operatorname{Re}\operatorname{St} \frac{\partial u_i}{\partial t}\,\phi^{[\mathrm{f}]} + R_\rho \operatorname{Re} u_j \frac{\partial u_i}{\partial x_j}\,\phi^{[\mathrm{f}]} \\ & - B_i\,\phi^{[\mathrm{f}]} - R_\rho \frac{\operatorname{Re}}{\operatorname{Fr}} G_i\,\phi^{[\mathrm{f}]} + \tau_{ij}\frac{\partial \phi^{[\mathrm{f}]}}{\partial x_j} \Bigg\}\,\mathrm{d}V \\ & - \iint_S \tau_{ij}\,n_j\,\phi^{[\mathrm{f}]}\,\mathrm{d}S = 0. \end{aligned} \tag{5.23}$$

Obtaining the weak form of the continuity equation is much more straightforward: we multiply the residual form of (5.11) by a (scalar) test function $\phi^{[\mathrm{p}]}$ and integrate over the domain to get

$$\mathcal{R}^{[\mathrm{p}]} = \iiint_V (\nabla\cdot\mathbf{u} - Q)\;\phi^{[\mathrm{p}]}\;\mathrm{d}V. \tag{5.24}$$

Again, we note that by assuming a Cartesian basis we obtain the form of the continuity equation given in (3.25):

$$\mathcal{R}^{[\mathrm{p}]} = \iiint_V \left(\frac{\partial u_j}{\partial x_j} - Q\right)\;\phi^{[\mathrm{p}]}\;\mathrm{d}V. \tag{5.25}$$

5.3 Weak form of the Navier–Stokes equations in cylindrical polar coordinates

Having obtained the weak form of the Navier–Stokes equations in a general orthogonal coordinate system it is straightforward to write them in terms of a cylindrical polar coordinate system in which the radial, axial and azimuthal components are denoted by r, z and θ respectively. The basis vectors for such a coordinate system can be written in terms of the Cartesian basis vectors $\mathbf{i}$, $\mathbf{j}$ and $\mathbf{k}$ in the following way:

$$\begin{aligned} \mathbf{e}_1 &= \mathbf{e}_r &&= \cos\theta\,\mathbf{i} + \sin\theta\,\mathbf{j}, \\ \mathbf{e}_2 &= \mathbf{e}_z &&= \mathbf{k}, \\ \mathbf{e}_3 &= \mathbf{e}_\theta &&= -\sin\theta\,\mathbf{i} + \cos\theta\,\mathbf{j}. \end{aligned} \tag{5.26}$$

From (5.26) it is clear that

$$\frac{\partial \mathbf{e}_r}{\partial \theta} = \mathbf{e}_\theta \qquad \text{and} \qquad \frac{\partial \mathbf{e}_\theta}{\partial \theta} = -\mathbf{e}_r, \tag{5.27}$$

and all other derivatives of the basis vectors with respect to the coordinate directions vanish. The gradient operator is defined to be

$$\nabla = \mathbf{e}_r \frac{\partial}{\partial r} + \mathbf{e}_z \frac{\partial}{\partial z} + \mathbf{e}_\theta \frac{1}{r}\frac{\partial}{\partial \theta}, \tag{5.28}$$

and the tensor product term $\nabla \otimes \mathbf{u}$ is therefore given by

$$\begin{aligned} \nabla \otimes \mathbf{u} &= \left(\mathbf{e}_r \frac{\partial}{\partial r} + \mathbf{e}_z \frac{\partial}{\partial z} + \mathbf{e}_\theta \frac{1}{r}\frac{\partial}{\partial \theta}\right) \otimes (u_r\,\mathbf{e}_r + u_z\,\mathbf{e}_z + u_\theta\,\mathbf{e}_\theta) \\ &= \frac{\partial u_r}{\partial r}\,\mathbf{e}_r \otimes \mathbf{e}_r + \frac{\partial u_z}{\partial r}\,\mathbf{e}_r \otimes \mathbf{e}_z + \frac{\partial u_\theta}{\partial r}\,\mathbf{e}_r \otimes \mathbf{e}_\theta \\ &\quad + \frac{\partial u_r}{\partial z}\,\mathbf{e}_z \otimes \mathbf{e}_r + \frac{\partial u_z}{\partial z}\,\mathbf{e}_z \otimes \mathbf{e}_z + \frac{\partial u_\theta}{\partial z}\,\mathbf{e}_z \otimes \mathbf{e}_\theta \\ &\quad + \left(\frac{1}{r}\frac{\partial u_r}{\partial \theta} - \frac{u_\theta}{r}\right)\mathbf{e}_\theta \otimes \mathbf{e}_r + \frac{1}{r}\frac{\partial u_z}{\partial \theta}\,\mathbf{e}_\theta \otimes \mathbf{e}_z + \left(\frac{1}{r}\frac{\partial u_\theta}{\partial \theta} + \frac{u_r}{r}\right)\mathbf{e}_\theta \otimes \mathbf{e}_\theta. \end{aligned} \tag{5.29}$$

Using (5.29) the stress tensor (5.12) can be written as

$$\begin{aligned} \boldsymbol{\tau} &= \left[-p + 2R_\mu \frac{\partial u_r}{\partial r}\right]\mathbf{e}_r \otimes \mathbf{e}_r + R_\mu \left[\frac{\partial u_z}{\partial r} + \frac{\partial u_r}{\partial z}\right]\mathbf{e}_r \otimes \mathbf{e}_z \\ &\quad + R_\mu \left[\frac{\partial u_\theta}{\partial r} + \frac{1}{r}\frac{\partial u_r}{\partial \theta} - \frac{u_\theta}{r}\right]\mathbf{e}_r \otimes \mathbf{e}_\theta + R_\mu \left[\frac{\partial u_r}{\partial z} + \frac{\partial u_z}{\partial r}\right]\mathbf{e}_z \otimes \mathbf{e}_r \\ &\quad + \left[-p + 2R_\mu \frac{\partial u_z}{\partial z}\right]\mathbf{e}_z \otimes \mathbf{e}_z + R_\mu \left[\frac{\partial u_\theta}{\partial z} + \frac{1}{r}\frac{\partial u_z}{\partial \theta}\right]\mathbf{e}_z \otimes \mathbf{e}_\theta \\ &\quad + R_\mu \left[\frac{1}{r}\frac{\partial u_r}{\partial \theta} - \frac{u_\theta}{r} + \frac{\partial u_\theta}{\partial r}\right]\mathbf{e}_\theta \otimes \mathbf{e}_r + R_\mu \left[\frac{1}{r}\frac{\partial u_z}{\partial \theta} + \frac{\partial u_\theta}{\partial z}\right]\mathbf{e}_\theta \otimes \mathbf{e}_z \\ &\quad + \left[-p + \frac{2R_\mu}{r}\frac{\partial u_\theta}{\partial \theta} + \frac{2R_\mu}{r}u_r\right]\mathbf{e}_\theta \otimes \mathbf{e}_\theta. \end{aligned} \tag{5.30}$$

From (5.14) we note that

$$\mathbf{e}_k \cdot (\mathbf{e}_i \otimes \mathbf{e}_j) = (\mathbf{e}_k \cdot \mathbf{e}_i)\,\mathbf{e}_j, \tag{5.31}$$

where i, j, k is any combination of r, z, θ, and we use this in combination with the fact that the basis vectors are orthogonal,

$$\mathbf{e}_i \cdot \mathbf{e}_j = \delta_{ij} \qquad \forall\, i, j, \tag{5.32}$$

to evaluate the advective term:

$$\begin{aligned} \mathbf{u} \cdot (\nabla \otimes \mathbf{u}) &= \left[u_r \frac{\partial u_r}{\partial r} + u_z \frac{\partial u_r}{\partial z} + \frac{u_\theta}{r}\frac{\partial u_r}{\partial \theta} - \frac{u_\theta^2}{r}\right]\mathbf{e}_r \\ &\quad + \left[u_r \frac{\partial u_z}{\partial r} + u_z \frac{\partial u_z}{\partial z} + \frac{u_\theta}{r}\frac{\partial u_z}{\partial \theta}\right]\mathbf{e}_z \\ &\quad + \left[u_r \frac{\partial u_\theta}{\partial r} + u_z \frac{\partial u_\theta}{\partial z} + \frac{u_\theta}{r}\frac{\partial u_\theta}{\partial \theta} + \frac{u_r u_\theta}{r}\right]\mathbf{e}_\theta. \end{aligned} \tag{5.33}$$

The three individual momentum equations are now obtained by taking the three test functions $\boldsymbol{\phi}^{[\mathrm{f}]} = \phi^{[\mathrm{f}]}\,\mathbf{e}_r$, $\boldsymbol{\phi}^{[\mathrm{f}]} = \phi^{[\mathrm{f}]}\,\mathbf{e}_z$ and $\boldsymbol{\phi}^{[\mathrm{f}]} = \phi^{[\mathrm{f}]}\,\mathbf{e}_\theta$ and resolving (5.21) into components.

Radial momentum equation ($\boldsymbol{\phi}^{[\mathrm{f}]} = \phi^{[\mathrm{f}]}\,\mathbf{e}_r$):

If we assume a test function of the form $\boldsymbol{\phi}^{[\mathrm{f}]} = \phi^{[\mathrm{f}]}\,\mathbf{e}_r$, the tensor product term $\nabla \otimes \boldsymbol{\phi}^{[\mathrm{f}]}$ is given by

$$\nabla \otimes \left(\phi^{[\mathrm{f}]}\,\mathbf{e}_r\right) = \frac{\partial \phi^{[\mathrm{f}]}}{\partial r}\,\mathbf{e}_r \otimes \mathbf{e}_r + \frac{\partial \phi^{[\mathrm{f}]}}{\partial z}\,\mathbf{e}_z \otimes \mathbf{e}_r + \frac{1}{r}\frac{\partial \phi^{[\mathrm{f}]}}{\partial \theta}\,\mathbf{e}_\theta \otimes \mathbf{e}_r + \frac{\phi^{[\mathrm{f}]}}{r}\,\mathbf{e}_\theta \otimes \mathbf{e}_\theta, \quad (5.34)$$

and from (5.15) and (5.32) we note that

$$(\mathbf{e}_i \otimes \mathbf{e}_j) : (\mathbf{e}_k \otimes \mathbf{e}_l) \quad (5.35)$$

is only non-zero if $i = l$ and $j = k$. Therefore using (5.30) we have

$$\begin{aligned}\boldsymbol{\tau} : \left[\nabla \otimes \left(\phi^{[\mathrm{f}]}\,\mathbf{e}_r\right)\right] = &\left[-p + 2R_\mu \frac{\partial u_r}{\partial r}\right]\frac{\partial \phi^{[\mathrm{f}]}}{\partial r} + R_\mu\left[\frac{\partial u_z}{\partial r} + \frac{\partial u_r}{\partial z}\right]\frac{\partial \phi^{[\mathrm{f}]}}{\partial z} \\ &+ R_\mu\left[\frac{\partial u_\theta}{\partial r} + \frac{1}{r}\frac{\partial u_r}{\partial \theta} - \frac{u_\theta}{r}\right]\frac{1}{r}\frac{\partial \phi^{[\mathrm{f}]}}{\partial \theta} + \left[-p + \frac{2R_\mu}{r}\frac{\partial u_\theta}{\partial \theta} + \frac{2R_\mu}{r}u_r\right]\frac{\phi^{[\mathrm{f}]}}{r}. \quad (5.36)\end{aligned}$$

From (5.13) we note that

$$(\mathbf{e}_i \otimes \mathbf{e}_j) \cdot \mathbf{e}_k = \mathbf{e}_i\,(\mathbf{e}_j \cdot \mathbf{e}_k) \quad (5.37)$$

where i, j, k is any combination of r, z, θ, and we use this in combination with (5.32) to evaluate the $\left(\boldsymbol{\tau} \cdot \boldsymbol{\phi}^{[\mathrm{f}]}\right)$ term:

$$\begin{aligned}\boldsymbol{\tau} \cdot \left(\phi^{[\mathrm{f}]}\,\mathbf{e}_r\right) = \phi^{[\mathrm{f}]}\Bigg\{&\left[-p + 2R_\mu \frac{\partial u_r}{\partial r}\right]\mathbf{e}_r + R_\mu\left[\frac{\partial u_r}{\partial z} + \frac{\partial u_z}{\partial r}\right]\mathbf{e}_z \\ &+ R_\mu\left[\frac{1}{r}\frac{\partial u_r}{\partial \theta} - \frac{u_\theta}{r} + \frac{\partial u_\theta}{\partial r}\right]\mathbf{e}_\theta\Bigg\}. \quad (5.38)\end{aligned}$$

Therefore we have

$$\left[\boldsymbol{\tau} \cdot \left(\phi^{[\mathrm{f}]}\,\mathbf{e}_r\right)\right] \cdot \mathbf{n} = \phi^{[\mathrm{f}]}\left(\tau_{rr}\,n_r + \tau_{rz}\,n_z + \tau_{r\theta}\,n_\theta\right), \quad (5.39)$$

where τ_{rr}, τ_{rz} and $\tau_{r\theta}$ are defined in (5.5). Finally, we substitute (5.33), (5.36) and (5.39) into (5.21) to write down the radial momentum equation:

$$\begin{aligned}\mathcal{R}_{\mathrm{r}}^{[\mathrm{f}]} = \iiint_V \Bigg\{ & R_\rho \,\mathrm{Re}\,\mathrm{St}\,\frac{\partial u_r}{\partial t}\phi^{[\mathrm{f}]} + R_\rho \,\mathrm{Re}\,\left[u_r\frac{\partial u_r}{\partial r} + u_z\frac{\partial u_r}{\partial z} + \frac{u_\theta}{r}\frac{\partial u_r}{\partial \theta} - \frac{u_\theta^2}{r}\right]\phi^{[\mathrm{f}]} \\ & - B_r\,\phi^{[\mathrm{f}]} - R_\rho\,\frac{\mathrm{Re}}{\mathrm{Fr}}G_r\,\phi^{[\mathrm{f}]} + \left[-p + 2R_\mu\frac{\partial u_r}{\partial r}\right]\frac{\partial \phi^{[\mathrm{f}]}}{\partial r} + R_\mu\left[\frac{\partial u_z}{\partial r} + \frac{\partial u_r}{\partial z}\right]\frac{\partial \phi^{[\mathrm{f}]}}{\partial z} \\ & + R_\mu\left[\frac{\partial u_\theta}{\partial r} + \frac{1}{r}\frac{\partial u_r}{\partial \theta} - \frac{u_\theta}{r}\right]\frac{1}{r}\frac{\partial \phi^{[\mathrm{f}]}}{\partial \theta} + \left[-p + \frac{2R_\mu}{r}\frac{\partial u_\theta}{\partial \theta} + \frac{2R_\mu}{r}u_r\right]\frac{\phi^{[\mathrm{f}]}}{r}\Bigg\}\,\mathrm{d}V \\ & - \iint_S \Big[\tau_{rr}\,n_r + \tau_{rz}\,n_z + \tau_{r\theta}\,n_\theta\Big]\phi^{[\mathrm{f}]}\,\mathrm{d}S = 0. \end{aligned} \tag{5.40}$$

Axial momentum equation ($\boldsymbol{\phi}^{[\mathrm{f}]} = \phi^{[\mathrm{f}]}\,\mathbf{e}_z$):

If we assume a test function of the form $\boldsymbol{\phi}^{[\mathrm{f}]} = \phi^{[\mathrm{f}]}\,\mathbf{e}_z$, the tensor product term $\nabla \otimes \boldsymbol{\phi}^{[\mathrm{f}]}$ is given by

$$\nabla \otimes \left(\phi^{[\mathrm{f}]}\,\mathbf{e}_z\right) = \frac{\partial \phi^{[\mathrm{f}]}}{\partial r}\,\mathbf{e}_r \otimes \mathbf{e}_z + \frac{\partial \phi^{[\mathrm{f}]}}{\partial z}\,\mathbf{e}_z \otimes \mathbf{e}_z + \frac{1}{r}\frac{\partial \phi^{[\mathrm{f}]}}{\partial \theta}\,\mathbf{e}_\theta \otimes \mathbf{e}_z, \tag{5.41}$$

and using (5.30) and (5.35) we have

$$\begin{aligned}\boldsymbol{\tau} : \left[\nabla \otimes \left(\phi^{[\mathrm{f}]}\,\mathbf{e}_z\right)\right] = {} & R_\mu\left[\frac{\partial u_r}{\partial z} + \frac{\partial u_z}{\partial r}\right]\frac{\partial \phi^{[\mathrm{f}]}}{\partial r} + \left[-p + 2R_\mu\frac{\partial u_z}{\partial z}\right]\frac{\partial \phi^{[\mathrm{f}]}}{\partial z} \\ & + R_\mu\left[\frac{\partial u_\theta}{\partial z} + \frac{1}{r}\frac{\partial u_z}{\partial \theta}\right]\frac{1}{r}\frac{\partial \phi^{[\mathrm{f}]}}{\partial \theta}. \end{aligned} \tag{5.42}$$

We use (5.37) and (5.32) to evaluate

$$\begin{aligned}\boldsymbol{\tau} \cdot \left(\phi^{[\mathrm{f}]}\,\mathbf{e}_z\right) = \phi^{[\mathrm{f}]}\Bigg\{ & R_\mu\left[\frac{\partial u_z}{\partial r} + \frac{\partial u_r}{\partial z}\right]\mathbf{e}_r + \left[-p + 2R_\mu\frac{\partial u_z}{\partial z}\right]\mathbf{e}_z \\ & + R_\mu\left[\frac{1}{r}\frac{\partial u_z}{\partial \theta} + \frac{\partial u_\theta}{\partial z}\right]\mathbf{e}_\theta\Bigg\}, \end{aligned} \tag{5.43}$$

and therefore we have

$$\left[\boldsymbol{\tau} \cdot \left(\phi^{[\mathrm{f}]}\,\mathbf{e}_z\right)\right] \cdot \mathbf{n} = \phi^{[\mathrm{f}]}\left(\tau_{zr}\,n_r + \tau_{zz}\,n_z + \tau_{z\theta}\,n_\theta\right), \tag{5.44}$$

where τ_{zr}, τ_{zz} and $\tau_{z\theta}$ are defined in (5.5). Finally, we substitute (5.33), (5.42) and (5.44) into (5.21) to write down the axial momentum equation:

$$\begin{aligned}\mathcal{R}_{\mathrm{z}}^{[\mathrm{f}]} = \iiint_V \Bigg\{ & R_\rho \,\mathrm{Re}\,\mathrm{St}\,\frac{\partial u_z}{\partial t}\phi^{[\mathrm{f}]} + R_\rho \,\mathrm{Re}\,\left[u_r\frac{\partial u_z}{\partial r} + u_z\frac{\partial u_z}{\partial z} + \frac{u_\theta}{r}\frac{\partial u_z}{\partial \theta}\right]\phi^{[\mathrm{f}]} \\ & - B_z\,\phi^{[\mathrm{f}]} - R_\rho\,\frac{\mathrm{Re}}{\mathrm{Fr}}G_z\,\phi^{[\mathrm{f}]} + R_\mu\left[\frac{\partial u_r}{\partial z} + \frac{\partial u_z}{\partial r}\right]\frac{\partial \phi^{[\mathrm{f}]}}{\partial r} \\ & + \left[-p + 2R_\mu\frac{\partial u_z}{\partial z}\right]\frac{\partial \phi^{[\mathrm{f}]}}{\partial z} + R_\mu\left[\frac{\partial u_\theta}{\partial z} + \frac{1}{r}\frac{\partial u_z}{\partial \theta}\right]\frac{1}{r}\frac{\partial \phi^{[\mathrm{f}]}}{\partial \theta}\Bigg\}\,\mathrm{d}V \\ & - \iint_S \Big[\tau_{zr}\,n_r + \tau_{zz}\,n_z + \tau_{z\theta}\,n_\theta\Big]\phi^{[\mathrm{f}]}\,\mathrm{d}S = 0. \quad (5.45)\end{aligned}$$

Azimuthal momentum equation ($\boldsymbol{\phi}^{[\mathbf{f}]} = \phi^{[\mathbf{f}]}\,\mathbf{e}_\theta$):

If we assume a test function of the form $\boldsymbol{\phi}^{[\mathrm{f}]} = \phi^{[\mathrm{f}]}\,\mathbf{e}_\theta$, the tensor product term $\nabla \otimes \boldsymbol{\phi}^{[\mathrm{f}]}$ is given by

$$\nabla \otimes \left(\phi^{[\mathrm{f}]}\,\mathbf{e}_\theta\right) = \frac{\partial \phi^{[\mathrm{f}]}}{\partial r}\,\mathbf{e}_r \otimes \mathbf{e}_\theta + \frac{\partial \phi^{[\mathrm{f}]}}{\partial z}\,\mathbf{e}_z \otimes \mathbf{e}_\theta + \frac{1}{r}\frac{\partial \phi^{[\mathrm{f}]}}{\partial \theta}\,\mathbf{e}_\theta \otimes \mathbf{e}_\theta - \frac{\phi^{[\mathrm{f}]}}{r}\,\mathbf{e}_\theta \otimes \mathbf{e}_r, \quad (5.46)$$

and using (5.30) and (5.35) we have

$$\begin{aligned}\boldsymbol{\tau} : \left[\nabla \otimes \left(\phi^{[\mathrm{f}]}\,\mathbf{e}_\theta\right)\right] = {} & R_\mu\left[\frac{1}{r}\frac{\partial u_r}{\partial \theta} - \frac{u_\theta}{r} + \frac{\partial u_\theta}{\partial r}\right]\frac{\partial \phi^{[\mathrm{f}]}}{\partial r} + R_\mu\left[\frac{1}{r}\frac{\partial u_z}{\partial \theta} + \frac{\partial u_\theta}{\partial z}\right]\frac{\partial \phi^{[\mathrm{f}]}}{\partial z} \\ & + \left[-p + \frac{2R_\mu}{r}\frac{\partial u_\theta}{\partial \theta} + \frac{2R_\mu}{r}u_r\right]\frac{1}{r}\frac{\partial \phi^{[\mathrm{f}]}}{\partial \theta} - R_\mu\left[\frac{\partial u_\theta}{\partial r} + \frac{1}{r}\frac{\partial u_r}{\partial \theta} - \frac{u_\theta}{r}\right]\frac{\phi^{[\mathrm{f}]}}{r}. \quad (5.47)\end{aligned}$$

We use (5.37) and (5.32) to evaluate

$$\begin{aligned}\boldsymbol{\tau} \cdot \left(\phi^{[\mathrm{f}]}\,\mathbf{e}_\theta\right) = \phi^{[\mathrm{f}]}\Bigg\{ & R_\mu\left[\frac{\partial u_\theta}{\partial r} + \frac{1}{r}\frac{\partial u_r}{\partial \theta} - \frac{u_\theta}{r}\right]\mathbf{e}_r + R_\mu\left[\frac{\partial u_\theta}{\partial z} + \frac{1}{r}\frac{\partial u_z}{\partial \theta}\right]\mathbf{e}_z \\ & + \left[-p + \frac{2R_\mu}{r}\frac{\partial u_\theta}{\partial \theta} + \frac{2R_\mu}{r}u_r\right]\mathbf{e}_\theta\Bigg\}, \quad (5.48)\end{aligned}$$

and therefore we have

$$\left[\boldsymbol{\tau} \cdot \left(\phi^{[\mathrm{f}]}\,\mathbf{e}_\theta\right)\right] \cdot \mathbf{n} = \phi^{[\mathrm{f}]}\left(\tau_{\theta r}\,n_r + \tau_{\theta z}\,n_z + \tau_{\theta\theta}\,n_\theta\right), \quad (5.49)$$

where $\tau_{\theta r}$, $\tau_{\theta z}$ and $\tau_{\theta\theta}$ are defined in (5.5). Finally, we substitute (5.33), (5.47) and (5.49) into (5.21) to write down the azimuthal momentum equation:

$$\begin{aligned}\mathcal{R}_{\theta}^{[\mathrm{f}]} = \iiint_V \Bigg\{ & R_\rho \,\mathrm{Re}\,\mathrm{St}\,\frac{\partial u_\theta}{\partial t}\phi^{[\mathrm{f}]} + R_\rho \,\mathrm{Re}\,\left[u_r\frac{\partial u_\theta}{\partial r} + u_z\frac{\partial u_\theta}{\partial z} + \frac{u_\theta}{r}\frac{\partial u_\theta}{\partial \theta} + \frac{u_r u_\theta}{r}\right]\phi^{[\mathrm{f}]} \\ & - B_\theta\,\phi^{[\mathrm{f}]} - R_\rho\,\frac{\mathrm{Re}}{\mathrm{Fr}}G_\theta\,\phi^{[\mathrm{f}]} + R_\mu\left[\frac{1}{r}\frac{\partial u_r}{\partial\theta} - \frac{u_\theta}{r} + \frac{\partial u_\theta}{\partial r}\right]\frac{\partial\phi^{[\mathrm{f}]}}{\partial r} \\ & + R_\mu\left[\frac{1}{r}\frac{\partial u_z}{\partial\theta} + \frac{\partial u_\theta}{\partial z}\right]\frac{\partial\phi^{[\mathrm{f}]}}{\partial z} + \left[-p + \frac{2R_\mu}{r}\frac{\partial u_\theta}{\partial\theta} + \frac{2R_\mu}{r}u_r\right]\frac{1}{r}\frac{\partial\phi^{[\mathrm{f}]}}{\partial\theta} \\ & - R_\mu\left[\frac{\partial u_\theta}{\partial r} + \frac{1}{r}\frac{\partial u_r}{\partial\theta} - \frac{u_\theta}{r}\right]\frac{\phi^{[\mathrm{f}]}}{r}\Bigg\}\,\mathrm{d}V \\ & - \iint_S \Big[\tau_{\theta r}\,n_r + \tau_{\theta z}\,n_z + \tau_{\theta\theta}\,n_\theta\Big]\phi^{[\mathrm{f}]}\,\mathrm{d}S = 0. \quad (5.50)\end{aligned}$$

Continuity equation:

From (5.24) and (5.28) we obtain the weak form of the continuity equation in a cylindrical polar coordinate system:

$$\mathcal{R}^{[\mathrm{p}]} = \iiint_V \left(\frac{\partial u_r}{\partial r} + \frac{u_r}{r} + \frac{\partial u_z}{\partial z} + \frac{1}{r}\frac{\partial u_\theta}{\partial\theta} - Q\right)\phi^{[\mathrm{p}]}\,\mathrm{d}V. \quad (5.51)$$

5.4 Weak form of the free surface boundary conditions in a general orthogonal coordinate system

In this section we shall derive the weak form of the conditions at a free boundary for a general orthogonal coordinate system. In this case it is convenient to employ tensor formulation, and therefore we begin by considering a general coordinate system ξ^i in three dimensions ($i = 1, 2, 3$). If $\mathbf{x}(\xi^1, \xi^2, \xi^3)$ is the position vector then the covariant base vectors are defined as

$$\mathbf{g}_i = \frac{\partial \mathbf{x}}{\partial \xi^i}, \quad (5.52)$$

and a vector $\mathbf{v}$ can be written in the covariant basis as

$$\mathbf{v} = v^i\,\mathbf{g}_i = v^1\frac{\partial\mathbf{x}}{\partial\xi^1} + v^2\frac{\partial\mathbf{x}}{\partial\xi^2} + v^3\frac{\partial\mathbf{x}}{\partial\xi^3}, \quad (5.53)$$

where v^1, v^2, v^3 are the contravariant components of $\mathbf{v}$ [Riley et al., 2002, pp. 370-2]. The covariant components of the metric tensor $\mathbf{g}$ are defined by

$$g_{ij} = \mathbf{g}_i \cdot \mathbf{g}_j, \quad (5.54)$$

and we then define the contravariant components of $\mathbf{g}$ such that $g^{ik}\, g_{kj} = \delta^i_j$, the identity matrix. From this it follows that the contravariant base vectors can be found using

$$\mathbf{g}^i = g^{ij}\, \mathbf{g}_j, \tag{5.55}$$

and the same vector $\mathbf{v}$ can therefore be written in the contravariant basis as

$$\mathbf{v} = v_i\, \mathbf{g}^i, \tag{5.56}$$

where v_1, v_2, v_3 are the covariant components of $\mathbf{v}$ [Riley et al., 2002, pp. 806-8].

Let us now consider a (two-dimensional) free surface described by the vector $\mathbf{X}(\zeta^1, \zeta^2)$, where ζ^α are two intrinsic coordinates that parametrise the surface. The covariant base vectors of the surface are then

$$\mathbf{a}_\alpha = \frac{\partial \mathbf{X}}{\partial \zeta^\alpha} \tag{5.57}$$

and the covariant components of the metric surface tensor $\mathbf{a}$ are

$$a_{\alpha\beta} = \mathbf{a}_\alpha \cdot \mathbf{a}_\beta. \tag{5.58}$$

As before the contravariant components of $\mathbf{a}$ are defined such that $a^{\alpha\gamma}\, a_{\gamma\beta} = \delta^\alpha_\beta$, and the contravariant base vectors of the surface are given by

$$\mathbf{a}^\alpha = a^{\alpha\beta}\, \mathbf{a}_\beta. \tag{5.59}$$

The dynamic condition

From (3.18) we have the dynamic boundary condition in the case where the fluid 'above' the free surface is considered to be totally inviscid

$$\tau^{ij}\, n_j = \frac{\kappa}{\mathrm{Ca}}\, n^i - p_{\mathrm{ext}}\, n^i, \tag{5.60}$$

where τ^{ij} are the contravariant components of the stress tensor and $\mathbf{n} = n^i\, \mathbf{g}_i = n_j\, \mathbf{g}^j$ is the (unit) normal vector to the surface written in terms of the global base vectors. Multiplying by a (scalar) test function $\phi^{[\mathrm{f}]}$ and integrating over the surface Ω yields

$$\iint_\Omega \tau^{ij}\, n_j\, \phi^{[\mathrm{f}]}\, \mathrm{d}S = \frac{1}{\mathrm{Ca}} \iint_\Omega \kappa\, n^i\, \phi^{[\mathrm{f}]}\, \mathrm{d}S - \iint_\Omega p_{\mathrm{ext}}\, n^i\, \phi^{[\mathrm{f}]}\, \mathrm{d}S, \tag{5.61}$$

and, as discussed in section 3.2.1, this condition can be used in the surface integral of the normal stress, provided that the stress-divergence form of the bulk equations is

used. If we express the i-th momentum equation ($i = 1, 2, 3$) as a sum of bulk terms, $\mathcal{R}_i^{[\text{f,bulk}]}$, terms arising from integrals over the free surface, $\mathcal{R}_i^{[\text{f,fs}]}$, and terms arising from integrals over the rest of the domain boundary, $\mathcal{R}_i^{[\text{f,non-fs}]}$, so that

$$\mathcal{R}_i^{[\text{f}]} = \mathcal{R}_i^{[\text{f,bulk}]} + \mathcal{R}_i^{[\text{f,fs}]} + \mathcal{R}_i^{[\text{f,non-fs}]}, \tag{5.62}$$

then the integral over the free surface can be written as

$$\mathcal{R}_i^{[\text{f,fs}]} = \frac{1}{\text{Ca}} \iint_\Omega \kappa\, n^i\, \phi^{[\text{f}]}\, \mathrm{d}S - \iint_\Omega p_{\text{ext}}\, n^i\, \phi^{[\text{f}]}\, \mathrm{d}S. \tag{5.63}$$

From [Green and Zerna, 1954, eqns. 1.13.34 and 1.13.47] we have that the product of the mean curvature of the surface with the normal vector is given by

$$\kappa\, \mathbf{n} = \frac{\partial \mathbf{a}^\alpha}{\partial \zeta^\alpha} + \bar{\Gamma}^\alpha_{\alpha\beta}\, \mathbf{a}^\beta, \tag{5.64}$$

where $\bar{\Gamma}$ is the Christoffel symbol of the second kind with respect to the surface and, using [Green and Zerna, 1954, eqn. 1.13.36], can be expressed in terms of the components of the metric surface tensor:

$$\bar{\Gamma}^\alpha_{\alpha\beta} = \frac{1}{2} a^{\alpha\gamma} \left(\frac{\partial a_{\alpha\gamma}}{\partial \zeta^\beta} + \frac{\partial a_{\beta\gamma}}{\partial \zeta^\alpha} - \frac{\partial a_{\alpha\beta}}{\partial \zeta^\gamma} \right) = \frac{1}{2} a^{\alpha\gamma} \frac{\partial a_{\alpha\gamma}}{\partial \zeta^\beta}. \tag{5.65}$$

If a is the determinant of the metric surface tensor then it follows that

$$\frac{\partial a}{\partial a_{\alpha\beta}} = a\, a^{\alpha\beta} \tag{5.66}$$

and

$$\frac{\partial \sqrt{a}}{\partial \zeta^\alpha} = \frac{1}{2\sqrt{a}} \frac{\partial a}{\partial \zeta^\alpha}. \tag{5.67}$$

Using these identities in (5.65) we have

$$\bar{\Gamma}^\alpha_{\alpha\beta} = \frac{1}{2a} \frac{\partial a}{\partial a_{\alpha\gamma}} \frac{\partial a_{\alpha\gamma}}{\partial \zeta^\beta} = \frac{1}{2a} \frac{\partial a}{\partial \zeta^\beta} = \frac{1}{\sqrt{a}} \frac{\partial \sqrt{a}}{\partial \zeta^\beta}, \tag{5.68}$$

which allows us to rewrite (5.64) as

$$\kappa\, \mathbf{n} = \frac{1}{\sqrt{a}} \frac{\partial \left(\sqrt{a}\, \mathbf{a}^\alpha \right)}{\partial \zeta^\alpha}. \tag{5.69}$$

The components of the normal vector in the global covariant basis are found by taking the scalar product of $\mathbf{n}$ with the global contravariant base vectors,

$$\kappa\, n^i = \frac{1}{\sqrt{a}} \frac{\partial \left(\sqrt{a}\, \mathbf{a}^\alpha \right)}{\partial \zeta^\alpha} \cdot \mathbf{g}^i, \tag{5.70}$$

and by using the product rule on $\frac{\partial}{\partial\zeta^\alpha}\left(\sqrt{a}\,\mathbf{a}^\alpha\cdot\mathbf{g}^i\,\phi^{[\mathrm{f}]}\right)$ we have

$$\frac{1}{\mathrm{Ca}}\iint_\Omega \kappa\, n^i\,\phi^{[\mathrm{f}]}\,\mathrm{d}S = \frac{1}{\mathrm{Ca}}\iint_\Omega \frac{1}{\sqrt{a}}\frac{\partial\left(\sqrt{a}\,\mathbf{a}^\alpha\cdot\mathbf{g}^i\,\phi^{[\mathrm{f}]}\right)}{\partial\zeta^\alpha}\,\mathrm{d}S - \frac{1}{\mathrm{Ca}}\iint_\Omega \mathbf{a}^\alpha\cdot\frac{\partial\mathbf{g}^i}{\partial\zeta^\alpha}\,\phi^{[\mathrm{f}]}\,\mathrm{d}S - \frac{1}{\mathrm{Ca}}\iint_\Omega \mathbf{a}^\alpha\cdot\mathbf{g}^i\,\frac{\partial\phi^{[\mathrm{f}]}}{\partial\zeta^\alpha}\,\mathrm{d}S. \quad (5.71)$$

The surface divergence theorem is given by [Green and Zerna, 1954, eqn. 1.13.61], which states that if $\mathbf{u} = u_\alpha\,\mathbf{a}^\alpha$ is the unit outward normal *in the surface* Ω to the closed curve $\partial\Omega$ that marks the surface's boundary, then

$$\iint_\Omega \frac{1}{\sqrt{a}}\frac{\partial\left(\sqrt{a}\,v^\alpha\right)}{\partial\zeta^\alpha}\,\mathrm{d}S = \oint_{\partial\Omega} u_\alpha\,v^\alpha\,\mathrm{d}\lambda, \quad (5.72)$$

where $\mathbf{v} = v^\alpha\,\mathbf{a}_\alpha$ is any vector in Ω. Applying (5.72) to the first integral in the right-hand side of (5.71) gives

$$\frac{1}{\mathrm{Ca}}\iint_\Omega \kappa\, n^i\,\phi^{[\mathrm{f}]}\,\mathrm{d}S = \frac{1}{\mathrm{Ca}}\oint_{\partial\Omega} u_\alpha\,\mathbf{a}^\alpha\cdot\mathbf{g}^i\,\phi^{[\mathrm{f}]}\,\mathrm{d}\lambda - \frac{1}{\mathrm{Ca}}\iint_\Omega \mathbf{a}^\alpha\cdot\frac{\partial\mathbf{g}^i}{\partial\zeta^\alpha}\,\phi^{[\mathrm{f}]}\,\mathrm{d}S - \frac{1}{\mathrm{Ca}}\iint_\Omega \mathbf{a}^\alpha\cdot\mathbf{g}^i\,\frac{\partial\phi^{[\mathrm{f}]}}{\partial\zeta^\alpha}\,\mathrm{d}S, \quad (5.73)$$

and we note that

$$u_\alpha\,\mathbf{a}^\alpha\cdot\mathbf{g}^i = \mathbf{u}\cdot\mathbf{g}^i = m^i, \quad (5.74)$$

where m^i are the components of the outward normal to $\partial\Omega$ in the *global* covariant basis. The unit vector $\mathbf{m} = m^i\,\mathbf{g}_i$ is therefore tangent to the surface Ω and normal to its bounding curve $\partial\Omega$. The final integrand of (5.73) can alternatively be expressed as

$$\left(\mathbf{a}^\alpha\,\frac{\partial\phi^{[\mathrm{f}]}}{\partial\zeta^\alpha}\right)\cdot\mathbf{g}^i = \left(\mathbf{a}^1\,\frac{\partial\phi^{[\mathrm{f}]}}{\partial\zeta^1} + \mathbf{a}^2\,\frac{\partial\phi^{[\mathrm{f}]}}{\partial\zeta^2}\right)\cdot\mathbf{g}^i, \quad (5.75)$$

and then (5.59) is used to write the terms on the left-hand side of the scalar product in (5.75) in the covariant basis,

$$\left(a^{11}\,\mathbf{a}_1 + a^{12}\,\mathbf{a}_2\right)\frac{\partial\phi^{[\mathrm{f}]}}{\partial\zeta^1} + \left(a^{21}\,\mathbf{a}_1 + a^{22}\,\mathbf{a}_2\right)\frac{\partial\phi^{[\mathrm{f}]}}{\partial\zeta^2}. \quad (5.76)$$

Using $a^{\alpha\gamma}\,a_{\gamma\beta} = \delta^\alpha_\beta$ it is straightforward to show that

$$a^{11}\,a = a_{22}, \qquad a^{12}\,a = -a_{12}, \qquad a^{21}\,a = -a_{21} \qquad \text{and} \qquad a^{22}\,a = a_{11}, \quad (5.77)$$

and hence (5.76) becomes

$$\frac{\mathbf{a}_1}{a}\left(a_{22}\,\frac{\partial\phi^{[\mathrm{f}]}}{\partial\zeta^1} - a_{21}\,\frac{\partial\phi^{[\mathrm{f}]}}{\partial\zeta^2}\right) + \frac{\mathbf{a}_2}{a}\left(a_{11}\,\frac{\partial\phi^{[\mathrm{f}]}}{\partial\zeta^2} - a_{12}\,\frac{\partial\phi^{[\mathrm{f}]}}{\partial\zeta^1}\right). \quad (5.78)$$

Using (5.74), (5.75), (5.78) and (5.73) gives

$$\frac{1}{\mathrm{Ca}}\iint_\Omega \kappa\, n^i\, \phi^{[\mathrm{f}]}\,\mathrm{d}S = \frac{1}{\mathrm{Ca}}\oint_{\partial\Omega} m^i\,\phi^{[\mathrm{f}]}\,\mathrm{d}\lambda - \frac{1}{\mathrm{Ca}}\iint_\Omega \mathbf{a}^\alpha\cdot\frac{\partial\mathbf{g}^i}{\partial\zeta^\alpha}\,\phi^{[\mathrm{f}]}\,\mathrm{d}S$$
$$-\frac{1}{\mathrm{Ca}}\iint_\Omega \frac{1}{a}\left[\mathbf{g}^i\cdot\mathbf{a}_1\left(a_{22}\frac{\partial\phi^{[\mathrm{f}]}}{\partial\zeta^1}-a_{21}\frac{\partial\phi^{[\mathrm{f}]}}{\partial\zeta^2}\right)+\mathbf{g}^i\cdot\mathbf{a}_2\left(a_{11}\frac{\partial\phi^{[\mathrm{f}]}}{\partial\zeta^2}-a_{12}\frac{\partial\phi^{[\mathrm{f}]}}{\partial\zeta^1}\right)\right]\mathrm{d}S, \tag{5.79}$$

and this can now be combined with (5.63) to write the integral over the free surface as

$$\mathcal{R}_i^{[\mathrm{f,fs}]} = -\iint_\Omega p_{\mathrm{ext}}\, n^i\,\phi^{[\mathrm{f}]}\,\mathrm{d}S + \frac{1}{\mathrm{Ca}}\oint_{\partial\Omega} m^i\,\phi^{[\mathrm{f}]}\,\mathrm{d}\lambda - \frac{1}{\mathrm{Ca}}\iint_\Omega \mathbf{a}^\alpha\cdot\frac{\partial\mathbf{g}^i}{\partial\zeta^\alpha}\,\phi^{[\mathrm{f}]}\,\mathrm{d}S$$
$$-\frac{1}{\mathrm{Ca}}\iint_\Omega \frac{1}{a}\left[\mathbf{g}^i\cdot\mathbf{a}_1\left(a_{22}\frac{\partial\phi^{[\mathrm{f}]}}{\partial\zeta^1}-a_{21}\frac{\partial\phi^{[\mathrm{f}]}}{\partial\zeta^2}\right)+\mathbf{g}^i\cdot\mathbf{a}_2\left(a_{11}\frac{\partial\phi^{[\mathrm{f}]}}{\partial\zeta^2}-a_{12}\frac{\partial\phi^{[\mathrm{f}]}}{\partial\zeta^1}\right)\right]\mathrm{d}S. \tag{5.80}$$

The kinematic condition

If we write the velocity $\mathbf{u}$ and the position vector to the free surface $\mathbf{X}$ in terms of the global contravariant basis,

$$\mathbf{u} = u_i\,\mathbf{g}^i \qquad \text{and} \qquad \mathbf{X} = X_i\,\mathbf{g}^i, \tag{5.81}$$

then the kinematic boundary condition (5.8) is given by

$$u_i\,n^i - \mathrm{St}\,\frac{\partial X_i}{\partial t}\,n^i = 0. \tag{5.82}$$

The weighted residual is therefore found by multiplying by a test function $\phi^{[\mathrm{f}]}$ and integrating over the surface Ω to give

$$\mathcal{R}^{[\mathrm{h}]} = \iint_\Omega \left(u_i\,n^i - \mathrm{St}\,\frac{\partial X_i}{\partial t}\,n^i\right)\phi^{[\mathrm{f}]}\,\mathrm{d}S \tag{5.83}$$

5.5 Specialisation to axisymmetric flows

5.5.1 Governing equations

We shall now consider the weak form of the governing equations for the special case of an axisymmetric flow that is independent of θ, and hence u_r, u_z, u_θ and p are functions

of r, z and t only. The weak form of the radial, axial and azimuthal momentum equations therefore become

$$\begin{aligned}\mathcal{R}_{\mathrm{r}}^{[\mathrm{f}]} = \iiint_V \Bigg\{ & R_\rho \,\mathrm{Re}\,\mathrm{St}\,\frac{\partial u_r}{\partial t}\phi^{[\mathrm{f}]} + R_\rho \,\mathrm{Re}\,\left[u_r\frac{\partial u_r}{\partial r} + u_z\frac{\partial u_r}{\partial z} - \frac{u_\theta^2}{r}\right]\phi^{[\mathrm{f}]} \\ & - B_r\,\phi^{[\mathrm{f}]} - R_\rho\,\frac{\mathrm{Re}}{\mathrm{Fr}}G_r\,\phi^{[\mathrm{f}]} + \left[-p + 2R_\mu\frac{\partial u_r}{\partial r}\right]\frac{\partial \phi^{[\mathrm{f}]}}{\partial r} \\ & + R_\mu\left[\frac{\partial u_z}{\partial r} + \frac{\partial u_r}{\partial z}\right]\frac{\partial \phi^{[\mathrm{f}]}}{\partial z} + \left[-p + \frac{2R_\mu}{r}u_r\right]\frac{\phi^{[\mathrm{f}]}}{r}\Bigg\}\,\mathrm{d}V \\ & - \iint_S \Big[\tau_{rr}\,n_r + \tau_{rz}\,n_z + \tau_{r\theta}\,n_\theta\Big]\phi^{[\mathrm{f}]}\,\mathrm{d}S = 0, \end{aligned} \tag{5.84}$$

$$\begin{aligned}\mathcal{R}_{\mathrm{z}}^{[\mathrm{f}]} = \iiint_V \Bigg\{ & R_\rho \,\mathrm{Re}\,\mathrm{St}\,\frac{\partial u_z}{\partial t}\phi^{[\mathrm{f}]} + R_\rho \,\mathrm{Re}\,\left[u_r\frac{\partial u_z}{\partial r} + u_z\frac{\partial u_z}{\partial z}\right]\phi^{[\mathrm{f}]} - B_z\,\phi^{[\mathrm{f}]} \\ & - R_\rho\,\frac{\mathrm{Re}}{\mathrm{Fr}}G_z\,\phi^{[\mathrm{f}]} + R_\mu\left[\frac{\partial u_r}{\partial z} + \frac{\partial u_z}{\partial r}\right]\frac{\partial \phi^{[\mathrm{f}]}}{\partial r} + \left[-p + 2R_\mu\frac{\partial u_z}{\partial z}\right]\frac{\partial \phi^{[\mathrm{f}]}}{\partial z}\Bigg\}\,\mathrm{d}V \\ & - \iint_S \Big[\tau_{zr}\,n_r + \tau_{zz}\,n_z + \tau_{z\theta}\,n_\theta\Big]\phi^{[\mathrm{f}]}\,\mathrm{d}S = 0 \end{aligned} \tag{5.85}$$

and

$$\begin{aligned}\mathcal{R}_{\theta}^{[\mathrm{f}]} = \iiint_V \Bigg\{ & R_\rho \,\mathrm{Re}\,\mathrm{St}\,\frac{\partial u_\theta}{\partial t}\phi^{[\mathrm{f}]} + R_\rho \,\mathrm{Re}\,\left[u_r\frac{\partial u_\theta}{\partial r} + u_z\frac{\partial u_\theta}{\partial z} + \frac{u_r u_\theta}{r}\right]\phi^{[\mathrm{f}]} \\ & - B_\theta\,\phi^{[\mathrm{f}]} - R_\rho\,\frac{\mathrm{Re}}{\mathrm{Fr}}G_\theta\,\phi^{[\mathrm{f}]} + R_\mu\left[\frac{\partial u_\theta}{\partial r} - \frac{u_\theta}{r}\right]\frac{\partial \phi^{[\mathrm{f}]}}{\partial r} \\ & + R_\mu\frac{\partial u_\theta}{\partial z}\frac{\partial \phi^{[\mathrm{f}]}}{\partial z} - R_\mu\left[\frac{\partial u_\theta}{\partial r} - \frac{u_\theta}{r}\right]\frac{\phi^{[\mathrm{f}]}}{r}\Bigg\}\,\mathrm{d}V \\ & - \iint_S \Big[\tau_{\theta r}\,n_r + \tau_{\theta z}\,n_z + \tau_{\theta\theta}\,n_\theta\Big]\phi^{[\mathrm{f}]}\,\mathrm{d}S = 0, \end{aligned} \tag{5.86}$$

where the components of the stress tensor are given by

$$\begin{aligned} \tau_{rr} &= -p + 2R_\mu\frac{\partial u_r}{\partial r}, \qquad \tau_{zz} = -p + 2R_\mu\frac{\partial u_z}{\partial z}, \\ \tau_{\theta\theta} &= -p + 2R_\mu\frac{u_r}{r}, \qquad \tau_{rz} = \tau_{zr} = R_\mu\left(\frac{\partial u_r}{\partial z} + \frac{\partial u_z}{\partial r}\right), \\ \tau_{r\theta} &= \tau_{\theta r} = R_\mu\left(\frac{\partial u_\theta}{\partial r} - \frac{u_\theta}{r}\right), \qquad \tau_{z\theta} = \tau_{\theta z} = R_\mu\frac{\partial u_\theta}{\partial z}. \end{aligned} \tag{5.87}$$

The weak form of the continuity equation for an axisymmetric flow is given by

$$\mathcal{R}^{[\mathrm{p}]} = \iiint_V \left(\frac{\partial u_r}{\partial r} + \frac{u_r}{r} + \frac{\partial u_z}{\partial z} - Q\right)\phi^{[\mathrm{p}]}\,\mathrm{d}V. \tag{5.88}$$

The above equations depend spatially on r and z only, and therefore the computational domain is two-dimensional. We note, however, that in general the azimuthal

component of the velocity is non-zero: hence despite only having two spatial directions we retain the three velocity components. In later chapters we will sometimes refer to this azimuthal component as the 'swirl'.

5.5.2 Free surface boundary conditions

In section 5.4 we described the surface integral terms for a general coordinate system ξ^i, and we shall now write down their form for an axisymmetric surface in cylindrical polar coordinates. If $\xi^1 = r$, $\xi^2 = z$ and $\xi^3 = \theta$ then the position vector can be written in terms of the Cartesian basis vectors $\mathbf{i}$, $\mathbf{j}$ and $\mathbf{k}$ as

$$\mathbf{x}(r, z, \theta) = r\cos\theta\,\mathbf{i} + r\sin\theta\,\mathbf{j} + z\,\mathbf{k}. \tag{5.89}$$

From (5.52) the covariant base vectors are given by

$$\begin{aligned} \mathbf{g}_1 &= \cos\theta\,\mathbf{i} + \sin\theta\,\mathbf{j}, \\ \mathbf{g}_2 &= \mathbf{k}, \\ \mathbf{g}_3 &= -r\sin\theta\,\mathbf{i} + r\cos\theta\,\mathbf{j}, \end{aligned} \tag{5.90}$$

and the non-zero covariant components of the global metric tensor (5.54) are

$$g_{11} = 1, \qquad g_{22} = 1 \qquad \text{and} \qquad g_{33} = r^2. \tag{5.91}$$

Its determinant is r^2 and we can find the contravariant components of $\mathbf{g}$ by inverting the matrix made up of the covariant components. We therefore have

$$g^{11} = 1, \qquad g^{22} = 1 \qquad \text{and} \qquad g^{33} = \frac{1}{r^2}, \tag{5.92}$$

which, using (5.55), allows us to construct the contravariant base vectors

$$\begin{aligned} \mathbf{g}^1 &= \cos\theta\,\mathbf{i} + \sin\theta\,\mathbf{j}, \\ \mathbf{g}^2 &= \mathbf{k}, \\ \mathbf{g}^3 &= -\frac{1}{r}\sin\theta\,\mathbf{i} + \frac{1}{r}\cos\theta\,\mathbf{j}. \end{aligned} \tag{5.93}$$

Let us now consider an axisymmetric surface S in a cylindrical polar coordinate system. We shall choose to parameterise it by θ and another surface coordinate, η, so that (in the notation introduced in section 5.4) $\zeta^1 = \eta$ and $\zeta^2 = \theta$. If we

establish an explicit connection between the global coordinate system, ξ^i, and the surface coordinates, ζ^α, then we can define the Eulerian position vector to the surface $\mathbf{X}$. We therefore let $\xi^1 = R(\zeta^1) = R(\eta)$, $\xi^2 = Z(\zeta^1) = Z(\eta)$ and $\xi^3 = \zeta^2 = \theta$, and write down the position vector

$$\mathbf{X}(\eta, \theta) = R(\eta)\cos\theta\,\mathbf{i} + R(\eta)\sin\theta\,\mathbf{j} + Z(\eta)\,\mathbf{k}. \tag{5.94}$$

It follows from (5.57) that the covariant base vectors of the surface are

$$\begin{aligned} \mathbf{a}_1 &= \frac{\mathrm{d}R}{\mathrm{d}\eta}\cos\theta\,\mathbf{i} + \frac{\mathrm{d}R}{\mathrm{d}\eta}\sin\theta\,\mathbf{j} + \frac{\mathrm{d}Z}{\mathrm{d}\eta}\,\mathbf{k}, \\ \mathbf{a}_2 &= -R\,\sin\theta\,\mathbf{i} + R\,\cos\theta\,\mathbf{j}, \end{aligned} \tag{5.95}$$

and the non-zero covariant components of the metric surface tensor (5.58) are

$$a_{11} = (\Delta S)^2 \qquad \text{and} \qquad a_{22} = R^2, \tag{5.96}$$

where

$$(\Delta S)^2 = \left(\frac{\mathrm{d}R}{\mathrm{d}\eta}\right)^2 + \left(\frac{\mathrm{d}Z}{\mathrm{d}\eta}\right)^2. \tag{5.97}$$

The determinant of the metric surface tensor is

$$a = R^2\,(\Delta S)^2\,, \tag{5.98}$$

and hence from (5.77) its non-zero contravariant components are

$$a^{11} = \frac{1}{(\Delta S)^2} \qquad \text{and} \qquad a^{22} = \frac{1}{R^2}. \tag{5.99}$$

From (5.59) we can now construct the contravariant base vectors of the surface,

$$\begin{aligned} \mathbf{a}^1 &= \frac{1}{(\Delta S)}\frac{\mathrm{d}R}{\mathrm{d}\eta}\cos\theta\,\mathbf{i} + \frac{1}{(\Delta S)}\frac{\mathrm{d}R}{\mathrm{d}\eta}\sin\theta\,\mathbf{j} + \frac{1}{(\Delta S)}\frac{\mathrm{d}Z}{\mathrm{d}\eta}\,\mathbf{k}, \\ \mathbf{a}^2 &= -\frac{1}{R}\sin\theta\,\mathbf{i} + \frac{1}{R}\,\cos\theta\,\mathbf{j}. \end{aligned} \tag{5.100}$$

The derivatives of the global contravariant base vectors $\mathbf{g}_i$ with respect to the surface coordinates ζ^α are

$$\begin{aligned} \frac{\partial \mathbf{g}^1}{\partial \eta} &= \mathbf{0}, & \frac{\partial \mathbf{g}^1}{\partial \theta} &= -\sin\theta\,\mathbf{i} + \cos\theta\,\mathbf{j}, \\ \frac{\partial \mathbf{g}^2}{\partial \eta} &= \mathbf{0}, & \frac{\partial \mathbf{g}^2}{\partial \theta} &= \mathbf{0}, \\ \frac{\partial \mathbf{g}^3}{\partial \eta} &= \frac{1}{R^2}\frac{\mathrm{d}R}{\mathrm{d}\eta}\sin\theta\,\mathbf{i} - \frac{1}{R^2}\frac{\mathrm{d}R}{\mathrm{d}\eta}\cos\theta\,\mathbf{j}, & \frac{\partial \mathbf{g}^3}{\partial \theta} &= -\frac{1}{R}\cos\theta\,\mathbf{i} - \frac{1}{R}\sin\theta\,\mathbf{j}. \end{aligned} \tag{5.101}$$

The dynamic condition

In order to evaluate (5.80) for a cylindrical polar system, we need to construct the following terms,

$$\begin{aligned}
\mathbf{a}^\alpha \cdot \frac{\partial \mathbf{g}^1}{\partial \zeta^\alpha} &= \frac{1}{R}, & \mathbf{g}^1 \cdot \mathbf{a}_1 &= \frac{\mathrm{d}R}{\mathrm{d}\eta}, & \mathbf{g}^1 \cdot \mathbf{a}_2 &= 0, \\
\mathbf{a}^\alpha \cdot \frac{\partial \mathbf{g}^2}{\partial \zeta^\alpha} &= 0, & \mathbf{g}^2 \cdot \mathbf{a}_1 &= \frac{\mathrm{d}Z}{\mathrm{d}\eta}, & \mathbf{g}^2 \cdot \mathbf{a}_2 &= 0, \\
\mathbf{a}^\alpha \cdot \frac{\partial \mathbf{g}^3}{\partial \zeta^\alpha} &= 0, & \mathbf{g}^3 \cdot \mathbf{a}_1 &= 0, & \mathbf{g}^3 \cdot \mathbf{a}_2 &= 1,
\end{aligned} \tag{5.102}$$

and the contribution to the i-th momentum equation from the integral over the free surface is therefore given by

$$\begin{aligned}
\mathcal{R}_i^{[\mathrm{f,fs}]} = &- \iint_\Omega p_{\mathrm{ext}}\, n^i\, \phi^{[\mathrm{f}]}\, \mathrm{d}S + \frac{1}{\mathrm{Ca}} \oint_{\partial\Omega} m^i\, \phi^{[\mathrm{f}]}\, \mathrm{d}\lambda - \frac{1}{\mathrm{Ca}} \iint_\Omega \mathbf{a}^\alpha \cdot \frac{\partial \mathbf{g}^i}{\partial \zeta^\alpha}\, \phi^{[\mathrm{f}]}\, \mathrm{d}S \\
&- \frac{1}{\mathrm{Ca}} \iint_\Omega \mathbf{g}^i \cdot \mathbf{a}_1 \left(\frac{1}{(\Delta S)^2} \frac{\mathrm{d}\phi^{[\mathrm{f}]}}{\mathrm{d}\eta} \right) \mathrm{d}S.
\end{aligned} \tag{5.103}$$

Considering each component separately and using (5.102) gives

$$\begin{aligned}
\mathcal{R}_1^{[\mathrm{f,fs}]} &= - \iint_\Omega p_{\mathrm{ext}}\, n^1\, \phi^{[\mathrm{f}]}\, \mathrm{d}S + \frac{1}{\mathrm{Ca}} \oint_{\partial\Omega} m^1\, \phi^{[\mathrm{f}]}\, \mathrm{d}\lambda \\
&\qquad - \frac{1}{\mathrm{Ca}} \iint_\Omega \left[\frac{\phi^{[\mathrm{f}]}}{R} + \frac{1}{(\Delta S)^2} \frac{\mathrm{d}R}{\mathrm{d}\eta} \frac{\mathrm{d}\phi^{[\mathrm{f}]}}{\mathrm{d}\eta} \right] \mathrm{d}S, \\
\mathcal{R}_2^{[\mathrm{f,fs}]} &= - \iint_\Omega p_{\mathrm{ext}}\, n^2\, \phi^{[\mathrm{f}]}\, \mathrm{d}S + \frac{1}{\mathrm{Ca}} \oint_{\partial\Omega} m^2\, \phi^{[\mathrm{f}]}\, \mathrm{d}\lambda - \frac{1}{\mathrm{Ca}} \iint_\Omega \frac{1}{(\Delta S)^2} \frac{\mathrm{d}Z}{\mathrm{d}\eta} \frac{\mathrm{d}\phi^{[\mathrm{f}]}}{\mathrm{d}\eta}\, \mathrm{d}S, \\
\mathcal{R}_3^{[\mathrm{f,fs}]} &= - \iint_\Omega p_{\mathrm{ext}}\, n^3\, \phi^{[\mathrm{f}]}\, \mathrm{d}S + \frac{1}{\mathrm{Ca}} \oint_{\partial\Omega} m^3\, \phi^{[\mathrm{f}]}\, \mathrm{d}\lambda
\end{aligned} \tag{5.104}$$

but we note that in order to be consistent with the form of the momentum equations derived in section 5.3 we require the components of the vectors $\mathbf{n}$ and $\mathbf{m}$ to be described with respect to the $\mathbf{e}_r$, $\mathbf{e}_z$ and $\mathbf{e}_\theta$ basis defined in (5.26). This basis is related to the current basis $\mathbf{g}_i$ by

$$\mathbf{e}_j = S_{ij}\, \mathbf{g}_i, \tag{5.105}$$

where $j = 1, 2, 3$ corresponds to r, z and θ respectively and $\mathbf{S}$ is the transformation matrix

$$\mathbf{S} = \begin{pmatrix} 1 & 0 & 0 \\ 0 & 1 & 0 \\ 0 & 0 & 1/r \end{pmatrix}. \tag{5.106}$$

The coefficients of $\mathbf{n}$ and $\mathbf{m}$ with respect to $\mathbf{e}_r$, $\mathbf{e}_z$ and $\mathbf{e}_\theta$ are therefore given by

$$n'_j = \left(S^{-1}\right)_{ij} n^i \qquad \text{and} \qquad m'_j = \left(S^{-1}\right)_{ij} m^i, \tag{5.107}$$

where $\mathbf{S}^{-1}$ is the inverse of $\mathbf{S}$, and hence[1]

$$\begin{aligned} n_r &= n^1, & n_z &= n^2, & n_\theta &= r\, n^3, \\ m_r &= m^1, & m_z &= m^2, & m_\theta &= r\, m^3, \end{aligned} \tag{5.108}$$

which allows us to rewrite (5.104) as

$$\begin{aligned} \mathcal{R}_{\mathrm{r}}^{[\mathrm{f,fs}]} &= -\iint_\Omega p_{\text{ext}}\, n_r\, \phi^{[\mathrm{f}]}\, \mathrm{d}S + \frac{1}{\mathrm{Ca}} \oint_{\partial\Omega} m_r\, \phi^{[\mathrm{f}]}\, \mathrm{d}\lambda \\ &\qquad - \frac{1}{\mathrm{Ca}} \iint_\Omega \left[\frac{\phi^{[\mathrm{f}]}}{R} + \frac{1}{(\Delta S)^2} \frac{\mathrm{d}R}{\mathrm{d}\eta} \frac{\mathrm{d}\phi^{[\mathrm{f}]}}{\mathrm{d}\eta} \right] \mathrm{d}S, \\ \mathcal{R}_{\mathrm{z}}^{[\mathrm{f,fs}]} &= -\iint_\Omega p_{\text{ext}}\, n_z\, \phi^{[\mathrm{f}]}\, \mathrm{d}S + \frac{1}{\mathrm{Ca}} \oint_{\partial\Omega} m_z\, \phi^{[\mathrm{f}]}\, \mathrm{d}\lambda - \frac{1}{\mathrm{Ca}} \iint_\Omega \frac{1}{(\Delta S)^2} \frac{\mathrm{d}Z}{\mathrm{d}\eta} \frac{\mathrm{d}\phi^{[\mathrm{f}]}}{\mathrm{d}\eta}\, \mathrm{d}S, \\ \mathcal{R}_{\theta}^{[\mathrm{f,fs}]} &= -\iint_\Omega \frac{p_{\text{ext}}\, n_\theta}{r}\, \phi^{[\mathrm{f}]}\, \mathrm{d}S + \frac{1}{\mathrm{Ca}} \oint_{\partial\Omega} \frac{m_\theta}{r}\, \phi^{[\mathrm{f}]}\, \mathrm{d}\lambda. \end{aligned} \tag{5.109}$$

Let us now consider the position vector to the free surface (5.94) written in terms of the $\mathbf{e}_r$, $\mathbf{e}_z$ and $\mathbf{e}_\theta$ basis defined in (5.26):

$$\mathbf{X}(\eta, \theta) = R(\eta)\, \mathbf{e}_r + Z(\eta)\, \mathbf{e}_z \tag{5.110}$$

A unit tangent vector to the surface in the direction of increasing η is given by

$$\mathbf{t} = \left[\frac{\partial \mathbf{X}}{\partial \eta} \cdot \frac{\partial \mathbf{X}}{\partial \eta} \right]^{-\frac{1}{2}} \frac{\partial \mathbf{X}}{\partial \eta} = \frac{1}{(\Delta S)} \left[\frac{\mathrm{d}R}{\mathrm{d}\eta}\, \mathbf{e}_r + \frac{\mathrm{d}Z}{\mathrm{d}\eta}\, \mathbf{e}_z \right], \tag{5.111}$$

and therefore

$$t_r = \frac{1}{(\Delta S)} \frac{\mathrm{d}R}{\mathrm{d}\eta} \qquad \text{and} \qquad t_z = \frac{1}{(\Delta S)} \frac{\mathrm{d}Z}{\mathrm{d}\eta}. \tag{5.112}$$

At any point on Ω a unit vector normal to the surface can be found using

$$\mathbf{n} = \Big[(\mathbf{a}_1 \times \mathbf{a}_2) \cdot (\mathbf{a}_1 \times \mathbf{a}_2) \Big]^{-\frac{1}{2}} (\mathbf{a}_1 \times \mathbf{a}_2), \tag{5.113}$$

and using (5.95) we therefore have

$$\mathbf{n} = \frac{1}{(\Delta S)} \left[-\frac{\mathrm{d}Z}{\mathrm{d}\eta} \cos\theta\, \mathbf{i} - \frac{\mathrm{d}Z}{\mathrm{d}\eta} \sin\theta\, \mathbf{j} + \frac{\mathrm{d}R}{\mathrm{d}\eta}\, \mathbf{k} \right], \tag{5.114}$$

[1] We note that since this coordinate system is orthonormal, there is no difference between the co- and contravariant components of either $\mathbf{n}$ or $\mathbf{m}$.

and hence from (5.26) obtain

$$n_r = -\frac{1}{(\Delta S)}\frac{\mathrm{d}Z}{\mathrm{d}\eta} = -t_z, \qquad n_z = \frac{1}{(\Delta S)}\frac{\mathrm{d}R}{\mathrm{d}\eta} = t_r, \qquad n_\theta = 0. \tag{5.115}$$

We also note that as the surface is independent of θ, the azimuthal component of $\mathbf{m}$ must be equal to zero. Using (5.112) and (5.115) we can therefore rewrite (5.109) as

$$\begin{aligned}
\mathcal{R}_{\mathrm{r}}^{[\mathrm{f,fs}]} &= \iint_\Omega p_{\mathrm{ext}}\, t_z\, \phi^{[\mathrm{f}]}\, \mathrm{d}S + \frac{1}{\mathrm{Ca}} \oint_{\partial\Omega} m_r\, \phi^{[\mathrm{f}]}\, \mathrm{d}\lambda \\
&\qquad\qquad -\frac{1}{\mathrm{Ca}} \iint_\Omega \left[\frac{\phi^{[\mathrm{f}]}}{R} + \frac{1}{(\Delta S)} t_r \frac{\mathrm{d}\phi^{[\mathrm{f}]}}{\mathrm{d}\eta}\right] \mathrm{d}S, \\
\mathcal{R}_{\mathrm{z}}^{[\mathrm{f,fs}]} &= -\iint_\Omega p_{\mathrm{ext}}\, t_r\, \phi^{[\mathrm{f}]}\, \mathrm{d}S + \frac{1}{\mathrm{Ca}} \oint_{\partial\Omega} m_z\, \phi^{[\mathrm{f}]}\, \mathrm{d}\lambda - \frac{1}{\mathrm{Ca}} \iint_\Omega \frac{1}{(\Delta S)} t_z \frac{\mathrm{d}\phi^{[\mathrm{f}]}}{\mathrm{d}\eta}\, \mathrm{d}S, \\
\mathcal{R}_{\theta}^{[\mathrm{f,fs}]} &= 0.
\end{aligned} \tag{5.116}$$

The kinematic condition

The components of the velocity $\mathbf{u}$ and the position vector to the free surface $\mathbf{X}$ with respect to the $\mathbf{e}_r$, $\mathbf{e}_z$ and $\mathbf{e}_\theta$ basis defined in (5.26) are given by

$$u'_j = \left(S^{-1}\right)_{ij} u_i \qquad \text{and} \qquad X'_j = \left(S^{-1}\right)_{ij} X_i, \tag{5.117}$$

where $\mathbf{S}$ is the transformation matrix that relates this basis to the global contravariant basis (5.93) and is defined by

$$\mathbf{S} = \begin{pmatrix} 1 & 0 & 0 \\ 0 & 1 & 0 \\ 0 & 0 & r \end{pmatrix}. \tag{5.118}$$

The weak form of the kinematic boundary condition is therefore given by

$$\begin{aligned}
\mathcal{R}^{[\mathrm{h}]} = \iint_\Omega \Bigg[& u_r\, n_r + u_z\, n_z + u_\theta\, n_\theta \\
& - \mathrm{St}\, \frac{\partial X_r}{\partial t}\, n_r - \mathrm{St}\, \frac{\partial X_z}{\partial t}\, n_z - \mathrm{St}\, \frac{\partial X_\theta}{\partial t}\, n_\theta \Bigg] \phi^{[\mathrm{f}]}\, \mathrm{d}S.
\end{aligned} \tag{5.119}$$

From (5.110) we can write the position vector to the surface at time t,

$$\mathbf{X}(\eta, \theta, t) = R(\eta, t)\, \mathbf{e}_r + Z(\eta, t)\, \mathbf{e}_z, \tag{5.120}$$

and therefore using (5.115) we can rewrite (5.119) as

$$\mathcal{R}^{[\mathrm{h}]} = \iint_\Omega \left[-u_r\, t_z + u_z\, t_r + \mathrm{St}\, \frac{\partial R}{\partial t}\, t_z - \mathrm{St}\, \frac{\partial Z}{\partial t}\, t_r \right] \phi^{[\mathrm{f}]}\, \mathrm{d}S. \tag{5.121}$$

5.5.3 Complete weak form

Having derived the weak form of the bulk axisymmetric Navier–Stokes equations in section 5.5.1 and the contributions made by a free boundary in section 5.5.2, we can now combine these results to write down the complete set of residual equations for an axisymmetric free surface problem. We note that the integral of an arbitrary function $f(x, y, z)$ over a surface S can alternatively be written as [Stewart, 2012, eqn. 16.7.2]

$$\iint_S f(x, y, z)\ \mathrm{d}S = \iint_S f(\mathbf{X}(\zeta^1, \zeta^2))\ |\mathbf{a}_1 \times \mathbf{a}_2|\ \mathrm{d}\zeta^1\,\mathrm{d}\zeta^2, \tag{5.122}$$

and from (5.95) we have

$$|\mathbf{a}_1 \times \mathbf{a}_2| = R\,(\Delta S)\,. \tag{5.123}$$

Combining (5.84)–(5.86) with (5.116) yields the three momentum equations,

$$\begin{aligned}
\mathcal{R}_{\mathrm{r}}^{[\mathrm{f}]} = \iiint_V \Bigg\{ & R_\rho \,\mathrm{Re}\,\mathrm{St}\, r \frac{\partial u_r}{\partial t}\phi^{[\mathrm{f}]} + R_\rho \,\mathrm{Re}\,\left[r u_r \frac{\partial u_r}{\partial r} + r u_z \frac{\partial u_r}{\partial z} - u_\theta^2 \right] \phi^{[\mathrm{f}]} \\
& - r B_r\, \phi^{[\mathrm{f}]} - R_\rho \frac{\mathrm{Re}}{\mathrm{Fr}}\, r\, G_r\, \phi^{[\mathrm{f}]} + \left[-rp + 2R_\mu r \frac{\partial u_r}{\partial r} \right] \frac{\partial \phi^{[\mathrm{f}]}}{\partial r} \\
& + R_\mu \left[r \frac{\partial u_z}{\partial r} + r \frac{\partial u_r}{\partial z} \right] \frac{\partial \phi^{[\mathrm{f}]}}{\partial z} + \left[-p + \frac{2R_\mu}{r} u_r \right] \phi^{[\mathrm{f}]} \Bigg\}\, \mathrm{d}r\,\mathrm{d}z\,\mathrm{d}\theta \\
& - \iint_{S/\Omega} r\,(\Delta S)\, \mathfrak{t}_r\, \phi^{[\mathrm{f}]}\ \mathrm{d}\eta\,\mathrm{d}\theta - \iint_\Omega r\,(\Delta S)\, p_{\mathrm{ext}}\, t_z\, \phi^{[\mathrm{f}]}\ \mathrm{d}\eta\,\mathrm{d}\theta \\
& - \frac{1}{\mathrm{Ca}} \oint_{\partial\Omega} m_r\, \phi^{[\mathrm{f}]}\ \mathrm{d}\lambda + \frac{1}{\mathrm{Ca}} \iint_\Omega \left[\phi^{[\mathrm{f}]}\,(\Delta S) + r\, t_r \frac{\mathrm{d}\phi^{[\mathrm{f}]}}{\mathrm{d}\eta} \right] \mathrm{d}\eta\,\mathrm{d}\theta,
\end{aligned} \tag{5.124}$$

$$\begin{aligned}
\mathcal{R}_{\mathrm{z}}^{[\mathrm{f}]} = \iiint_V \Bigg\{ & R_\rho \,\mathrm{Re}\,\mathrm{St}\, r \frac{\partial u_z}{\partial t}\phi^{[\mathrm{f}]} + R_\rho \,\mathrm{Re}\,\left[r u_r \frac{\partial u_z}{\partial r} + r u_z \frac{\partial u_z}{\partial z} \right] \phi^{[\mathrm{f}]} \\
& - r B_z\, \phi^{[\mathrm{f}]} - R_\rho \frac{\mathrm{Re}}{\mathrm{Fr}}\, r\, G_z\, \phi^{[\mathrm{f}]} + R_\mu \left[r \frac{\partial u_r}{\partial z} + r \frac{\partial u_z}{\partial r} \right] \frac{\partial \phi^{[\mathrm{f}]}}{\partial r} \\
& + \left[-rp + 2R_\mu r \frac{\partial u_z}{\partial z} \right] \frac{\partial \phi^{[\mathrm{f}]}}{\partial z} \Bigg\}\, \mathrm{d}r\,\mathrm{d}z\,\mathrm{d}\theta \\
& - \iint_{S/\Omega} r\,(\Delta S)\, \mathfrak{t}_z\, \phi^{[\mathrm{f}]}\ \mathrm{d}\eta\,\mathrm{d}\theta + \iint_\Omega r\,(\Delta S)\, p_{\mathrm{ext}}\, t_r\, \phi^{[\mathrm{f}]}\ \mathrm{d}\eta\,\mathrm{d}\theta \\
& - \frac{1}{\mathrm{Ca}} \oint_{\partial\Omega} m_z\, \phi^{[\mathrm{f}]}\ \mathrm{d}\lambda + \frac{1}{\mathrm{Ca}} \iint_\Omega r\, t_z \frac{\mathrm{d}\phi^{[\mathrm{f}]}}{\mathrm{d}\eta}\ \mathrm{d}\eta\,\mathrm{d}\theta
\end{aligned} \tag{5.125}$$

and

$$\mathcal{R}_{\theta}^{[\mathrm{f}]} = \iiint_V \Bigg\{ R_\rho \,\mathrm{Re}\,\mathrm{St}\, r \frac{\partial u_\theta}{\partial t}\phi^{[\mathrm{f}]} + R_\rho \,\mathrm{Re}\, \left[r u_r \frac{\partial u_\theta}{\partial r} + r u_z \frac{\partial u_\theta}{\partial z} + u_r u_\theta \right] \phi^{[\mathrm{f}]} \\ - r B_\theta \,\phi^{[\mathrm{f}]} - R_\rho \frac{\mathrm{Re}}{\mathrm{Fr}}\, r\, G_\theta \,\phi^{[\mathrm{f}]} + R_\mu \left[r \frac{\partial u_\theta}{\partial r} - u_\theta \right] \frac{\partial \phi^{[\mathrm{f}]}}{\partial r} \\ + R_\mu r \frac{\partial u_\theta}{\partial z}\frac{\partial \phi^{[\mathrm{f}]}}{\partial z} - R_\mu \left[\frac{\partial u_\theta}{\partial r} - \frac{u_\theta}{r} \right] \phi^{[\mathrm{f}]} \Bigg\} \,\mathrm{d}r\,\mathrm{d}z\,\mathrm{d}\theta \\ - \iint_{S/\Omega} r\,(\Delta S)\, \mathfrak{t}_\theta \,\phi^{[\mathrm{f}]} \,\mathrm{d}\eta\,\mathrm{d}\theta, \quad (5.126)$$

where we note that we have replaced $R(\eta)$ in the free surface terms with the global radial coordinate r since they are precisely the same quantity[2]. From (5.88) we have the continuity equation,

$$\mathcal{R}^{[\mathrm{p}]} = \iiint_V \left(r \frac{\partial u_r}{\partial r} + u_r + r \frac{\partial u_z}{\partial z} - r\,Q \right) \phi^{[\mathrm{p}]} \,\mathrm{d}r\,\mathrm{d}z\,\mathrm{d}\theta, \quad (5.127)$$

and from (5.121) the kinematic boundary condition,

$$\mathcal{R}^{[\mathrm{h}]} = \iint_\Omega r\,(\Delta S) \left[-u_r\, t_z + u_z\, t_r + \mathrm{St}\, \frac{\partial r}{\partial t}\, t_z - \mathrm{St}\, \frac{\partial z}{\partial t}\, t_r \right] \phi^{[\mathrm{f}]} \,\mathrm{d}\eta\,\mathrm{d}\theta, \quad (5.128)$$

where again we have used the fact that $\xi^1 = r = R(\eta)$ and $\xi^2 = z = Z(\eta)$ on the boundary.

We integrate with respect to θ between zero and 2π to obtain

$$\mathcal{R}_{\mathrm{r}}^{[\mathrm{f}]} = \iint_D \Bigg\{ R_\rho \,\mathrm{Re}\,\mathrm{St}\, r \frac{\partial u_r}{\partial t}\phi^{[\mathrm{f}]} + R_\rho \,\mathrm{Re}\, \left[r u_r \frac{\partial u_r}{\partial r} + r u_z \frac{\partial u_r}{\partial z} - u_\theta^2 \right] \phi^{[\mathrm{f}]} \\ - r B_r \,\phi^{[\mathrm{f}]} - R_\rho \frac{\mathrm{Re}}{\mathrm{Fr}}\, r\, G_r \,\phi^{[\mathrm{f}]} + \left[-rp + 2R_\mu r \frac{\partial u_r}{\partial r} \right] \frac{\partial \phi^{[\mathrm{f}]}}{\partial r} \\ + R_\mu \left[r \frac{\partial u_z}{\partial r} + r \frac{\partial u_r}{\partial z} \right] \frac{\partial \phi^{[\mathrm{f}]}}{\partial z} + \left[-p + \frac{2R_\mu}{r} u_r \right] \phi^{[\mathrm{f}]} \Bigg\} \,\mathrm{d}r\,\mathrm{d}z \\ - \int_{\partial D/\Omega} r\,(\Delta S)\, \mathfrak{t}_r \,\phi^{[\mathrm{f}]} \,\mathrm{d}\eta - \int_\Omega r\,(\Delta S)\, p_{\mathrm{ext}}\, t_z \,\phi^{[\mathrm{f}]} \,\mathrm{d}\eta \\ - \frac{1}{\mathrm{Ca}} \Big[r\, m_r \,\phi^{[\mathrm{f}]} \Big]_{\partial\Omega} + \frac{1}{\mathrm{Ca}} \int_\Omega \left[\phi^{[\mathrm{f}]}\,(\Delta S) + r\, t_r \frac{\mathrm{d}\phi^{[\mathrm{f}]}}{\mathrm{d}\eta} \right] \mathrm{d}\eta, \quad (5.129)$$

[2]Recall that we defined $\xi^1 = r = R(\eta)$ in section 5.5.2.

$$\mathcal{R}_{\mathrm{z}}^{[\mathrm{f}]} = \int\!\!\int_D \Bigg\{ R_\rho \,\mathrm{Re}\,\mathrm{St}\, r\frac{\partial u_z}{\partial t}\phi^{[\mathrm{f}]} + R_\rho \,\mathrm{Re}\,\left[ru_r\frac{\partial u_z}{\partial r} + ru_z\frac{\partial u_z}{\partial z}\right]\phi^{[\mathrm{f}]} \\ -rB_z\,\phi^{[\mathrm{f}]} - R_\rho\frac{\mathrm{Re}}{\mathrm{Fr}}\,r\,G_z\,\phi^{[\mathrm{f}]} + R_\mu\left[r\frac{\partial u_r}{\partial z} + r\frac{\partial u_z}{\partial r}\right]\frac{\partial \phi^{[\mathrm{f}]}}{\partial r} \\ + \left[-rp + 2R_\mu r\frac{\partial u_z}{\partial z}\right]\frac{\partial \phi^{[\mathrm{f}]}}{\partial z}\Bigg\}\,\mathrm{d}r\,\mathrm{d}z \\ - \int_{\partial D/\Omega} r\,(\Delta S)\,\mathfrak{t}_z\,\phi^{[\mathrm{f}]}\,\mathrm{d}\eta + \int_\Omega r\,(\Delta S)\,p_{\mathrm{ext}}\,t_r\,\phi^{[\mathrm{f}]}\,\mathrm{d}\eta \\ - \frac{1}{\mathrm{Ca}}\Big[r\,m_z\,\phi^{[\mathrm{f}]}\Big]_{\partial\Omega} + \frac{1}{\mathrm{Ca}}\int_\Omega r\,t_z\frac{\mathrm{d}\phi^{[\mathrm{f}]}}{\mathrm{d}\eta}\,\mathrm{d}\eta, \quad (5.130)$$

$$\mathcal{R}_{\theta}^{[\mathrm{f}]} = \int\!\!\int_D \Bigg\{ R_\rho \,\mathrm{Re}\,\mathrm{St}\, r\frac{\partial u_\theta}{\partial t}\phi^{[\mathrm{f}]} + R_\rho \,\mathrm{Re}\,\left[ru_r\frac{\partial u_\theta}{\partial r} + ru_z\frac{\partial u_\theta}{\partial z} + u_r u_\theta\right]\phi^{[\mathrm{f}]} \\ -rB_\theta\,\phi^{[\mathrm{f}]} - R_\rho\frac{\mathrm{Re}}{\mathrm{Fr}}\,r\,G_\theta\,\phi^{[\mathrm{f}]} + R_\mu\left[r\frac{\partial u_\theta}{\partial r} - u_\theta\right]\frac{\partial \phi^{[\mathrm{f}]}}{\partial r} \\ + R_\mu r\frac{\partial u_\theta}{\partial z}\frac{\partial \phi^{[\mathrm{f}]}}{\partial z} - R_\mu\left[\frac{\partial u_\theta}{\partial r} - \frac{u_\theta}{r}\right]\phi^{[\mathrm{f}]}\Bigg\}\,\mathrm{d}r\,\mathrm{d}z \\ - \int_{\partial D/\Omega} r\,(\Delta S)\,\mathfrak{t}_\theta\,\phi^{[\mathrm{f}]}\,\mathrm{d}\eta, \quad (5.131)$$

$$\mathcal{R}^{[\mathrm{p}]} = \int\!\!\int_D \left(r\frac{\partial u_r}{\partial r} + u_r + r\frac{\partial u_z}{\partial z} - r\,Q\right)\phi^{[\mathrm{p}]}\,\mathrm{d}r\,\mathrm{d}z, \quad (5.132)$$

and

$$\mathcal{R}^{[\mathrm{h}]} = \int_\Omega r\,(\Delta S)\left[-u_r\,t_z + u_z\,t_r + \mathrm{St}\,\frac{\partial r}{\partial t}\,t_z - \mathrm{St}\,\frac{\partial z}{\partial t}\,t_r\right]\phi^{[\mathrm{f}]}\,\mathrm{d}\eta, \quad (5.133)$$

where we have ignored the factors of 2π that premultiply (5.129)–(5.133).

5.5.4 Discrete residual equations

To complete this discussion we must write down the elemental residual equations which were actually be implemented in `oomph-lib` in order to compute the finite element solution of (5.129)–(5.133). The equations are discretised as described in section 3.3, with the integration over each element performed in local coordinates. The bulk elemental residual equations are therefore given by

$$\mathcal{R}_{\mathrm{r}l}^{[\mathrm{f,bulk}]} = \int_{-1}^{1}\int_{-1}^{1} \Bigg\{ R_\rho \,\mathrm{Re}\,\mathrm{St}\, r\frac{\partial u_r}{\partial t}\psi_l^{[\mathrm{f}]} + R_\rho \,\mathrm{Re}\,\left[ru_r\frac{\partial u_r}{\partial r} + ru_z\frac{\partial u_r}{\partial z} - u_\theta^2\right]\psi_l^{[\mathrm{f}]} \\ -rB_r\,\psi_l^{[\mathrm{f}]} - R_\rho\frac{\mathrm{Re}}{\mathrm{Fr}}\,r\,G_r\,\psi_l^{[\mathrm{f}]} + \left[-rp + 2R_\mu r\frac{\partial u_r}{\partial r}\right]\frac{\partial \psi_l^{[\mathrm{f}]}}{\partial r} \\ + R_\mu\left[r\frac{\partial u_z}{\partial r} + r\frac{\partial u_r}{\partial z}\right]\frac{\partial \psi_l^{[\mathrm{f}]}}{\partial z} + \left[-p + \frac{2R_\mu}{r}u_r\right]\psi_l^{[\mathrm{f}]}\Bigg\}\,\mathcal{J}_B\,\mathrm{d}s_1\,\mathrm{d}s_2, \quad (5.134)$$

$$\mathcal{R}_{zl}^{[\mathrm{f,bulk}]} = \int_{-1}^{1}\int_{-1}^{1}\Bigg\{R_\rho\,\mathrm{Re}\,\mathrm{St}\,r\frac{\partial u_z}{\partial t}\psi_l^{[\mathrm{f}]} + R_\rho\,\mathrm{Re}\,\left[ru_r\frac{\partial u_z}{\partial r} + ru_z\frac{\partial u_z}{\partial z}\right]\psi_l^{[\mathrm{f}]} \\ -rB_z\,\psi_l^{[\mathrm{f}]} - R_\rho\,\frac{\mathrm{Re}}{\mathrm{Fr}}\,r\,G_z\,\psi_l^{[\mathrm{f}]} + R_\mu\left[r\frac{\partial u_r}{\partial z} + r\frac{\partial u_z}{\partial r}\right]\frac{\partial \psi_l^{[\mathrm{f}]}}{\partial r} \\ + \left[-rp + 2R_\mu r\frac{\partial u_z}{\partial z}\right]\frac{\partial \psi_l^{[\mathrm{f}]}}{\partial z}\Bigg\}\,\mathcal{J}_B\,\mathrm{d}s_1\,\mathrm{d}s_2, \quad (5.135)$$

$$\mathcal{R}_{\theta l}^{[\mathrm{f,bulk}]} = \int_{-1}^{1}\int_{-1}^{1}\Bigg\{R_\rho\,\mathrm{Re}\,\mathrm{St}\,r\frac{\partial u_\theta}{\partial t}\psi_l^{[\mathrm{f}]} + R_\rho\,\mathrm{Re}\,\left[ru_r\frac{\partial u_\theta}{\partial r} + ru_z\frac{\partial u_\theta}{\partial z} + u_r u_\theta\right]\psi_l^{[\mathrm{f}]} \\ -rB_\theta\,\psi_l^{[\mathrm{f}]} - R_\rho\,\frac{\mathrm{Re}}{\mathrm{Fr}}\,r\,G_\theta\,\psi_l^{[\mathrm{f}]} + R_\mu\left[r\frac{\partial u_\theta}{\partial r} - u_\theta\right]\frac{\partial \psi_l^{[\mathrm{f}]}}{\partial r} \\ + R_\mu r\frac{\partial u_\theta}{\partial z}\frac{\partial \psi_l^{[\mathrm{f}]}}{\partial z} - R_\mu\left[\frac{\partial u_\theta}{\partial r} - \frac{u_\theta}{r}\right]\psi_l^{[\mathrm{f}]}\Bigg\}\,\mathcal{J}_B\,\mathrm{d}s_1\,\mathrm{d}s_2, \quad (5.136)$$

and

$$\mathcal{R}_l^{[\mathrm{p}]} = \int_{-1}^{1}\int_{-1}^{1}\left(r\frac{\partial u_r}{\partial r} + u_r + r\frac{\partial u_z}{\partial z} - r\,Q\right)\psi_l^{[\mathrm{p}]}\,\mathcal{J}_B\,\mathrm{d}s_1\,\mathrm{d}s_2. \quad (5.137)$$

where $\mathcal{J}_B = \det\left[\partial x_j/\partial s_i\right]$ is the Jacobian of the mapping between local and global coordinates. As described in section 3.3.5, contributions to the momentum equations arising from the boundary integral terms are computed using one-dimensional 'face' elements, and are given by

$$\mathcal{R}_{rl}^{[\mathrm{f,boundary}]} = -\int_{-1}^{1} r\,\mathfrak{t}_r\,\psi_l^{[\mathrm{f}]}\,\mathcal{J}_S\,\mathrm{d}s, \quad (5.138)$$

$$\mathcal{R}_{zl}^{[\mathrm{f,boundary}]} = -\int_{-1}^{1} r\,\mathfrak{t}_z\,\psi_l^{[\mathrm{f}]}\,\mathcal{J}_S\,\mathrm{d}s \quad (5.139)$$

and

$$\mathcal{R}_{\theta l}^{[\mathrm{f,boundary}]} = -\int_{-1}^{1} r\,\mathfrak{t}_\theta\,\psi_l^{[\mathrm{f}]}\,\mathcal{J}_S\,\mathrm{d}s \quad (5.140)$$

on non-Dirichlet, non-free surface boundaries, and

$$\mathcal{R}_{rl}^{[\mathrm{f,boundary}]} = -\int_{-1}^{1} r\,p_{\mathrm{ext}}\,t_z\,\psi_l^{[\mathrm{f}]}\,\mathcal{J}_S\,\mathrm{d}s + \frac{1}{\mathrm{Ca}}\int_{-1}^{1}\left[\psi_l^{[\mathrm{f}]}\mathcal{J}_S + r\,t_r\frac{\mathrm{d}\psi_l^{[\mathrm{f}]}}{\mathrm{d}s}\right]\mathrm{d}s \quad (5.141)$$

and

$$\mathcal{R}_{zl}^{[\mathrm{f,boundary}]} = \int_{-1}^{1} r\,p_{\mathrm{ext}}\,t_r\,\psi_l^{[\mathrm{f}]}\,\mathcal{J}_S\,\mathrm{d}s + \frac{1}{\mathrm{Ca}}\int_{-1}^{1} r\,t_z\frac{\mathrm{d}\psi_l^{[\mathrm{f}]}}{\mathrm{d}s}\,\mathrm{d}s \quad (5.142)$$

on free surface boundaries, where

$$\mathcal{J}_S = (\Delta S)\,\frac{\mathrm{d}\eta}{\mathrm{d}s} \quad (5.143)$$

is the Jacobian of the mapping between local and global coordinates in the face elements. As usual, the point contributions

$$\mathcal{R}_{\mathrm{r}l}^{[\mathrm{f,boundary}]} = -\frac{1}{\mathrm{Ca}}\left[r\, m_r\, \psi_l^{[\mathrm{f}]}\right]_{\partial\Omega} \tag{5.144}$$

and

$$\mathcal{R}_{\mathrm{z}l}^{[\mathrm{f,boundary}]} = -\frac{1}{\mathrm{Ca}}\left[r\, m_z\, \psi_l^{[\mathrm{f}]}\right]_{\partial\Omega} \tag{5.145}$$

need to be added at the two contact points at either side of the free surface. Finally, at a free boundary we also require the kinematic condition,

$$\mathcal{R}_l^{[\mathrm{h}]} = \int_{-1}^{1} r\left[-u_r\, t_z + u_z\, t_r + \mathrm{St}\,\frac{\partial r}{\partial t}\, t_z - \mathrm{St}\,\frac{\partial z}{\partial t}\, t_r\right]\psi_l^{[\mathrm{f}]}\, \mathcal{J}_S\, \mathrm{d}s. \tag{5.146}$$

5.5.5 Implementation

In `oomph-lib` the `get_residual(...)` and `get_jacobian(...)` functions for the axisymmetric Navier–Stokes equations are implemented in the `AxisymmetricNavierStokesEquations` class, which implements the governing equations but contains no specific geometrical information. Concrete implementations are therefore provided by the `AxisymmetricQTaylorHoodElement` and `AxisymmetricQCrouzeixRaviartElement` classes, which inherit from the `AxisymmetricNavierStokesEquations` and `QElement<2,3>` classes. We provide a comprehensive introduction to this equation class, and its implementation in `oomph-lib`, in a tutorial located in the

`doc/axisym_navier_stokes/spin_up/`

directory. This tutorial introduces the equations in the context of an axisymmetric spin-up problem, and the source for the corresponding driver code is located in

`demo_drivers/axisym_navier_stokes/spin_up/spin_up.cc.`

As discussed in section 3.3.6, the common interfaces and functions for all fluid interface elements are implemented in the `FluidInterfaceElement` base class. The specific interface element which implements the boundary conditions at an axisymmetric surface is then implemented in the `AxisymmetricFluidInterfaceElement` class, which is derived from this base class. This is the direct equivalent of the `LineFluidInterfaceElement` class used in the two-dimensional problems discussed in the previous two chapters, and as such the same structure is used to add the 'machinery' that is

specific to the chosen node-update strategy: the `SpineLineFluidInterfaceElement` and `ElasticLineFluidInterfaceElement` classes both inherit from `AxisymmetricFluidInterfaceElement` and provide the appropriate functionality.

Chapter 6

Applications of the axisymmetric free surface Navier–Stokes equations

In chapter 4 we applied the two-dimensional free surface Navier–Stokes equations to two relaxing interface problems, and validated the implementation of these equations in `oomph-lib` against analytical predictions obtained from linear analysis. We shall now use the same technique to validate the formulation derived in the previous chapter for axisymmetric free surfaces in a cylindrical polar coordinate system. The two problems studied here are directly analogous to those studied in chapter 4: this time, however, the fluid occupies a cylindrical domain orientated in such a way that its axis of symmetry is normal to the equilibrium position of the interface.

6.1 Relaxation oscillations of a fluid layer

Let us consider the problem sketched in figure 6.1, in which we have a single, incompressible, viscous fluid layer governed by the axisymmetric Navier–Stokes equations

$$\begin{aligned}
\mathrm{Re}\,\mathrm{St}\,\frac{\partial u_r}{\partial t} + \mathrm{Re}\,\left[u_r\frac{\partial u_r}{\partial r} - \frac{u_\theta^2}{r} + u_z\frac{\partial u_r}{\partial z}\right] &= -\frac{\partial p}{\partial r} + \frac{\partial^2 u_r}{\partial r^2} + \frac{1}{r}\frac{\partial u_r}{\partial r} - \frac{u_r}{r^2} + \frac{\partial^2 u_r}{\partial z^2},\\
\mathrm{Re}\,\mathrm{St}\,\frac{\partial u_z}{\partial t} + \mathrm{Re}\,\left[u_r\frac{\partial u_z}{\partial r} + u_z\frac{\partial u_z}{\partial z}\right] &= -\frac{\partial p}{\partial z} - \frac{\mathrm{Re}}{\mathrm{Fr}} + \frac{\partial^2 u_z}{\partial r^2} + \frac{1}{r}\frac{\partial u_z}{\partial r} + \frac{\partial^2 u_z}{\partial z^2},\\
\mathrm{Re}\,\mathrm{St}\,\frac{\partial u_\theta}{\partial t} + \mathrm{Re}\,\left[u_r\frac{\partial u_\theta}{\partial r} + \frac{u_r u_\theta}{r} + u_z\frac{\partial u_\theta}{\partial z}\right] &= \frac{\partial^2 u_\theta}{\partial r^2} + \frac{1}{r}\frac{\partial u_\theta}{\partial r} - \frac{u_\theta}{r^2} + \frac{\partial^2 u_\theta}{\partial z^2}
\end{aligned} \tag{6.1}$$

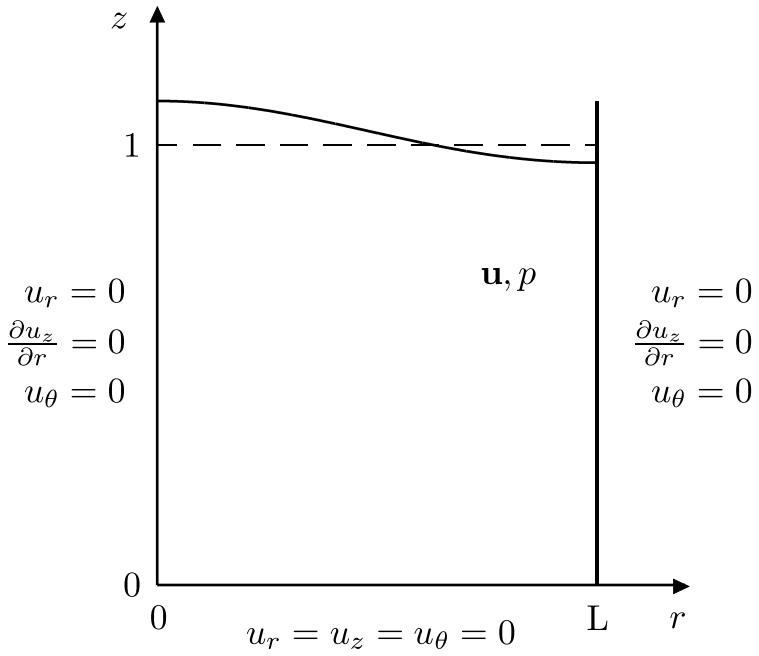

Figure 6.1: Sketch of an axisymmetric single layer free surface problem, where the axis of symmetry is located at $r = 0$. The equilibrium position of the interface corresponds to $z = 1$ and is represented by the dashed line.

and

$$\frac{\partial u_r}{\partial r} + \frac{u_r}{r} + \frac{\partial u_z}{\partial z} = 0, \tag{6.2}$$

with gravity acting in the negative z direction. The domain is $r \in [0, L]$, $z \in [0, 1]$ and is symmetric about the line $r = 0$, which corresponds to the axis of the cylindrical container. As in the Cartesian example (studied in section 4.1) we wish to compare the numerical solution of this problem to results obtained from a linear analysis, and as such require a domain which is capable of capturing a single linearised separable eigenmode of the system of equations. For an axisymmetric system such as this, a standard separation-of-variables approach reveals that the radial part of the solution is formed of a linear combination of Bessel functions of the first kind, of order zero. In order for the initial deformation of the interface to be volume conserving, however, we will require the surface to meet the 'outer wall' of the domain at right angles[1]: we must therefore treat the solid boundary at $r = L$ as a 'slippery wall' at which the fluid is unconstrained in the axial direction. Hence we apply the non-penetration conditions $u_r = u_\theta = 0$ at both the axis of symmetry and the outer wall (the left and right domain

[1]The reasons for this are discussed in detail on page 109 of the current section.

boundaries), and the usual no-slip condition $u_r = u_z = u_\theta = 0$ at the bottom solid boundary. The free surface is located at $\mathbf{X}$ and is subject to the kinematic condition,

$$\left(u_i - \mathrm{St}\,\frac{\partial X_i}{\partial t} \right) n_i = 0, \tag{6.3}$$

and the dynamic condition,

$$\tau_{ij}\, n_j = \frac{1}{\mathrm{Ca}}\,\kappa\, n_i - p_{\mathrm{ext}}\, n_i, \tag{6.4}$$

where the stress tensor is defined as

$$\begin{aligned} \tau_{rr} &= -p + 2\frac{\partial u_r}{\partial r}, & \tau_{zz} &= -p + 2\frac{\partial u_z}{\partial z}, \\ \tau_{\theta\theta} &= -p + 2\frac{u_r}{r}, & \tau_{rz} = \tau_{zr} &= \frac{\partial u_r}{\partial z} + \frac{\partial u_z}{\partial r}, \\ \tau_{r\theta} = \tau_{\theta r} &= \frac{\partial u_\theta}{\partial r} - \frac{u_\theta}{r}, & \tau_{z\theta} = \tau_{\theta z} &= \frac{\partial u_\theta}{\partial z}. \end{aligned} \tag{6.5}$$

This problem was solved numerically in `oomph-lib` using both Taylor–Hood and Crouzeix–Raviart elements. The problem domain was discretised into a 12×12 element mesh whose deformation in response to the motion of the free surface boundary was facilitated by a spine-based node update strategy (section 3.3.4). The time-derivatives were discretised using a second-order-accurate BDF scheme with a (non-dimensionalised) timestep of 0.0025. The free-surface boundary conditions (6.3 and 6.4) were implemented by attaching one-dimensional 'face' elements to the upper boundaries of the bulk elements adjacent to the free boundary.

The initial shape of the interface is defined by

$$\mathbf{X} = r\,\mathbf{e}_r + [1.0 + \epsilon J_0(kr)]\;\mathbf{e}_z, \tag{6.6}$$

where ϵ is a small parameter controlling the amplitude of the deflection away from the equilibrium position and k is a wavenumber. $J_0(kr)$ is a zeroth-order Bessel function of the first kind, so chosen because it is an eigenmode of the system and has the required property that its derivative with respect to r vanishes at $r = 0$, which ensures that the interface is smooth at the symmetry boundary. In order for the equilibrium state of the system to be such that the interface is a flat line at $z = 1$, we require an initial deformation which is volume conserving. We must therefore satisfy

$$\int_0^L r\, J_0(kr)\, dr = 0, \tag{6.7}$$

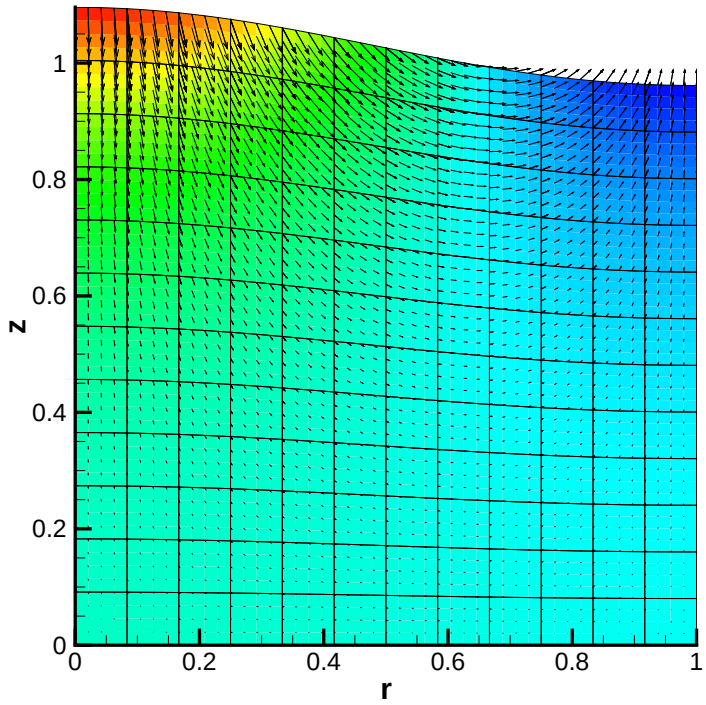

Figure 6.2: Pressure contour plot for the axisymmetric single layer relaxing interface problem at time $t = 0.005$, with superimposed velocity vectors. A mesh of 12×12 Crouzeix–Raviart elements and a second-order-accurate BDF timestepping scheme with a non-dimensionalised timestep of 0.0025 were used, for the parameters $\mathrm{Re} = \mathrm{Re}\,\mathrm{St} = \mathrm{Re}/\mathrm{Fr} = 5.0$, $\mathrm{Ca} = 0.01$, $L = 1$ and $\epsilon = 0.1$. The (non-dimensional) pressure ranges from -56 to 144, with areas of highest and lowest pressure shown in red and blue respectively. As in the Cartesian example (chapter 4), the hydrostatic pressure gradient is present yet sufficiently small that its effect cannot be seen in the colour contours.

and note that this condition is met if $J_1(k) = 0$: hence the values of the wavenumber k are constrained to be zeroes of $J_1(k)$. The properties of Bessel functions are such that the derivative of $J_0(kr)$ with respect to r, evaluated at any point along the r-axis which corresponds to a zero of $J_1(kr)$, is itself zero, and therefore the appropriate velocity boundary condition in the axial direction must be the traction-free condition $\partial u_z/\partial r = 0$. This condition could be physically realised by having a 'slippery' outer wall where the contact line can move and the contact angle is fixed at 90^o.

Figure 6.2 shows a contour plot of the pressure distribution with superimposed velocity vectors at the second timestep ($t = 0.005$), for the parameters $\mathrm{Re} = \mathrm{Re}\,\mathrm{St} = \mathrm{Re}/\mathrm{Fr} = 5.0$, $\mathrm{Ca} = 0.01$ and $L = 1$. The simulation was started impulsively with an

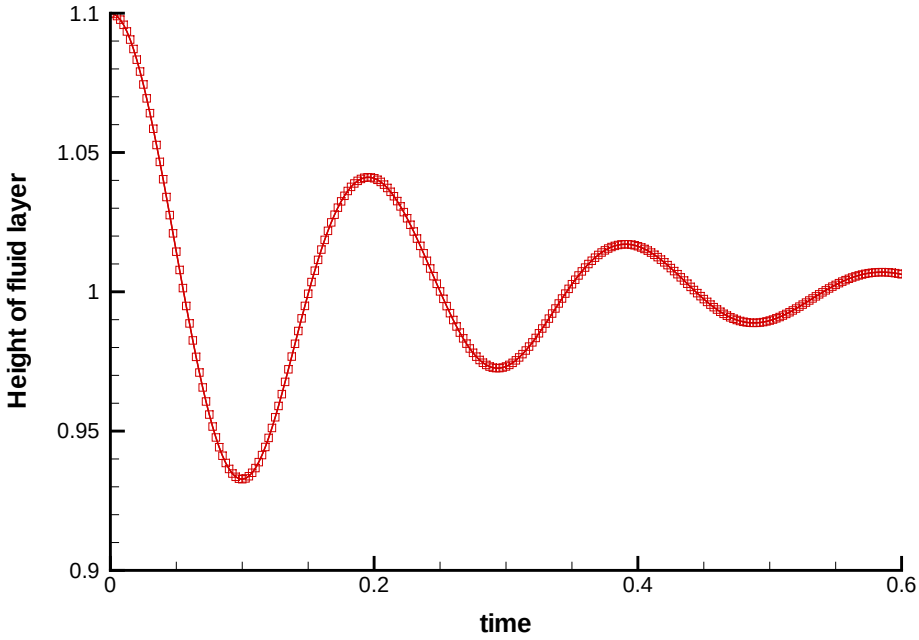

Figure 6.3: Time-trace of the height of the fluid layer at the edge of the domain for the parameters $\mathrm{Re} = \mathrm{Re}\,\mathrm{St} = \mathrm{Re}/\mathrm{Fr} = 5.0$, $\mathrm{Ca} = 0.01$, $L = 1$ and $\epsilon = 0.1$. A mesh of 12×12 Crouzeix–Raviart elements and a second-order-accurate BDF timestepping scheme with a non-dimensionalised timestep of 0.0025 were used.

initial free surface perturbation amplitude of 10% of the domain width ($\epsilon = 0.1$).

The physical description of this problem is the same as in the Cartesian case (section 4.1). As the simulation begins the restoring forces of surface tension and gravitational acceleration act to revert the deformed interface it to its equilibrium position. The surface oscillations are damped as the energy in the system is dissipated through viscous forces, until eventually the interface settles down to its undeformed state. This viscous damping effect can be seen in the time-trace of the height of the fluid layer at the edge of the domain, shown in figure 6.3.

6.1.1 Validation against an analytical dispersion relation

We shall validate the numerical simulations described above in the same way that we validated their Cartesian counterparts (described in section 4.1.1). We start by considering the problem sketched in figure 6.4, in which we are solving the axisymmetric Navier–Stokes equations (6.1 and 6.2) in a domain chosen so that the equilibrium

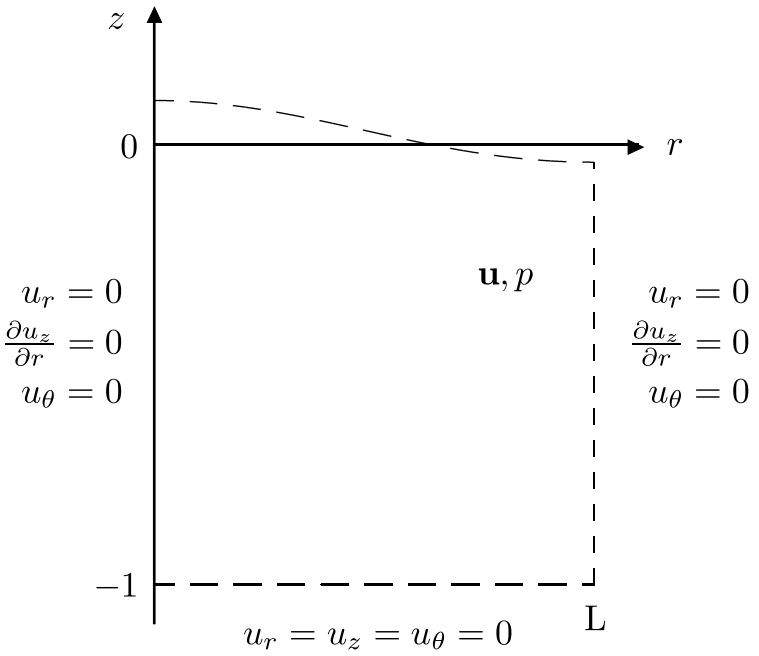

Figure 6.4: Sketch of the problem domain used to derive the dispersion relation for an axisymmetric single-layer free surface problem. As in the Cartesian example, it is convenient to set the problem up so that the equilibrium position of the interface corresponds to the line $z = 0$.

position of the interface corresponds to the line $z = 0$. As in the Cartesian case the position of the free boundary is described by defining its 'height', h, as a function of the horizontal coordinate, and the position vector to the surface can therefore be expressed as

$$\mathbf{X}(r,t) = r\,\mathbf{e}_r + h(r,t)\,\mathbf{e}_z. \tag{6.8}$$

A unit vector normal to a line specified by $z = h(r,t)$ is given by

$$\mathbf{n} = \left[1 + \left(\frac{\partial h}{\partial r}\right)^2\right]^{-\frac{1}{2}} \left(-\frac{\partial h}{\partial r}\,\mathbf{e}_r + \mathbf{e}_z\right), \tag{6.9}$$

and the curvature can be expressed as

$$\kappa = \frac{\partial^2 h}{\partial r^2}\left[1 + \left(\frac{\partial h}{\partial r}\right)^2\right]^{-\frac{3}{2}} + \frac{1}{r}\frac{\partial h}{\partial r}\left[1 + \left(\frac{\partial h}{\partial r}\right)^2\right]^{-\frac{1}{2}}. \tag{6.10}$$

Using (6.8) and (6.9) the kinematic condition (6.3) becomes

$$-u_r\frac{\partial h}{\partial r} + u_z - \mathrm{St}\,\frac{\partial h}{\partial t} = 0, \tag{6.11}$$

and using (6.9) and (6.10) the dynamic condition (6.4) is given by

$$-\frac{\partial h}{\partial r}\tau_{rr} + \tau_{rz} = -\frac{1}{\mathrm{Ca}}\frac{\partial h}{\partial r}\left\{\frac{\partial^2 h}{\partial r^2}\left[1 + \left(\frac{\partial h}{\partial r}\right)^2\right]^{-\frac{3}{2}} + \frac{1}{r}\frac{\partial h}{\partial r}\left[1 + \left(\frac{\partial h}{\partial r}\right)^2\right]^{-\frac{1}{2}}\right\} \tag{6.12}$$

and

$$-\frac{\partial h}{\partial r}\tau_{zr}+\tau_{zz}=\frac{1}{\mathrm{Ca}}\left\{\frac{\partial^2 h}{\partial r^2}\left[1+\left(\frac{\partial h}{\partial r}\right)^2\right]^{-\frac{3}{2}}+\frac{1}{r}\frac{\partial h}{\partial r}\left[1+\left(\frac{\partial h}{\partial r}\right)^2\right]^{-\frac{1}{2}}\right\},$$

where the external pressure has been set to zero. The definition of the stress tensor (6.5) can now be used to write these conditions as

$$\begin{aligned}\frac{\partial h}{\partial r}p-2\frac{\partial h}{\partial r}\frac{\partial u_r}{\partial r}+\frac{\partial u_r}{\partial z}+\frac{\partial u_z}{\partial r}&\\ =-\frac{1}{\mathrm{Ca}}\frac{\partial h}{\partial r}\left\{\frac{\partial^2 h}{\partial r^2}\left[1+\left(\frac{\partial h}{\partial r}\right)^2\right]^{-\frac{3}{2}}+\frac{1}{r}\frac{\partial h}{\partial r}\left[1+\left(\frac{\partial h}{\partial r}\right)^2\right]^{-\frac{1}{2}}\right\}&\end{aligned}\tag{6.13}$$

and

$$\begin{aligned}-\frac{\partial h}{\partial r}\left(\frac{\partial u_z}{\partial r}+\frac{\partial u_r}{\partial z}\right)-p+2\frac{\partial u_z}{\partial z}&\\ =\frac{1}{\mathrm{Ca}}\left\{\frac{\partial^2 h}{\partial r^2}\left[1+\left(\frac{\partial h}{\partial r}\right)^2\right]^{-\frac{3}{2}}+\frac{1}{r}\frac{\partial h}{\partial r}\left[1+\left(\frac{\partial h}{\partial r}\right)^2\right]^{-\frac{1}{2}}\right\}.&\end{aligned}\tag{6.14}$$

As in the Cartesian example we choose the trivial solution

$$\bar{h}=0,\qquad \bar{u}_r=\bar{u}_z=\bar{u}_\theta=0\qquad\text{and}\qquad \bar{p}=-\frac{\mathrm{Re}}{\mathrm{Fr}}\,z\tag{6.15}$$

to be the base state to which we will introduce an infinitesimal perturbation. Substituting

$$\begin{gathered}u_r=\bar{u}_r+\epsilon\,\hat{u}_r,\qquad u_z=\bar{u}_z+\epsilon\,\hat{u}_z,\qquad u_\theta=\bar{u}_\theta+\epsilon\,\hat{u}_\theta,\\ h=\bar{h}+\epsilon\,\hat{h}\qquad\text{and}\qquad p=\bar{p}+\epsilon\,\hat{p},\end{gathered}\tag{6.16}$$

where $\epsilon\ll 1$, into the governing equations (6.1 and 6.2) yields

$$\begin{aligned}\mathrm{Re}\,\mathrm{St}\,\frac{\partial\hat{u}_r}{\partial t}&=-\frac{\partial\hat{p}}{\partial r}+\frac{\partial^2\hat{u}_r}{\partial r^2}+\frac{1}{r}\frac{\partial\hat{u}_r}{\partial r}-\frac{\hat{u}_r}{r^2}+\frac{\partial^2\hat{u}_r}{\partial z^2},\\ \mathrm{Re}\,\mathrm{St}\,\frac{\partial\hat{u}_z}{\partial t}&=-\frac{\partial\hat{p}}{\partial z}+\frac{\partial^2\hat{u}_z}{\partial r^2}+\frac{1}{r}\frac{\partial\hat{u}_z}{\partial r}+\frac{\partial^2\hat{u}_z}{\partial z^2},\\ \mathrm{Re}\,\mathrm{St}\,\frac{\partial\hat{u}_\theta}{\partial t}&=\frac{\partial^2\hat{u}_\theta}{\partial r^2}+\frac{1}{r}\frac{\partial\hat{u}_\theta}{\partial r}-\frac{\hat{u}_\theta}{r^2}+\frac{\partial^2\hat{u}_\theta}{\partial z^2}\end{aligned}\tag{6.17}$$

and

$$\frac{\partial\hat{u}_r}{\partial r}+\frac{\hat{u}_r}{r}+\frac{\partial\hat{u}_z}{\partial z}=0,\tag{6.18}$$

where we have neglected orders of ϵ^2 and higher. The kinematic condition (6.11) must be evaluated at the interface, $h = \epsilon\,\hat{h}$, but we use Taylor's theorem to express u_z as a power series about $z = 0$ so that we can instead evaluate it at the undeformed position of the free boundary,

$$\hat{u}_z|_{z=0} = \mathrm{St}\,\frac{\partial \hat{h}}{\partial t}, \tag{6.19}$$

where terms of order ϵ^2 and higher have been neglected. The dynamic conditions (6.13 and 6.14) contain terms raised to negative powers, and we expand these using the binomial theorem,

$$\left[1 + \left(\frac{\partial h}{\partial r}\right)^2\right]^{-\frac{n}{2}} = \left[1 + \epsilon^2\left(\frac{\partial \hat{h}}{\partial r}\right)^2\right]^{-\frac{n}{2}} = 1 + \mathrm{O}(\epsilon^2), \tag{6.20}$$

before using (6.16) and (6.15) to give

$$\left.\frac{\partial \hat{u}_r}{\partial z}\right|_{z=0} + \left.\frac{\partial \hat{u}_z}{\partial r}\right|_{z=0} = 0 \tag{6.21}$$

and

$$-\,\hat{p}|_{z=0} + 2\,\left.\frac{\partial \hat{u}_z}{\partial z}\right|_{z=0} + \frac{\mathrm{Re}}{\mathrm{Fr}}\hat{h} = \frac{1}{\mathrm{Ca}}\left(\frac{\partial^2 \hat{h}}{\partial r^2} + \frac{1}{r}\frac{\partial \hat{h}}{\partial r}\right), \tag{6.22}$$

where we have again used Taylor's theorem to allow us to evaluate these conditions at $z = 0$. Finally, we have the following Dirichlet boundary conditions:

$$\hat{u}_r|_{z=-1} = 0, \qquad \hat{u}_z|_{z=-1} = 0, \qquad \hat{u}_\theta|_{z=-1} = 0, \tag{6.23}$$

$$\hat{u}_r|_{r=0} = 0, \qquad \hat{u}_\theta|_{r=0} = 0, \tag{6.24}$$

$$\hat{u}_r|_{r=L} = 0, \qquad \text{and} \qquad \hat{u}_\theta|_{r=L} = 0. \tag{6.25}$$

The governing equations, (6.18) and (6.17), and boundary conditions, (6.19) and (6.21)–(6.25), have now been linearised and we propose a separable solution of the form

$$\begin{aligned}
\hat{h}(r,t) &= H\,J_0(kr)\,e^{\lambda t},\\
\hat{u}_r(r,z,t) &= U(z)\,J_1(kr)\,e^{\lambda t},\\
\hat{u}_z(r,z,t) &= W(z)\,J_0(kr)\,e^{\lambda t},\\
\hat{u}_\theta(r,z,t) &= 0 \quad \text{and}\\
\hat{p}(r,z,t) &= P(z)\,J_0(kr)\,e^{\lambda t},
\end{aligned} \tag{6.26}$$

where J_ν is a Bessel function of the first kind of ν-th order. Because the perturbation that we are introducing, $\hat{h}(r,t)$, is an eigenmode of the system and is independent of θ, we can infer that the swirl, $\hat{u}_\theta$, is zero for all time. $J_1(0) = 0$ and hence the symmetry boundary condition at the axis (6.24) is automatically satisfied, but we note that (6.26) only satisfies the symmetry condition at the outer wall (6.25) if k is chosen so that $J_1(k) = 0$.

Substituting (6.26) into the linearised governing equations (6.17) and (6.18) yields

$$\begin{aligned}
\operatorname{Re}\operatorname{St}\lambda U J_1(kr) =& -P\frac{\partial}{\partial r}\Big[J_0(kr)\Big] + U\frac{\partial^2}{\partial r^2}\Big[J_1(kr)\Big] \\
&+ \frac{U}{r}\frac{\partial}{\partial r}\Big[J_1(kr)\Big] - \frac{U}{r^2}J_1(kr) + \frac{\mathrm{d}^2U}{\mathrm{d}z^2}J_1(kr), \\
\operatorname{Re}\operatorname{St}\lambda W J_0(kr) =& -\frac{\mathrm{d}P}{\mathrm{d}z}J_0(kr) + W\frac{\partial^2}{\partial r^2}\Big[J_0(kr)\Big] \\
&+ \frac{W}{r}\frac{\partial}{\partial r}\Big[J_0(kr)\Big] + \frac{\mathrm{d}^2W}{\mathrm{d}z^2}J_0(kr)
\end{aligned} \tag{6.27}$$

and

$$U\frac{\partial}{\partial r}\Big[J_1(kr)\Big] + \frac{U}{r}J_1(kr) + \frac{\mathrm{d}W}{\mathrm{d}z}J_0(kr) = 0. \tag{6.28}$$

The following property of Bessel functions,

$$\frac{\mathrm{d}}{\mathrm{d}z}\Big[z^{-\nu}J_\nu(z)\Big] = -z^{-\nu}J_{\nu+1}(z), \tag{6.29}$$

allows us to evaluate their derivatives and hence we obtain

$$\begin{aligned}
\operatorname{Re}\operatorname{St}\lambda U J_1(kr) &= kPJ_1(kr) + \frac{\mathrm{d}^2U}{\mathrm{d}z^2}J_1(kr) + U\left[k^2J_3(kr) - \frac{4k}{r}J_2(kr)\right], \\
\operatorname{Re}\operatorname{St}\lambda W J_0(kr) &= -\frac{\mathrm{d}P}{\mathrm{d}z}J_0(kr) + \frac{\mathrm{d}^2W}{\mathrm{d}z^2}J_0(kr) \\
&\qquad + W\left[k^2J_2(kr) - \frac{2k}{r}J_1(kr)\right]
\end{aligned} \tag{6.30}$$

and

$$U\left[\frac{2}{r}J_1(kr) - kJ_2(kr)\right] + \frac{\mathrm{d}W}{\mathrm{d}z}J_0(kr) = 0. \tag{6.31}$$

We can combine Bessel functions of different orders using

$$J_{\nu-1}(kr) + J_{\nu+1}(kr) = \frac{2\nu}{kr}J_\nu(kr), \tag{6.32}$$

and applying this to (6.30) and (6.31) yields

$$\mathrm{Re}\,\mathrm{St}\,\lambda\,U = kP + \frac{\mathrm{d}^2U}{\mathrm{d}z^2} - k^2U, \tag{6.33}$$

$$\mathrm{Re}\,\mathrm{St}\,\lambda\,W = -\frac{\mathrm{d}P}{\mathrm{d}z} + \frac{\mathrm{d}^2W}{\mathrm{d}z^2} - k^2W \tag{6.34}$$

and

$$kU + \frac{\mathrm{d}W}{\mathrm{d}z} = 0. \tag{6.35}$$

We can now rearrange (6.35) for U and substitute it into (6.33) to give

$$P = \frac{1}{k^2}\frac{\mathrm{d}^3W}{\mathrm{d}z^3} - \left(1 + \frac{\mathrm{Re}\,\mathrm{St}\,\lambda}{k^2}\right)\frac{\mathrm{d}W}{\mathrm{d}z}, \tag{6.36}$$

where we have rearranged for P. We then differentiate this expression with respect to z and substitute it into (6.34) to obtain a fourth-order ODE in W,

$$\frac{\mathrm{d}^4W}{\mathrm{d}z^4} - \left(\mathrm{Re}\,\mathrm{St}\,\lambda + 2k^2\right)\frac{\mathrm{d}^2W}{\mathrm{d}z^2} + k^2\left(\mathrm{Re}\,\mathrm{St}\,\lambda + k^2\right)W = 0. \tag{6.37}$$

The coefficients of W are all constant and hence assuming a solution of the form $W(z) = Ae^{mz}$ yields the general solution

$$W(z) = Ae^{kz} + Be^{-kz} + Ce^{\beta z} + De^{-\beta z}, \tag{6.38}$$

where $\beta = \sqrt{\mathrm{Re}\,\mathrm{St}\,\lambda + k^2}$ and we have assumed that $\mathrm{Re}\,\mathrm{St} > 0$. Using (6.35) and (6.36) we can also obtain general solutions for $U(z)$,

$$U(z) = -Ae^{kz} + Be^{-kz} - \frac{\beta}{k}Ce^{\beta z} + \frac{\beta}{k}De^{-\beta z}, \tag{6.39}$$

and $P(z)$,

$$P(z) = -\frac{\mathrm{Re}\,\mathrm{St}\,\lambda}{k}Ae^{kz} + \frac{\mathrm{Re}\,\mathrm{St}\,\lambda}{k}Be^{-kz}. \tag{6.40}$$

A, B, C and D are constant coefficients to be determined from the boundary conditions, and we therefore substitute the same ansatz (6.26) into (6.19), (6.21), (6.22) and (6.23) to obtain the separated forms of the kinematic,

$$W(0) = \mathrm{St}\,H\,\lambda, \tag{6.41}$$

dynamic,

$$\left.\frac{\mathrm{d}U}{\mathrm{d}z}\right|_{z=0} - k\,W(0) = 0 \tag{6.42}$$

and

$$-P(0) + 2\left.\frac{\mathrm{d}W}{\mathrm{d}z}\right|_{z=0} + \left(\frac{k^2}{\mathrm{Ca}} + \frac{\mathrm{Re}}{\mathrm{Fr}}\right) H = 0, \tag{6.43}$$

and Dirichlet conditions,

$$U(-1) = 0 \qquad \text{and} \qquad W(-1) = 0. \tag{6.44}$$

We can now use the general solutions of $U(z)$, $W(z)$ and $P(z)$ in (6.41)–(6.44) to obtain the following homogeneous linear system,

$$\begin{aligned}
A + B + C + D - \mathrm{St}\,\lambda H &= 0, \\
2k^2 (A + B) + \left(\mathrm{Re}\,\mathrm{St}\,\lambda + 2k^2\right)(C + D) &= 0, \\
\frac{\mathrm{Re}\,\mathrm{St}\,\lambda + 2k^2}{k}(A - B) + 2\beta (C - D) + \left(\frac{k^2}{\mathrm{Ca}} + \frac{\mathrm{Re}}{\mathrm{Fr}}\right) H &= 0, \\
-Ae^{-k} + Be^{k} - \frac{\beta}{k} Ce^{-\beta} + \frac{\beta}{k} De^{\beta} &= 0, \\
Ae^{-k} + Be^{k} + Ce^{-\beta} + De^{\beta} &= 0.
\end{aligned} \tag{6.45}$$

As usual this system of five equations in the five unknowns A, B, C, D and H can be written in matrix form, and there exists a non-trivial solution only if the determinant of the matrix made up of the coefficients of the unknowns is equal to zero. We solve this equation numerically as before to obtain a dispersion relation $\lambda(k)$, and compare this analytical result to `oomph-lib`'s computations for given values of k. As discussed in section 6.1 we require the values of k to be such that $J_1(kr) = 0$ at $r = L$, the domain boundary. A disadvantage of this from a numerical point of view is that for each subsequent root of $J_1(kr)$ the free boundary becomes increasingly complex spatially and therefore requires more elements to resolve it properly. We choose to use an alternative (but equivalent) approach where we instead vary the width of the domain, and fix the initial shape of the surface so that the right-hand side of the domain always corresponds to the first root of $J_1(kr)$. As the first root of $J_1(z)$ is $z = 3.8317$, varying the width of the domain from $L = 0.24$ to $L = 2.0$ is equivalent to varying k between 15.9654 and 1.91585.

An initial deflection amplitude of 1% of the domain width was chosen to be 'sufficiently small' that the nonlinear terms would be negligible, and the growth rate and

frequency of the oscillation was determined from a time-trace of the left-hand edge of the interface (such as the one plotted in figure 6.3) using the same Levenberg–Marquardt fitting technique as before. The comparison is shown in figure 6.5, where the real and imaginary parts of λ are plotted as lines and the points are the results generated using `oomph-lib`. We note that, as in the Cartesian case, our numerical results agree very well with those predicted by the linear theory.

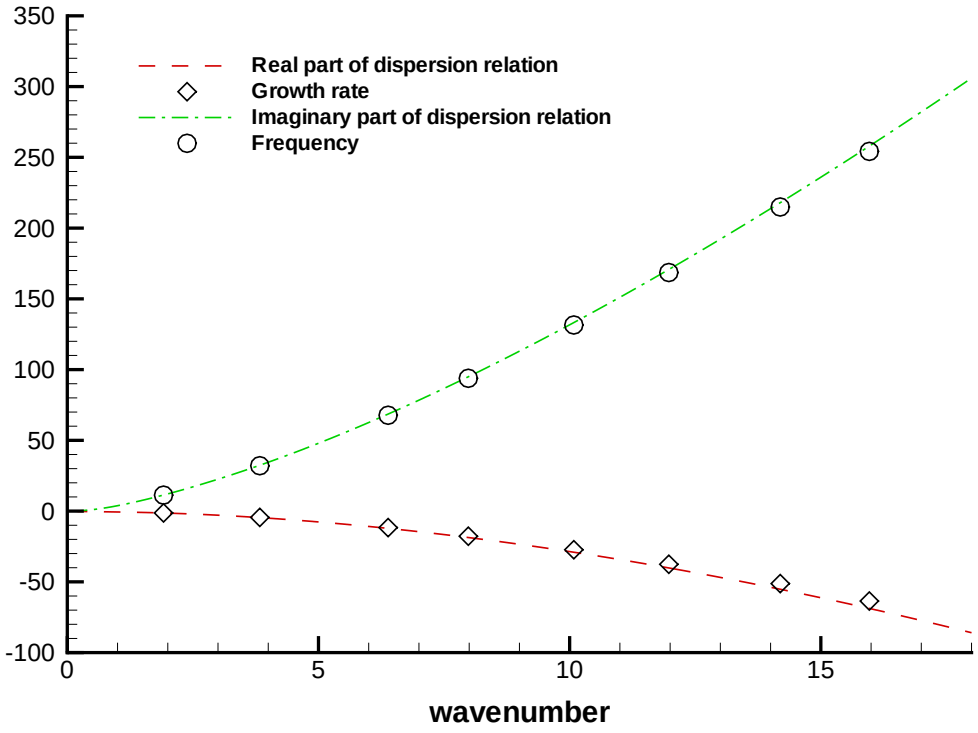

Figure 6.5: Validation of the `oomph-lib` code (points) by comparison with an analytical dispersion relation (lines) for the axisymmetric single-layer interface problem. The `oomph-lib` simulations employ a 12×12 element mesh and a second-order BDF timestepper with a (non-dimensionalised) timestep of 0.0025, for the parameters $\mathrm{Re} = \mathrm{Re}\,\mathrm{St} = \mathrm{Re}/\mathrm{Fr} = 5.0$, $\mathrm{Ca} = 0.01$ and $\epsilon = 0.01$.

6.1.2 Implementation

The problem discussed above was implemented as a demonstration code in `oomph-lib`, and its source file,

`single_layer_free_surface_axisym.cc`,

is located in the

```
demo_drivers/axisym_navier_stokes/single_layer_free_surface_axisym/
```

directory.

6.2 Relaxation oscillations of an interface between two viscous fluids

We will now briefly extend the problem discussed in section 6.1 to one involving two immiscible, incompressible viscous fluids separated by an interface, as sketched in figure 6.6. As in the Cartesian two-layer example (section 4.2), the formulation only requires slight modification from that described for the single-layer case. The governing equations in the lower fluid are exactly as before (6.1 and 6.2), while the momentum equation in the upper fluid requires modification to include the density and viscosity ratios:

$$R_\rho \,\mathrm{Re}\left[\mathrm{St}\,\frac{\partial u_r}{\partial t} + u_r\frac{\partial u_r}{\partial r} - \frac{u_\theta^2}{r} + u_z\frac{\partial u_r}{\partial z}\right] = -\frac{\partial p}{\partial r} + R_\mu\left[\frac{\partial^2 u_r}{\partial r^2} + \frac{1}{r}\frac{\partial u_r}{\partial r} - \frac{u_r}{r^2} + \frac{\partial^2 u_r}{\partial z^2}\right],$$

$$R_\rho \,\mathrm{Re}\left[\mathrm{St}\,\frac{\partial u_z}{\partial t} + u_r\frac{\partial u_z}{\partial r} + u_z\frac{\partial u_z}{\partial z}\right] = -\frac{\partial p}{\partial z} - R_\rho\,\frac{\mathrm{Re}}{\mathrm{Fr}} + R_\mu\left[\frac{\partial^2 u_z}{\partial r^2} + \frac{1}{r}\frac{\partial u_z}{\partial r} + \frac{\partial^2 u_z}{\partial z^2}\right]$$

and

$$R_\rho \,\mathrm{Re}\left[\mathrm{St}\,\frac{\partial u_\theta}{\partial t} + u_r\frac{\partial u_\theta}{\partial r} + \frac{u_r u_\theta}{r} + u_z\frac{\partial u_\theta}{\partial z}\right] = R_\mu\left[\frac{\partial^2 u_\theta}{\partial r^2} + \frac{1}{r}\frac{\partial u_\theta}{\partial r} - \frac{u_\theta}{r^2} + \frac{\partial^2 u_\theta}{\partial z^2}\right]. \tag{6.46}$$

The domain is very similar to that of the single-layer case, with non-penetration conditions $u_r = u_\theta = 0$ applied at both the axis of symmetry ($r = 0$) and the outer wall ($r = L$), and no-slip conditions $u_r = u_z = u_\theta = 0$ applied on the top ($z = 2$) and bottom ($z = 0$) solid boundaries. Gravity acts in the negative z direction. The interface is located at $\mathbf{X}$ and is subject to the kinematic condition (6.3) and the dynamic condition,

$$\tau_{ij}^{[1]}\, n_j^{[1]} = \tau_{ij}^{[2]}\, n_j^{[1]} + \frac{1}{\mathrm{Ca}}\kappa\, n_i^{[1]}, \tag{6.47}$$

where the lower and upper fluids are denoted by [1] and [2] respectively. The stress tensor in the lower fluid is identical to that in the single-layer case (6.5), and the stress tensor in the upper fluid is defined in (5.87).

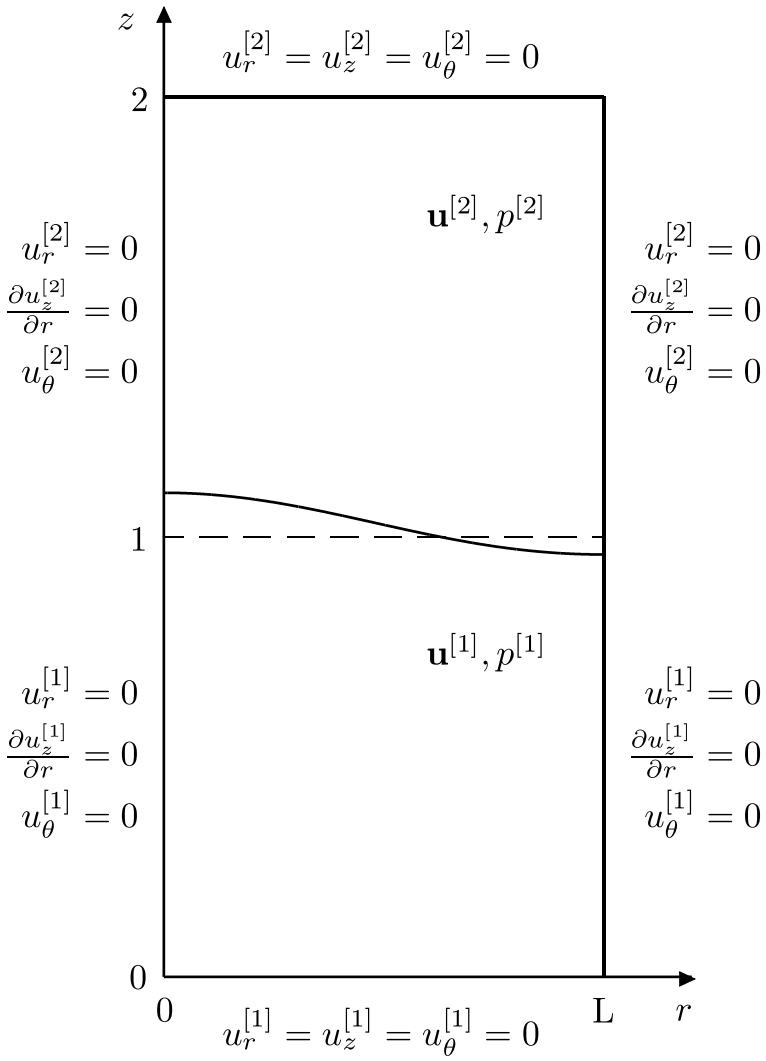

Figure 6.6: Sketch of an axisymmetric two layer interface problem, where the axis of symmetry is located at $r = 0$. The equilibrium position of the interface is located at $z = 1$ and is represented by the dashed line.

This problem was solved numerically in `oomph-lib` using a very similar approach to the previous example (discussed in section 6.1). The two regions of the mesh corresponding to the two fluid layers were each discretised using 12×12 Crouzeix–Raviart elements, since Taylor–Hood elements cannot accomodate the pressure jump at the interface. The usual spine-based node update strategy was used to deform the mesh in response to the motion of the interface, and the time-derivatives were again discretised using a second-order-accurate BDF scheme with a (non-dimensionalised) timestep of 0.005.

The simulation was started impulsively from the initial conditions of zero velocity everywhere and an interfacial deformation as before (6.6), and ran for 240 timesteps.

Figure 6.7 shows a time-trace of the height of the fluid layer at the edge of the domain for the parameters $\mathrm{Re} = \mathrm{Re}\,\mathrm{St} = \mathrm{Re}/\mathrm{Fr} = 5.0$, $\mathrm{Ca} = 0.01$, $R_\rho = 0.5$, $R_\mu = 0.1$, $L = 1$ and an initial deflection amplitude of $\epsilon = 0.1$.

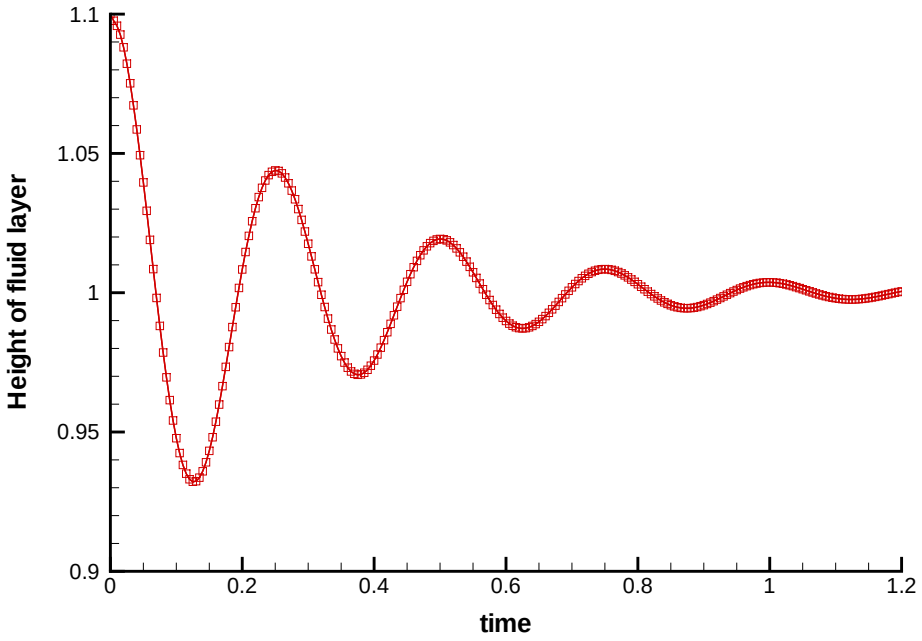

Figure 6.7: Time-trace of the height of the interface at the point $r = 0$ for the parameters $\mathrm{Re} = \mathrm{Re}\,\mathrm{St} = \mathrm{Re}/\mathrm{Fr} = 5.0$, $\mathrm{Ca} = 0.01$, $R_\rho = 0.5$, $R_\mu = 0.1$, $L = 1$ and $\epsilon = 0.1$. A mesh of 12×24 Crouzeix–Raviart elements and a second-order-accurate BDF timestepping scheme with a non-dimensionalised timestep of 0.005 were used.

6.2.1 Validation against an analytical dispersion relation

The simulations described above were validated against an analytical test case in a similar manner to those discussed in section 6.1. We consider a domain $r \in [0, L]$, $z \in [-1, 1]$, with gravity acting in the negative z direction, in which two fluids governed by the Navier–Stokes equations are separated by an interface located at $z = 0$. For sufficiently small amplitudes the governing equations can be linearised about the trivial steady base state

$$\bar{h} = 0, \qquad \bar{u}_r^{[1]} = \bar{u}_z^{[1]} = \bar{u}_\theta^{[1]} = \bar{u}_r^{[2]} = \bar{u}_z^{[2]} = \bar{u}_\theta^{[2]} = 0,$$

$$\bar{p}^{[1]} = -R_\rho^{[1]} \frac{\mathrm{Re}}{\mathrm{Fr}} (z + 1) \qquad \text{and} \qquad \bar{p}^{[2]} = -\frac{\mathrm{Re}}{\mathrm{Fr}} \left(R_\rho^{[1]} + R_\rho^{[2]} z \right) \tag{6.48}$$

to give

$$R_\rho^{[\beta]}\mathrm{Re}\,\mathrm{St}\,\frac{\partial \hat{u}_r^{[\beta]}}{\partial t} = -\frac{\partial \hat{p}^{[\beta]}}{\partial r} + R_\mu^{[\beta]}\left[\frac{\partial^2 \hat{u}_r^{[\beta]}}{\partial r^2} + \frac{1}{r}\frac{\partial \hat{u}_r^{[\beta]}}{\partial r} - \frac{\hat{u}_r^{[\beta]}}{r^2} + \frac{\partial^2 \hat{u}_r^{[\beta]}}{\partial z^2}\right],$$

$$R_\rho^{[\beta]}\mathrm{Re}\,\mathrm{St}\,\frac{\partial \hat{u}_z^{[\beta]}}{\partial t} = -\frac{\partial \hat{p}^{[\beta]}}{\partial z} + R_\mu^{[\beta]}\left[\frac{\partial^2 \hat{u}_z^{[\beta]}}{\partial r^2} + \frac{1}{r}\frac{\partial \hat{u}_z^{[\beta]}}{\partial r} + \frac{\partial^2 \hat{u}_z^{[\beta]}}{\partial z^2}\right],$$

$$R_\rho^{[\beta]}\mathrm{Re}\,\mathrm{St}\,\frac{\partial \hat{u}_\theta^{[\beta]}}{\partial t} = R_\mu^{[\beta]}\left[\frac{\partial^2 \hat{u}_\theta^{[\beta]}}{\partial r^2} + \frac{1}{r}\frac{\partial \hat{u}_\theta^{[\beta]}}{\partial r} - \frac{\hat{u}_\theta^{[\beta]}}{r^2} + \frac{\partial^2 \hat{u}_\theta^{[\beta]}}{\partial z^2}\right] \tag{6.49}$$

and

$$\frac{\partial \hat{u}_r^{[\beta]}}{\partial r} + \frac{\hat{u}_r^{[\beta]}}{r} + \frac{\partial \hat{u}_z^{[\beta]}}{\partial z} = 0, \tag{6.50}$$

where $\beta = 1, 2$ and we note that $R_\rho^{[1]} = R_\mu^{[1]} = 1$. The linearised form of the kinematic boundary condition is as before,

$$\hat{u}_z^{[\beta]}\big|_{z=0} = \mathrm{St}\,\frac{\partial \hat{h}}{\partial t}, \tag{6.51}$$

and the two components of the linearised dynamic condition are

$$R_\mu^{[1]}\left.\frac{\partial \hat{u}_r^{[1]}}{\partial z}\right|_{z=0} + R_\mu^{[1]}\left.\frac{\partial \hat{u}_z^{[1]}}{\partial r}\right|_{z=0} = R_\mu^{[2]}\left.\frac{\partial \hat{u}_r^{[2]}}{\partial z}\right|_{z=0} + R_\mu^{[2]}\left.\frac{\partial \hat{u}_z^{[2]}}{\partial r}\right|_{z=0} \tag{6.52}$$

and

$$-\hat{p}^{[1]}\big|_{z=0} + 2R_\mu^{[1]}\left.\frac{\partial \hat{u}_z^{[1]}}{\partial z}\right|_{z=0} = -\hat{p}^{[2]}\big|_{z=0} + 2R_\mu^{[2]}\left.\frac{\partial \hat{u}_z^{[2]}}{\partial z}\right|_{z=0} + \frac{1}{\mathrm{Ca}}\left[\frac{\partial^2 \hat{h}}{\partial r^2} + \frac{1}{r}\frac{\partial \hat{h}}{\partial r}\right] - \frac{\mathrm{Re}}{\mathrm{Fr}}\left(R_\rho^{[1]} - R_\rho^{[2]}\right)\hat{h}. \tag{6.53}$$

Additionally we have the following Dirichlet conditions at the top and bottom solid boundaries,

$$\hat{u}_r^{[1]}\big|_{z=-1} = \hat{u}_z^{[1]}\big|_{z=-1} = \left.\hat{u}_\theta^{[1]}\right|_{z=-1} = 0, \tag{6.54}$$

$$\hat{u}_r^{[2]}\big|_{z=1} = \hat{u}_z^{[2]}\big|_{z=1} = \left.\hat{u}_\theta^{[2]}\right|_{z=1} = 0, \tag{6.55}$$

and we note that the radial and azimuthal components of the velocity must be continuous across the interface,

$$\hat{u}_r^{[1]}\big|_{z=0} = \hat{u}_r^{[2]}\big|_{z=0} \qquad \text{and} \qquad \left.\hat{u}_\theta^{[1]}\right|_{z=0} = \left.\hat{u}_\theta^{[2]}\right|_{z=0}. \tag{6.56}$$

Continuity of the vertical component of velocity across the interface can be ensured by evaluating the kinematic condition (6.51) for both fluids. Substitution of the ansatz

$$\begin{aligned}
\hat{h}(r,t) &= H\, J_0(kr)\, e^{\lambda t},\\
\hat{u}_r^{[\beta]}(r,z,t) &= U^{[\beta]}(z)\, J_1(kr)\, e^{\lambda t},\\
\hat{u}_z^{[\beta]}(r,z,t) &= W^{[\beta]}(z)\, J_0(kr)\, e^{\lambda t},\\
\hat{u}_\theta^{[\beta]}(r,z,t) &= 0 \quad \text{and}\\
\hat{p}^{[\beta]}(r,z,t) &= P^{[\beta]}(z)\, J_0(kr)\, e^{\lambda t}
\end{aligned} \tag{6.57}$$

into the linearised governing equations and boundary conditions yields the following linear system,

$$\begin{aligned}
A^{[1]} + B^{[1]} + C^{[1]} + D^{[1]} - \mathrm{St}\,\lambda H &= 0,\\
A^{[2]} + B^{[2]} + C^{[2]} + D^{[2]} - \mathrm{St}\,\lambda H &= 0,\\
R_\mu^{[1]} A^{[1]} + R_\mu^{[1]} B^{[1]} + \left(\frac{R_\rho^{[1]}\mathrm{Re}\,\mathrm{St}\,\lambda}{2k^2} + R_\mu^{[1]}\right)\left(C^{[1]} + D^{[1]}\right)&\\
-R_\mu^{[2]} A^{[2]} - R_\mu^{[2]} B^{[2]} - \left(\frac{R_\rho^{[2]}\mathrm{Re}\,\mathrm{St}\,\lambda}{2k^2} + R_\mu^{[2]}\right)\left(C^{[2]} + D^{[2]}\right) &= 0,\\
\left(\frac{R_\rho^{[1]}\mathrm{Re}\,\mathrm{St}\,\lambda}{k} + 2R_\mu^{[1]}k\right)\left(A^{[1]} - B^{[1]}\right) + 2R_\mu^{[1]} a_1 \left(C^{[1]} - D^{[1]}\right)&\\
- \left(\frac{R_\rho^{[2]}\mathrm{Re}\,\mathrm{St}\,\lambda}{k} + 2R_\mu^{[2]}k\right)\left(A^{[2]} - B^{[2]}\right) - 2R_\mu^{[2]} a_2 \left(C^{[2]} - D^{[2]}\right)&\\
+ \left(\frac{k^2}{\mathrm{Ca}} + \frac{\mathrm{Re}}{\mathrm{Fr}}\left(R_\rho^{[1]} - R_\rho^{[2]}\right)\right) H &= 0,\\
-A^{[1]} e^{-k} + B^{[1]} e^{k} - \frac{a_1}{k} C^{[1]} e^{-a_1} + \frac{a_1}{k} D^{[1]} e^{a_1} &= 0,\\
A^{[1]} e^{-k} + B^{[1]} e^{k} + C^{[1]} e^{-a_1} + D^{[1]} e^{a_1} &= 0,\\
-A^{[2]} e^{k} + B^{[2]} e^{-k} - \frac{a_2}{k} C^{[2]} e^{a_2} + \frac{a_2}{k} D^{[2]} e^{-a_2} &= 0,\\
A^{[2]} e^{k} + B^{[2]} e^{-k} + C^{[2]} e^{a_2} + D^{[2]} e^{-a_2} &= 0,\\
-A^{[1]} + B^{[1]} - \frac{a_1}{k} C^{[1]} + \frac{a_1}{k} D^{[1]} + A^{[2]} - B^{[2]} + \frac{a_2}{k} C^{[2]} - \frac{a_2}{k} D^{[2]} &= 0,
\end{aligned}$$

where $a_\beta = \left[\left(R_\rho^{[\beta]}\mathrm{Re}\,\mathrm{St}\,\lambda/R_\mu^{[\beta]}\right) + k^2\right]^{1/2}$. The dispersion relation $\lambda(k)$ was obtained using the same procedure as before (section 6.1.1), and figure 6.8 compares the real and imaginary parts of λ with the growth rate and frequency of the oscillating interface as computed by `oomph-lib` for a range of wavenumbers k. An initial deflection amplitude of 1% of the domain width was again chosen for this validation exercise.

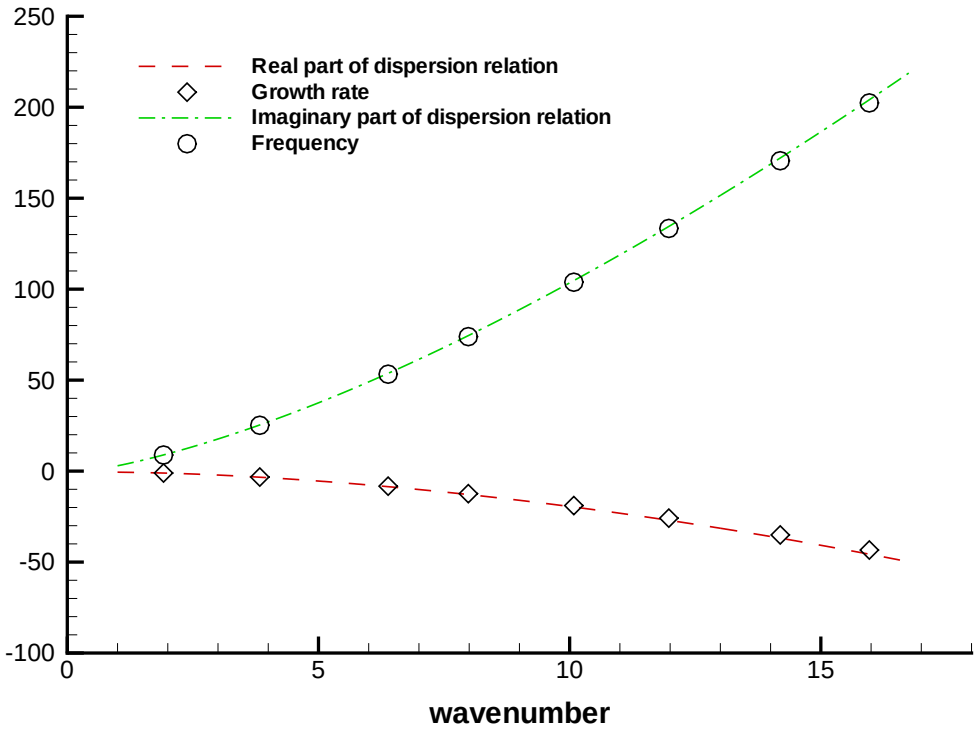

Figure 6.8: Validation of the `oomph-lib` code (points) by comparison with an analytical dispersion relation (lines) for the axisymmetric two-layer interface problem. The `oomph-lib` simulations employ a 12×24 element mesh and a second-order BDF timestepper with a (non-dimensionalised) timestep of 0.005, for the parameters $\mathrm{Re} = \mathrm{Re}\,\mathrm{St} = \mathrm{Re}/\mathrm{Fr} = 5.0$, $\mathrm{Ca} = 0.01$, $R_\rho = 0.5$, $R_\mu = 0.1$ and $\epsilon = 0.01$.

6.2.2 Implementation

As in the case of the single-layer example, the problem discussed above was implemented as an `oomph-lib` demonstration code, and its source,

```
spine_two_layer_interface_axisym.cc,
```

is located in the

```
demo_drivers/axisym_navier_stokes/two_layer_interface_axisym/
```

directory. The same problem was also implemented using a pseudo-solid node-update strategy, and its source file,

```
elastic_two_layer_interface_axisym.cc,
```

is located in the same directory. There is excellent agreement between the results generated by the two implementations of this problem, and the pseudo-solid version of this driver code was also comprehensively documented in a tutorial located in the

```
doc/axisym_navier_stokes/two_layer_interface_axisym/
```

directory.

Chapter 7

Perturbations to axisymmetric flows: Part one

Having discussed the finite element formulation of the Navier–Stokes equations in cylindrical polar coordinates, and their implementation within the `oomph-lib` framework, we shall now move on to considering the effect of introducing a (small) non-axisymmetric perturbation to an axisymmetric base state. We will introduce this formulation in two parts: first, in the current chapter, we derive the set of equations which describe a linear, non-axisymmetric perturbation to the bulk axisymmetric Navier–Stokes equations. In the subsequent chapter we then illustrate the application of these equations by considering two single-phase problems. The second part of this discussion will then begin in chapter 9, where we derive the equations describing a linear perturbation to the free boundary conditions. Finally, chapter 10 considers the effect of introducing a linear perturbation to a two-phase flow.

7.1 Linearisation of the bulk equations

We begin by considering just the bulk terms in the weak form of the Navier–Stokes equations in a cylindrical polar coordinate system. From (5.40), (5.45) and (5.50) the

radial, axial and azimuthal momentum equations are given by

$$\begin{aligned}\mathcal{R}_{\mathrm{r}}^{[\mathrm{f,bulk}]} = \iiint_V \Bigg\{ & R_\rho \,\mathrm{Re}\left[\mathrm{St}\, r\frac{\partial u_r}{\partial t} + r u_r\frac{\partial u_r}{\partial r} + r u_z\frac{\partial u_r}{\partial z} + u_\theta\frac{\partial u_r}{\partial \theta} - u_\theta^2\right]\phi^{[\mathrm{f}]} \\ & - r B_r\,\phi^{[\mathrm{f}]} - R_\rho\,\frac{\mathrm{Re}}{\mathrm{Fr}}\, r\, G_r\,\phi^{[\mathrm{f}]} + r\left[-p + 2R_\mu\frac{\partial u_r}{\partial r}\right]\frac{\partial \phi^{[\mathrm{f}]}}{\partial r} \\ & + R_\mu r\left[\frac{\partial u_z}{\partial r} + \frac{\partial u_r}{\partial z}\right]\frac{\partial \phi^{[\mathrm{f}]}}{\partial z} + R_\mu\left[\frac{\partial u_\theta}{\partial r} + \frac{1}{r}\frac{\partial u_r}{\partial \theta} - \frac{u_\theta}{r}\right]\frac{\partial \phi^{[\mathrm{f}]}}{\partial \theta} \\ & + \left[-p + \frac{2R_\mu}{r}\frac{\partial u_\theta}{\partial \theta} + \frac{2R_\mu}{r}u_r\right]\phi^{[\mathrm{f}]}\Bigg\}\,\mathrm{d}r\,\mathrm{d}z\,\mathrm{d}\theta, \end{aligned} \tag{7.1}$$

$$\begin{aligned}\mathcal{R}_{\mathrm{z}}^{[\mathrm{f,bulk}]} = \iiint_V \Bigg\{ & R_\rho \,\mathrm{Re}\left[\mathrm{St}\, r\frac{\partial u_z}{\partial t} + r u_r\frac{\partial u_z}{\partial r} + r u_z\frac{\partial u_z}{\partial z} + u_\theta\frac{\partial u_z}{\partial \theta}\right]\phi^{[\mathrm{f}]} \\ & - r B_z\,\phi^{[\mathrm{f}]} - R_\rho\,\frac{\mathrm{Re}}{\mathrm{Fr}}\, r\, G_z\,\phi^{[\mathrm{f}]} + R_\mu r\left[\frac{\partial u_r}{\partial z} + \frac{\partial u_z}{\partial r}\right]\frac{\partial \phi^{[\mathrm{f}]}}{\partial r} \\ & + r\left[-p + 2R_\mu\frac{\partial u_z}{\partial z}\right]\frac{\partial \phi^{[\mathrm{f}]}}{\partial z} + R_\mu\left[\frac{\partial u_\theta}{\partial z} + \frac{1}{r}\frac{\partial u_z}{\partial \theta}\right]\frac{\partial \phi^{[\mathrm{f}]}}{\partial \theta}\Bigg\}\,\mathrm{d}r\,\mathrm{d}z\,\mathrm{d}\theta \end{aligned} \tag{7.2}$$

and

$$\begin{aligned}\mathcal{R}_{\theta}^{[\mathrm{f,bulk}]} = \iiint_V \Bigg\{ & R_\rho \,\mathrm{Re}\left[\mathrm{St}\, r\frac{\partial u_\theta}{\partial t} + r u_r\frac{\partial u_\theta}{\partial r} + r u_z\frac{\partial u_\theta}{\partial z} + u_\theta\frac{\partial u_\theta}{\partial \theta} + u_r u_\theta\right]\phi^{[\mathrm{f}]} \\ & - r B_\theta\,\phi^{[\mathrm{f}]} - R_\rho\,\frac{\mathrm{Re}}{\mathrm{Fr}}\, r\, G_\theta\,\phi^{[\mathrm{f}]} + R_\mu\left[\frac{\partial u_r}{\partial \theta} - u_\theta + r\frac{\partial u_\theta}{\partial r}\right]\frac{\partial \phi^{[\mathrm{f}]}}{\partial r} \\ & + R_\mu\left[\frac{\partial u_z}{\partial \theta} + r\frac{\partial u_\theta}{\partial z}\right]\frac{\partial \phi^{[\mathrm{f}]}}{\partial z} + \left[-p + \frac{2R_\mu}{r}\frac{\partial u_\theta}{\partial \theta} + \frac{2R_\mu}{r}u_r\right]\frac{\partial \phi^{[\mathrm{f}]}}{\partial \theta} \\ & - R_\mu\left[\frac{\partial u_\theta}{\partial r} + \frac{1}{r}\frac{\partial u_r}{\partial \theta} - \frac{u_\theta}{r}\right]\phi^{[\mathrm{f}]}\Bigg\}\,\mathrm{d}r\,\mathrm{d}z\,\mathrm{d}\theta, \end{aligned} \tag{7.3}$$

where we have explicitly specified the variables of integration. The continuity equation (5.51) is given by

$$\mathcal{R}^{[\mathrm{p}]} = \iiint_V \left(r\frac{\partial u_r}{\partial r} + u_r + r\frac{\partial u_z}{\partial z} + \frac{\partial u_\theta}{\partial \theta} - rQ\right)\,\phi^{[\mathrm{p}]}\,\mathrm{d}r\,\mathrm{d}z\,\mathrm{d}\theta. \tag{7.4}$$

These equations are discretised as discussed in section 3.3 to obtain the elemental

residual equations

$$\mathcal{R}_{rl}^{[\mathrm{f,bulk}]} = \int_{-1}^{1}\int_{-1}^{1}\int_{\theta=0}^{2\pi}\Bigg\{R_\rho\,\mathrm{Re}\,\Bigg[\mathrm{St}\,r\frac{\delta u_r}{\delta t} + r\left(u_r - \mathrm{St}\,u_r^{[\mathrm{M}]}\right)\frac{\partial u_r}{\partial r} + r\left(u_z - \mathrm{St}\,u_z^{[\mathrm{M}]}\right)\frac{\partial u_r}{\partial z} + \left(u_\theta - \mathrm{St}\,u_\theta^{[\mathrm{M}]}\right)\frac{\partial u_r}{\partial \theta} - u_\theta^2\Bigg]\phi_l^{[\mathrm{f}]} - rB_r\,\phi_l^{[\mathrm{f}]} - R_\rho\frac{\mathrm{Re}}{\mathrm{Fr}}\,r\,G_r\,\phi_l^{[\mathrm{f}]} + r\left[-p + 2R_\mu\frac{\partial u_r}{\partial r}\right]\frac{\partial \phi_l^{[\mathrm{f}]}}{\partial r} + R_\mu r\left[\frac{\partial u_z}{\partial r} + \frac{\partial u_r}{\partial z}\right]\frac{\partial \phi_l^{[\mathrm{f}]}}{\partial z} + R_\mu\left[\frac{\partial u_\theta}{\partial r} + \frac{1}{r}\frac{\partial u_r}{\partial \theta} - \frac{u_\theta}{r}\right]\frac{\partial \phi_l^{[\mathrm{f}]}}{\partial \theta} + \left[-p + \frac{2R_\mu}{r}\frac{\partial u_\theta}{\partial \theta} + \frac{2R_\mu}{r}u_r\right]\phi_l^{[\mathrm{f}]}\Bigg\}\,\mathcal{J}_B\,\mathrm{d}s_1\,\mathrm{d}s_2\,\mathrm{d}\theta, \quad (7.5)$$

$$\mathcal{R}_{zl}^{[\mathrm{f,bulk}]} = \int_{-1}^{1}\int_{-1}^{1}\int_{\theta=0}^{2\pi}\Bigg\{R_\rho\,\mathrm{Re}\,\Bigg[\mathrm{St}\,r\frac{\delta u_z}{\delta t} + r\left(u_r - \mathrm{St}\,u_r^{[\mathrm{M}]}\right)\frac{\partial u_z}{\partial r} + r\left(u_z - \mathrm{St}\,u_z^{[\mathrm{M}]}\right)\frac{\partial u_z}{\partial z} + \left(u_\theta - \mathrm{St}\,u_\theta^{[\mathrm{M}]}\right)\frac{\partial u_z}{\partial \theta}\Bigg]\phi_l^{[\mathrm{f}]} - rB_z\,\phi_l^{[\mathrm{f}]} - R_\rho\frac{\mathrm{Re}}{\mathrm{Fr}}\,r\,G_z\,\phi_l^{[\mathrm{f}]} + R_\mu r\left[\frac{\partial u_r}{\partial z} + \frac{\partial u_z}{\partial r}\right]\frac{\partial \phi_l^{[\mathrm{f}]}}{\partial r} + r\left[-p + 2R_\mu\frac{\partial u_z}{\partial z}\right]\frac{\partial \phi_l^{[\mathrm{f}]}}{\partial z} + R_\mu\left[\frac{\partial u_\theta}{\partial z} + \frac{1}{r}\frac{\partial u_z}{\partial \theta}\right]\frac{\partial \phi_l^{[\mathrm{f}]}}{\partial \theta}\Bigg\}\,\mathcal{J}_B\,\mathrm{d}s_1\,\mathrm{d}s_2\,\mathrm{d}\theta, \quad (7.6)$$

$$\mathcal{R}_{\theta l}^{[\mathrm{f,bulk}]} = \int_{-1}^{1}\int_{-1}^{1}\int_{\theta=0}^{2\pi}\Bigg\{R_\rho\,\mathrm{Re}\,\Bigg[\mathrm{St}\,r\frac{\delta u_\theta}{\delta t} + r\left(u_r - \mathrm{St}\,u_r^{[\mathrm{M}]}\right)\frac{\partial u_\theta}{\partial r} + r\left(u_z - \mathrm{St}\,u_z^{[\mathrm{M}]}\right)\frac{\partial u_\theta}{\partial z} + \left(u_\theta - \mathrm{St}\,u_\theta^{[\mathrm{M}]}\right)\frac{\partial u_\theta}{\partial \theta} + u_r u_\theta\Bigg]\phi_l^{[\mathrm{f}]} - rB_\theta\,\phi_l^{[\mathrm{f}]} - R_\rho\frac{\mathrm{Re}}{\mathrm{Fr}}\,r\,G_\theta\,\phi_l^{[\mathrm{f}]} + R_\mu\left[\frac{\partial u_r}{\partial \theta} - u_\theta + r\frac{\partial u_\theta}{\partial r}\right]\frac{\partial \phi_l^{[\mathrm{f}]}}{\partial r} + R_\mu\left[\frac{\partial u_z}{\partial \theta} + r\frac{\partial u_\theta}{\partial z}\right]\frac{\partial \phi_l^{[\mathrm{f}]}}{\partial z} + \left[-p + \frac{2R_\mu}{r}\frac{\partial u_\theta}{\partial \theta} + \frac{2R_\mu}{r}u_r\right]\frac{\partial \phi_l^{[\mathrm{f}]}}{\partial \theta} - R_\mu\left[\frac{\partial u_\theta}{\partial r} + \frac{1}{r}\frac{\partial u_r}{\partial \theta} - \frac{u_\theta}{r}\right]\phi_l^{[\mathrm{f}]}\Bigg\}\,\mathcal{J}_B\,\mathrm{d}s_1\,\mathrm{d}s_2\,\mathrm{d}\theta \quad (7.7)$$

and

$$\mathcal{R}_l^{[\mathrm{p}]} = \int_{-1}^{1}\int_{-1}^{1}\int_{\theta=0}^{2\pi}\left(r\frac{\partial u_r}{\partial r} + u_r + r\frac{\partial u_z}{\partial z} + \frac{\partial u_\theta}{\partial \theta} - rQ\right)\phi_l^{[\mathrm{p}]}\,\mathcal{J}_B\,\mathrm{d}s_1\,\mathrm{d}s_2\,\mathrm{d}\theta, \quad (7.8)$$

where (3.86) has been used to write $\partial u_i/\partial t$ in terms of the rate of change of u_i at a fixed set of local coordinates, $\delta u_i/\delta t$, and the mesh velocity terms, $u_a^{[\mathrm{M}]}\,\partial u_i/\partial x_a$. The Jacobian of the mapping between local s_i and global ξ_i coordinates is given by

$$\mathcal{J}_{ij} = \frac{\partial \xi_j}{\partial s_i}, \quad (7.9)$$

where $\xi_1 = r$, $\xi_2 = z$ and $\xi_3 = s_3 = \theta$ as before, and its determinant is denoted by $\mathcal{J}_B$. Note that in (7.5)–(7.8) the variables u_r, u_z, u_θ, p, r and z are all functions of the local coordinates s_1, s_2 and θ, and terms of the form $\partial v/\partial \xi_i$ are evaluated using

$$\frac{\partial v}{\partial \xi_i} = \left(\mathcal{J}^{-1}\right)_{ij} \frac{\partial v}{\partial s_j}, \tag{7.10}$$

where v is any particular variable.

In order to linearise the governing equations (7.5)–(7.8) about a non-linear, axisymmetric base state we write the solution u_r, u_z, u_θ and p in the following way:

$$\begin{aligned} u_r(s_1, s_2, \theta, t) &= \bar{u}_r(s_1, s_2, t) + \epsilon\, \hat{u}_r(s_1, s_2, \theta, t), \\ u_z(s_1, s_2, \theta, t) &= \bar{u}_z(s_1, s_2, t) + \epsilon\, \hat{u}_z(s_1, s_2, \theta, t), \\ u_\theta(s_1, s_2, \theta, t) &= \bar{u}_\theta(s_1, s_2, t) + \epsilon\, \hat{u}_\theta(s_1, s_2, \theta, t) \quad \text{and} \\ p(s_1, s_2, \theta, t) &= \bar{p}(s_1, s_2, t) + \epsilon\, \hat{p}(s_1, s_2, \theta, t), \end{aligned} \tag{7.11}$$

where ϵ is a small, positive non-dimensional parameter ($\epsilon \ll 1$). Here we have decomposed the velocity and pressure fields into components corresponding to a base state ($\bar{\mathbf{u}}$ and $\bar{p}$) and a perturbation to this base state ($\hat{\mathbf{u}}$ and $\hat{p}$). We also decompose the Eulerian coordinates r and z in the same way:

$$\begin{aligned} r(s_1, s_2, \theta, t) &= \bar{r}(s_1, s_2, t) + \epsilon\, \hat{r}(s_1, s_2, \theta, t) \quad \text{and} \\ z(s_1, s_2, \theta, t) &= \bar{z}(s_1, s_2, t) + \epsilon\, \hat{z}(s_1, s_2, \theta, t). \end{aligned} \tag{7.12}$$

Note that the decomposition of the coordinates in this manner is not required for problems which are to be solved on a fixed mesh, such as the single-fluid problems which will be discussed in chapter 8. However, this formulation will become necessary when solving two-layer problems (such as those discussed in chapter 10) since we require the mesh to deform in response to changes in the shape of the interface, and in order to avoid later repetition we will therefore include it at this point in the discussion.

Before substituting this ansatz into (7.5)–(7.8) it is convenient to evaluate certain groups of terms explicitly. We begin by observing that by writing $1/r$ in the form

$$\frac{1}{r} = \left(\bar{r} + \epsilon \hat{r}\right)^{-1} = \frac{1}{\bar{r}} \left(1 + \epsilon \frac{\hat{r}}{\bar{r}}\right)^{-1} \tag{7.13}$$

we can use the binomial expansion to show that

$$\frac{1}{r} = \frac{1}{\bar{r}} - \epsilon \frac{\hat{r}}{\bar{r}^2} + \mathrm{O}(\epsilon^2). \tag{7.14}$$

Next we substitute (7.12) into the definition of the Jacobian of the mapping (7.9) to obtain

$$\mathcal{J}_{ij} = \begin{pmatrix} \frac{\partial \bar{r}}{\partial s_1} + \epsilon \frac{\partial \hat{r}}{\partial s_1} & \frac{\partial \bar{z}}{\partial s_1} + \epsilon \frac{\partial \hat{z}}{\partial s_1} & 0 \\ \frac{\partial \bar{r}}{\partial s_2} + \epsilon \frac{\partial \hat{r}}{\partial s_2} & \frac{\partial \bar{z}}{\partial s_2} + \epsilon \frac{\partial \hat{z}}{\partial s_2} & 0 \\ \epsilon \frac{\partial \hat{r}}{\partial \theta} & \epsilon \frac{\partial \hat{z}}{\partial \theta} & 1 \end{pmatrix}, \tag{7.15}$$

the determinant of which is given by

$$\mathcal{J}_B(s_1, s_2, \theta, t) = \frac{\partial \bar{r}}{\partial s_1}\frac{\partial \bar{z}}{\partial s_2} - \frac{\partial \bar{r}}{\partial s_2}\frac{\partial \bar{z}}{\partial s_1} + \epsilon \left[\frac{\partial \bar{r}}{\partial s_1}\frac{\partial \hat{z}}{\partial s_2} + \frac{\partial \bar{z}}{\partial s_2}\frac{\partial \hat{r}}{\partial s_1} - \frac{\partial \bar{r}}{\partial s_2}\frac{\partial \hat{z}}{\partial s_1} - \frac{\partial \bar{z}}{\partial s_1}\frac{\partial \hat{r}}{\partial s_2} \right] + \mathrm{O}(\epsilon^2). \tag{7.16}$$

For convenience of notation we write this as

$$\mathcal{J}_B = \bar{\mathcal{J}}_B + \epsilon \hat{\mathcal{J}}_B + \mathrm{O}(\epsilon^2),$$

where

$$\bar{\mathcal{J}}_B = \frac{\partial \bar{r}}{\partial s_1}\frac{\partial \bar{z}}{\partial s_2} - \frac{\partial \bar{z}}{\partial s_1}\frac{\partial \bar{r}}{\partial s_2} \tag{7.17}$$

and

$$\hat{\mathcal{J}}_B = \frac{\partial \bar{r}}{\partial s_1}\frac{\partial \hat{z}}{\partial s_2} + \frac{\partial \bar{z}}{\partial s_2}\frac{\partial \hat{r}}{\partial s_1} - \frac{\partial \bar{r}}{\partial s_2}\frac{\partial \hat{z}}{\partial s_1} - \frac{\partial \bar{z}}{\partial s_1}\frac{\partial \hat{r}}{\partial s_2}. \tag{7.18}$$

The reciprocal of this quantity can be evaluated by first writing

$$\frac{1}{\mathcal{J}_B} = \left(\bar{\mathcal{J}}_B + \epsilon \hat{\mathcal{J}}_B + \mathrm{O}(\epsilon^2) \right)^{-1} = \frac{1}{\bar{\mathcal{J}}_B} \left(1 + \epsilon \frac{\hat{\mathcal{J}}_B}{\bar{\mathcal{J}}_B} + \mathrm{O}(\epsilon^2) \right)^{-1} \tag{7.19}$$

and then once again performing a binomial expansion to obtain

$$\frac{1}{\mathcal{J}_B} = \frac{1}{\bar{\mathcal{J}}_B} - \epsilon \frac{\hat{\mathcal{J}}_B}{\bar{\mathcal{J}}_B^2} + \mathrm{O}(\epsilon^2). \tag{7.20}$$

The inverse of the Jacobian of the mapping (7.15) is given by

$$\left(\mathcal{J}^{-1}\right)_{ij} = \frac{1}{\mathcal{J}_B} \begin{pmatrix} \frac{\partial \bar{z}}{\partial s_2} + \epsilon \frac{\partial \hat{z}}{\partial s_2} & -\frac{\partial \bar{r}}{\partial s_2} - \epsilon \frac{\partial \hat{r}}{\partial s_2} & \epsilon \left[\frac{\partial \bar{r}}{\partial s_2}\frac{\partial \hat{z}}{\partial \theta} - \frac{\partial \bar{z}}{\partial s_2}\frac{\partial \hat{r}}{\partial \theta} \right] + \mathrm{O}(\epsilon^2) \\ -\frac{\partial \bar{z}}{\partial s_1} - \epsilon \frac{\partial \hat{z}}{\partial s_1} & \frac{\partial \bar{r}}{\partial s_1} + \epsilon \frac{\partial \hat{r}}{\partial s_1} & \epsilon \left[\frac{\partial \bar{z}}{\partial s_1}\frac{\partial \hat{r}}{\partial \theta} - \frac{\partial \bar{r}}{\partial s_1}\frac{\partial \hat{z}}{\partial \theta} \right] + \mathrm{O}(\epsilon^2) \\ 0 & 0 & \bar{\mathcal{J}}_B + \epsilon \hat{\mathcal{J}}_B + \mathrm{O}(\epsilon^2) \end{pmatrix}^T, \tag{7.21}$$

and using (7.20) we can write

$$\left(\mathcal{J}^{-1}\right)_{ij} = \bar{K}_{ij} + \epsilon \hat{K}_{ij} + \mathrm{O}(\epsilon^2), \tag{7.22}$$

where

$$\bar{K}_{ij} = \begin{pmatrix} \frac{1}{\bar{\mathcal{J}}_B}\frac{\partial \bar{z}}{\partial s_2} & -\frac{1}{\bar{\mathcal{J}}_B}\frac{\partial \bar{z}}{\partial s_1} & 0 \\ -\frac{1}{\bar{\mathcal{J}}_B}\frac{\partial \bar{r}}{\partial s_2} & \frac{1}{\bar{\mathcal{J}}_B}\frac{\partial \bar{r}}{\partial s_1} & 0 \\ 0 & 0 & 1 \end{pmatrix} \tag{7.23}$$

and

$$\hat{K}_{ij} = \begin{pmatrix} \frac{1}{\bar{\mathcal{J}}_B}\frac{\partial \hat{z}}{\partial s_2} - \frac{\hat{\mathcal{J}}_B}{\bar{\mathcal{J}}_B^2}\frac{\partial \bar{z}}{\partial s_2} & -\frac{1}{\bar{\mathcal{J}}_B}\frac{\partial \hat{z}}{\partial s_1} + \frac{\hat{\mathcal{J}}_B}{\bar{\mathcal{J}}_B^2}\frac{\partial \bar{z}}{\partial s_1} & 0 \\ -\frac{1}{\bar{\mathcal{J}}_B}\frac{\partial \hat{r}}{\partial s_2} + \frac{\hat{\mathcal{J}}_B}{\bar{\mathcal{J}}_B^2}\frac{\partial \bar{r}}{\partial s_2} & \frac{1}{\bar{\mathcal{J}}_B}\frac{\partial \hat{r}}{\partial s_1} - \frac{\hat{\mathcal{J}}_B}{\bar{\mathcal{J}}_B^2}\frac{\partial \bar{r}}{\partial s_1} & 0 \\ \frac{1}{\bar{\mathcal{J}}_B}\left(\frac{\partial \bar{r}}{\partial s_2}\frac{\partial \hat{z}}{\partial \theta} - \frac{\partial \bar{z}}{\partial s_2}\frac{\partial \hat{r}}{\partial \theta}\right) & \frac{1}{\bar{\mathcal{J}}_B}\left(\frac{\partial \bar{z}}{\partial s_1}\frac{\partial \hat{r}}{\partial \theta} - \frac{\partial \bar{r}}{\partial s_1}\frac{\partial \hat{z}}{\partial \theta}\right) & 0 \end{pmatrix}. \tag{7.24}$$

Derivatives of a given (arbitrary) field $v = v(s_1, s_2, \theta, t)$ with respect to the global Eulerian coordinates $\xi_1 = r$, $\xi_2 = z$ and $\xi_3 = \theta$ are evaluated using (7.10). By analogy with (7.11) we let

$$v(s_1, s_2, \theta, t) = \bar{v}(s_1, s_2, t) + \epsilon\, \hat{v}(s_1, s_2, \theta, t) \tag{7.25}$$

and then use (7.22) to rewrite (7.10) as

$$\frac{\partial v}{\partial \xi_i} = \bar{K}_{ij}\frac{\partial \bar{v}}{\partial s_j} + \epsilon\left[\bar{K}_{ij}\frac{\partial \hat{v}}{\partial s_j} + \hat{K}_{ij}\frac{\partial \bar{v}}{\partial s_j}\right] + \mathrm{O}(\epsilon^2). \tag{7.26}$$

Once again for notational convenience we write

$$\frac{\partial v}{\partial \xi_i} = \overline{\frac{\partial v}{\partial \xi_i}} + \epsilon\widehat{\frac{\partial v}{\partial \xi_i}} + \mathrm{O}(\epsilon^2), \tag{7.27}$$

where

$$\overline{\frac{\partial v}{\partial \xi_i}} = \bar{K}_{ij}\frac{\partial \bar{v}}{\partial s_j} \tag{7.28}$$

and

$$\widehat{\frac{\partial v}{\partial \xi_i}} = \bar{K}_{ij}\frac{\partial \hat{v}}{\partial s_j} + \hat{K}_{ij}\frac{\partial \bar{v}}{\partial s_j}. \tag{7.29}$$

Derivatives of the (fluid) finite element test functions $\phi_l^{[\mathrm{f}]}$ with respect to the global Eulerian coordinates are evaluated in the same way. We can write $\partial\phi_l^{[\mathrm{f}]}/\partial\xi_i$ as

$$\frac{\partial \phi_l^{[\mathrm{f}]}}{\partial \xi_i} = \overline{\frac{\partial \phi_l^{[\mathrm{f}]}}{\partial \xi_i}} + \epsilon\widehat{\frac{\partial \phi_l^{[\mathrm{f}]}}{\partial \xi_i}} + \mathrm{O}(\epsilon^2), \tag{7.30}$$

where

$$\overline{\frac{\partial \phi_l^{[\mathrm{f}]}}{\partial \xi_i}} = \bar{K}_{ij}\frac{\partial \phi_l^{[\mathrm{f}]}}{\partial s_j} \tag{7.31}$$

and

$$\widehat{\frac{\partial \phi_l^{[\mathrm{f}]}}{\partial \xi_i}} = \hat{K}_{ij}\frac{\partial \phi_l^{[\mathrm{f}]}}{\partial s_j}. \tag{7.32}$$

Finally, from (3.88) we have the definition of the interpolated mesh velocity,

$$u_a^{[\mathrm{M}]} = \sum_{j=1}^{N_{\mathrm{node}}} \frac{dX_{aj}}{dt}\phi_j^{[\mathrm{f}]}, \tag{7.33}$$

and note that by analogy with (3.87) we can write this as

$$u_a^{[\mathrm{M}]} = \frac{\delta x_a}{\delta t}. \tag{7.34}$$

From (7.12) we can therefore write

$$u_r^{[\mathrm{M}]} = \frac{\delta \bar{r}}{\delta t} + \epsilon\frac{\delta \hat{r}}{\delta t}, \qquad u_z^{[\mathrm{M}]} = \frac{\delta \bar{z}}{\delta t} + \epsilon\frac{\delta \hat{z}}{\delta t} \qquad \text{and} \qquad u_\theta^{[\mathrm{M}]} = 0, \tag{7.35}$$

where $\bar{u}_r^{[\mathrm{M}]} = \delta\bar{r}/\delta t$, $\bar{u}_z^{[\mathrm{M}]} = \delta\bar{z}/\delta t$, $\hat{u}_r^{[\mathrm{M}]} = \delta\hat{r}/\delta t$ and $\hat{u}_z^{[\mathrm{M}]} = \delta\hat{z}/\delta t$.

We can now substitute the ansatz (7.11) and (7.12) into the governing equations (7.5)–(7.8) to obtain

$$\begin{aligned}
\mathcal{R}_{\mathrm{r}l}^{[\mathrm{f,bulk}]} &= \int_{-1}^{1}\int_{-1}^{1}\int_{\theta=0}^{2\pi}\left\{\bar{A}_{\mathrm{r}l}^{[\mathrm{f}]}\bar{\mathcal{J}}_B + \epsilon\left[\hat{A}_{\mathrm{r}l}^{[\mathrm{f}]}\bar{\mathcal{J}}_B + \bar{A}_{\mathrm{r}l}^{[\mathrm{f}]}\hat{\mathcal{J}}_B\right]\right\}\mathrm{d}s_1\,\mathrm{d}s_2\,\mathrm{d}\theta + \mathrm{O}(\epsilon^2),\\
\mathcal{R}_{\mathrm{z}l}^{[\mathrm{f,bulk}]} &= \int_{-1}^{1}\int_{-1}^{1}\int_{\theta=0}^{2\pi}\left\{\bar{A}_{\mathrm{z}l}^{[\mathrm{f}]}\bar{\mathcal{J}}_B + \epsilon\left[\hat{A}_{\mathrm{z}l}^{[\mathrm{f}]}\bar{\mathcal{J}}_B + \bar{A}_{\mathrm{z}l}^{[\mathrm{f}]}\hat{\mathcal{J}}_B\right]\right\}\mathrm{d}s_1\,\mathrm{d}s_2\,\mathrm{d}\theta + \mathrm{O}(\epsilon^2),\\
\mathcal{R}_{\theta l}^{[\mathrm{f,bulk}]} &= \int_{-1}^{1}\int_{-1}^{1}\int_{\theta=0}^{2\pi}\left\{\bar{A}_{\theta l}^{[\mathrm{f}]}\bar{\mathcal{J}}_B + \epsilon\left[\hat{A}_{\theta l}^{[\mathrm{f}]}\bar{\mathcal{J}}_B + \bar{A}_{\theta l}^{[\mathrm{f}]}\hat{\mathcal{J}}_B\right]\right\}\mathrm{d}s_1\,\mathrm{d}s_2\,\mathrm{d}\theta + \mathrm{O}(\epsilon^2) \quad \text{and}\\
\mathcal{R}_{l}^{[\mathrm{p}]} &= \int_{-1}^{1}\int_{-1}^{1}\int_{\theta=0}^{2\pi}\left\{\bar{A}_{l}^{[\mathrm{p}]}\bar{\mathcal{J}}_B + \epsilon\left[\hat{A}_{l}^{[\mathrm{p}]}\bar{\mathcal{J}}_B + \bar{A}_{l}^{[\mathrm{p}]}\hat{\mathcal{J}}_B\right]\right\}\mathrm{d}s_1\,\mathrm{d}s_2\,\mathrm{d}\theta + \mathrm{O}(\epsilon^2),
\end{aligned} \tag{7.36}$$

where

$$\begin{aligned}
\bar{A}_{\mathrm{r}l}^{[\mathrm{f}]} = R_\rho\,\mathrm{Re}\,\Bigg[&\mathrm{St}\,\bar{r}\frac{\delta\bar{u}_r}{\delta t} + \bar{r}\left(\bar{u}_r - \mathrm{St}\,\bar{u}_r^{[\mathrm{M}]}\right)\overline{\frac{\partial u_r}{\partial r}} + \bar{r}\left(\bar{u}_z - \mathrm{St}\,\bar{u}_z^{[\mathrm{M}]}\right)\overline{\frac{\partial u_r}{\partial z}}\\
&+ \left(\bar{u}_\theta - \mathrm{St}\,\bar{u}_\theta^{[\mathrm{M}]}\right)\overline{\frac{\partial u_r}{\partial \theta}} - \bar{u}_\theta^2\Bigg]\phi_l^{[\mathrm{f}]} - \bar{r}\,B_r\,\phi_l^{[\mathrm{f}]} - R_\rho\frac{\mathrm{Re}}{\mathrm{Fr}}\bar{r}\,G_r\,\phi_l^{[\mathrm{f}]}\\
&+ \bar{r}\left[-\bar{p} + 2R_\mu\overline{\frac{\partial u_r}{\partial r}}\right]\overline{\frac{\partial \phi_l^{[\mathrm{f}]}}{\partial r}} + R_\mu\bar{r}\left[\overline{\frac{\partial u_z}{\partial r}} + \overline{\frac{\partial u_r}{\partial z}}\right]\overline{\frac{\partial \phi_l^{[\mathrm{f}]}}{\partial z}}\\
&+ R_\mu\left[\overline{\frac{\partial u_\theta}{\partial r}} + \frac{1}{\bar{r}}\overline{\frac{\partial u_r}{\partial \theta}} - \frac{\bar{u}_\theta}{\bar{r}}\right]\overline{\frac{\partial \phi_l^{[\mathrm{f}]}}{\partial \theta}} + \left[-\bar{p} + \frac{2R_\mu}{\bar{r}}\overline{\frac{\partial u_\theta}{\partial \theta}} + \frac{2R_\mu}{\bar{r}}\bar{u}_r\right]\phi_l^{[\mathrm{f}]},
\end{aligned} \tag{7.37}$$

$$\bar{A}_{zl}^{[\mathrm{f}]} = R_\rho \,\mathrm{Re}\,\Bigg[\mathrm{St}\,\bar{r}\frac{\delta \bar{u}_z}{\delta t} + \bar{r}\left(\bar{u}_r - \mathrm{St}\,\bar{u}_r^{[\mathrm{M}]}\right)\overline{\frac{\partial u_z}{\partial r}} + \bar{r}\left(\bar{u}_z - \mathrm{St}\,\bar{u}_z^{[\mathrm{M}]}\right)\overline{\frac{\partial u_z}{\partial z}} + \left(\bar{u}_\theta - \mathrm{St}\,\bar{u}_\theta^{[\mathrm{M}]}\right)\overline{\frac{\partial u_z}{\partial \theta}}\Bigg]\phi_l^{[\mathrm{f}]} - \bar{r}\,B_z\,\phi_l^{[\mathrm{f}]} - R_\rho\,\frac{\mathrm{Re}}{\mathrm{Fr}}\,\bar{r}\,G_z\,\phi_l^{[\mathrm{f}]} + R_\mu\bar{r}\left[\overline{\frac{\partial u_r}{\partial z}} + \overline{\frac{\partial u_z}{\partial r}}\right]\overline{\frac{\partial \phi_l^{[\mathrm{f}]}}{\partial r}} + \bar{r}\left[-\bar{p} + 2R_\mu\overline{\frac{\partial u_z}{\partial z}}\right]\overline{\frac{\partial \phi_l^{[\mathrm{f}]}}{\partial z}} + R_\mu\left[\frac{1}{\bar{r}}\overline{\frac{\partial u_z}{\partial \theta}} + \overline{\frac{\partial u_\theta}{\partial z}}\right]\overline{\frac{\partial \phi_l^{[\mathrm{f}]}}{\partial \theta}}, \quad (7.38)$$

$$\bar{A}_{\theta l}^{[\mathrm{f}]} = R_\rho \,\mathrm{Re}\,\Bigg[\mathrm{St}\,\bar{r}\frac{\delta \bar{u}_\theta}{\delta t} + \bar{r}\left(\bar{u}_r - \mathrm{St}\,\bar{u}_r^{[\mathrm{M}]}\right)\overline{\frac{\partial u_\theta}{\partial r}} + \bar{r}\left(\bar{u}_z - \mathrm{St}\,\bar{u}_z^{[\mathrm{M}]}\right)\overline{\frac{\partial u_\theta}{\partial z}} + \left(\bar{u}_\theta - \mathrm{St}\,\bar{u}_\theta^{[\mathrm{M}]}\right)\overline{\frac{\partial u_\theta}{\partial \theta}} + \bar{u}_\theta\bar{u}_r\Bigg]\phi_l^{[\mathrm{f}]} - \bar{r}\,B_\theta\,\phi_l^{[\mathrm{f}]} - R_\rho\,\frac{\mathrm{Re}}{\mathrm{Fr}}\,\bar{r}\,G_\theta\,\phi_l^{[\mathrm{f}]} + R_\mu\left[\bar{r}\overline{\frac{\partial u_\theta}{\partial r}} + \overline{\frac{\partial u_r}{\partial \theta}} - \bar{u}_\theta\right]\overline{\frac{\partial \phi_l^{[\mathrm{f}]}}{\partial r}} + R_\mu\left[\overline{\frac{\partial u_z}{\partial \theta}} + \bar{r}\overline{\frac{\partial u_\theta}{\partial z}}\right]\overline{\frac{\partial \phi_l^{[\mathrm{f}]}}{\partial z}} + \left[-\bar{p} + \frac{2R_\mu}{\bar{r}}\overline{\frac{\partial u_\theta}{\partial \theta}} + \frac{2R_\mu}{\bar{r}}\bar{u}_r\right]\overline{\frac{\partial \phi_l^{[\mathrm{f}]}}{\partial \theta}} - R_\mu\left[\overline{\frac{\partial u_\theta}{\partial r}} + \frac{1}{\bar{r}}\overline{\frac{\partial u_r}{\partial \theta}} - \frac{\bar{u}_\theta}{\bar{r}}\right]\phi_l^{[\mathrm{f}]}, \quad (7.39)$$

$$\bar{A}_l^{[\mathrm{p}]} = \left[\bar{r}\overline{\frac{\partial u_r}{\partial r}} + \bar{u}_r + \bar{r}\overline{\frac{\partial u_z}{\partial z}} + \overline{\frac{\partial u_\theta}{\partial \theta}} - \bar{r}Q\right]\phi_l^{[\mathrm{p}]}, \quad (7.40)$$

$$\hat{A}_{\mathrm{rl}}^{[\mathrm{f}]} = R_\rho \,\mathrm{Re}\left[\mathrm{St}\,\bar{r}\frac{\delta\hat{u}_r}{\delta t} + \mathrm{St}\,\hat{r}\frac{\delta\bar{u}_r}{\delta t} + \bar{r}\left(\bar{u}_r - \mathrm{St}\,\bar{u}_r^{[\mathrm{M}]}\right)\widehat{\frac{\partial u_r}{\partial r}} + \bar{r}\left(\hat{u}_r - \mathrm{St}\,\hat{u}_r^{[\mathrm{M}]}\right)\overline{\frac{\partial u_r}{\partial r}}\right.$$
$$+\hat{r}\left(\bar{u}_r - \mathrm{St}\,\bar{u}_r^{[\mathrm{M}]}\right)\overline{\frac{\partial u_r}{\partial r}} + \bar{r}\left(\bar{u}_z - \mathrm{St}\,\bar{u}_z^{[\mathrm{M}]}\right)\widehat{\frac{\partial u_r}{\partial z}} + \bar{r}\left(\hat{u}_z - \mathrm{St}\,\hat{u}_z^{[\mathrm{M}]}\right)\overline{\frac{\partial u_r}{\partial z}}$$
$$+\hat{r}\left(\bar{u}_z - \mathrm{St}\,\bar{u}_z^{[\mathrm{M}]}\right)\overline{\frac{\partial u_r}{\partial z}} + \left(\bar{u}_\theta - \mathrm{St}\,\bar{u}_\theta^{[\mathrm{M}]}\right)\widehat{\frac{\partial u_r}{\partial \theta}} + \left(\hat{u}_\theta - \mathrm{St}\,\hat{u}_\theta^{[\mathrm{M}]}\right)\overline{\frac{\partial u_r}{\partial \theta}}$$
$$\left.-2\bar{u}_\theta\hat{u}_\theta\right]\phi_l^{[\mathrm{f}]} - \hat{r}\,B_r\,\phi_l^{[\mathrm{f}]} - R_\rho\,\frac{\mathrm{Re}}{\mathrm{Fr}}\,\hat{r}\,G_r\,\phi_l^{[\mathrm{f}]} - \bar{r}\bar{p}\widehat{\frac{\partial\phi_l^{[\mathrm{f}]}}{\partial r}}$$
$$-\bar{r}\hat{p}\overline{\frac{\partial\phi_l^{[\mathrm{f}]}}{\partial r}} - \hat{r}\bar{p}\overline{\frac{\partial\phi_l^{[\mathrm{f}]}}{\partial r}} + 2R_\mu\left[\bar{r}\overline{\frac{\partial u_r}{\partial r}}\widehat{\frac{\partial\phi_l^{[\mathrm{f}]}}{\partial r}} + \bar{r}\widehat{\frac{\partial u_r}{\partial r}}\overline{\frac{\partial\phi_l^{[\mathrm{f}]}}{\partial r}} + \hat{r}\overline{\frac{\partial u_r}{\partial r}}\overline{\frac{\partial\phi_l^{[\mathrm{f}]}}{\partial r}}\right]$$
$$+R_\mu\left[\overline{\frac{\partial u_\theta}{\partial r}}\widehat{\frac{\partial\phi_l^{[\mathrm{f}]}}{\partial\theta}} + \widehat{\frac{\partial u_\theta}{\partial r}}\overline{\frac{\partial\phi_l^{[\mathrm{f}]}}{\partial\theta}} + \frac{1}{\bar{r}}\overline{\frac{\partial u_r}{\partial\theta}}\widehat{\frac{\partial\phi_l^{[\mathrm{f}]}}{\partial\theta}} + \frac{1}{\bar{r}}\widehat{\frac{\partial u_r}{\partial\theta}}\overline{\frac{\partial\phi_l^{[\mathrm{f}]}}{\partial\theta}} - \frac{\hat{r}}{\bar{r}^2}\overline{\frac{\partial u_r}{\partial\theta}}\overline{\frac{\partial\phi_l^{[\mathrm{f}]}}{\partial\theta}}\right.$$
$$\left.-\frac{\bar{u}_\theta}{\bar{r}}\widehat{\frac{\partial\phi_l^{[\mathrm{f}]}}{\partial\theta}} - \frac{\hat{u}_\theta}{\bar{r}}\overline{\frac{\partial\phi_l^{[\mathrm{f}]}}{\partial\theta}} + \frac{\hat{r}\bar{u}_\theta}{\bar{r}^2}\overline{\frac{\partial\phi_l^{[\mathrm{f}]}}{\partial\theta}}\right] + R_\mu\left[\bar{r}\overline{\frac{\partial u_z}{\partial r}}\widehat{\frac{\partial\phi_l^{[\mathrm{f}]}}{\partial z}} + \bar{r}\widehat{\frac{\partial u_z}{\partial r}}\overline{\frac{\partial\phi_l^{[\mathrm{f}]}}{\partial z}}\right.$$
$$+\hat{r}\overline{\frac{\partial u_z}{\partial r}}\overline{\frac{\partial\phi_l^{[\mathrm{f}]}}{\partial z}} + \bar{r}\overline{\frac{\partial u_r}{\partial z}}\widehat{\frac{\partial\phi_l^{[\mathrm{f}]}}{\partial z}} + \bar{r}\widehat{\frac{\partial u_r}{\partial z}}\overline{\frac{\partial\phi_l^{[\mathrm{f}]}}{\partial z}} + \hat{r}\overline{\frac{\partial u_r}{\partial z}}\overline{\frac{\partial\phi_l^{[\mathrm{f}]}}{\partial z}}\Bigg]$$
$$+\left[-\hat{p} + \frac{2R_\mu}{\bar{r}}\widehat{\frac{\partial u_\theta}{\partial\theta}} - \frac{2R_\mu\hat{r}}{\bar{r}^2}\overline{\frac{\partial u_\theta}{\partial\theta}} + \frac{2R_\mu\hat{u}_r}{\bar{r}} - \frac{2R_\mu\hat{r}\bar{u}_r}{\bar{r}^2}\right]\phi_l^{[\mathrm{f}]}, \quad (7.41)$$

$$\hat{A}_{\mathrm{zl}}^{[\mathrm{f}]} = R_\rho\,\mathrm{Re}\left[\mathrm{St}\,\bar{r}\frac{\delta\hat{u}_z}{\delta t} + \mathrm{St}\,\hat{r}\frac{\delta\bar{u}_z}{\delta t} + \bar{r}\left(\bar{u}_r - \mathrm{St}\,\bar{u}_r^{[\mathrm{M}]}\right)\widehat{\frac{\partial u_z}{\partial r}} + \bar{r}\left(\hat{u}_r - \mathrm{St}\,\hat{u}_r^{[\mathrm{M}]}\right)\overline{\frac{\partial u_z}{\partial r}}\right.$$
$$+\hat{r}\left(\bar{u}_r - \mathrm{St}\,\bar{u}_r^{[\mathrm{M}]}\right)\overline{\frac{\partial u_z}{\partial r}} + \bar{r}\left(\bar{u}_z - \mathrm{St}\,\bar{u}_z^{[\mathrm{M}]}\right)\widehat{\frac{\partial u_z}{\partial z}} + \bar{r}\left(\hat{u}_z - \mathrm{St}\,\hat{u}_z^{[\mathrm{M}]}\right)\overline{\frac{\partial u_z}{\partial z}}$$
$$\left.+\hat{r}\left(\bar{u}_z - \mathrm{St}\,\bar{u}_z^{[\mathrm{M}]}\right)\overline{\frac{\partial u_z}{\partial z}} + \left(\bar{u}_\theta - \mathrm{St}\,\bar{u}_\theta^{[\mathrm{M}]}\right)\widehat{\frac{\partial u_z}{\partial\theta}} + \left(\hat{u}_\theta - \mathrm{St}\,\hat{u}_\theta^{[\mathrm{M}]}\right)\overline{\frac{\partial u_z}{\partial\theta}}\right]\phi_l^{[\mathrm{f}]}$$
$$-\hat{r}\,B_z\,\phi_l^{[\mathrm{f}]} - R_\rho\,\frac{\mathrm{Re}}{\mathrm{Fr}}\,\hat{r}\,G_z\,\phi_l^{[\mathrm{f}]} + R_\mu\left[\bar{r}\overline{\frac{\partial u_z}{\partial r}}\widehat{\frac{\partial\phi_l^{[\mathrm{f}]}}{\partial r}} + \bar{r}\widehat{\frac{\partial u_z}{\partial r}}\overline{\frac{\partial\phi_l^{[\mathrm{f}]}}{\partial r}}\right.$$
$$\left.+\hat{r}\overline{\frac{\partial u_z}{\partial r}}\overline{\frac{\partial\phi_l^{[\mathrm{f}]}}{\partial r}} + \bar{r}\overline{\frac{\partial u_r}{\partial z}}\widehat{\frac{\partial\phi_l^{[\mathrm{f}]}}{\partial r}} + \bar{r}\widehat{\frac{\partial u_r}{\partial z}}\overline{\frac{\partial\phi_l^{[\mathrm{f}]}}{\partial r}} + \hat{r}\overline{\frac{\partial u_r}{\partial z}}\overline{\frac{\partial\phi_l^{[\mathrm{f}]}}{\partial r}}\right]$$
$$-\bar{r}\bar{p}\widehat{\frac{\partial\phi_l^{[\mathrm{f}]}}{\partial z}} - \bar{r}\hat{p}\overline{\frac{\partial\phi_l^{[\mathrm{f}]}}{\partial z}} - \hat{r}\bar{p}\overline{\frac{\partial\phi_l^{[\mathrm{f}]}}{\partial z}} + 2R_\mu\left[\bar{r}\overline{\frac{\partial u_z}{\partial z}}\widehat{\frac{\partial\phi_l^{[\mathrm{f}]}}{\partial z}} + \bar{r}\widehat{\frac{\partial u_z}{\partial z}}\overline{\frac{\partial\phi_l^{[\mathrm{f}]}}{\partial z}} + \hat{r}\overline{\frac{\partial u_z}{\partial z}}\overline{\frac{\partial\phi_l^{[\mathrm{f}]}}{\partial z}}\right]$$
$$+R_\mu\left[\frac{1}{\bar{r}}\overline{\frac{\partial u_z}{\partial\theta}}\widehat{\frac{\partial\phi_l^{[\mathrm{f}]}}{\partial\theta}} + \frac{1}{\bar{r}}\widehat{\frac{\partial u_z}{\partial\theta}}\overline{\frac{\partial\phi_l^{[\mathrm{f}]}}{\partial\theta}} - \frac{\hat{r}}{\bar{r}^2}\overline{\frac{\partial u_z}{\partial\theta}}\overline{\frac{\partial\phi_l^{[\mathrm{f}]}}{\partial\theta}} + \overline{\frac{\partial u_\theta}{\partial z}}\widehat{\frac{\partial\phi_l^{[\mathrm{f}]}}{\partial\theta}} + \widehat{\frac{\partial u_\theta}{\partial z}}\overline{\frac{\partial\phi_l^{[\mathrm{f}]}}{\partial\theta}}\right], \quad (7.42)$$

$$\hat{A}^{[\mathrm{f}]}_{\theta l} = R_\rho \,\mathrm{Re}\left[\mathrm{St}\,\bar{r}\frac{\delta\hat{u}_\theta}{\delta t} + \mathrm{St}\,\hat{r}\frac{\delta\bar{u}_\theta}{\delta t} + \bar{r}\left(\bar{u}_r - \mathrm{St}\,\bar{u}_r^{[\mathrm{M}]}\right)\widehat{\frac{\partial u_\theta}{\partial r}} + \bar{r}\left(\hat{u}_r - \mathrm{St}\,\hat{u}_r^{[\mathrm{M}]}\right)\overline{\frac{\partial u_\theta}{\partial r}}\right.$$
$$+ \hat{r}\left(\bar{u}_r - \mathrm{St}\,\bar{u}_r^{[\mathrm{M}]}\right)\overline{\frac{\partial u_\theta}{\partial r}} + \bar{r}\left(\bar{u}_z - \mathrm{St}\,\bar{u}_z^{[\mathrm{M}]}\right)\widehat{\frac{\partial u_\theta}{\partial z}} + \bar{r}\left(\hat{u}_z - \mathrm{St}\,\hat{u}_z^{[\mathrm{M}]}\right)\overline{\frac{\partial u_\theta}{\partial z}}$$
$$+ \hat{r}\left(\bar{u}_z - \mathrm{St}\,\bar{u}_z^{[\mathrm{M}]}\right)\overline{\frac{\partial u_\theta}{\partial z}} + \left(\bar{u}_\theta - \mathrm{St}\,\bar{u}_\theta^{[\mathrm{M}]}\right)\widehat{\frac{\partial u_\theta}{\partial \theta}} + \left(\hat{u}_\theta - \mathrm{St}\,\hat{u}_\theta^{[\mathrm{M}]}\right)\overline{\frac{\partial u_\theta}{\partial \theta}}$$
$$\left. + \bar{u}_\theta\hat{u}_r + \hat{u}_\theta\bar{u}_r\right]\phi_l^{[\mathrm{f}]} - \hat{r}\,B_\theta\,\phi_l^{[\mathrm{f}]} - R_\rho\,\frac{\mathrm{Re}}{\mathrm{Fr}}\,\hat{r}\,G_\theta\,\phi_l^{[\mathrm{f}]} + R_\mu\left[\bar{r}\overline{\frac{\partial u_\theta}{\partial r}}\widehat{\frac{\partial \phi_l^{[\mathrm{f}]}}{\partial r}}\right.$$
$$\left. + \bar{r}\widehat{\frac{\partial u_\theta}{\partial r}}\overline{\frac{\partial \phi_l^{[\mathrm{f}]}}{\partial r}} + \hat{r}\overline{\frac{\partial u_\theta}{\partial r}}\overline{\frac{\partial \phi_l^{[\mathrm{f}]}}{\partial r}} + \overline{\frac{\partial u_r}{\partial \theta}}\widehat{\frac{\partial \phi_l^{[\mathrm{f}]}}{\partial r}} + \widehat{\frac{\partial u_r}{\partial \theta}}\overline{\frac{\partial \phi_l^{[\mathrm{f}]}}{\partial r}} - \bar{u}_\theta\widehat{\frac{\partial \phi_l^{[\mathrm{f}]}}{\partial r}} - \hat{u}_\theta\overline{\frac{\partial \phi_l^{[\mathrm{f}]}}{\partial r}}\right]$$
$$+ R_\mu\left[\overline{\frac{\partial u_z}{\partial \theta}}\widehat{\frac{\partial \phi_l^{[\mathrm{f}]}}{\partial z}} + \widehat{\frac{\partial u_z}{\partial \theta}}\overline{\frac{\partial \phi_l^{[\mathrm{f}]}}{\partial z}} + \bar{r}\overline{\frac{\partial u_\theta}{\partial z}}\widehat{\frac{\partial \phi_l^{[\mathrm{f}]}}{\partial z}} + \bar{r}\widehat{\frac{\partial u_\theta}{\partial z}}\overline{\frac{\partial \phi_l^{[\mathrm{f}]}}{\partial z}} + \hat{r}\overline{\frac{\partial u_\theta}{\partial z}}\overline{\frac{\partial \phi_l^{[\mathrm{f}]}}{\partial z}}\right]$$
$$- \bar{p}\widehat{\frac{\partial \phi_l^{[\mathrm{f}]}}{\partial \theta}} - \hat{p}\overline{\frac{\partial \phi_l^{[\mathrm{f}]}}{\partial \theta}} + 2R_\mu\left[\frac{1}{\bar{r}}\overline{\frac{\partial u_\theta}{\partial \theta}}\widehat{\frac{\partial \phi_l^{[\mathrm{f}]}}{\partial \theta}} + \frac{1}{\bar{r}}\widehat{\frac{\partial u_\theta}{\partial \theta}}\overline{\frac{\partial \phi_l^{[\mathrm{f}]}}{\partial \theta}} - \frac{\hat{r}}{\bar{r}^2}\overline{\frac{\partial u_\theta}{\partial \theta}}\overline{\frac{\partial \phi_l^{[\mathrm{f}]}}{\partial \theta}} + \frac{\bar{u}_r}{\bar{r}}\widehat{\frac{\partial \phi_l^{[\mathrm{f}]}}{\partial \theta}}\right.$$
$$\left. + \frac{\hat{u}_r}{\bar{r}}\overline{\frac{\partial \phi_l^{[\mathrm{f}]}}{\partial \theta}} - \frac{\hat{r}\bar{u}_r}{\bar{r}^2}\overline{\frac{\partial \phi_l^{[\mathrm{f}]}}{\partial \theta}}\right] - R_\mu\left[\widehat{\frac{\partial u_\theta}{\partial r}} + \frac{1}{\bar{r}}\widehat{\frac{\partial u_r}{\partial \theta}} - \frac{\hat{r}}{\bar{r}^2}\overline{\frac{\partial u_r}{\partial \theta}} - \frac{\hat{u}_\theta}{\bar{r}} + \frac{\hat{r}\bar{u}_\theta}{\bar{r}^2}\right]\phi_l^{[\mathrm{f}]} \quad (7.43)$$

and

$$\hat{A}^{[\mathrm{p}]}_l = \left[\bar{r}\widehat{\frac{\partial u_r}{\partial r}} + \hat{r}\overline{\frac{\partial u_r}{\partial r}} + \hat{u}_r + \widehat{\frac{\partial u_\theta}{\partial \theta}} + \bar{r}\widehat{\frac{\partial u_z}{\partial z}} + \hat{r}\overline{\frac{\partial u_z}{\partial z}} - \hat{r}Q\right]\phi_l^{[\mathrm{p}]}. \quad (7.44)$$

We use (7.28) to evaluate the following terms which are used in (7.37)–(7.44):

$$\begin{aligned}
\overline{\frac{\partial u_i}{\partial r}} &= \frac{1}{\bar{\mathcal{J}}_B}\left(\frac{\partial \bar{z}}{\partial s_2}\frac{\partial \bar{u}_i}{\partial s_1} - \frac{\partial \bar{z}}{\partial s_1}\frac{\partial \bar{u}_i}{\partial s_2}\right), & \overline{\frac{\partial p}{\partial r}} &= \frac{1}{\bar{\mathcal{J}}_B}\left(\frac{\partial \bar{z}}{\partial s_2}\frac{\partial \bar{p}}{\partial s_1} - \frac{\partial \bar{z}}{\partial s_1}\frac{\partial \bar{p}}{\partial s_2}\right),\\
\overline{\frac{\partial u_i}{\partial z}} &= \frac{1}{\bar{\mathcal{J}}_B}\left(\frac{\partial \bar{r}}{\partial s_1}\frac{\partial \bar{u}_i}{\partial s_2} - \frac{\partial \bar{r}}{\partial s_2}\frac{\partial \bar{u}_i}{\partial s_1}\right), & \overline{\frac{\partial p}{\partial z}} &= \frac{1}{\bar{\mathcal{J}}_B}\left(\frac{\partial \bar{r}}{\partial s_1}\frac{\partial \bar{p}}{\partial s_2} - \frac{\partial \bar{r}}{\partial s_2}\frac{\partial \bar{p}}{\partial s_1}\right),\\
\overline{\frac{\partial u_i}{\partial \theta}} &= 0, & \overline{\frac{\partial p}{\partial \theta}} &= 0.
\end{aligned} \quad (7.45)$$

Similarly, (7.29) is used to evaluate

$$\begin{aligned}
\widehat{\frac{\partial u_i}{\partial r}} &= \frac{1}{\bar{\mathcal{J}}_B}\left[\frac{\partial \bar{z}}{\partial s_2}\frac{\partial \hat{u}_i}{\partial s_1} + \frac{\partial \hat{z}}{\partial s_2}\frac{\partial \bar{u}_i}{\partial s_1} - \frac{\partial \bar{z}}{\partial s_1}\frac{\partial \hat{u}_i}{\partial s_2} - \frac{\partial \hat{z}}{\partial s_1}\frac{\partial \bar{u}_i}{\partial s_2}\right] - \frac{\hat{\mathcal{J}}_B}{\bar{\mathcal{J}}_B}\overline{\frac{\partial u_i}{\partial r}},\\
\widehat{\frac{\partial p}{\partial r}} &= \frac{1}{\bar{\mathcal{J}}_B}\left[\frac{\partial \bar{z}}{\partial s_2}\frac{\partial \hat{p}}{\partial s_1} + \frac{\partial \hat{z}}{\partial s_2}\frac{\partial \bar{p}}{\partial s_1} - \frac{\partial \bar{z}}{\partial s_1}\frac{\partial \hat{p}}{\partial s_2} - \frac{\partial \hat{z}}{\partial s_1}\frac{\partial \bar{p}}{\partial s_2}\right] - \frac{\hat{\mathcal{J}}_B}{\bar{\mathcal{J}}_B}\overline{\frac{\partial p}{\partial r}},\\
\widehat{\frac{\partial u_i}{\partial z}} &= \frac{1}{\bar{\mathcal{J}}_B}\left[\frac{\partial \bar{r}}{\partial s_1}\frac{\partial \hat{u}_i}{\partial s_2} + \frac{\partial \hat{r}}{\partial s_1}\frac{\partial \bar{u}_i}{\partial s_2} - \frac{\partial \bar{r}}{\partial s_2}\frac{\partial \hat{u}_i}{\partial s_1} - \frac{\partial \hat{r}}{\partial s_2}\frac{\partial \bar{u}_i}{\partial s_1}\right] - \frac{\hat{\mathcal{J}}_B}{\bar{\mathcal{J}}_B}\overline{\frac{\partial u_i}{\partial z}},\\
\widehat{\frac{\partial p}{\partial z}} &= \frac{1}{\bar{\mathcal{J}}_B}\left[\frac{\partial \bar{r}}{\partial s_1}\frac{\partial \hat{p}}{\partial s_2} + \frac{\partial \hat{r}}{\partial s_1}\frac{\partial \bar{p}}{\partial s_2} - \frac{\partial \bar{r}}{\partial s_2}\frac{\partial \hat{p}}{\partial s_1} - \frac{\partial \hat{r}}{\partial s_2}\frac{\partial \bar{p}}{\partial s_1}\right] - \frac{\hat{\mathcal{J}}_B}{\bar{\mathcal{J}}_B}\overline{\frac{\partial p}{\partial z}},\\
\widehat{\frac{\partial u_i}{\partial \theta}} &= \frac{\partial \hat{u}_i}{\partial \theta} - \overline{\frac{\partial u_i}{\partial r}}\frac{\partial \hat{r}}{\partial \theta} - \overline{\frac{\partial u_i}{\partial z}}\frac{\partial \hat{z}}{\partial \theta},\\
\widehat{\frac{\partial p}{\partial \theta}} &= \frac{\partial \hat{p}}{\partial \theta} - \overline{\frac{\partial p}{\partial r}}\frac{\partial \hat{r}}{\partial \theta} - \overline{\frac{\partial p}{\partial z}}\frac{\partial \hat{z}}{\partial \theta}.
\end{aligned} \tag{7.46}$$

Finally, (7.31) and (7.32) are used to evaluate

$$\begin{aligned}
\overline{\frac{\partial \phi_l^{[\mathrm{f}]}}{\partial r}} &= \frac{1}{\bar{\mathcal{J}}_B}\left(\frac{\partial \bar{z}}{\partial s_2}\frac{\partial \phi_l^{[\mathrm{f}]}}{\partial s_1} - \frac{\partial \bar{z}}{\partial s_1}\frac{\partial \phi_l^{[\mathrm{f}]}}{\partial s_2}\right),\\
\overline{\frac{\partial \phi_l^{[\mathrm{f}]}}{\partial z}} &= \frac{1}{\bar{\mathcal{J}}_B}\left(\frac{\partial \bar{r}}{\partial s_1}\frac{\partial \phi_l^{[\mathrm{f}]}}{\partial s_2} - \frac{\partial \bar{r}}{\partial s_2}\frac{\partial \phi_l^{[\mathrm{f}]}}{\partial s_1}\right),\\
\overline{\frac{\partial \phi_l^{[\mathrm{f}]}}{\partial \theta}} &= \frac{\partial \phi_l^{[\mathrm{f}]}}{\partial \theta},\\
\widehat{\frac{\partial \phi_l^{[\mathrm{f}]}}{\partial r}} &= \frac{1}{\bar{\mathcal{J}}_B}\left(\frac{\partial \hat{z}}{\partial s_2}\frac{\partial \phi_l^{[\mathrm{f}]}}{\partial s_1} - \frac{\partial \hat{z}}{\partial s_1}\frac{\partial \phi_l^{[\mathrm{f}]}}{\partial s_2}\right) - \frac{\hat{\mathcal{J}}_B}{\bar{\mathcal{J}}_B}\overline{\frac{\partial \phi_l^{[\mathrm{f}]}}{\partial r}},\\
\widehat{\frac{\partial \phi_l^{[\mathrm{f}]}}{\partial z}} &= \frac{1}{\bar{\mathcal{J}}_B}\left(\frac{\partial \hat{r}}{\partial s_1}\frac{\partial \phi_l^{[\mathrm{f}]}}{\partial s_2} - \frac{\partial \hat{r}}{\partial s_2}\frac{\partial \phi_l^{[\mathrm{f}]}}{\partial s_1}\right) - \frac{\hat{\mathcal{J}}_B}{\bar{\mathcal{J}}_B}\overline{\frac{\partial \phi_l^{[\mathrm{f}]}}{\partial z}},\\
\widehat{\frac{\partial \phi_l^{[\mathrm{f}]}}{\partial \theta}} &= -\overline{\frac{\partial \phi_l^{[\mathrm{f}]}}{\partial r}}\frac{\partial \hat{r}}{\partial \theta} - \overline{\frac{\partial \phi_l^{[\mathrm{f}]}}{\partial z}}\frac{\partial \hat{z}}{\partial \theta}.
\end{aligned} \tag{7.47}$$

7.2 The base state

Let us briefly consider just the terms in (7.36) that are of order one. We recall from (7.11) that the 'base state solution' $(\bar{\mathbf{u}}, \bar{p})$ is independent of θ, and therefore we can discretise $\bar{u}_r$, $\bar{u}_z$, $\bar{u}_\theta$ and $\bar{p}$ in the manner outlined in section 3.3.2,

$$\begin{aligned}
\bar{u}_r(s_1,s_2) &= \sum_{j=1}^{n_u} U_j\,\psi_j^{[\mathrm{f}]}(s_1,s_2), \qquad \bar{u}_z(s_1,s_2) = \sum_{j=1}^{n_u} W_j\,\psi_j^{[\mathrm{f}]}(s_1,s_2),\\
\bar{u}_\theta(s_1,s_2) &= \sum_{j=1}^{n_u} V_j\,\psi_j^{[\mathrm{f}]}(s_1,s_2), \qquad \bar{p}(s_1,s_2) = \sum_{j=1}^{n_p} P_j\,\psi_j^{[\mathrm{p}]}(s_1,s_2),
\end{aligned} \tag{7.48}$$

where explicit references to the time dependence of the nodal values U_j, W_j, V_j and P_j have been suppressed for the time being. The (unperturbed) Eulerian coordinates $\bar{r}$ and $\bar{z}$ are discretised in a similar manner,

$$\bar{r}(s_1,s_2)=\sum_{j=1}^{n} X_{1j}\,\psi_j^{[\mathrm{f}]}(s_1,s_2) \qquad \text{and} \qquad \bar{z}(s_1,s_2)=\sum_{j=1}^{n} X_{2j}\,\psi_j^{[\mathrm{f}]}(s_1,s_2). \tag{7.49}$$

As usual we employ the Galerkin method to expand the test functions in terms of the same basis functions with which the solution is represented, and so we choose

$$\phi_l^{[\mathrm{f}]}=\psi_l^{[\mathrm{f}]}(s_1,s_2) \qquad \text{and} \qquad \phi_l^{[\mathrm{p}]}=\psi_l^{[\mathrm{p}]}(s_1,s_2). \tag{7.50}$$

It follows that $\partial\phi_l^{[\mathrm{f}]}/\partial\theta=0$ and hence from (7.47)

$$\overline{\frac{\partial\phi_l^{[\mathrm{f}]}}{\partial\theta}}=0. \tag{7.51}$$

Putting all this together, the terms of order one in (7.36) are therefore

$$\begin{aligned}\bar{\mathcal{R}}_{rl}^{[\mathrm{f,bulk}]}=2\pi\int_{-1}^{1}\int_{-1}^{1}\Bigg\{&R_\rho\,\mathrm{Re}\,\Bigg[\mathrm{St}\,\bar{r}\frac{\delta\bar{u}_r}{\delta t}+\bar{r}\,(\bar{u}_r-\mathrm{St}\,\bar{u}_r^{[\mathrm{M}]})\,\overline{\frac{\partial u_r}{\partial r}}\\&+\bar{r}\,(\bar{u}_z-\mathrm{St}\,\bar{u}_z^{[\mathrm{M}]})\,\overline{\frac{\partial u_r}{\partial z}}-\bar{u}_\theta^2\Bigg]\psi_l^{[\mathrm{f}]}-\bar{r}\,B_r\,\psi_l^{[\mathrm{f}]}\\&-R_\rho\,\frac{\mathrm{Re}}{\mathrm{Fr}}\,\bar{r}\,G_r\,\psi_l^{[\mathrm{f}]}+\bar{r}\left[-\bar{p}+2R_\mu\overline{\frac{\partial u_r}{\partial r}}\right]\overline{\frac{\partial\psi_l^{[\mathrm{f}]}}{\partial r}}\\&+R_\mu\bar{r}\left[\overline{\frac{\partial u_z}{\partial r}}+\overline{\frac{\partial u_r}{\partial z}}\right]\overline{\frac{\partial\psi_l^{[\mathrm{f}]}}{\partial z}}+\left[-\bar{p}+\frac{2R_\mu}{\bar{r}}\bar{u}_r\right]\psi_l^{[\mathrm{f}]}\Bigg\}\,\bar{\mathcal{J}}_B\;\mathrm{d}s_1\,\mathrm{d}s_2,\end{aligned} \tag{7.52}$$

$$\begin{aligned}\bar{\mathcal{R}}_{zl}^{[\mathrm{f,bulk}]}=2\pi\int_{-1}^{1}\int_{-1}^{1}\Bigg\{&R_\rho\,\mathrm{Re}\,\Bigg[\mathrm{St}\,\bar{r}\frac{\delta\bar{u}_z}{\delta t}+\bar{r}\,(\bar{u}_r-\mathrm{St}\,\bar{u}_r^{[\mathrm{M}]})\,\overline{\frac{\partial u_z}{\partial r}}\\&+\bar{r}\,(\bar{u}_z-\mathrm{St}\,\bar{u}_z^{[\mathrm{M}]})\,\overline{\frac{\partial u_z}{\partial z}}\Bigg]\psi_l^{[\mathrm{f}]}-\bar{r}\,B_z\,\psi_l^{[\mathrm{f}]}-R_\rho\,\frac{\mathrm{Re}}{\mathrm{Fr}}\,\bar{r}\,G_z\,\psi_l^{[\mathrm{f}]}\\&+R_\mu\bar{r}\left[\overline{\frac{\partial u_r}{\partial z}}+\overline{\frac{\partial u_z}{\partial r}}\right]\overline{\frac{\partial\psi_l^{[\mathrm{f}]}}{\partial r}}+\bar{r}\left[-\bar{p}+2R_\mu\overline{\frac{\partial u_z}{\partial z}}\right]\overline{\frac{\partial\psi_l^{[\mathrm{f}]}}{\partial z}}\Bigg\}\,\bar{\mathcal{J}}_B\;\mathrm{d}s_1\,\mathrm{d}s_2,\end{aligned} \tag{7.53}$$

$$\begin{aligned}\bar{\mathcal{R}}_{\theta l}^{[\mathrm{f,bulk}]}=2\pi\int_{-1}^{1}\int_{-1}^{1}\Bigg\{&R_\rho\,\mathrm{Re}\,\Bigg[\mathrm{St}\,\bar{r}\frac{\delta\bar{u}_\theta}{\delta t}+\bar{r}\,(\bar{u}_r-\mathrm{St}\,\bar{u}_r^{[\mathrm{M}]})\,\overline{\frac{\partial u_\theta}{\partial r}}\\&+\bar{r}\,(\bar{u}_z-\mathrm{St}\,\bar{u}_z^{[\mathrm{M}]})\,\overline{\frac{\partial u_\theta}{\partial z}}+\bar{u}_\theta\bar{u}_r\Bigg]\psi_l^{[\mathrm{f}]}-\bar{r}\,B_\theta\,\psi_l^{[\mathrm{f}]}\\&-R_\rho\,\frac{\mathrm{Re}}{\mathrm{Fr}}\,\bar{r}\,G_\theta\,\psi_l^{[\mathrm{f}]}+R_\mu\left[\bar{r}\overline{\frac{\partial u_\theta}{\partial r}}-\bar{u}_\theta\right]\overline{\frac{\partial\psi_l^{[\mathrm{f}]}}{\partial r}}\\&+R_\mu\bar{r}\overline{\frac{\partial u_\theta}{\partial z}}\overline{\frac{\partial\psi_l^{[\mathrm{f}]}}{\partial z}}-R_\mu\left[\overline{\frac{\partial u_\theta}{\partial r}}-\frac{\bar{u}_\theta}{\bar{r}}\right]\psi_l^{[\mathrm{f}]}\Bigg\}\,\bar{\mathcal{J}}_B\;\mathrm{d}s_1\,\mathrm{d}s_2\end{aligned} \tag{7.54}$$

and

$$\bar{\mathcal{R}}_l^{[\mathrm{p}]} = 2\pi \int_{-1}^{1}\int_{-1}^{1} \left[\bar{r}\overline{\frac{\partial u_r}{\partial r}} + \bar{u}_r + \bar{r}\overline{\frac{\partial u_z}{\partial z}} - \bar{r}Q\right] \psi_l^{[\mathrm{p}]}\, \bar{\mathcal{J}}_B \, \mathrm{d}s_1\, \mathrm{d}s_2, \tag{7.55}$$

where we have performed the integral over θ. Comparison with (5.84), (5.85), (5.86) and (5.88) reveals that these are precisely the axisymmetric Navier–Stokes equations, as expected.

7.3 Perturbation to the base state

Let us now consider the terms in (7.36) that are of order ϵ. Because the domain in which we are solving the governing equations is periodic in the θ direction, we can represent any function $f(s_1, s_2, \theta, t)$ as a Fourier series,

$$f(s_1, s_2, \theta, t) = \sum_{k=0}^{\infty} \Big[F_k^C(s_1, s_2, t)\cos k\theta + F_k^S(s_1, s_2, t)\sin k\theta\Big], \tag{7.56}$$

where the 'mode number' k is an integer and the 'Fourier coefficients' F_k^C and F_k^S are functions of the two remaining spatial coordinates and time. We note that F_0^S is undefined (since $\sin(0) = 0$) but choose to write the decomposition in this way to make the following discussion more concise. We therefore let

$$\begin{aligned}
\hat{u}_r(s_1, s_2, \theta, t) &= \sum_{k=0}^{\infty} \Big[U_k^C(s_1, s_2, t)\cos k\theta + U_k^S(s_1, s_2, t)\sin k\theta\Big], \\
\hat{u}_z(s_1, s_2, \theta, t) &= \sum_{k=0}^{\infty} \Big[W_k^C(s_1, s_2, t)\cos k\theta + W_k^S(s_1, s_2, t)\sin k\theta\Big], \\
\hat{u}_\theta(s_1, s_2, \theta, t) &= \sum_{k=0}^{\infty} \Big[V_k^C(s_1, s_2, t)\cos k\theta + V_k^S(s_1, s_2, t)\sin k\theta\Big], \\
\hat{p}(s_1, s_2, \theta, t) &= \sum_{k=0}^{\infty} \Big[P_k^C(s_1, s_2, t)\cos k\theta + P_k^S(s_1, s_2, t)\sin k\theta\Big], \\
\hat{r}(s_1, s_2, \theta, t) &= \sum_{k=0}^{\infty} \Big[R_k^C(s_1, s_2, t)\cos k\theta + R_k^S(s_1, s_2, t)\sin k\theta\Big] \quad \text{and} \\
\hat{z}(s_1, s_2, \theta, t) &= \sum_{k=0}^{\infty} \Big[Z_k^C(s_1, s_2, t)\cos k\theta + Z_k^S(s_1, s_2, t)\sin k\theta\Big].
\end{aligned} \tag{7.57}$$

The finite element solution of $\hat{u}_r$ within the element is then represented by

$$\hat{u}_r(s_1, s_2, \theta) = \sum_{k=0}^{\infty} \left\{ \sum_{j=1}^{n_u} \left(U_k^C\right)_j \psi_j^{[\mathrm{f}]}(s_1, s_2)\cos k\theta + \sum_{j=1}^{n_u} \left(U_k^S\right)_j \psi_j^{[\mathrm{f}]}(s_1, s_2)\sin k\theta \right\}, \tag{7.58}$$

where we have again suppressed any explicit references to the time dependence of the nodal values $\left(U_k^C\right)_j$ and $\left(U_k^S\right)_j$. The finite element solutions of $\hat{u}_z$, $\hat{u}_\theta$, $\hat{p}$, $\hat{r}$ and $\hat{z}$ follow in a similar way. The Galerkin method requires us to choose the two sets of test functions,

$$\phi_l^{[\mathrm{f,C}]} = \psi_l^{[\mathrm{f}]}(s_1, s_2)\cos m\theta, \qquad \phi_l^{[\mathrm{p,C}]} = \psi_l^{[\mathrm{p}]}(s_1, s_2)\cos m\theta \tag{7.59}$$

and

$$\phi_l^{[\mathrm{f,S}]} = \psi_l^{[\mathrm{f}]}(s_1, s_2)\sin m\theta, \qquad \phi_l^{[\mathrm{p,S}]} = \psi_l^{[\mathrm{p}]}(s_1, s_2)\sin m\theta. \tag{7.60}$$

From (7.47) we have

$$\begin{aligned}
\overline{\frac{\partial \phi_l^{[\mathrm{f,C}]}}{\partial r}} &= \frac{\partial \psi_l^{[\mathrm{f}]}}{\partial r}\cos m\theta, & \overline{\frac{\partial \phi_l^{[\mathrm{f,S}]}}{\partial r}} &= \frac{\partial \psi_l^{[\mathrm{f}]}}{\partial r}\sin m\theta, \\
\overline{\frac{\partial \phi_l^{[\mathrm{f,C}]}}{\partial z}} &= \frac{\partial \psi_l^{[\mathrm{f}]}}{\partial z}\cos m\theta, & \overline{\frac{\partial \phi_l^{[\mathrm{f,S}]}}{\partial z}} &= \frac{\partial \psi_l^{[\mathrm{f}]}}{\partial z}\sin m\theta, \\
\overline{\frac{\partial \phi_l^{[\mathrm{f,C}]}}{\partial \theta}} &= -m\psi_l^{[\mathrm{f}]}\sin m\theta, & \overline{\frac{\partial \phi_l^{[\mathrm{f,S}]}}{\partial \theta}} &= m\psi_l^{[\mathrm{f}]}\cos m\theta
\end{aligned} \tag{7.61}$$

and

$$\widehat{\frac{\partial \phi_l^{[\mathrm{f,C}]}}{\partial r}} = \frac{1}{\bar{\mathcal{J}}_B}\left[\frac{\partial \psi_l^{[\mathrm{f}]}}{\partial s_1}\sum_{k=0}^{\infty}\frac{\partial Z_k^C}{\partial s_2}\cos k\theta + \frac{\partial \psi_l^{[\mathrm{f}]}}{\partial s_1}\sum_{k=0}^{\infty}\frac{\partial Z_k^S}{\partial s_2}\sin k\theta \right.$$
$$\left. -\frac{\partial \psi_l^{[\mathrm{f}]}}{\partial s_2}\sum_{k=0}^{\infty}\frac{\partial Z_k^C}{\partial s_1}\cos k\theta - \frac{\partial \psi_l^{[\mathrm{f}]}}{\partial s_2}\sum_{k=0}^{\infty}\frac{\partial Z_k^S}{\partial s_1}\sin k\theta\right]\cos m\theta - \frac{\hat{\mathcal{J}}_B}{\bar{\mathcal{J}}_B}\overline{\frac{\partial \phi_l^{[\mathrm{f,C}]}}{\partial r}}$$

$$\widehat{\frac{\partial \phi_l^{[\mathrm{f,S}]}}{\partial r}} = \frac{1}{\bar{\mathcal{J}}_B}\left[\frac{\partial \psi_l^{[\mathrm{f}]}}{\partial s_1}\sum_{k=0}^{\infty}\frac{\partial Z_k^C}{\partial s_2}\cos k\theta + \frac{\partial \psi_l^{[\mathrm{f}]}}{\partial s_1}\sum_{k=0}^{\infty}\frac{\partial Z_k^S}{\partial s_2}\sin k\theta \right.$$
$$\left. -\frac{\partial \psi_l^{[\mathrm{f}]}}{\partial s_2}\sum_{k=0}^{\infty}\frac{\partial Z_k^C}{\partial s_1}\cos k\theta - \frac{\partial \psi_l^{[\mathrm{f}]}}{\partial s_2}\sum_{k=0}^{\infty}\frac{\partial Z_k^S}{\partial s_1}\sin k\theta\right]\sin m\theta - \frac{\hat{\mathcal{J}}_B}{\bar{\mathcal{J}}_B}\overline{\frac{\partial \phi_l^{[\mathrm{f,S}]}}{\partial r}}$$

$$\widehat{\frac{\partial \phi_l^{[\mathrm{f,C}]}}{\partial z}} = \frac{1}{\bar{\mathcal{J}}_B}\left[\frac{\partial \psi_l^{[\mathrm{f}]}}{\partial s_2}\sum_{k=0}^{\infty}\frac{\partial R_k^C}{\partial s_1}\cos k\theta + \frac{\partial \psi_l^{[\mathrm{f}]}}{\partial s_2}\sum_{k=0}^{\infty}\frac{\partial R_k^S}{\partial s_1}\sin k\theta \right.$$
$$\left. -\frac{\partial \psi_l^{[\mathrm{f}]}}{\partial s_1}\sum_{k=0}^{\infty}\frac{\partial R_k^C}{\partial s_2}\cos k\theta - \frac{\partial \psi_l^{[\mathrm{f}]}}{\partial s_1}\sum_{k=0}^{\infty}\frac{\partial R_k^S}{\partial s_2}\sin k\theta\right]\cos m\theta - \frac{\hat{\mathcal{J}}_B}{\bar{\mathcal{J}}_B}\overline{\frac{\partial \phi_l^{[\mathrm{f,C}]}}{\partial z}}$$

$$\widehat{\frac{\partial \phi_l^{[\mathrm{f,S}]}}{\partial z}} = \frac{1}{\bar{\mathcal{J}}_B}\left[\frac{\partial \psi_l^{[\mathrm{f}]}}{\partial s_2}\sum_{k=0}^{\infty}\frac{\partial R_k^C}{\partial s_1}\cos k\theta + \frac{\partial \psi_l^{[\mathrm{f}]}}{\partial s_2}\sum_{k=0}^{\infty}\frac{\partial R_k^S}{\partial s_1}\sin k\theta \right.$$
$$\left. -\frac{\partial \psi_l^{[\mathrm{f}]}}{\partial s_1}\sum_{k=0}^{\infty}\frac{\partial R_k^C}{\partial s_2}\cos k\theta - \frac{\partial \psi_l^{[\mathrm{f}]}}{\partial s_1}\sum_{k=0}^{\infty}\frac{\partial R_k^S}{\partial s_2}\sin k\theta\right]\sin m\theta - \frac{\hat{\mathcal{J}}_B}{\bar{\mathcal{J}}_B}\overline{\frac{\partial \phi_l^{[\mathrm{f,S}]}}{\partial z}}$$

$$\widehat{\frac{\partial \phi_l^{[\mathrm{f,C}]}}{\partial \theta}} = \left[-\frac{\partial \psi_l^{[\mathrm{f}]}}{\partial r}\sum_{k=0}^{\infty}kR_k^S\cos k\theta + \frac{\partial \psi_l^{[\mathrm{f}]}}{\partial r}\sum_{k=0}^{\infty}kR_k^C\sin k\theta \right.$$
$$\left. -\frac{\partial \psi_l^{[\mathrm{f}]}}{\partial z}\sum_{k=0}^{\infty}kZ_k^S\cos k\theta + \frac{\partial \psi_l^{[\mathrm{f}]}}{\partial z}\sum_{k=0}^{\infty}kZ_k^C\sin k\theta\right]\cos m\theta$$

$$\widehat{\frac{\partial \phi_l^{[\mathrm{f,S}]}}{\partial \theta}} = \left[-\frac{\partial \psi_l^{[\mathrm{f}]}}{\partial r}\sum_{k=0}^{\infty}kR_k^S\cos k\theta + \frac{\partial \psi_l^{[\mathrm{f}]}}{\partial r}\sum_{k=0}^{\infty}kR_k^C\sin k\theta \right.$$
$$\left. -\frac{\partial \psi_l^{[\mathrm{f}]}}{\partial z}\sum_{k=0}^{\infty}kZ_k^S\cos k\theta + \frac{\partial \psi_l^{[\mathrm{f}]}}{\partial z}\sum_{k=0}^{\infty}kZ_k^C\sin k\theta\right]\sin m\theta \tag{7.62}$$

where we have defined

$$\frac{\partial \psi_l^{[\mathrm{f}]}}{\partial r} = \frac{1}{\bar{\mathcal{J}}_B}\left(\frac{\partial \bar{z}}{\partial s_2}\frac{\partial \psi_l^{[\mathrm{f}]}}{\partial s_1} - \frac{\partial \bar{z}}{\partial s_1}\frac{\partial \psi_l^{[\mathrm{f}]}}{\partial s_2}\right) \tag{7.63}$$

and

$$\frac{\partial \psi_l^{[\mathrm{f}]}}{\partial z} = \frac{1}{\bar{\mathcal{J}}_B}\left(\frac{\partial \bar{r}}{\partial s_1}\frac{\partial \psi_l^{[\mathrm{f}]}}{\partial s_2} - \frac{\partial \bar{r}}{\partial s_2}\frac{\partial \psi_l^{[\mathrm{f}]}}{\partial s_1}\right), \tag{7.64}$$

and from (7.18) we have

$$\begin{aligned}\hat{\mathcal{J}}_B &= \sum_{k=0}^{\infty}\left[\left(\frac{\partial\bar{r}}{\partial s_1}\frac{\partial Z_k^C}{\partial s_2}+\frac{\partial\bar{z}}{\partial s_2}\frac{\partial R_k^C}{\partial s_1}-\frac{\partial\bar{r}}{\partial s_2}\frac{\partial Z_k^C}{\partial s_1}-\frac{\partial\bar{z}}{\partial s_1}\frac{\partial R_k^C}{\partial s_2}\right)\cos k\theta\right] \\ &\quad+\sum_{k=0}^{\infty}\left[\left(\frac{\partial\bar{r}}{\partial s_1}\frac{\partial Z_k^S}{\partial s_2}+\frac{\partial\bar{z}}{\partial s_2}\frac{\partial R_k^S}{\partial s_1}-\frac{\partial\bar{r}}{\partial s_2}\frac{\partial Z_k^S}{\partial s_1}-\frac{\partial\bar{z}}{\partial s_1}\frac{\partial R_k^S}{\partial s_2}\right)\sin k\theta\right]. \quad (7.65)\end{aligned}$$

When we perform the integral over θ, we will exploit the fact that all the terms of a Fourier serier are mutually orthogonal, and therefore

$$\begin{aligned}\int_0^{2\pi}\sin k\theta\cos m\theta\,\mathrm{d}\theta &= 0 \qquad \text{for all } k \text{ and } m, \\ \int_0^{2\pi}\cos k\theta\cos m\theta\,\mathrm{d}\theta &= \begin{cases} 2\pi & \text{for } k=m=0 \\ \pi & \text{for } k=m>0 \\ 0 & \text{for } k\neq m \end{cases}\end{aligned}$$

and

$$\int_0^{2\pi}\sin k\theta\sin m\theta\,\mathrm{d}\theta = \begin{cases} 2\pi & \text{for } k=m=0 \\ \pi & \text{for } k=m>0 \\ 0 & \text{for } k\neq m \end{cases}. \quad (7.66)$$

Using this result we note that from (7.65)

$$\int_0^{2\pi}\hat{\mathcal{J}}_B\cos m\theta\,\mathrm{d}\theta=\gamma_m\,\pi\,\hat{\mathcal{J}}_m^C \qquad \text{and} \qquad \int_0^{2\pi}\hat{\mathcal{J}}_B\sin m\theta\,\mathrm{d}\theta=\gamma_m\,\pi\,\hat{\mathcal{J}}_m^S, \quad (7.67)$$

where we have defined

$$\hat{\mathcal{J}}_m^C=\frac{\partial\bar{r}}{\partial s_1}\frac{\partial Z_k^C}{\partial s_2}+\frac{\partial\bar{z}}{\partial s_2}\frac{\partial R_k^C}{\partial s_1}-\frac{\partial\bar{r}}{\partial s_2}\frac{\partial Z_k^C}{\partial s_1}-\frac{\partial\bar{z}}{\partial s_1}\frac{\partial R_k^C}{\partial s_2} \quad (7.68)$$

and

$$\hat{\mathcal{J}}_m^S=\frac{\partial\bar{r}}{\partial s_1}\frac{\partial Z_k^S}{\partial s_2}+\frac{\partial\bar{z}}{\partial s_2}\frac{\partial R_k^S}{\partial s_1}-\frac{\partial\bar{r}}{\partial s_2}\frac{\partial Z_k^S}{\partial s_1}-\frac{\partial\bar{z}}{\partial s_1}\frac{\partial R_k^S}{\partial s_2}, \quad (7.69)$$

and we introduce the quantity

$$\gamma_m=\begin{cases} 2 & \text{for } m=0 \\ 1 & \text{for } m>0 \end{cases}. \quad (7.70)$$

If we also introduce the quantities

$$\left(\frac{\partial\psi_l^{[\mathrm{f}]}}{\partial R}\right)_m^C = \frac{1}{\bar{\mathcal{J}}_B}\left(\frac{\partial\psi_l^{[\mathrm{f}]}}{\partial s_1}\frac{\partial Z_m^C}{\partial s_2} - \frac{\partial\psi_l^{[\mathrm{f}]}}{\partial s_2}\frac{\partial Z_m^C}{\partial s_1}\right),$$
$$\left(\frac{\partial\psi_l^{[\mathrm{f}]}}{\partial R}\right)_m^S = \frac{1}{\bar{\mathcal{J}}_B}\left(\frac{\partial\psi_l^{[\mathrm{f}]}}{\partial s_1}\frac{\partial Z_m^S}{\partial s_2} - \frac{\partial\psi_l^{[\mathrm{f}]}}{\partial s_2}\frac{\partial Z_m^S}{\partial s_1}\right),$$
$$\left(\frac{\partial\psi_l^{[\mathrm{f}]}}{\partial Z}\right)_m^C = \frac{1}{\bar{\mathcal{J}}_B}\left(\frac{\partial\psi_l^{[\mathrm{f}]}}{\partial s_2}\frac{\partial R_m^C}{\partial s_1} - \frac{\partial\psi_l^{[\mathrm{f}]}}{\partial s_1}\frac{\partial R_m^C}{\partial s_2}\right) \quad \text{and}$$
$$\left(\frac{\partial\psi_l^{[\mathrm{f}]}}{\partial Z}\right)_m^S = \frac{1}{\bar{\mathcal{J}}_B}\left(\frac{\partial\psi_l^{[\mathrm{f}]}}{\partial s_2}\frac{\partial R_m^S}{\partial s_1} - \frac{\partial\psi_l^{[\mathrm{f}]}}{\partial s_1}\frac{\partial R_m^S}{\partial s_2}\right), \tag{7.71}$$

then from (7.62) the integral over the spatial derivatives of the test functions are given by

$$\int_0^{2\pi}\widehat{\frac{\partial\phi_l^{[\mathrm{f,C}]}}{\partial r}}\,\mathrm{d}\theta = \gamma_m\,\pi\left[\left(\frac{\partial\psi_l^{[\mathrm{f}]}}{\partial R}\right)_m^C - \frac{\hat{\mathcal{J}}_m^C}{\bar{\mathcal{J}}_B}\frac{\partial\psi_l^{[\mathrm{f}]}}{\partial r}\right],$$
$$\int_0^{2\pi}\widehat{\frac{\partial\phi_l^{[\mathrm{f,S}]}}{\partial r}}\,\mathrm{d}\theta = \gamma_m\,\pi\left[\left(\frac{\partial\psi_l^{[\mathrm{f}]}}{\partial R}\right)_m^S - \frac{\hat{\mathcal{J}}_m^S}{\bar{\mathcal{J}}_B}\frac{\partial\psi_l^{[\mathrm{f}]}}{\partial r}\right],$$
$$\int_0^{2\pi}\widehat{\frac{\partial\phi_l^{[\mathrm{f,C}]}}{\partial z}}\,\mathrm{d}\theta = \gamma_m\,\pi\left[\left(\frac{\partial\psi_l^{[\mathrm{f}]}}{\partial Z}\right)_m^C - \frac{\hat{\mathcal{J}}_m^C}{\bar{\mathcal{J}}_B}\frac{\partial\psi_l^{[\mathrm{f}]}}{\partial z}\right],$$
$$\int_0^{2\pi}\widehat{\frac{\partial\phi_l^{[\mathrm{f,S}]}}{\partial z}}\,\mathrm{d}\theta = \gamma_m\,\pi\left[\left(\frac{\partial\psi_l^{[\mathrm{f}]}}{\partial Z}\right)_m^S - \frac{\hat{\mathcal{J}}_m^S}{\bar{\mathcal{J}}_B}\frac{\partial\psi_l^{[\mathrm{f}]}}{\partial z}\right],$$
$$\int_0^{2\pi}\widehat{\frac{\partial\phi_l^{[\mathrm{f,C}]}}{\partial\theta}}\,\mathrm{d}\theta = -\gamma_m\,\pi\,m\left[R_m^S\frac{\partial\psi_l^{[\mathrm{f}]}}{\partial r} + Z_m^S\frac{\partial\psi_l^{[\mathrm{f}]}}{\partial z}\right] \quad \text{and}$$
$$\int_0^{2\pi}\widehat{\frac{\partial\phi_l^{[\mathrm{f,S}]}}{\partial\theta}}\,\mathrm{d}\theta = \gamma_m\,\pi\,m\left[R_m^C\frac{\partial\psi_l^{[\mathrm{f}]}}{\partial r} + Z_m^C\frac{\partial\psi_l^{[\mathrm{f}]}}{\partial z}\right]. \tag{7.72}$$

It is also convenient to define the following quantities:

$$\left(\frac{\partial U}{\partial R}\right)_m^C = \frac{1}{\bar{\mathcal{J}}_B}\left[\frac{\partial\bar{z}}{\partial s_2}\frac{\partial U_m^C}{\partial s_1} + \frac{\partial\bar{u}_r}{\partial s_1}\frac{\partial Z_m^C}{\partial s_2} - \frac{\partial\bar{z}}{\partial s_1}\frac{\partial U_m^C}{\partial s_2} - \frac{\partial\bar{u}_r}{\partial s_2}\frac{\partial Z_m^C}{\partial s_1}\right],$$
$$\left(\frac{\partial U}{\partial R}\right)_m^S = \frac{1}{\bar{\mathcal{J}}_B}\left[\frac{\partial\bar{z}}{\partial s_2}\frac{\partial U_m^S}{\partial s_1} + \frac{\partial\bar{u}_r}{\partial s_1}\frac{\partial Z_m^S}{\partial s_2} - \frac{\partial\bar{z}}{\partial s_1}\frac{\partial U_m^S}{\partial s_2} - \frac{\partial\bar{u}_r}{\partial s_2}\frac{\partial Z_m^S}{\partial s_1}\right],$$
$$\left(\frac{\partial W}{\partial R}\right)_m^C = \frac{1}{\bar{\mathcal{J}}_B}\left[\frac{\partial\bar{z}}{\partial s_2}\frac{\partial W_m^C}{\partial s_1} + \frac{\partial\bar{u}_z}{\partial s_1}\frac{\partial Z_m^C}{\partial s_2} - \frac{\partial\bar{z}}{\partial s_1}\frac{\partial W_m^C}{\partial s_2} - \frac{\partial\bar{u}_z}{\partial s_2}\frac{\partial Z_m^C}{\partial s_1}\right],$$
$$\left(\frac{\partial W}{\partial R}\right)_m^S = \frac{1}{\bar{\mathcal{J}}_B}\left[\frac{\partial\bar{z}}{\partial s_2}\frac{\partial W_m^S}{\partial s_1} + \frac{\partial\bar{u}_z}{\partial s_1}\frac{\partial Z_m^S}{\partial s_2} - \frac{\partial\bar{z}}{\partial s_1}\frac{\partial W_m^S}{\partial s_2} - \frac{\partial\bar{u}_z}{\partial s_2}\frac{\partial Z_m^S}{\partial s_1}\right],$$

$$\left(\frac{\partial V}{\partial R}\right)_m^C = \frac{1}{\bar{\mathcal{J}}_B}\left[\frac{\partial \bar{z}}{\partial s_2}\frac{\partial V_m^C}{\partial s_1} + \frac{\partial \bar{u}_\theta}{\partial s_1}\frac{\partial Z_m^C}{\partial s_2} - \frac{\partial \bar{z}}{\partial s_1}\frac{\partial V_m^C}{\partial s_2} - \frac{\partial \bar{u}_\theta}{\partial s_2}\frac{\partial Z_m^C}{\partial s_1}\right],$$

$$\left(\frac{\partial V}{\partial R}\right)_m^S = \frac{1}{\bar{\mathcal{J}}_B}\left[\frac{\partial \bar{z}}{\partial s_2}\frac{\partial V_m^S}{\partial s_1} + \frac{\partial \bar{u}_\theta}{\partial s_1}\frac{\partial Z_m^S}{\partial s_2} - \frac{\partial \bar{z}}{\partial s_1}\frac{\partial V_m^S}{\partial s_2} - \frac{\partial \bar{u}_\theta}{\partial s_2}\frac{\partial Z_m^S}{\partial s_1}\right],$$

$$\left(\frac{\partial U}{\partial Z}\right)_m^C = \frac{1}{\bar{\mathcal{J}}_B}\left[\frac{\partial \bar{r}}{\partial s_1}\frac{\partial U_m^C}{\partial s_2} + \frac{\partial \bar{u}_r}{\partial s_2}\frac{\partial R_m^C}{\partial s_1} - \frac{\partial \bar{r}}{\partial s_2}\frac{\partial U_m^C}{\partial s_1} - \frac{\partial \bar{u}_r}{\partial s_1}\frac{\partial R_m^C}{\partial s_2}\right],$$

$$\left(\frac{\partial U}{\partial Z}\right)_m^S = \frac{1}{\bar{\mathcal{J}}_B}\left[\frac{\partial \bar{r}}{\partial s_1}\frac{\partial U_m^S}{\partial s_2} + \frac{\partial \bar{u}_r}{\partial s_2}\frac{\partial R_m^S}{\partial s_1} - \frac{\partial \bar{r}}{\partial s_2}\frac{\partial U_m^S}{\partial s_1} - \frac{\partial \bar{u}_r}{\partial s_1}\frac{\partial R_m^S}{\partial s_2}\right],$$

$$\left(\frac{\partial W}{\partial Z}\right)_m^C = \frac{1}{\bar{\mathcal{J}}_B}\left[\frac{\partial \bar{r}}{\partial s_1}\frac{\partial W_m^C}{\partial s_2} + \frac{\partial \bar{u}_z}{\partial s_2}\frac{\partial R_m^C}{\partial s_1} - \frac{\partial \bar{r}}{\partial s_2}\frac{\partial W_m^C}{\partial s_1} - \frac{\partial \bar{u}_z}{\partial s_1}\frac{\partial R_m^C}{\partial s_2}\right],$$

$$\left(\frac{\partial W}{\partial Z}\right)_m^S = \frac{1}{\bar{\mathcal{J}}_B}\left[\frac{\partial \bar{r}}{\partial s_1}\frac{\partial W_m^S}{\partial s_2} + \frac{\partial \bar{u}_z}{\partial s_2}\frac{\partial R_m^S}{\partial s_1} - \frac{\partial \bar{r}}{\partial s_2}\frac{\partial W_m^S}{\partial s_1} - \frac{\partial \bar{u}_z}{\partial s_1}\frac{\partial R_m^S}{\partial s_2}\right],$$

$$\left(\frac{\partial V}{\partial Z}\right)_m^C = \frac{1}{\bar{\mathcal{J}}_B}\left[\frac{\partial \bar{r}}{\partial s_1}\frac{\partial V_m^C}{\partial s_2} + \frac{\partial \bar{u}_\theta}{\partial s_2}\frac{\partial R_m^C}{\partial s_1} - \frac{\partial \bar{r}}{\partial s_2}\frac{\partial V_m^C}{\partial s_1} - \frac{\partial \bar{u}_\theta}{\partial s_1}\frac{\partial R_m^C}{\partial s_2}\right] \text{ and}$$

$$\left(\frac{\partial V}{\partial Z}\right)_m^S = \frac{1}{\bar{\mathcal{J}}_B}\left[\frac{\partial \bar{r}}{\partial s_1}\frac{\partial V_m^S}{\partial s_2} + \frac{\partial \bar{u}_\theta}{\partial s_2}\frac{\partial R_m^S}{\partial s_1} - \frac{\partial \bar{r}}{\partial s_2}\frac{\partial V_m^S}{\partial s_1} - \frac{\partial \bar{u}_\theta}{\partial s_1}\frac{\partial R_m^S}{\partial s_2}\right]. \tag{7.73}$$

Using (7.73) and (7.66) we can evaluate the integrals over θ of the spatial derivatives of the perturbed velocities and pressures (7.46):

$$\int_0^{2\pi} \widehat{\frac{\partial u_r}{\partial r}} \cos m\theta \,\mathrm{d}\theta = \gamma_m \pi \left[\left(\frac{\partial U}{\partial R}\right)_m^C - \frac{\hat{\mathcal{J}}_m^C}{\bar{\mathcal{J}}_B}\overline{\frac{\partial u_r}{\partial r}}\right],$$

$$\int_0^{2\pi} \widehat{\frac{\partial u_r}{\partial r}} \sin m\theta \,\mathrm{d}\theta = \gamma_m \pi \left[\left(\frac{\partial U}{\partial R}\right)_m^S - \frac{\hat{\mathcal{J}}_m^S}{\bar{\mathcal{J}}_B}\overline{\frac{\partial u_r}{\partial r}}\right],$$

$$\int_0^{2\pi} \widehat{\frac{\partial u_z}{\partial r}} \cos m\theta \,\mathrm{d}\theta = \gamma_m \pi \left[\left(\frac{\partial W}{\partial R}\right)_m^C - \frac{\hat{\mathcal{J}}_m^C}{\bar{\mathcal{J}}_B}\overline{\frac{\partial u_z}{\partial r}}\right],$$

$$\int_0^{2\pi} \widehat{\frac{\partial u_z}{\partial r}} \sin m\theta \,\mathrm{d}\theta = \gamma_m \pi \left[\left(\frac{\partial W}{\partial R}\right)_m^S - \frac{\hat{\mathcal{J}}_m^S}{\bar{\mathcal{J}}_B}\overline{\frac{\partial u_z}{\partial r}}\right],$$

$$\int_0^{2\pi} \widehat{\frac{\partial u_\theta}{\partial r}} \cos m\theta \,\mathrm{d}\theta = \gamma_m \pi \left[\left(\frac{\partial V}{\partial R}\right)_m^C - \frac{\hat{\mathcal{J}}_m^C}{\bar{\mathcal{J}}_B}\overline{\frac{\partial u_\theta}{\partial r}}\right],$$

$$\int_0^{2\pi} \widehat{\frac{\partial u_\theta}{\partial r}} \sin m\theta \,\mathrm{d}\theta = \gamma_m \pi \left[\left(\frac{\partial V}{\partial R}\right)_m^S - \frac{\hat{\mathcal{J}}_m^S}{\bar{\mathcal{J}}_B}\overline{\frac{\partial u_\theta}{\partial r}}\right], \tag{7.74}$$

$$
\begin{aligned}
\int_0^{2\pi} \widehat{\frac{\partial u_r}{\partial z}} \cos m\theta \,\mathrm{d}\theta &= \gamma_m \,\pi \left[\left(\frac{\partial U}{\partial Z} \right)_m^C - \frac{\hat{\mathcal{J}}_m^C}{\bar{\mathcal{J}}_B} \overline{\frac{\partial u_r}{\partial z}} \right], \\
\int_0^{2\pi} \widehat{\frac{\partial u_r}{\partial z}} \sin m\theta \,\mathrm{d}\theta &= \gamma_m \,\pi \left[\left(\frac{\partial U}{\partial Z} \right)_m^S - \frac{\hat{\mathcal{J}}_m^S}{\bar{\mathcal{J}}_B} \overline{\frac{\partial u_r}{\partial z}} \right], \\
\int_0^{2\pi} \widehat{\frac{\partial u_z}{\partial z}} \cos m\theta \,\mathrm{d}\theta &= \gamma_m \,\pi \left[\left(\frac{\partial W}{\partial Z} \right)_m^C - \frac{\hat{\mathcal{J}}_m^C}{\bar{\mathcal{J}}_B} \overline{\frac{\partial u_z}{\partial z}} \right], \\
\int_0^{2\pi} \widehat{\frac{\partial u_z}{\partial z}} \sin m\theta \,\mathrm{d}\theta &= \gamma_m \,\pi \left[\left(\frac{\partial W}{\partial Z} \right)_m^S - \frac{\hat{\mathcal{J}}_m^S}{\bar{\mathcal{J}}_B} \overline{\frac{\partial u_z}{\partial z}} \right], \\
\int_0^{2\pi} \widehat{\frac{\partial u_\theta}{\partial z}} \cos m\theta \,\mathrm{d}\theta &= \gamma_m \,\pi \left[\left(\frac{\partial V}{\partial Z} \right)_m^C - \frac{\hat{\mathcal{J}}_m^C}{\bar{\mathcal{J}}_B} \overline{\frac{\partial u_\theta}{\partial z}} \right], \\
\int_0^{2\pi} \widehat{\frac{\partial u_\theta}{\partial z}} \sin m\theta \,\mathrm{d}\theta &= \gamma_m \,\pi \left[\left(\frac{\partial V}{\partial Z} \right)_m^S - \frac{\hat{\mathcal{J}}_m^S}{\bar{\mathcal{J}}_B} \overline{\frac{\partial u_\theta}{\partial z}} \right], \qquad (7.75)
\end{aligned}
$$

$$
\begin{aligned}
\int_0^{2\pi} \widehat{\frac{\partial u_r}{\partial \theta}} \cos m\theta \,\mathrm{d}\theta &= \gamma_m \,\pi \, m \left[U_m^S - \overline{\frac{\partial u_r}{\partial r}} R_m^S - \overline{\frac{\partial u_r}{\partial z}} Z_m^S \right], \\
\int_0^{2\pi} \widehat{\frac{\partial u_r}{\partial \theta}} \sin m\theta \,\mathrm{d}\theta &= \gamma_m \,\pi \, m \left[-U_m^C + \overline{\frac{\partial u_r}{\partial r}} R_m^C + \overline{\frac{\partial u_r}{\partial z}} Z_m^C \right], \\
\int_0^{2\pi} \widehat{\frac{\partial u_z}{\partial \theta}} \cos m\theta \,\mathrm{d}\theta &= \gamma_m \,\pi \, m \left[W_m^S - \overline{\frac{\partial u_z}{\partial r}} R_m^S - \overline{\frac{\partial u_z}{\partial z}} Z_m^S \right], \\
\int_0^{2\pi} \widehat{\frac{\partial u_z}{\partial \theta}} \sin m\theta \,\mathrm{d}\theta &= \gamma_m \,\pi \, m \left[-W_m^C + \overline{\frac{\partial u_z}{\partial r}} R_m^C + \overline{\frac{\partial u_z}{\partial z}} Z_m^C \right], \\
\int_0^{2\pi} \widehat{\frac{\partial u_\theta}{\partial \theta}} \cos m\theta \,\mathrm{d}\theta &= \gamma_m \,\pi \, m \left[V_m^S - \overline{\frac{\partial u_\theta}{\partial r}} R_m^S - \overline{\frac{\partial u_\theta}{\partial z}} Z_m^S \right], \\
\int_0^{2\pi} \widehat{\frac{\partial u_\theta}{\partial \theta}} \sin m\theta \,\mathrm{d}\theta &= \gamma_m \,\pi \, m \left[-V_m^C + \overline{\frac{\partial u_\theta}{\partial r}} R_m^C + \overline{\frac{\partial u_\theta}{\partial z}} Z_m^C \right], \\
\int_0^{2\pi} \widehat{\frac{\partial p}{\partial \theta}} \cos m\theta \,\mathrm{d}\theta &= \gamma_m \,\pi \, m \left[P_m^S - \overline{\frac{\partial p}{\partial r}} R_m^S - \overline{\frac{\partial p}{\partial z}} Z_m^S \right] \quad \text{and} \\
\int_0^{2\pi} \widehat{\frac{\partial p}{\partial \theta}} \sin m\theta \,\mathrm{d}\theta &= \gamma_m \,\pi \, m \left[-P_m^C + \overline{\frac{\partial p}{\partial r}} R_m^C + \overline{\frac{\partial p}{\partial z}} Z_m^C \right]. \qquad (7.76)
\end{aligned}
$$

Finally, using (7.61)–(7.76) we can write down the terms of order ϵ in (7.36). We first choose the form of $\phi_l^{[\mathrm{f}]}$ and $\phi_l^{[\mathrm{p}]}$ given in (7.59), and perform the integral over θ to

obtain the radial momentum equation,

$$
\begin{aligned}
\hat{\mathcal{R}}^{[\mathrm{fC,bulk}]}_{\mathrm{r}ml} = \gamma_m\,\pi\int_{-1}^{1}\int_{-1}^{1}\Bigg\{ R_\rho\,\mathrm{Re}\,\Bigg[& \mathrm{St}\,\bar{r}\frac{\delta U_m^C}{\delta t}\bar{\mathcal{J}}_B + \mathrm{St}\,R_m^C\frac{\delta \bar{u}_r}{\delta t}\bar{\mathcal{J}}_B + \mathrm{St}\,\bar{r}\frac{\delta \bar{u}_r}{\delta t}\hat{\mathcal{J}}_m^C \\
& + \bar{r}\left(\bar{u}_r - \mathrm{St}\,\bar{u}_r^{[\mathrm{M}]}\right)\left(\frac{\partial U}{\partial R}\right)_m^C\bar{\mathcal{J}}_B + \bar{r}\left(U_m^C - \mathrm{St}\,\frac{\delta R_m^C}{\delta t}\right)\overline{\frac{\partial u_r}{\partial r}}\bar{\mathcal{J}}_B \\
& + R_m^C\left(\bar{u}_r - \mathrm{St}\,\bar{u}_r^{[\mathrm{M}]}\right)\overline{\frac{\partial u_r}{\partial r}}\bar{\mathcal{J}}_B + \bar{r}\left(\bar{u}_z - \mathrm{St}\,\bar{u}_z^{[\mathrm{M}]}\right)\left(\frac{\partial U}{\partial Z}\right)_m^C\bar{\mathcal{J}}_B \\
& + \bar{r}\left(W_m^C - \mathrm{St}\,\frac{\delta Z_m^C}{\delta t}\right)\overline{\frac{\partial u_r}{\partial z}}\bar{\mathcal{J}}_B + R_m^C\left(\bar{u}_z - \mathrm{St}\,\bar{u}_z^{[\mathrm{M}]}\right)\overline{\frac{\partial u_r}{\partial z}}\bar{\mathcal{J}}_B \\
& + m\bar{u}_\theta\left(U_m^S - \overline{\frac{\partial u_r}{\partial r}}R_m^S - \overline{\frac{\partial u_r}{\partial z}}Z_m^S\right)\bar{\mathcal{J}}_B - 2\bar{u}_\theta V_m^C\bar{\mathcal{J}}_B - \bar{u}_\theta^2\hat{\mathcal{J}}_m^C\Bigg]\,\psi_l^{[\mathrm{f}]} \\
& - \left(R_m^C\bar{\mathcal{J}}_B + \bar{r}\hat{\mathcal{J}}_m^C\right)B_r\,\psi_l^{[\mathrm{f}]} - R_\rho\,\frac{\mathrm{Re}}{\mathrm{Fr}}\left(R_m^C\bar{\mathcal{J}}_B + \bar{r}\hat{\mathcal{J}}_m^C\right)G_r\,\psi_l^{[\mathrm{f}]} \\
& - \bar{r}\bar{p}\left(\frac{\partial \psi_l^{[\mathrm{f}]}}{\partial R}\right)_m^C\bar{\mathcal{J}}_B - \bar{r}P_m^C\frac{\partial \psi_l^{[\mathrm{f}]}}{\partial r}\bar{\mathcal{J}}_B - R_m^C\bar{p}\frac{\partial \psi_l^{[\mathrm{f}]}}{\partial r}\bar{\mathcal{J}}_B \\
& + 2R_\mu\Bigg[\bar{r}\left(\frac{\partial U}{\partial R}\right)_m^C\frac{\partial \psi_l^{[\mathrm{f}]}}{\partial r}\bar{\mathcal{J}}_B + \bar{r}\overline{\frac{\partial u_r}{\partial r}}\left(\frac{\partial \psi_l^{[\mathrm{f}]}}{\partial R}\right)_m^C\bar{\mathcal{J}}_B \\
& + R_m^C\overline{\frac{\partial u_r}{\partial r}}\frac{\partial \psi_l^{[\mathrm{f}]}}{\partial r}\bar{\mathcal{J}}_B - \bar{r}\overline{\frac{\partial u_r}{\partial r}}\frac{\partial \psi_l^{[\mathrm{f}]}}{\partial r}\hat{\mathcal{J}}_m^C\Bigg] \\
& + R_\mu\Bigg[\bar{r}\left(\frac{\partial W}{\partial R}\right)_m^C\frac{\partial \psi_l^{[\mathrm{f}]}}{\partial z}\bar{\mathcal{J}}_B + \bar{r}\overline{\frac{\partial u_z}{\partial r}}\left(\frac{\partial \psi_l^{[\mathrm{f}]}}{\partial Z}\right)_m^C\bar{\mathcal{J}}_B + R_m^C\overline{\frac{\partial u_z}{\partial r}}\frac{\partial \psi_l^{[\mathrm{f}]}}{\partial z}\bar{\mathcal{J}}_B \\
& - \bar{r}\overline{\frac{\partial u_z}{\partial r}}\frac{\partial \psi_l^{[\mathrm{f}]}}{\partial z}\hat{\mathcal{J}}_m^C + \bar{r}\left(\frac{\partial U}{\partial Z}\right)_m^C\frac{\partial \psi_l^{[\mathrm{f}]}}{\partial z}\bar{\mathcal{J}}_B + \bar{r}\overline{\frac{\partial u_r}{\partial z}}\left(\frac{\partial \psi_l^{[\mathrm{f}]}}{\partial Z}\right)_m^C\bar{\mathcal{J}}_B \\
& + R_m^C\overline{\frac{\partial u_r}{\partial z}}\frac{\partial \psi_l^{[\mathrm{f}]}}{\partial z}\bar{\mathcal{J}}_B - \bar{r}\overline{\frac{\partial u_r}{\partial z}}\frac{\partial \psi_l^{[\mathrm{f}]}}{\partial z}\hat{\mathcal{J}}_m^C - m\left(\frac{\partial V}{\partial R}\right)_m^S\bar{\mathcal{J}}_B\psi_l^{[\mathrm{f}]} \\
& - m\overline{\frac{\partial u_\theta}{\partial r}}\left(\frac{\partial \psi_l^{[\mathrm{f}]}}{\partial r}R_m^S + \frac{\partial \psi_l^{[\mathrm{f}]}}{\partial z}Z_m^S\right)\bar{\mathcal{J}}_B + \frac{m}{\bar{r}}\bar{u}_\theta\left(\frac{\partial \psi_l^{[\mathrm{f}]}}{\partial r}R_m^S + \frac{\partial \psi_l^{[\mathrm{f}]}}{\partial z}Z_m^S\right)\bar{\mathcal{J}}_B\Bigg] \\
& + R_\mu\Bigg[\frac{m^2}{\bar{r}}\left(U_m^C - \overline{\frac{\partial u_r}{\partial r}}R_m^C - \overline{\frac{\partial u_r}{\partial z}}Z_m^C\right)\bar{\mathcal{J}}_B + \frac{m}{\bar{r}}V_m^S\bar{\mathcal{J}}_B \\
& - \frac{m}{\bar{r}^2}R_m^S\bar{u}_\theta\bar{\mathcal{J}}_B + \frac{m}{\bar{r}}\bar{u}_\theta\hat{\mathcal{J}}_m^S\Bigg]\,\psi_l^{[\mathrm{f}]} - \left(P_m^C\bar{\mathcal{J}}_B + \bar{p}\hat{\mathcal{J}}_m^C\right)\psi_l^{[\mathrm{f}]} \\
& + 2R_\mu\Bigg[\frac{m}{\bar{r}}\left(V_m^S - \overline{\frac{\partial u_\theta}{\partial r}}R_m^S - \overline{\frac{\partial u_\theta}{\partial z}}Z_m^S\right)\bar{\mathcal{J}}_B + \frac{1}{\bar{r}}U_m^C\bar{\mathcal{J}}_B \\
& - \frac{1}{\bar{r}^2}R_m^C\bar{u}_r\bar{\mathcal{J}}_B + \frac{1}{\bar{r}}\bar{u}_r\hat{\mathcal{J}}_m^C\Bigg]\,\psi_l^{[\mathrm{f}]}\Bigg\}\,\mathrm{d}s_1\,\mathrm{d}s_2, \qquad (7.77)
\end{aligned}
$$

axial momentum equation,

$$
\begin{aligned}
\hat{\mathcal{R}}_{zml}^{[\mathrm{fC,bulk}]} = \gamma_m \, \pi \int_{-1}^{1} \int_{-1}^{1} \Bigg\{ & R_\rho \, \mathrm{Re} \, \Bigg[\mathrm{St} \, \bar{r} \frac{\delta W_m^C}{\delta t} \bar{\mathcal{J}}_B + \mathrm{St} \, R_m^C \frac{\delta \bar{u}_z}{\delta t} \bar{\mathcal{J}}_B + \mathrm{St} \, \bar{r} \frac{\delta \bar{u}_z}{\delta t} \hat{\mathcal{J}}_m^C \\
& + \bar{r} \left(\bar{u}_r - \mathrm{St} \, \bar{u}_r^{[\mathrm{M}]} \right) \left(\frac{\partial W}{\partial R} \right)_m^C \bar{\mathcal{J}}_B + \bar{r} \left(U_m^C - \mathrm{St} \, \frac{\delta R_m^C}{\delta t} \right) \overline{\frac{\partial u_z}{\partial r}} \bar{\mathcal{J}}_B \\
& + R_m^C \left(\bar{u}_r - \mathrm{St} \, \bar{u}_r^{[\mathrm{M}]} \right) \overline{\frac{\partial u_z}{\partial r}} \bar{\mathcal{J}}_B + \bar{r} \left(\bar{u}_z - \mathrm{St} \, \bar{u}_z^{[\mathrm{M}]} \right) \left(\frac{\partial W}{\partial Z} \right)_m^C \bar{\mathcal{J}}_B \\
& + \bar{r} \left(W_m^C - \mathrm{St} \, \frac{\delta Z_m^C}{\delta t} \right) \overline{\frac{\partial u_z}{\partial z}} \bar{\mathcal{J}}_B + R_m^C \left(\bar{u}_z - \mathrm{St} \, \bar{u}_z^{[\mathrm{M}]} \right) \overline{\frac{\partial u_z}{\partial z}} \bar{\mathcal{J}}_B \\
& + m \bar{u}_\theta \left(W_m^S - \overline{\frac{\partial u_z}{\partial r}} R_m^S - \overline{\frac{\partial u_z}{\partial z}} Z_m^S \right) \bar{\mathcal{J}}_B \Bigg] \psi_l^{[\mathrm{f}]} \\
& - \left(R_m^C \bar{\mathcal{J}}_B + \bar{r} \hat{\mathcal{J}}_m^C \right) B_z \, \psi_l^{[\mathrm{f}]} - R_\rho \frac{\mathrm{Re}}{\mathrm{Fr}} \left(R_m^C \bar{\mathcal{J}}_B + \bar{r} \hat{\mathcal{J}}_m^C \right) G_z \, \psi_l^{[\mathrm{f}]} \\
& + R_\mu \Bigg[\bar{r} \left(\frac{\partial W}{\partial R} \right)_m^C \frac{\partial \psi_l^{[\mathrm{f}]}}{\partial r} \bar{\mathcal{J}}_B + \bar{r} \overline{\frac{\partial u_z}{\partial r}} \left(\frac{\partial \psi_l^{[\mathrm{f}]}}{\partial R} \right)_m^C \bar{\mathcal{J}}_B + R_m^C \overline{\frac{\partial u_z}{\partial r}} \frac{\partial \psi_l^{[\mathrm{f}]}}{\partial r} \bar{\mathcal{J}}_B \\
& - \bar{r} \overline{\frac{\partial u_z}{\partial r}} \frac{\partial \psi_l^{[\mathrm{f}]}}{\partial r} \hat{\mathcal{J}}_m^C + \bar{r} \left(\frac{\partial U}{\partial Z} \right)_m^C \frac{\partial \psi_l^{[\mathrm{f}]}}{\partial r} \bar{\mathcal{J}}_B + \bar{r} \overline{\frac{\partial u_r}{\partial z}} \left(\frac{\partial \psi_l^{[\mathrm{f}]}}{\partial R} \right)_m^C \bar{\mathcal{J}}_B \\
& + R_m^C \overline{\frac{\partial u_r}{\partial z}} \frac{\partial \psi_l^{[\mathrm{f}]}}{\partial r} \bar{\mathcal{J}}_B - \bar{r} \overline{\frac{\partial u_r}{\partial z}} \frac{\partial \psi_l^{[\mathrm{f}]}}{\partial r} \hat{\mathcal{J}}_m^C - m \overline{\frac{\partial u_\theta}{\partial z}} \left(\frac{\partial \psi_l^{[\mathrm{f}]}}{\partial r} R_m^S + \frac{\partial \psi_l^{[\mathrm{f}]}}{\partial z} Z_m^S \right) \bar{\mathcal{J}}_B \Bigg] \\
& - \bar{r} \bar{p} \left(\frac{\partial \psi_l^{[\mathrm{f}]}}{\partial Z} \right)_m^C \bar{\mathcal{J}}_B - \bar{r} P_m^C \frac{\partial \psi_l^{[\mathrm{f}]}}{\partial z} \bar{\mathcal{J}}_B - R_m^C \bar{p} \frac{\partial \psi_l^{[\mathrm{f}]}}{\partial z} \bar{\mathcal{J}}_B \\
& + 2 R_\mu \Bigg[\bar{r} \left(\frac{\partial W}{\partial Z} \right)_m^C \bar{\mathcal{J}}_B \frac{\partial \psi_l^{[\mathrm{f}]}}{\partial z} + \bar{r} \overline{\frac{\partial u_z}{\partial z}} \left(\frac{\partial \psi_l^{[\mathrm{f}]}}{\partial Z} \right)_m^C \bar{\mathcal{J}}_B \\
& + R_m^C \overline{\frac{\partial u_z}{\partial z}} \frac{\partial \psi_l^{[\mathrm{f}]}}{\partial z} \bar{\mathcal{J}}_B - \bar{r} \overline{\frac{\partial u_z}{\partial z}} \frac{\partial \psi_l^{[\mathrm{f}]}}{\partial z} \hat{\mathcal{J}}_m^C \Bigg] \\
& + R_\mu \left[\frac{m^2}{\bar{r}} \left(W_m^C - \overline{\frac{\partial u_z}{\partial r}} R_m^C - \overline{\frac{\partial u_z}{\partial z}} Z_m^C \right) \bar{\mathcal{J}}_B - m \left(\frac{\partial V}{\partial Z} \right)_m^S \bar{\mathcal{J}}_B \right] \psi_l^{[\mathrm{f}]} \Bigg\} \, \mathrm{d}s_1 \, \mathrm{d}s_2,
\end{aligned}
\tag{7.78}
$$

azimuthal momentum equation,

$$
\begin{aligned}
\hat{\mathcal{R}}^{[\mathrm{fC,bulk}]}_{\theta ml} = \gamma_m \, \pi \int_{-1}^{1} \int_{-1}^{1} \Bigg\{ & R_\rho \, \mathrm{Re} \, \Bigg[\mathrm{St} \, \bar{r} \frac{\delta V_m^C}{\delta t} \bar{\mathcal{J}}_B + \mathrm{St} \, R_m^C \frac{\delta \bar{u}_\theta}{\delta t} \bar{\mathcal{J}}_B + \mathrm{St} \, \bar{r} \frac{\delta \bar{u}_\theta}{\delta t} \hat{\mathcal{J}}_m^C \\
& + \bar{r} \left(\bar{u}_r - \mathrm{St} \, \bar{u}_r^{[\mathrm{M}]} \right) \left(\frac{\partial V}{\partial R} \right)_m^C \bar{\mathcal{J}}_B + \bar{r} \left(U_m^C - \mathrm{St} \, \frac{\delta R_m^C}{\delta t} \right) \overline{\frac{\partial u_\theta}{\partial r}} \bar{\mathcal{J}}_B \\
& + R_m^C \left(\bar{u}_r - \mathrm{St} \, \bar{u}_r^{[\mathrm{M}]} \right) \overline{\frac{\partial u_\theta}{\partial r}} \bar{\mathcal{J}}_B + \bar{r} \left(\bar{u}_z - \mathrm{St} \, \bar{u}_z^{[\mathrm{M}]} \right) \left(\frac{\partial V}{\partial Z} \right)_m^C \bar{\mathcal{J}}_B \\
& + \bar{r} \left(W_m^C - \mathrm{St} \, \frac{\delta Z_m^C}{\delta t} \right) \overline{\frac{\partial u_\theta}{\partial z}} \bar{\mathcal{J}}_B + R_m^C \left(\bar{u}_z - \mathrm{St} \, \bar{u}_z^{[\mathrm{M}]} \right) \overline{\frac{\partial u_\theta}{\partial z}} \bar{\mathcal{J}}_B \\
& + m \bar{u}_\theta \left(V_m^S - \overline{\frac{\partial u_\theta}{\partial r}} R_m^S - \overline{\frac{\partial u_\theta}{\partial z}} Z_m^S \right) \bar{\mathcal{J}}_B \\
& + \bar{u}_\theta U_m^C \bar{\mathcal{J}}_B + V_m^C \bar{u}_r \bar{\mathcal{J}}_B + \bar{u}_\theta \bar{u}_r \hat{\mathcal{J}}_m^C \Bigg] \, \psi_l^{[\mathrm{f}]} \\
& - \left(R_m^C \bar{\mathcal{J}}_B + \bar{r} \hat{\mathcal{J}}_m^C \right) B_\theta \, \psi_l^{[\mathrm{f}]} - R_\rho \, \frac{\mathrm{Re}}{\mathrm{Fr}} \left(R_m^C \bar{\mathcal{J}}_B + \bar{r} \hat{\mathcal{J}}_m^C \right) G_\theta \, \psi_l^{[\mathrm{f}]} \\
& + R_\mu \Bigg[\bar{r} \left(\frac{\partial V}{\partial R} \right)_m^C \frac{\partial \psi_l^{[\mathrm{f}]}}{\partial r} \bar{\mathcal{J}}_B + \bar{r} \overline{\frac{\partial u_\theta}{\partial r}} \left(\frac{\partial \psi_l^{[\mathrm{f}]}}{\partial R} \right)_m^C \bar{\mathcal{J}}_B + R_m^C \overline{\frac{\partial u_\theta}{\partial r}} \frac{\partial \psi_l^{[\mathrm{f}]}}{\partial r} \bar{\mathcal{J}}_B \\
& - \bar{r} \overline{\frac{\partial u_\theta}{\partial r}} \frac{\partial \psi_l^{[\mathrm{f}]}}{\partial r} \hat{\mathcal{J}}_m^C - V_m^C \frac{\partial \psi_l^{[\mathrm{f}]}}{\partial r} \bar{\mathcal{J}}_B - \bar{u}_\theta \left(\frac{\partial \psi_l^{[\mathrm{f}]}}{\partial R} \right)_m^C \bar{\mathcal{J}}_B \\
& + m \left(U_m^S - \overline{\frac{\partial u_r}{\partial r}} R_m^S - \overline{\frac{\partial u_r}{\partial z}} Z_m^S \right) \frac{\partial \psi_l^{[\mathrm{f}]}}{\partial r} \bar{\mathcal{J}}_B \\
& + \bar{r} \left(\frac{\partial V}{\partial Z} \right)_m^C \frac{\partial \psi_l^{[\mathrm{f}]}}{\partial z} \bar{\mathcal{J}}_B + \bar{r} \overline{\frac{\partial u_\theta}{\partial z}} \left(\frac{\partial \psi_l^{[\mathrm{f}]}}{\partial Z} \right)_m^C \bar{\mathcal{J}}_B + R_m^C \overline{\frac{\partial u_\theta}{\partial z}} \frac{\partial \psi_l^{[\mathrm{f}]}}{\partial z} \bar{\mathcal{J}}_B \\
& - \bar{r} \overline{\frac{\partial u_\theta}{\partial z}} \frac{\partial \psi_l^{[\mathrm{f}]}}{\partial z} \hat{\mathcal{J}}_m^C + m \left(W_m^S - \overline{\frac{\partial u_z}{\partial r}} R_m^S - \overline{\frac{\partial u_z}{\partial z}} Z_m^S \right) \frac{\partial \psi_l^{[\mathrm{f}]}}{\partial z} \bar{\mathcal{J}}_B \\
& - \frac{2m}{\bar{r}} \bar{u}_r \left(\frac{\partial \psi_l^{[\mathrm{f}]}}{\partial r} R_m^S + \frac{\partial \psi_l^{[\mathrm{f}]}}{\partial z} Z_m^S \right) \bar{\mathcal{J}}_B \Bigg] \\
& + m \left[\bar{p} R_m^S \frac{\partial \psi_l^{[\mathrm{f}]}}{\partial r} \bar{\mathcal{J}}_B + \bar{p} Z_m^S \frac{\partial \psi_l^{[\mathrm{f}]}}{\partial z} \bar{\mathcal{J}}_B + P_m^S \psi_l^{[\mathrm{f}]} \bar{\mathcal{J}}_B + \bar{p} \psi_l^{[\mathrm{f}]} \hat{\mathcal{J}}_m^S \right] \\
& + R_\mu \Bigg[- \frac{2m^2}{\bar{r}} \left(- V_m^C + \overline{\frac{\partial u_\theta}{\partial r}} R_m^C + \overline{\frac{\partial u_\theta}{\partial z}} Z_m^C \right) \bar{\mathcal{J}}_B \\
& - \frac{2m}{\bar{r}} U_m^S \bar{\mathcal{J}}_B + \frac{2m}{\bar{r}^2} R_m^S \bar{u}_r \bar{\mathcal{J}}_B - \frac{2m}{\bar{r}} \bar{u}_r \hat{\mathcal{J}}_m^S \\
& - \left(\frac{\partial V}{\partial R} \right)_m^C \bar{\mathcal{J}}_B - \frac{m}{\bar{r}} \left(U_m^S - \overline{\frac{\partial u_r}{\partial r}} R_m^S - \overline{\frac{\partial u_r}{\partial z}} Z_m^S \right) \bar{\mathcal{J}}_B \\
& + \frac{1}{\bar{r}} V_m^C \bar{\mathcal{J}}_B - \frac{1}{\bar{r}^2} R_m^C \bar{u}_\theta \bar{\mathcal{J}}_B + \frac{1}{\bar{r}} \bar{u}_\theta \hat{\mathcal{J}}_m^C \Bigg] \, \psi_l^{[\mathrm{f}]} \Bigg\} \, \mathrm{d}s_1 \, \mathrm{d}s_2
\end{aligned}
\tag{7.79}
$$

and continuity equation

$$\hat{\mathcal{R}}^{[\mathrm{pC}]}_{ml} = \gamma_m \, \pi \int_{-1}^{1} \int_{-1}^{1} \left\{ \bar{r} \left(\frac{\partial U}{\partial R} \right)^C_m \bar{\mathcal{J}}_B + R^C_m \overline{\frac{\partial u_r}{\partial r}} \bar{\mathcal{J}}_B + U^C_m \bar{\mathcal{J}}_B \right.$$
$$+ \bar{u}_r \hat{\mathcal{J}}^C_m + \bar{r} \left(\frac{\partial W}{\partial Z} \right)^C_m \bar{\mathcal{J}}_B + R^C_m \overline{\frac{\partial u_z}{\partial z}} \bar{\mathcal{J}}_B$$
$$+ m \left(V^S_m - \overline{\frac{\partial u_\theta}{\partial r}} R^S_m - \overline{\frac{\partial u_\theta}{\partial z}} Z^S_m \right) \bar{\mathcal{J}}_B$$
$$\left. - \left(R^C_m \bar{\mathcal{J}}_B + \bar{r} \hat{\mathcal{J}}^C_m \right) Q \right\} \psi^{[\mathrm{p}]}_l \, \mathrm{d}s_1 \, \mathrm{d}s_2. \quad (7.80)$$

We then choose the form of $\phi^{[\mathrm{f}]}_l$ and $\phi^{[\mathrm{p}]}_l$ given in (7.60), and again perform the integral

over θ to obtain the radial momentum equation,

$$
\begin{aligned}
\hat{\mathcal{R}}^{[\mathrm{fS,bulk}]}_{\mathrm{r}ml} = \gamma_m\,\pi \int_{-1}^{1}\int_{-1}^{1} \Bigg\{ & R_\rho\,\mathrm{Re}\,\Bigg[\mathrm{St}\,\bar{r}\frac{\delta U_m^S}{\delta t}\bar{\mathcal{J}}_B + \mathrm{St}\,R_m^S\frac{\delta \bar{u}_r}{\delta t}\bar{\mathcal{J}}_B + \mathrm{St}\,\bar{r}\frac{\delta \bar{u}_r}{\delta t}\hat{\mathcal{J}}_m^S \\
& + \bar{r}\left(\bar{u}_r - \mathrm{St}\,\bar{u}_r^{[\mathrm{M}]}\right)\left(\frac{\partial U}{\partial R}\right)_m^S \bar{\mathcal{J}}_B + \bar{r}\left(U_m^S - \mathrm{St}\,\frac{\delta R_m^S}{\delta t}\right)\overline{\frac{\partial u_r}{\partial r}}\bar{\mathcal{J}}_B \\
& + R_m^S\left(\bar{u}_r - \mathrm{St}\,\bar{u}_r^{[\mathrm{M}]}\right)\overline{\frac{\partial u_r}{\partial r}}\bar{\mathcal{J}}_B + \bar{r}\left(\bar{u}_z - \mathrm{St}\,\bar{u}_z^{[\mathrm{M}]}\right)\left(\frac{\partial U}{\partial Z}\right)_m^S \bar{\mathcal{J}}_B \\
& + \bar{r}\left(W_m^S - \mathrm{St}\,\frac{\delta Z_m^S}{\delta t}\right)\overline{\frac{\partial u_r}{\partial z}}\bar{\mathcal{J}}_B + R_m^S\left(\bar{u}_z - \mathrm{St}\,\bar{u}_z^{[\mathrm{M}]}\right)\overline{\frac{\partial u_r}{\partial z}}\bar{\mathcal{J}}_B \\
& + m\bar{u}_\theta\left(-U_m^C + \overline{\frac{\partial u_r}{\partial r}}R_m^C + \overline{\frac{\partial u_r}{\partial z}}Z_m^C\right)\bar{\mathcal{J}}_B - 2\bar{u}_\theta V_m^S\bar{\mathcal{J}}_B - \bar{u}_\theta^2\hat{\mathcal{J}}_m^S\Bigg]\,\psi_l^{[\mathrm{f}]} \\
& - \left(R_m^S\bar{\mathcal{J}}_B + \bar{r}\hat{\mathcal{J}}_m^S\right)B_r\,\psi_l^{[\mathrm{f}]} - R_\rho\,\frac{\mathrm{Re}}{\mathrm{Fr}}\left(R_m^S\bar{\mathcal{J}}_B + \bar{r}\hat{\mathcal{J}}_m^S\right)G_r\,\psi_l^{[\mathrm{f}]} \\
& - \bar{r}\bar{p}\left(\frac{\partial \psi_l^{[\mathrm{f}]}}{\partial R}\right)_m^S\bar{\mathcal{J}}_B - \bar{r}P_m^S\frac{\partial \psi_l^{[\mathrm{f}]}}{\partial r}\bar{\mathcal{J}}_B - R_m^S\bar{p}\frac{\partial \psi_l^{[\mathrm{f}]}}{\partial r}\bar{\mathcal{J}}_B \\
& + 2R_\mu\Bigg[\bar{r}\left(\frac{\partial U}{\partial R}\right)_m^S\frac{\partial \psi_l^{[\mathrm{f}]}}{\partial r}\bar{\mathcal{J}}_B + \bar{r}\overline{\frac{\partial u_r}{\partial r}}\left(\frac{\partial \psi_l^{[\mathrm{f}]}}{\partial R}\right)_m^S\bar{\mathcal{J}}_B \\
& + R_m^S\overline{\frac{\partial u_r}{\partial r}}\frac{\partial \psi_l^{[\mathrm{f}]}}{\partial r}\bar{\mathcal{J}}_B - \bar{r}\overline{\frac{\partial u_r}{\partial r}}\frac{\partial \psi_l^{[\mathrm{f}]}}{\partial r}\hat{\mathcal{J}}_m^S\Bigg] \\
& + R_\mu\Bigg[\bar{r}\left(\frac{\partial W}{\partial R}\right)_m^S\frac{\partial \psi_l^{[\mathrm{f}]}}{\partial z}\bar{\mathcal{J}}_B + \bar{r}\overline{\frac{\partial u_z}{\partial r}}\left(\frac{\partial \psi_l^{[\mathrm{f}]}}{\partial Z}\right)_m^S\bar{\mathcal{J}}_B + R_m^S\overline{\frac{\partial u_z}{\partial r}}\frac{\partial \psi_l^{[\mathrm{f}]}}{\partial z}\bar{\mathcal{J}}_B \\
& - \bar{r}\overline{\frac{\partial u_z}{\partial r}}\frac{\partial \psi_l^{[\mathrm{f}]}}{\partial z}\hat{\mathcal{J}}_m^S + \bar{r}\left(\frac{\partial U}{\partial Z}\right)_m^S\frac{\partial \psi_l^{[\mathrm{f}]}}{\partial z}\bar{\mathcal{J}}_B + \bar{r}\overline{\frac{\partial u_r}{\partial z}}\left(\frac{\partial \psi_l^{[\mathrm{f}]}}{\partial Z}\right)_m^S\bar{\mathcal{J}}_B \\
& + R_m^S\overline{\frac{\partial u_r}{\partial z}}\frac{\partial \psi_l^{[\mathrm{f}]}}{\partial z}\bar{\mathcal{J}}_B - \bar{r}\overline{\frac{\partial u_r}{\partial z}}\frac{\partial \psi_l^{[\mathrm{f}]}}{\partial z}\hat{\mathcal{J}}_m^S + m\left(\frac{\partial V}{\partial R}\right)_m^C\bar{\mathcal{J}}_B\psi_l^{[\mathrm{f}]} \\
& + m\overline{\frac{\partial u_\theta}{\partial r}}\left(\frac{\partial \psi_l^{[\mathrm{f}]}}{\partial r}R_m^C + \frac{\partial \psi_l^{[\mathrm{f}]}}{\partial z}Z_m^C\right)\bar{\mathcal{J}}_B - \frac{m}{\bar{r}}\bar{u}_\theta\left(\frac{\partial \psi_l^{[\mathrm{f}]}}{\partial r}R_m^C + \frac{\partial \psi_l^{[\mathrm{f}]}}{\partial z}Z_m^C\right)\bar{\mathcal{J}}_B\Bigg] \\
& + R_\mu\Bigg[\frac{m^2}{\bar{r}}\left(U_m^S - \overline{\frac{\partial u_r}{\partial r}}R_m^S - \overline{\frac{\partial u_r}{\partial z}}Z_m^S\right)\psi_l^{[\mathrm{f}]}\bar{\mathcal{J}}_B - \frac{m}{\bar{r}}V_m^C\psi_l^{[\mathrm{f}]}\bar{\mathcal{J}}_B \\
& + \frac{m}{\bar{r}^2}R_m^C\bar{u}_\theta\psi_l^{[\mathrm{f}]}\bar{\mathcal{J}}_B - \frac{m}{\bar{r}}\bar{u}_\theta\psi_l^{[\mathrm{f}]}\hat{\mathcal{J}}_m^C\Bigg]\,\psi_l^{[\mathrm{f}]} - \left(P_m^S\bar{\mathcal{J}}_B + \bar{p}\hat{\mathcal{J}}_m^S\right)\psi_l^{[\mathrm{f}]} \\
& + 2R_\mu\Bigg[\frac{m}{\bar{r}}\left(-V_m^C + \overline{\frac{\partial u_\theta}{\partial r}}R_m^C + \overline{\frac{\partial u_\theta}{\partial z}}Z_m^C\right)\bar{\mathcal{J}}_B + \frac{1}{\bar{r}}U_m^S\bar{\mathcal{J}}_B \\
& - \frac{1}{\bar{r}^2}R_m^S\bar{u}_r\bar{\mathcal{J}}_B + \frac{1}{\bar{r}}\bar{u}_r\hat{\mathcal{J}}_m^S\Bigg]\,\psi_l^{[\mathrm{f}]}\Bigg\}\,\mathrm{d}s_1\,\mathrm{d}s_2,
\end{aligned}
\tag{7.81}
$$

axial momentum equation,

$$\begin{aligned}
\hat{\mathcal{R}}^{[\mathrm{fS,bulk}]}_{zml} = \gamma_m\,\pi\int_{-1}^{1}\int_{-1}^{1}\Bigg\{ & R_\rho\,\mathrm{Re}\,\Bigg[\mathrm{St}\,\bar{r}\frac{\delta W_m^S}{\delta t}\bar{\mathcal{J}}_B + \mathrm{St}\,R_m^S\frac{\delta \bar{u}_z}{\delta t}\bar{\mathcal{J}}_B + \mathrm{St}\,\bar{r}\frac{\delta \bar{u}_z}{\delta t}\hat{\mathcal{J}}_m^S \\
& + \bar{r}\left(\bar{u}_r - \mathrm{St}\,\bar{u}_r^{[\mathrm{M}]}\right)\left(\frac{\partial W}{\partial R}\right)_m^S\bar{\mathcal{J}}_B + \bar{r}\left(U_m^S - \mathrm{St}\,\frac{\delta R_m^S}{\delta t}\right)\overline{\frac{\partial u_z}{\partial r}}\bar{\mathcal{J}}_B \\
& + R_m^S\left(\bar{u}_r - \mathrm{St}\,\bar{u}_r^{[\mathrm{M}]}\right)\overline{\frac{\partial u_z}{\partial r}}\bar{\mathcal{J}}_B + \bar{r}\left(\bar{u}_z - \mathrm{St}\,\bar{u}_z^{[\mathrm{M}]}\right)\left(\frac{\partial W}{\partial Z}\right)_m^S\bar{\mathcal{J}}_B \\
& + \bar{r}\left(W_m^S - \mathrm{St}\,\frac{\delta Z_m^S}{\delta t}\right)\overline{\frac{\partial u_z}{\partial z}}\bar{\mathcal{J}}_B + R_m^S\left(\bar{u}_z - \mathrm{St}\,\bar{u}_z^{[\mathrm{M}]}\right)\overline{\frac{\partial u_z}{\partial z}}\bar{\mathcal{J}}_B \\
& + m\bar{u}_\theta\left(-W_m^C + \overline{\frac{\partial u_z}{\partial r}}R_m^C + \overline{\frac{\partial u_z}{\partial z}}Z_m^C\right)\bar{\mathcal{J}}_B\Bigg]\psi_l^{[\mathrm{f}]} \\
& - \left(R_m^S\bar{\mathcal{J}}_B + \bar{r}\hat{\mathcal{J}}_m^S\right)B_z\,\psi_l^{[\mathrm{f}]} - R_\rho\frac{\mathrm{Re}}{\mathrm{Fr}}\left(R_m^S\bar{\mathcal{J}}_B + \bar{r}\hat{\mathcal{J}}_m^S\right)G_z\,\psi_l^{[\mathrm{f}]} \\
& + R_\mu\Bigg[\bar{r}\left(\frac{\partial W}{\partial R}\right)_m^S\frac{\partial \psi_l^{[\mathrm{f}]}}{\partial r}\bar{\mathcal{J}}_B + \bar{r}\overline{\frac{\partial u_z}{\partial r}}\left(\frac{\partial \psi_l^{[\mathrm{f}]}}{\partial R}\right)_m^S\bar{\mathcal{J}}_B + R_m^S\overline{\frac{\partial u_z}{\partial r}}\frac{\partial \psi_l^{[\mathrm{f}]}}{\partial r}\bar{\mathcal{J}}_B \\
& - \bar{r}\overline{\frac{\partial u_z}{\partial r}}\frac{\partial \psi_l^{[\mathrm{f}]}}{\partial r}\hat{\mathcal{J}}_m^S + \bar{r}\left(\frac{\partial U}{\partial Z}\right)_m^S\frac{\partial \psi_l^{[\mathrm{f}]}}{\partial r}\bar{\mathcal{J}}_B + \bar{r}\overline{\frac{\partial u_r}{\partial z}}\left(\frac{\partial \psi_l^{[\mathrm{f}]}}{\partial R}\right)_m^S\bar{\mathcal{J}}_B \\
& + R_m^S\overline{\frac{\partial u_r}{\partial z}}\frac{\partial \psi_l^{[\mathrm{f}]}}{\partial r}\bar{\mathcal{J}}_B - \bar{r}\overline{\frac{\partial u_r}{\partial z}}\frac{\partial \psi_l^{[\mathrm{f}]}}{\partial r}\hat{\mathcal{J}}_m^S + m\overline{\frac{\partial u_\theta}{\partial z}}\left(\frac{\partial \psi_l^{[\mathrm{f}]}}{\partial r}R_m^C + \frac{\partial \psi_l^{[\mathrm{f}]}}{\partial z}Z_m^C\right)\bar{\mathcal{J}}_B\Bigg] \\
& - \bar{r}\bar{p}\left(\frac{\partial \psi_l^{[\mathrm{f}]}}{\partial Z}\right)_m^S\bar{\mathcal{J}}_B - \bar{r}P_m^S\frac{\partial \psi_l^{[\mathrm{f}]}}{\partial z}\bar{\mathcal{J}}_B - R_m^S\bar{p}\frac{\partial \psi_l^{[\mathrm{f}]}}{\partial z}\bar{\mathcal{J}}_B \\
& + 2R_\mu\Bigg[\bar{r}\left(\frac{\partial W}{\partial Z}\right)_m^S\frac{\partial \psi_l^{[\mathrm{f}]}}{\partial z}\bar{\mathcal{J}}_B + \bar{r}\overline{\frac{\partial u_z}{\partial z}}\left(\frac{\partial \psi_l^{[\mathrm{f}]}}{\partial Z}\right)_m^S\bar{\mathcal{J}}_B \\
& + R_m^S\overline{\frac{\partial u_z}{\partial z}}\frac{\partial \psi_l^{[\mathrm{f}]}}{\partial z}\bar{\mathcal{J}}_B - \bar{r}\overline{\frac{\partial u_z}{\partial z}}\frac{\partial \psi_l^{[\mathrm{f}]}}{\partial z}\hat{\mathcal{J}}_m^S\Bigg] \\
& + R_\mu\left[\frac{m^2}{\bar{r}}\left(W_m^S - \overline{\frac{\partial u_z}{\partial r}}R_m^S - \overline{\frac{\partial u_z}{\partial z}}Z_m^S\right)\bar{\mathcal{J}}_B + m\left(\frac{\partial V}{\partial Z}\right)_m^C\bar{\mathcal{J}}_B\right]\psi_l^{[\mathrm{f}]}\Bigg\}\,\mathrm{d}s_1\,\mathrm{d}s_2,
\end{aligned} \tag{7.82}$$

azimuthal momentum equation,

$$
\begin{aligned}
\hat{\mathcal{R}}^{[\mathrm{fS,bulk}]}_{\theta ml} = \gamma_m \, \pi \int_{-1}^{1} \int_{-1}^{1} \Bigg\{ & R_\rho \, \mathrm{Re} \, \Bigg[\mathrm{St} \, \bar{r} \frac{\delta V_m^S}{\delta t} \bar{\mathcal{J}}_B + \mathrm{St} \, R_m^S \frac{\delta \bar{u}_\theta}{\delta t} \bar{\mathcal{J}}_B + \mathrm{St} \, \bar{r} \frac{\delta \bar{u}_\theta}{\delta t} \hat{\mathcal{J}}_m^S \\
& + \bar{r} \left(\bar{u}_r - \mathrm{St} \, \bar{u}_r^{[\mathrm{M}]} \right) \left(\frac{\partial V}{\partial R} \right)_m^S \bar{\mathcal{J}}_B + \bar{r} \left(U_m^S - \mathrm{St} \, \frac{\delta R_m^S}{\delta t} \right) \overline{\frac{\partial u_\theta}{\partial r}} \bar{\mathcal{J}}_B \\
& + R_m^S \left(\bar{u}_r - \mathrm{St} \, \bar{u}_r^{[\mathrm{M}]} \right) \overline{\frac{\partial u_\theta}{\partial r}} \bar{\mathcal{J}}_B + \bar{r} \left(\bar{u}_z - \mathrm{St} \, \bar{u}_z^{[\mathrm{M}]} \right) \left(\frac{\partial V}{\partial Z} \right)_m^S \bar{\mathcal{J}}_B \\
& + \bar{r} \left(W_m^S - \mathrm{St} \, \frac{\delta Z_m^S}{\delta t} \right) \overline{\frac{\partial u_\theta}{\partial z}} \bar{\mathcal{J}}_B + R_m^S \left(\bar{u}_z - \mathrm{St} \, \bar{u}_z^{[\mathrm{M}]} \right) \overline{\frac{\partial u_\theta}{\partial z}} \bar{\mathcal{J}}_B \\
& + m \bar{u}_\theta \left(-V_m^C + \overline{\frac{\partial u_\theta}{\partial r}} R_m^C + \overline{\frac{\partial u_\theta}{\partial z}} Z_m^C \right) \bar{\mathcal{J}}_B \\
& + \bar{u}_\theta U_m^S \bar{\mathcal{J}}_B + V_m^S \bar{u}_r \bar{\mathcal{J}}_B + \bar{u}_\theta \bar{u}_r \hat{\mathcal{J}}_m^S \Bigg] \psi_l^{[\mathrm{f}]} \\
& - \left(R_m^S \bar{\mathcal{J}}_B + \bar{r} \hat{\mathcal{J}}_m^S \right) B_\theta \, \psi_l^{[\mathrm{f}]} - R_\rho \, \frac{\mathrm{Re}}{\mathrm{Fr}} \left(R_m^S \bar{\mathcal{J}}_B + \bar{r} \hat{\mathcal{J}}_m^S \right) G_\theta \, \psi_l^{[\mathrm{f}]} \\
& + R_\mu \Bigg[\bar{r} \left(\frac{\partial V}{\partial R} \right)_m^S \frac{\partial \psi_l^{[\mathrm{f}]}}{\partial r} \bar{\mathcal{J}}_B + \bar{r} \overline{\frac{\partial u_\theta}{\partial r}} \left(\frac{\partial \psi_l^{[\mathrm{f}]}}{\partial R} \right)_m^S \bar{\mathcal{J}}_B + R_m^S \overline{\frac{\partial u_\theta}{\partial r}} \frac{\partial \psi_l^{[\mathrm{f}]}}{\partial r} \bar{\mathcal{J}}_B \\
& - \bar{r} \overline{\frac{\partial u_\theta}{\partial r}} \frac{\partial \psi_l^{[\mathrm{f}]}}{\partial r} \hat{\mathcal{J}}_m^S - V_m^S \frac{\partial \psi_l^{[\mathrm{f}]}}{\partial r} \bar{\mathcal{J}}_B - \bar{u}_\theta \left(\frac{\partial \psi_l^{[\mathrm{f}]}}{\partial R} \right)_m^S \bar{\mathcal{J}}_B \\
& + m \left(-U_m^C + \overline{\frac{\partial u_r}{\partial r}} R_m^C + \overline{\frac{\partial u_r}{\partial z}} Z_m^C \right) \frac{\partial \psi_l^{[\mathrm{f}]}}{\partial r} \bar{\mathcal{J}}_B \\
& + \bar{r} \left(\frac{\partial V}{\partial Z} \right)_m^S \frac{\partial \psi_l^{[\mathrm{f}]}}{\partial z} \bar{\mathcal{J}}_B + \bar{r} \overline{\frac{\partial u_\theta}{\partial z}} \left(\frac{\partial \psi_l^{[\mathrm{f}]}}{\partial Z} \right)_m^S \bar{\mathcal{J}}_B + R_m^S \overline{\frac{\partial u_\theta}{\partial z}} \frac{\partial \psi_l^{[\mathrm{f}]}}{\partial z} \bar{\mathcal{J}}_B \\
& - \bar{r} \overline{\frac{\partial u_\theta}{\partial z}} \frac{\partial \psi_l^{[\mathrm{f}]}}{\partial z} \hat{\mathcal{J}}_m^S + m \left(-W_m^C + \overline{\frac{\partial u_z}{\partial r}} R_m^C + \overline{\frac{\partial u_z}{\partial z}} Z_m^C \right) \frac{\partial \psi_l^{[\mathrm{f}]}}{\partial z} \bar{\mathcal{J}}_B \\
& + \frac{2m}{\bar{r}} \bar{u}_r \left(\frac{\partial \psi_l^{[\mathrm{f}]}}{\partial r} R_m^C + \frac{\partial \psi_l^{[\mathrm{f}]}}{\partial z} Z_m^C \right) \bar{\mathcal{J}}_B \Bigg] \\
& - m \left[\bar{p} R_m^C \frac{\partial \psi_l^{[\mathrm{f}]}}{\partial r} \bar{\mathcal{J}}_B + \bar{p} Z_m^C \frac{\partial \psi_l^{[\mathrm{f}]}}{\partial z} \bar{\mathcal{J}}_B + P_m^C \psi_l^{[\mathrm{f}]} \bar{\mathcal{J}}_B + \bar{p} \psi_l^{[\mathrm{f}]} \hat{\mathcal{J}}_m^C \right] \\
& + R_\mu \Bigg[\frac{2m^2}{\bar{r}} \left(V_m^S - \overline{\frac{\partial u_\theta}{\partial r}} R_m^S - \overline{\frac{\partial u_\theta}{\partial z}} Z_m^S \right) \bar{\mathcal{J}}_B \\
& + \frac{2m}{\bar{r}} U_m^C \bar{\mathcal{J}}_B - \frac{2m}{\bar{r}^2} R_m^C \bar{u}_r \bar{\mathcal{J}}_B + \frac{2m}{\bar{r}} \bar{u}_r \hat{\mathcal{J}}_m^C \\
& - \left(\frac{\partial V}{\partial R} \right)_m^S \bar{\mathcal{J}}_B + \frac{m}{\bar{r}} \left(U_m^C - \overline{\frac{\partial u_r}{\partial r}} R_m^C - \overline{\frac{\partial u_r}{\partial z}} Z_m^C \right) \bar{\mathcal{J}}_B \\
& + \frac{1}{\bar{r}} V_m^S \bar{\mathcal{J}}_B - \frac{\bar{u}_\theta}{\bar{r}^2} R_m^S \bar{\mathcal{J}}_B + \frac{1}{\bar{r}} \bar{u}_\theta \hat{\mathcal{J}}_m^S \Bigg] \psi_l^{[\mathrm{f}]} \Bigg\} \, \mathrm{d}s_1 \, \mathrm{d}s_2
\end{aligned}
\tag{7.83}
$$

and continuity equation

$$\hat{\mathcal{R}}^{[\mathrm{pS}]}_{ml} = \gamma_m \, \pi \int_{-1}^{1} \int_{-1}^{1} \Bigg\{ \bar{r} \left(\frac{\partial U}{\partial R} \right)^S_m \bar{\mathcal{J}}_B + R^S_m \overline{\frac{\partial u_r}{\partial r}} \bar{\mathcal{J}}_B + U^S_m \bar{\mathcal{J}}_B + \bar{u}_r \hat{\mathcal{J}}^S_m + \bar{r} \left(\frac{\partial W}{\partial Z} \right)^S_m \bar{\mathcal{J}}_B + R^S_m \overline{\frac{\partial u_z}{\partial z}} \bar{\mathcal{J}}_B - m \left(V^C_m - \overline{\frac{\partial u_\theta}{\partial r}} R^C_m - \overline{\frac{\partial u_\theta}{\partial z}} Z^C_m \right) \bar{\mathcal{J}}_B - \left(R^S_m \bar{\mathcal{J}}_B + \bar{r} \hat{\mathcal{J}}^S_m \right) Q \Bigg\} \psi^{[\mathrm{p}]}_l \, \mathrm{d}s_1 \, \mathrm{d}s_2. \quad (7.84)$$

We can solve the governing equations described in (7.36) by considering two separate problems. The first of these will be called the 'base problem' and corresponds to the terms of order one in (7.36). Its governing equations are the (non-linear) axisymmetric Navier–Stokes equations (7.52)–(7.55) described in section 7.2. We will refer to the second problem, which corresponds to the terms of order ϵ in (7.36), as the 'perturbation problem', since it describes a linear, non-axisymmetric perturbation to the base state. There is a one-way coupling between these problems in the sense that the solution of the perturbation problem depends on the base flow solution.

The governing equations for the perturbation problem are (7.77)–(7.84), and we note that the θ-dependence has been replaced by a parameter m which corresponds to the wavenumber of the particular Fourier mode in which we are interested. Since the equations are linear, the Fourier modes fully decouple: this then allows us to solve each mode separately. By performing this decomposition, therefore, we have transformed the three-dimensional perturbation problem into an infinite sum of two-dimensional problems. In practice we always truncate the sum over Fourier modes to some finite number.

7.4 Implementation

We implemented equations (7.77)–(7.84) in the `get_residual(...)` and `get_jacobian(...)` functions of a newly-developed `LinearisedAxisymmetricNavierStokesEquations` class. Wherever possible, we mirrored the inheritance structure of the 'standard' Navier–Stokes equations, and as such this class implements the governing equations but contains no specific geometrical information. Concrete implementations were developed

via the `LinearisedAxisymmetricQTaylorHoodElement` and `LinearisedAxisymmetric-QCrouzeixRaviartElement` classes, which inherit from the `LinearisedAxisymmetric-NavierStokesEquations` and `QElement<2,3>` classes.

Recall that the solution of the perturbation equations is dependent on the base flow. In a finite element context this means that in order to evaluate the `get_residual(...)` and `get_jacobian(...)` functions in the `LinearisedAxisymmetricNavierStokes-Equations` class we require the values of certain fields, which have been computed as part of the base state solution, evaluated at the Eulerian position corresponding to a given integration point in the perturbation problem. This one-way coupling is achieved in `oomph-lib` by ensuring that the elements that we use to compute the perturbation equations inherit from the `ElementWithExternalElement` class: this endows the elements with the functionality to determine, for each of the integration points,

(i) which element in the base state problem occupies the spatial coordinates of that integration point, and

(ii) the local coordinates in that element which correspond to that integration point.

Once this look-up scheme has been established using `oomph-lib`'s multi-domain 'machinery' it is straightforward to determine the base state problem's finite element solution for the required quantity, evaluated at the appropriate point in the domain. One benefit of this 'multi-domain' approach is that it is not necessary for the base flow and perturbation problems to utilise the same spatial discretisation. In general one would not expect the flow fields in the two problems to have the same spatial structure, and so it is advantageous to be able to employ different refinement patterns in each problem.

With this in mind, we developed the `LinearisedAxisymmetricQTaylorHoodMulti-DomainElement` and `LinearisedAxisymmetricQCrouzeixRaviartMultiDomainElement` classes: these classes are derived from the `LinearisedAxisymmetricQTaylorHood-Element` and `LinearisedAxisymmetricQCrouzeixRaviartElement` classes respectively, but also inherit from `ElementWithExternalElement` and hence gain the additional functionality described above. These classes define the interactions between the perturbation elements themselves and the 'external' base flow elements by overloading the

virtual functions defined in `LinearisedAxisymmetricNavierStokesEquations` which are required to return the value of particular base flow quantities. A (slightly simplified) inheritance diagram for the `LinearisedAxisymmetricQCrouzeixRaviartMultiDomainElement` class is shown in figure 7.1, where we only go as far 'up' the hierarchy as the `FiniteElement` base class.

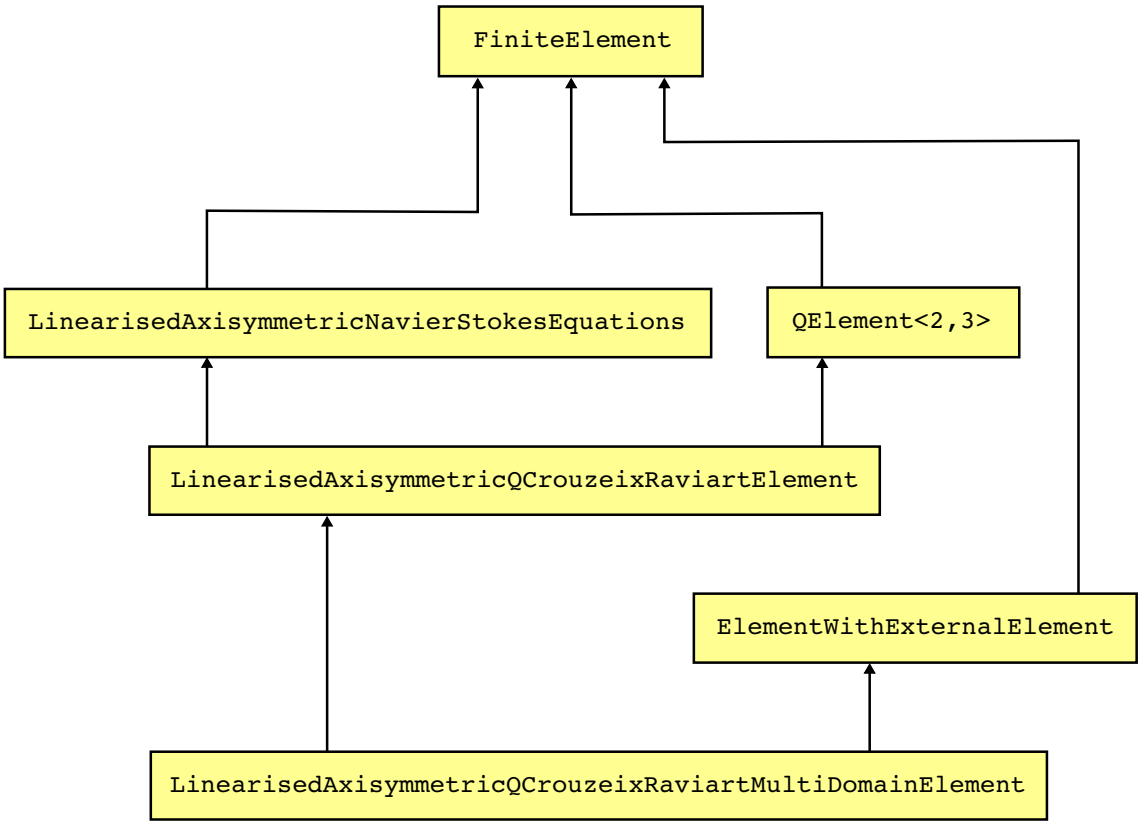

Figure 7.1: Inheritance diagram for the `LinearisedAxisymmetricQCrouzeixRaviartMultiDomainElement` class, where we only go as far 'up' as the `FiniteElement` base class. This schematic is slightly simplified, as in reality there are actually a number of levels of abstraction between `QElement<DIM,NNODE_1D>` and `FiniteElement`.

Chapter 8

Applications to single-phase flows

In the previous chapter we linearised the three-dimensional Navier–Stokes equations in a cylindrical polar coordinate system about an axisymmetric base flow. We shall now illustrate the use of these 'perturbation equations' by applying them to two single-fluid problems. The first of these considers the stability of the flow of a viscous fluid between two exactly counter-rotating disks. In this case the base flow is steady but non-trivial, and we assess the stability of this solution to linear, non-axisymmetric perturbations by time-evolving the perturbation equations. We use the power method to determine the growth rates of modes with different azimuthal mode numbers, and compare our results with those of the study conducted by Nore et al. in their paper *Survey of instability thresholds of flow between exactly counter-rotating disks* [Nore et al., 2004]. The second application considers the stability of the flow in an annular region between two concentric cylinders of infinite extent. The inner cylinder rotates at constant angular velocity while the outer cylinder is driven sinusoidally in time, giving rise to an unsteady, axisymmetric base flow. The stability of this flow to axisymmetric disturbances is then investigated via the time-evolution of the perturbation equations, where we set the mode number to zero. Stability thresholds are determined for a range of forcing amplitudes, and we compare these results with those of the study conducted by Murray et al. in their paper *Stabilization of Taylor–Couette flow due to time-periodic outer cylinder oscillation* [Murray et al., 1990].

We note that both of these problems are computed on a fixed mesh, and hence there are no perturbations to the nodal positions. In terms of the variables used in the governing equations for the linear perturbation problem (7.77)–(7.84) we therefore

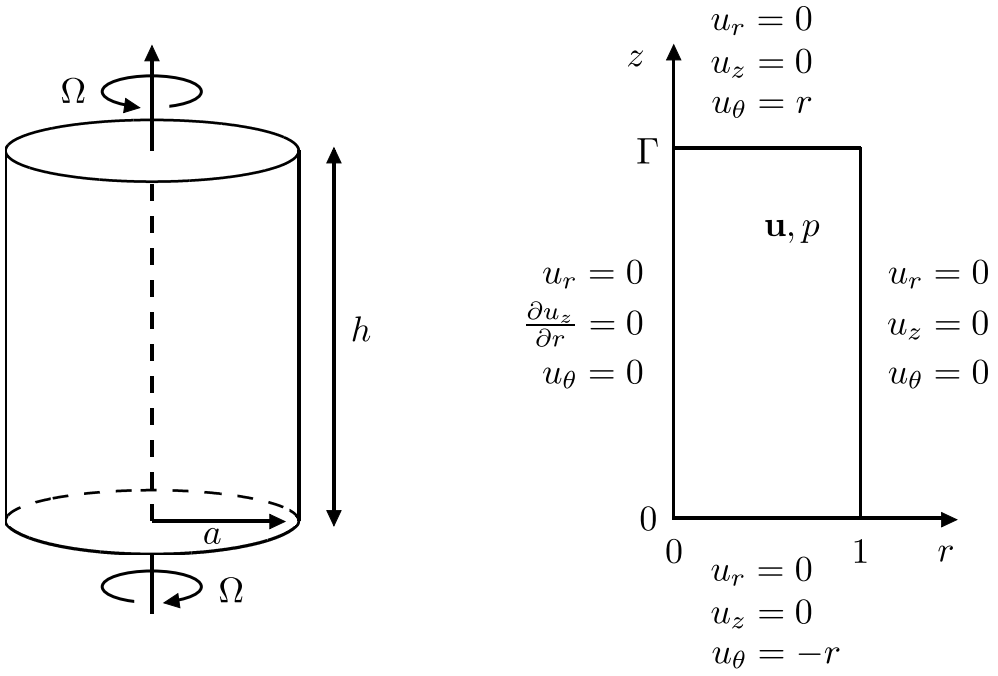

(a) Physical domain

(b) Computational domain

Figure 8.1: Sketch of the counter-rotating disks problem. The computational domain represents a radial 'slice' of the physical domain, where $r = 0$ corresponds to the centreline of the cylindrical cavity and $r = 1$ corresponds to the outer (solid) boundary.

have

$$R_m^C = R_m^S = 0 \qquad \text{and} \qquad Z_m^C = Z_m^S = 0 \tag{8.1}$$

for all values of the azimuthal mode number m, and it follows from (7.68) and (7.69) that

$$\hat{\mathcal{J}}_m^C = 0 \qquad \text{and} \qquad \hat{\mathcal{J}}_m^S = 0 \tag{8.2}$$

as well. Hence these test problems are not able to validate the terms associated with a moving mesh, and we will address this issue in chapter 10.

8.1 Stability of the flow between counter-rotating disks

8.1.1 The base flow

Let us consider the problem sketched in figure 8.1(a), in which we have a cylindrical cavity of radius a and height h filled with an incompressible fluid. The upper and

lower 'lids' are disks which rotate at constant angular velocity Ω and $-\Omega$ respectively, and (in the absence of gravitational forces) this gives rise to a steady, axisymmetric base flow governed by

$$\begin{aligned}
\mathrm{Re}\left[u_r\frac{\partial u_r}{\partial r}-\frac{u_\theta^2}{r}+u_z\frac{\partial u_r}{\partial z}\right] &= -\frac{\partial p}{\partial r}+\frac{\partial^2 u_r}{\partial r^2}+\frac{1}{r}\frac{\partial u_r}{\partial r}-\frac{u_r}{r^2}+\frac{\partial^2 u_r}{\partial z^2},\\
\mathrm{Re}\left[u_r\frac{\partial u_z}{\partial r}+u_z\frac{\partial u_z}{\partial z}\right] &= -\frac{\partial p}{\partial z}+\frac{\partial^2 u_z}{\partial r^2}+\frac{1}{r}\frac{\partial u_z}{\partial r}+\frac{\partial^2 u_z}{\partial z^2},\\
\mathrm{Re}\left[u_r\frac{\partial u_\theta}{\partial r}+\frac{u_r u_\theta}{r}+u_z\frac{\partial u_\theta}{\partial z}\right] &= \frac{\partial^2 u_\theta}{\partial r^2}+\frac{1}{r}\frac{\partial u_\theta}{\partial r}-\frac{u_\theta}{r^2}+\frac{\partial^2 u_\theta}{\partial z^2}
\end{aligned} \tag{8.3}$$

and

$$\frac{\partial u_r}{\partial r}+\frac{u_r}{r}+\frac{\partial u_z}{\partial z}=0. \tag{8.4}$$

We choose the length, velocity and time scales to be the cylinder radius, tangential velocity and rotation period respectively so that

$$\mathcal{L}=a, \qquad \mathcal{U}=a\,\Omega \qquad \text{and} \qquad \mathcal{T}=\frac{1}{2\pi\Omega}, \tag{8.5}$$

and the Reynolds number is therefore defined to be

$$\mathrm{Re}=\frac{a^2\,\Omega\,\rho}{\mu}, \tag{8.6}$$

where ρ is the fluid density and μ the dynamic viscosity. The domain in which these equations are to be solved is sketched in 8.1(b), where $\Gamma = h/a$ is the aspect ratio. We apply the symmetry condition $u_r = u_\theta = 0$ at the axis ($r = 0$) and the no-slip condition at the stationary side wall and the upper and lower rotating disks, so that

$$\begin{aligned}
u_r=u_z=u_\theta=0 \qquad &\text{at} \quad r=1,\\
u_r=u_z=0, \qquad u_\theta=-r \qquad &\text{at} \quad z=0 \qquad \text{and}\\
u_r=u_z=0, \qquad u_\theta=r \qquad &\text{at} \quad z=\Gamma.
\end{aligned} \tag{8.7}$$

This base flow was computed numerically in `oomph-lib` with a mesh that was initially set up to contain 30×30 elements. A refineable implementation of the axisymmetric Navier–Stokes equations was used so that the mesh could adapt itself automatically based on a posteriori error estimates provided by `oomph-lib`'s implementation of the 'Z2' error estimator, [Zienkiewicz and Zhu, 1992a] and [Zienkiewicz and Zhu, 1992b]. The flow was computed using both Taylor–Hood and Crouzeix–Raviart elements for validation purposes. In this problem the fluid velocity is prescribed along

the entire domain boundary, and the fluid pressure is therefore only determined up to an arbitrary constant. This indeterminacy was overcome by prescribing the value of the pressure at a single point in the domain. We note from (8.7) that at the point at which the upper and lower boundaries meet the outer wall there is discontinuity in the azimuthal velocity, and this was compensated for by 'smoothing' the azimuthal boundary condition on the upper and lower lids so that

$$u_\theta = \begin{cases} -r & \text{at} \quad z = 0 \quad \text{for} \quad 0 < r \leq \beta \\ -\beta\frac{1-r}{1-\beta} & \text{at} \quad z = 0 \quad \text{for} \quad \beta < r < 1 \end{cases} \tag{8.8}$$

and

$$u_\theta = \begin{cases} r & \text{at} \quad z = \Gamma \quad \text{for} \quad 0 < r \leq \beta \\ \beta\frac{1-r}{1-\beta} & \text{at} \quad z = \Gamma \quad \text{for} \quad \beta < r < 1 \end{cases}, \tag{8.9}$$

where β is the fraction along the lid at which we wish the smoothing to start. A value of $\beta = 0.96$ was used for all of these computations.

The base flow solution was obtained by first performing a steady Newton solve for the zero Reynolds number case, and then using that solution as an initial guess for the Newton solver when computing the flow at the desired Reynolds number. For larger Reynolds numbers this initial guess turned out to be insufficient and the Newton method would fail to converge: in these cases some additional continuation steps were performed. We note that according to Nore et al. (figure 11(a), solid circle markers) the base flow has a unique solution for the entire range of Reynolds numbers considered in the current work. This result was confirmed by a later study conducted by Hewitt and Hazel [Hewitt and Hazel, 2007, Fig. 5].

A plot of the solution using refineable Taylor–Hood elements for $\mathrm{Re} = 500$ and $\Gamma = 1$ is shown in figure 8.2, where the colour contours on the left and right-hand sides of the plot illustrate the pressure and the azimuthal velocity respectively as functions of r and z. On the pressure plot, dark blue and bright red correspond to the minimum and maximum values of the pressure respectively. The legend to the right of the azimuthal velocity plot describes the contours in terms of the non-dimensional velocity. Streamlines on both plots track the motion of the in-plane recirculation of the fluid. Examination of figure 8.2 reveals that the mesh refines most in areas where there are steep velocity gradients: these areas correspond to the narrow 'gap' between the rotating lids and the stationary outer wall. We note that the form of the recirculation

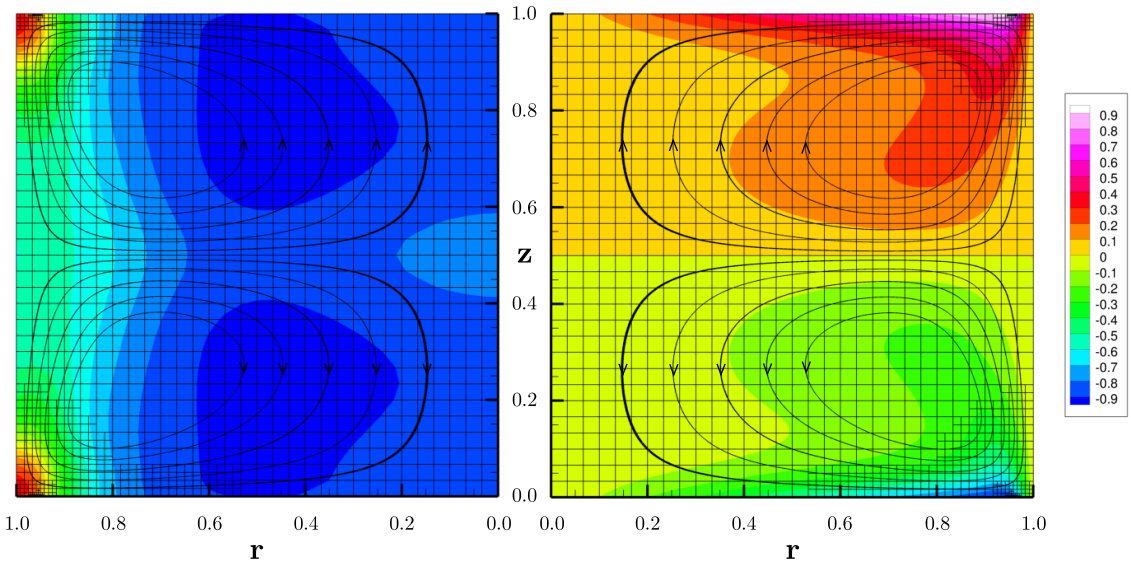

Figure 8.2: Base flow computed using Taylor–Hood elements for Re $= 500$ and $\Gamma = 1$. In both plots the symmetry axis is located at the 'centre' of the page, so that the radial coordinate always extends 'outwards'. The left-hand plot displays colour contours of pressure which vary linearly between the maximum value of 27.4, shown in red, and the minimum value of -3.1, shown in blue. The right-hand plot displays colour contours of the azimuthal velocity, as described by the legend to the right of the figure. On both plots superimposed streamlines track the in-plane velocity.

zones and the azimuthal velocity contours match those described by Nore et al. in figures 1(c) and 4(a) respectively [Nore et al., 2004].

8.1.2 Determining stability thresholds

We now wish to assess the stability of the base flow computed in section 8.1.1 to small, non-axisymmetric perturbations. If the base solution is $(\bar{\mathbf{u}}, \bar{p})$ then we can write the sum of this flow and a small, non-axisymmetric, time-dependent perturbation as

$$\begin{aligned} \mathbf{u} &= \bar{\mathbf{u}}(r,z) + \epsilon\,\hat{\mathbf{u}}(r,z,\theta,t), \\ p &= \bar{p}(r,z) + \epsilon\,\hat{p}(r,z,\theta,t), \end{aligned} \tag{8.10}$$

where $\epsilon \ll 1$. If we substitute this ansatz into the governing equations (5.3) and (5.4), and consider only the terms of order ϵ, then we obtain a linear system of the form

$$\frac{\partial \hat{\mathbf{u}}}{\partial t} + \mathcal{L}_1(\bar{\mathbf{u}}, \bar{p})\,\hat{\mathbf{u}} + \mathcal{L}_2(\bar{\mathbf{u}}, \bar{p})\,\hat{p} = 0, \tag{8.11}$$

where $\mathcal{L}_1$ and $\mathcal{L}_2$ are linear operators which depend on the base flow.

Let us now consider the formulation discussed in chapter 7, where the weak form of the three-dimensional Navier–Stokes equations in cylindrical polar coordinates were linearised by application of the ansatz specified in (7.11) and (7.12). After performing Fourier series expansions of all fields in the azimuthal direction, the resultant weak form of this 'perturbation problem' was stated in (7.77)–(7.84). Each of the eight fields in this problem is discretised in the usual finite element way,

$$U_m^C(s_1,s_2) = \sum_{j=1}^{n_u} (\hat{U}_m^C)_j \, \psi_j^{[\mathrm{f}]}(s_1,s_2), \qquad U_m^S(s_1,s_2) = \sum_{j=1}^{n_u} (\hat{U}_m^S)_j \, \psi_j^{[\mathrm{f}]}(s_1,s_2),$$

$$W_m^C(s_1,s_2) = \sum_{j=1}^{n_u} (\hat{W}_m^C)_j \, \psi_j^{[\mathrm{f}]}(s_1,s_2), \qquad W_m^S(s_1,s_2) = \sum_{j=1}^{n_u} (\hat{W}_m^S)_j \, \psi_j^{[\mathrm{f}]}(s_1,s_2),$$

$$V_m^C(s_1,s_2) = \sum_{j=1}^{n_u} (\hat{V}_m^C)_j \, \psi_j^{[\mathrm{f}]}(s_1,s_2), \qquad V_m^S(s_1,s_2) = \sum_{j=1}^{n_u} (\hat{V}_m^S)_j \, \psi_j^{[\mathrm{f}]}(s_1,s_2),$$

$$P_m^C(s_1,s_2) = \sum_{j=1}^{n_p} (\hat{P}_m^C)_j \, \psi_j^{[\mathrm{p}]}(s_1,s_2), \qquad P_m^S(s_1,s_2) = \sum_{j=1}^{n_p} (\hat{P}_m^S)_j \, \psi_j^{[\mathrm{p}]}(s_1,s_2),$$

where n_u and n_p are the number of velocity and pressure degrees of freedom in each element, respectively, and $(\hat{U}_m^C)_j$, $(\hat{U}_m^S)_j$, …, $(\hat{P}_m^S)_j$ are the values of the respective fields at the j-th local node. Let us now consider the vector $\hat{\mathbf{U}}_m^C$ of all nodal values of U_m^C in the *entire problem*. The length of $\hat{\mathbf{U}}_m^C$ will be equal to the number of nodes in the global mesh at which the value of U_m^C is an unknown. We can now construct the vector

$$\mathbf{Z} = \left[\hat{\mathbf{U}}_m^C \;\; \hat{\mathbf{U}}_m^S \;\; \hat{\mathbf{W}}_m^C \;\; \hat{\mathbf{W}}_m^S \;\; \hat{\mathbf{V}}_m^C \;\; \hat{\mathbf{V}}_m^S \;\; \hat{\mathbf{P}}_m^C \;\; \hat{\mathbf{P}}_m^S \right]^T, \tag{8.12}$$

where the vectors $\hat{\mathbf{U}}_m^S, \hat{\mathbf{W}}_m^C, \ldots, \hat{\mathbf{P}}_m^S$ are defined in an equivalent manner to $\hat{\mathbf{U}}_m^C$. $\mathbf{Z}$ is a vector containing all of the unknown variables in the discretised problem, and we can use it to write the system of linear equations in 'matrix-vector' form,

$$\mathcal{M} \frac{\partial \mathbf{Z}}{\partial t} + \mathcal{A}(\bar{\mathbf{u}}, \bar{p}) \, \mathbf{Z} = 0, \tag{8.13}$$

where $\mathcal{A}$ and $\mathcal{M}$ are square matrices of size N, the number of degrees of freedom in the problem. We now employ a backward Euler timestepping scheme with timestep Δt to obtain

$$\mathcal{M} \left(\frac{\mathbf{Z}_{n+1} - \mathbf{Z}_n}{\Delta t} \right) + \mathcal{A}(\bar{\mathbf{u}}, \bar{p}) \, \mathbf{Z}_{n+1} = 0, \tag{8.14}$$

where $\mathbf{Z}_n$ is the solution at the n-th timestep. Rearranging (8.14) gives

$$\mathbf{Z}_{n+1} = \mathcal{B} \, \mathbf{Z}_n, \tag{8.15}$$

where

$$\mathcal{B} = (\mathcal{M} + \Delta t\, \mathcal{A})^{-1}\, \mathcal{M}. \tag{8.16}$$

The eigenvectors of $\mathcal{B}$ form a complete basis for the N–dimensional vector space, and hence we can express the initial state of the system $\mathbf{Z}_0$ as a linear combination of these eigenvectors $\mathbf{x}_i$,

$$\mathbf{Z}_0 = \sum_{i=1}^{N} \alpha_i\, \mathbf{x}_i, \tag{8.17}$$

where α_i are constant coefficients. Since $\mathcal{B}\,\mathbf{x}_i = \lambda_i\,\mathbf{x}_i$, where λ_i is the eigenvalue corresponding to $\mathbf{x}_i$, it follows that

$$\mathcal{B}\,\mathbf{Z}_0 = \sum_{i=1}^{N} \lambda_i\, \alpha_i\, \mathbf{x}_i, \tag{8.18}$$

and then from (8.15) the solution at the n-th timestep is given by

$$\mathbf{Z}_n \;=\; \mathcal{B}^n\, \mathbf{Z}_0 \;=\; \sum_{i=1}^{N} \lambda_i^n\, \alpha_i\, \mathbf{x}_i. \tag{8.19}$$

Assuming that our initial state $\mathbf{Z}_0$ is a linear combination of *all* eigenvectors of $\mathcal{B}$ (i.e. $\alpha_i > 0 \quad \forall\, i$), then it is clear from (8.19) that if the magnitudes of all the corresponding eigenvalues λ_i are less than one then the perturbation will eventually decay to zero and the base flow is stable. If, however, one or more of the eigenvalues are equal to or greater than one then the corresponding eigenvector(s) will grow in magnitude and the base flow is unstable. This means that in order to determine the stability of the base flow at a given Reynolds number we require the value of the dominating eigenvalue of $\mathcal{B}$: that is, the eigenvalue of greatest magnitude. A simple way to compute this is by use of the 'power method'.

The power method

The power method is an algorithm designed to compute the dominant eigenvalue (and corresponding eigenvector) of an arbitrary square matrix M of size $N \times N$. We based our implementation of this algorithm in `oomph-lib` on that outlined in [Bai et al., 2000, Algorithm 4.1]. We start with the initial guess $\mathbf{y} = \mathbf{Z}_0$, and then loop over the following set of instructions:

1. Define $\mathbf{v} = \mathbf{y}/\|\mathbf{y}\|_2$, where $\|\mathbf{y}\|_2$ is the L^2-norm of $\mathbf{y}$.

2. Perform the matrix-vector product $\mathbf{y} = M\,\mathbf{v}$.

3. Compute the scalar product $\theta = \mathbf{v} \cdot \mathbf{y}$.

4. Compute $c = \|\mathbf{y} - \theta\mathbf{v}\|_2/\sqrt{N}$, and then test this quantity against the product of the absolute value of θ and a pre-defined tolerance ϵ.

We perform the loop outlined above until the convergence criterion $c < \epsilon\,|\theta|$ is met, and at this point we stop and accept the dominating eigenvalue to be θ and its corresponding eigenvector to be $\mathbf{v}$. Note the addition of the factor of $1/\sqrt{N}$ in step (4): this is so that c is independent of the number of degrees of freedom in the discretised problem. If the largest and second-largest eigenvalues of M in magnitude are denoted by λ_1 and λ_2 respectively, then the convergence rate of this method is governed by $|\lambda_2/\lambda_1|$. By constructing matrices for which the eigenvalues were known we were able to test our implementation of this algorithm to ensure that the correct rate of convergence was obtained.

8.1.3 Perturbation to the base flow

Having established that the stability of the base flow is determined by the dominating eigenvalue of $\mathcal{B}$, we now require a scheme to determine $\mathcal{B}$ itself. From (8.15) we see that $\mathcal{B}$ is the linear operator that acts upon the unknowns in the discretised linear perturbation problem in order to advance to the solution at the next timestep. Therefore for each iteration of the power method we shall perform one timestep of the governing equations, which are the linearised perturbation equations (7.77)–(7.84) as formulated in section 7.3. As discussed at the beginning of this chapter, however, a significant number of terms are equal to zero. In the interests of clarity we shall state these equations again here, with only the non-zero terms. The momentum equations

which arise through taking the 'cosine' test functions (7.59) are

$$\hat{\mathcal{R}}^{[\mathrm{fC}]}_{\mathrm{r}ml} = \gamma_m \pi \int_{-1}^{1}\int_{-1}^{1} \Bigg\{ \mathrm{Re}\ \Bigg[\mathrm{St}\,\bar{r}\frac{\delta U_m^C}{\delta t} + \bar{r}\bar{u}_r\left(\frac{\partial U}{\partial R}\right)_m^C + \bar{r}U_m^C\overline{\frac{\partial u_r}{\partial r}} + \bar{r}\bar{u}_z\left(\frac{\partial U}{\partial Z}\right)_m^C + \bar{r}W_m^C\overline{\frac{\partial u_r}{\partial z}} + m\bar{u}_\theta U_m^S - 2\bar{u}_\theta V_m^C \Bigg] \psi_l^{[\mathrm{f}]} - \left(\bar{r}\frac{\partial \psi_l^{[\mathrm{f}]}}{\partial r} + \psi_l^{[\mathrm{f}]}\right) P_m^C + 2\bar{r}\left(\frac{\partial U}{\partial R}\right)_m^C \frac{\partial \psi_l^{[\mathrm{f}]}}{\partial r} + \bar{r}\left[\left(\frac{\partial W}{\partial R}\right)_m^C + \left(\frac{\partial U}{\partial Z}\right)_m^C\right]\frac{\partial \psi_l^{[\mathrm{f}]}}{\partial z} - m\left(\frac{\partial V}{\partial R}\right)_m^S \psi_l^{[\mathrm{f}]} + \frac{1}{\bar{r}}\Bigg[\left(m^2+2\right)U_m^C + 3mV_m^S\Bigg]\psi_l^{[\mathrm{f}]}\Bigg\}\,\bar{\mathcal{J}}_B\ \mathrm{d}s_1\,\mathrm{d}s_2, \tag{8.20}$$

$$\hat{\mathcal{R}}^{[\mathrm{fC}]}_{\mathrm{z}ml} = \gamma_m \pi \int_{-1}^{1}\int_{-1}^{1} \Bigg\{ \mathrm{Re}\ \Bigg[\mathrm{St}\,\bar{r}\frac{\delta W_m^C}{\delta t} + \bar{r}\bar{u}_r\left(\frac{\partial W}{\partial R}\right)_m^C + \bar{r}U_m^C\overline{\frac{\partial u_z}{\partial r}} + \bar{r}\bar{u}_z\left(\frac{\partial W}{\partial Z}\right)_m^C + \bar{r}W_m^C\overline{\frac{\partial u_z}{\partial z}} + m\bar{u}_\theta W_m^S \Bigg] \psi_l^{[\mathrm{f}]} + \bar{r}\left[\left(\frac{\partial W}{\partial R}\right)_m^C + \left(\frac{\partial U}{\partial Z}\right)_m^C\right]\frac{\partial \psi_l^{[\mathrm{f}]}}{\partial r} + \bar{r}\left[2\left(\frac{\partial W}{\partial Z}\right)_m^C - P_m^C\right]\frac{\partial \psi_l^{[\mathrm{f}]}}{\partial z} + \left[\frac{m^2}{\bar{r}}W_m^C - m\left(\frac{\partial V}{\partial Z}\right)_m^S\right]\psi_l^{[\mathrm{f}]}\Bigg\}\,\bar{\mathcal{J}}_B\ \mathrm{d}s_1\,\mathrm{d}s_2 \tag{8.21}$$

and

$$\hat{\mathcal{R}}^{[\mathrm{fC}]}_{\theta ml} = \gamma_m \pi \int_{-1}^{1}\int_{-1}^{1} \Bigg\{ \mathrm{Re}\ \Bigg[\mathrm{St}\,\bar{r}\frac{\delta V_m^C}{\delta t} + \bar{r}\bar{u}_r\left(\frac{\partial V}{\partial R}\right)_m^C + \bar{r}U_m^C\overline{\frac{\partial u_\theta}{\partial r}} + \bar{r}\bar{u}_z\left(\frac{\partial V}{\partial Z}\right)_m^C + \bar{r}W_m^C\overline{\frac{\partial u_\theta}{\partial z}} + m\bar{u}_\theta V_m^S + \bar{u}_\theta U_m^C + V_m^C\bar{u}_r \Bigg] \psi_l^{[\mathrm{f}]} + \left[\bar{r}\left(\frac{\partial V}{\partial R}\right)_m^C - V_m^C + mU_m^S\right]\frac{\partial \psi_l^{[\mathrm{f}]}}{\partial r} + \left[\bar{r}\left(\frac{\partial V}{\partial Z}\right)_m^C + mW_m^S\right]\frac{\partial \psi_l^{[\mathrm{f}]}}{\partial z} + mP_m^S\psi_l^{[\mathrm{f}]} + \left[\frac{2m^2+1}{\bar{r}}V_m^C - \frac{3m}{\bar{r}}U_m^S - \left(\frac{\partial V}{\partial R}\right)_m^C\right]\psi_l^{[\mathrm{f}]}\Bigg\}\,\bar{\mathcal{J}}_B\ \mathrm{d}s_1\,\mathrm{d}s_2, \tag{8.22}$$

and the continuity equation is

$$\hat{\mathcal{R}}^{[\mathrm{pC}]}_{ml} = \gamma_m \pi \int_{-1}^{1}\int_{-1}^{1} \left[\bar{r}\left(\frac{\partial U}{\partial R}\right)_m^C + U_m^C + \bar{r}\left(\frac{\partial W}{\partial Z}\right)_m^C + mV_m^S\right]\psi_l^{[\mathrm{p}]}\,\bar{\mathcal{J}}_B\ \mathrm{d}s_1\,\mathrm{d}s_2. \tag{8.23}$$

The 'sine counterparts' that arise through taking the 'sine' test functions (7.60) are

$$\hat{\mathcal{R}}^{[\mathrm{fS}]}_{\mathrm{r}ml} = \gamma_m\,\pi\int_{-1}^{1}\int_{-1}^{1}\Bigg\{\mathrm{Re}\,\Bigg[\mathrm{St}\,\bar{r}\frac{\delta U_m^S}{\delta t} + \bar{r}\bar{u}_r\left(\frac{\partial U}{\partial R}\right)_m^S + \bar{r}U_m^S\overline{\frac{\partial u_r}{\partial r}} + \bar{r}\bar{u}_z\left(\frac{\partial U}{\partial Z}\right)_m^S + \bar{r}W_m^S\overline{\frac{\partial u_r}{\partial z}} - m\bar{u}_\theta U_m^C - 2\bar{u}_\theta V_m^S\Bigg]\psi_l^{[\mathrm{f}]} - \left(\bar{r}\frac{\partial\psi_l^{[\mathrm{f}]}}{\partial r} + \psi_l^{[\mathrm{f}]}\right)P_m^S + 2\bar{r}\left(\frac{\partial U}{\partial R}\right)_m^S\frac{\partial\psi_l^{[\mathrm{f}]}}{\partial r} + \bar{r}\left[\left(\frac{\partial W}{\partial R}\right)_m^S + \left(\frac{\partial U}{\partial Z}\right)_m^S\right]\frac{\partial\psi_l^{[\mathrm{f}]}}{\partial z} + m\left(\frac{\partial V}{\partial R}\right)_m^C\psi_l^{[\mathrm{f}]} + \frac{1}{\bar{r}}\Bigg[\left(m^2+2\right)U_m^S - 3mV_m^C\Bigg]\psi_l^{[\mathrm{f}]}\Bigg\}\,\bar{\mathcal{J}}_B\;\mathrm{d}s_1\,\mathrm{d}s_2, \tag{8.24}$$

$$\hat{\mathcal{R}}^{[\mathrm{fS}]}_{\mathrm{z}ml} = \gamma_m\,\pi\int_{-1}^{1}\int_{-1}^{1}\Bigg\{\mathrm{Re}\,\Bigg[\mathrm{St}\,\bar{r}\frac{\delta W_m^S}{\delta t} + \bar{r}\bar{u}_r\left(\frac{\partial W}{\partial R}\right)_m^S + \bar{r}U_m^S\overline{\frac{\partial u_z}{\partial r}} + \bar{r}\bar{u}_z\left(\frac{\partial W}{\partial Z}\right)_m^S + \bar{r}W_m^S\overline{\frac{\partial u_z}{\partial z}} - m\bar{u}_\theta W_m^C\Bigg]\psi_l^{[\mathrm{f}]} + \bar{r}\left[\left(\frac{\partial W}{\partial R}\right)_m^S + \left(\frac{\partial U}{\partial Z}\right)_m^S\right]\frac{\partial\psi_l^{[\mathrm{f}]}}{\partial r} + \bar{r}\left[2\left(\frac{\partial W}{\partial Z}\right)_m^S - P_m^S\right]\frac{\partial\psi_l^{[\mathrm{f}]}}{\partial z} + \left[\frac{m^2}{\bar{r}}W_m^S + m\left(\frac{\partial V}{\partial Z}\right)_m^C\right]\psi_l^{[\mathrm{f}]}\Bigg\}\,\bar{\mathcal{J}}_B\;\mathrm{d}s_1\,\mathrm{d}s_2, \tag{8.25}$$

$$\hat{\mathcal{R}}^{[\mathrm{fS}]}_{\theta ml} = \gamma_m\,\pi\int_{-1}^{1}\int_{-1}^{1}\Bigg\{\mathrm{Re}\,\Bigg[\mathrm{St}\,\bar{r}\frac{\delta V_m^S}{\delta t} + \bar{r}\bar{u}_r\left(\frac{\partial V}{\partial R}\right)_m^S + \bar{r}U_m^S\overline{\frac{\partial u_\theta}{\partial r}} + \bar{r}\bar{u}_z\left(\frac{\partial V}{\partial Z}\right)_m^S + \bar{r}W_m^S\overline{\frac{\partial u_\theta}{\partial z}} - m\bar{u}_\theta V_m^C + \bar{u}_\theta U_m^S + V_m^S\bar{u}_r\Bigg]\psi_l^{[\mathrm{f}]} + \left[\bar{r}\left(\frac{\partial V}{\partial R}\right)_m^S - V_m^S - mU_m^C\right]\frac{\partial\psi_l^{[\mathrm{f}]}}{\partial r} + \left[\bar{r}\left(\frac{\partial V}{\partial Z}\right)_m^S - mW_m^C\right]\frac{\partial\psi_l^{[\mathrm{f}]}}{\partial z} - mP_m^C\psi_l^{[\mathrm{f}]} + \left[\frac{2m^2+1}{\bar{r}}V_m^S + \frac{3m}{\bar{r}}U_m^C - \left(\frac{\partial V}{\partial R}\right)_m^S\right]\psi_l^{[\mathrm{f}]}\Bigg\}\,\bar{\mathcal{J}}_B\;\mathrm{d}s_1\,\mathrm{d}s_2 \tag{8.26}$$

and

$$\hat{\mathcal{R}}^{[\mathrm{pS}]}_{ml} = \gamma_m\,\pi\int_{-1}^{1}\int_{-1}^{1}\left[\bar{r}\left(\frac{\partial U}{\partial R}\right)_m^S + U_m^S + \bar{r}\left(\frac{\partial W}{\partial Z}\right)_m^S - mV_m^C\right]\psi_l^{[\mathrm{p}]}\,\bar{\mathcal{J}}_B\;\mathrm{d}s_1\,\mathrm{d}s_2. \tag{8.27}$$

These equations are to be solved in a two-dimensional domain of radius 1 and height Γ, and are subject to the Dirichlet boundary conditions

$$U_m^C = U_m^S = W_m^C = W_m^S = V_m^C = V_m^S = 0 \tag{8.28}$$

on all solid boundaries. The boundary conditions at the symmetry axis ($r = 0$) differ depending on the azimuthal mode number m. For the axisymmetric mode we have the same condition here as in the base state,

$$U_0^C = U_0^S = \frac{\partial W_0^C}{\partial r} = \frac{\partial W_0^S}{\partial r} = V_0^C = V_0^S = 0, \tag{8.29}$$

whereas for non-zero, even-numbered modes we must additionally prescribe that the axial velocity is zero to avoid there being a discontinuity in the field at this boundary. On odd-numbered modes, however, the 'usual' symmetry condition must be relaxed as it is physically allowable for the fluid to have finite radial and azimuthal velocity at the symmetry axis. Consequently, the boundary conditions at $r = 0$ for non-zero modes are

$$U_m^C = U_m^S = W_m^C = W_m^S = V_m^C = V_m^S = 0 \tag{8.30}$$

for even m and

$$\frac{\partial U_m^C}{\partial r} = \frac{\partial U_m^S}{\partial r} = W_m^C = W_m^S = \frac{\partial V_m^C}{\partial r} = \frac{\partial V_m^S}{\partial r} = 0 \tag{8.31}$$

for odd m.

To solve this problem in `oomph-lib`, both `LinearisedAxisymmetricQTaylorHoodMultiDomainElement` and `LinearisedAxisymmetricQCrouzeixRaviartMultiDomainElement` were used here[1]. The problem domain was discretised using a uniform mesh of 50×50 elements and the BDF1 (or 'backward Euler') timestepper was employed, so as to match the formulation discussed in section 8.1.2. As remarked earlier, the only requirement for the initial conditions is that the resulting vector of global unknowns not be orthogonal to the dominant eigenvector. Bai et al. [Bai et al., 2000] remark that this is unlikely to occur if the initial conditions are chosen at random. We therefore choose to prescribe that all six velocity fields are given initially by

$$f(r, z) = 4rz(r - 1)(z - \Gamma), \tag{8.32}$$

[1]See section 7.4 for a discussion of the implementation of these elements.

a smoothly-varying function of r and z that satisfies the homogenous boundary conditions.

Having set up the linear problem, the overall stability problem was solved in the following way. For a given Reynolds number, the steady base flow was computed as discussed in section 8.1.1. A linear perturbation problem was then set up as described above, for a particular azimuthal mode m. We then performed the power method, where for every iteration one timestep of the system of equations was taken. Because the problem is linear and the base state is steady, the global Jacobian matrix is the same at each timestep: this allowed us to compute it once, store it, and then reapply it at each successive power method iteration. Once the power method had converged, the resulting dominating eigenvalue was used to determine whether or not the base flow is stable at the Reynolds number in question.

The results given in Nore et al. [Nore et al., 2004] were used as a guide to establish roughly where we expected the stability thresholds to lie. The actual thresholds were then computed by first choosing a value of the Reynolds number below the expected threshold, and carrying out the above procedure to determine the stability of the flow at this parameter. The Reynolds number was then increased slightly, and the procedure performed again. The advantages of performing this automatic 'continuation'-like routine are twofold: firstly, the initial guess for the base flow solution at the advanced Reynolds number is chosen to be the solution found using the 'old' Reynolds number. Since the two solutions are very similar this is an excellent initial guess and the Newton method therefore requires very few steps to converge. Secondly, the dominant eigenvector computed at the 'old' Reynolds number is used for the initial conditions for the power method at the advanced Reynolds number. Since we are attempting to 'trace' this eigenvector as the magnitude of its corresponding eigenvalue crosses the threshold $\lambda_{\text{crit}} = 1$, this choice of starting vector allows the power method to converge in significantly fewer iterations than if we constantly reset to the initial conditions specified in (8.32).

Once a range of problems at various Reynolds numbers had been solved, the stability threshold was determined by plotting the dominant eigenvalue against Reynolds number. Figure 8.3 shows such a plot for the azimuthal mode $m = 2$, where the two

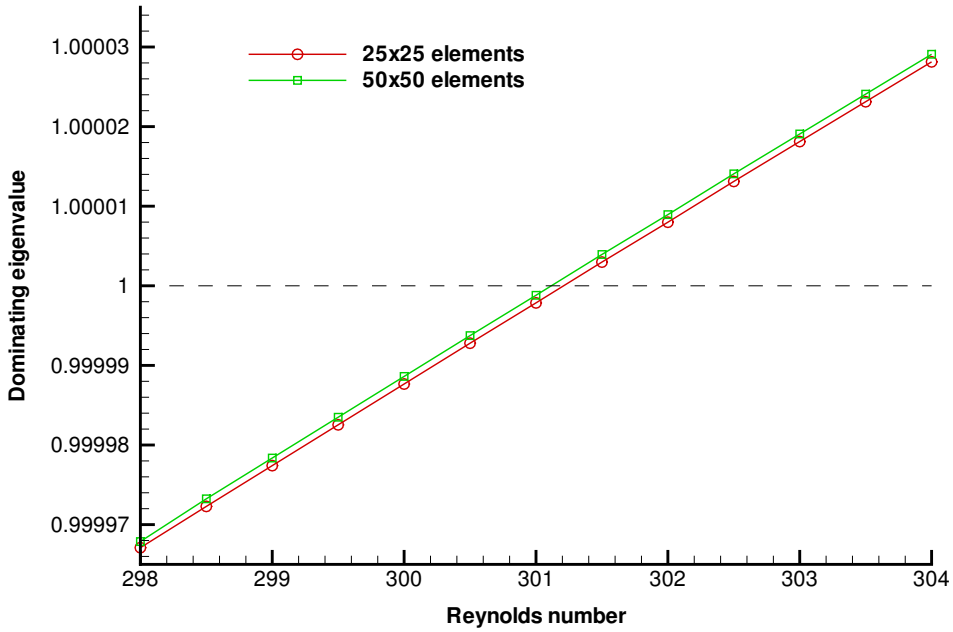

Figure 8.3: Plot of dominant eigenvalue against Reynolds number for the $m = 2$ mode, shown for two different spatial resolutions. The data plotted here were generated using `LinearisedAxisymmetricQTaylorHoodMultiDomainElements`, but the use of their Crouzeix–Raviart counterparts would result in a near-identical plot. A BDF1 timestepper with a non-dimensionalised timestep of 0.005 was employed, and the aspect ratio was set to $\Gamma = 1$. The Reynolds number was increased in steps of 0.5.

lines correspond to the same set of problems computed at two different spatial resolutions. From this we infer that (to the nearest integer value) the critical Reynolds number at which the flow goes unstable is $\mathrm{Re} = 301$.

8.1.4 Comparison with Nore et al.

The motivation for studying this particular problem was so that the linear perturbation equations (on stationary meshes) could be validated by comparison against the study conducted by Nore et al. [Nore et al., 2004]. Although a large portion of this paper discusses the effect that changing the aspect ratio Γ has on the stability thresholds, we restrict ourselves to cases where $\Gamma = 1$. The results generated by Nore et al. were computed in the following way. First a stable steady base flow was computed for $\mathrm{Re} = 100$ and fixed Γ using an unsteady axisymmetric code. The flow fields were represented in cylindrical coordinates, with a staggered non-uniform grid used in the

(r, z)–plane. The refinement of the grid was concentrated at the top, bottom and outer boundaries, as well as at the line of constant z exactly half-way between the top and bottom boundaries. The base flow was represented by the azimuthal velocity and a stream-function ψ defining the radial and axial velocities via $\nabla\psi \times \mathbf{e}_r/r$, and the Navier–Stokes equations were spatially discretised using mimetic finite-difference operators. Once the (steady) $\mathrm{Re} = 100$ solution was established by time integration of the unsteady code, successive steady states (which may be unstable to axisymmetric perturbations) were computed using a Newton–Raphson method. The large linear systems which arise as a consequence of this method were solved using a preconditioned Krylov subspace solver.

To carry out the linear stability analysis of the axisymmetric steady state a non-axisymmetric code was used, with velocity and pressure components expanded as truncated Fourier series over N_θ modes in the azimuthal direction. The governing equations are

$$\frac{\partial \mathbf{v}}{\partial t} + (\mathbf{V} \cdot \nabla)\,\mathbf{v} + (\mathbf{v} \cdot \nabla)\,\mathbf{V} = -\nabla p + \frac{1}{\mathrm{Re}}\nabla^2 \mathbf{v} \tag{8.33}$$

and

$$\nabla \cdot \mathbf{v} = 0, \tag{8.34}$$

where $(\mathbf{v}, p)$ are the perturbation variables and $\mathbf{V}$ represents the previously computed base flow. The velocity $\mathbf{v}$ was subject to homogeneous boundary conditions. The temporal evolution of this system was performed by a second-order implicit discretisation of the linear terms and explicit Adams-Bashforth type extrapolation of the 'linearised versions' of the nonlinear terms. Velocity-pressure coupling was handled by means of an incremental projection method. As in the formulation described in this thesis, the stability computation decoupled into a series of subproblems each associated with a different azimuthal mode number m, which meant that time integration from an arbitrary initial condition corresponded to performing N_θ parallel computations of the Fourier-decomposed system. The leading eigenvalues were computed using an implicitly restarted Arnoldi method within the `ARPACK` software library [Lehoucq et al., 1998]. The critical Reynolds numbers Re_m for each mode are those for which the real part of the dominant eigenvalue is equal to zero, and their values were determined by interpolation. Hence the critical Reynolds number for the overall flow was determined by finding the minimum Re_m, and the corresponding value of m gave the critical

Study	Spatial resolution	Critical Re_m				
		1	2	3	4	5
Nore et al.	100×100 gridpoints (uniform spacing)	420	299	312	387	533
	64×100 gridpoints (non-uniform spacing)	420	300	312	387	534
This work	25×25 elements	423	301	314	389	536
	50×50 elements	423	301	314	389	536

Table 8.1: Comparison of the critical Reynolds numbers at which modes 1–5 go unstable between this work and the study conducted by Nore et al. In both works results for two different spatial resolutions are given. All thresholds agree to within 1% of each other.

mode.

Table 8.1 compares the results of the study performed in this thesis with that performed by Nore et al., where two different spatial resolutions have been used in each case. Nore et al. give results for both a uniform and a non-uniform grid, where in the non-uniform case they use a larger number of grid points in the axial direction than in the radial direction. We compare these results to those computed in the manner discussed in sections 8.1.1–8.1.3, where quadratic finite elements have been used. We note that our results agree to within 1% to those computed by Nore et al., which is the same tolerance as quoted by these authors when validating their code against results presented by a study by Gelfgat et al. for a rotor-stator flow [Gelfgat et al., 2001].

We note from (8.16) that the matrix $\mathcal{B}$, the eigenvalues of which determine the linear stability of the base flow, depends on the duration of the timestep Δt. To investigate the effect of this dependancy we re-computed the threshold of the $m = 2$ mode using several different values of the timestep, and the results are shown in figure 8.4. For all values of the timestep, the simulations were run with two different spatial resolutions, 25×25 and 50×50 elements. Since the two spatial resolutions give very similar results, only the results for the finer resolution runs are shown here for clarity. We note that (as expected) the critical Reynolds number is independent of Δt, but the slope of the lines vary in a systematic way, with a larger timestep corresponding to a steeper gradient. This is to be expected: taking a larger timestep per iteration of the power method results in larger growth (or decay) of the dominant eigenvector

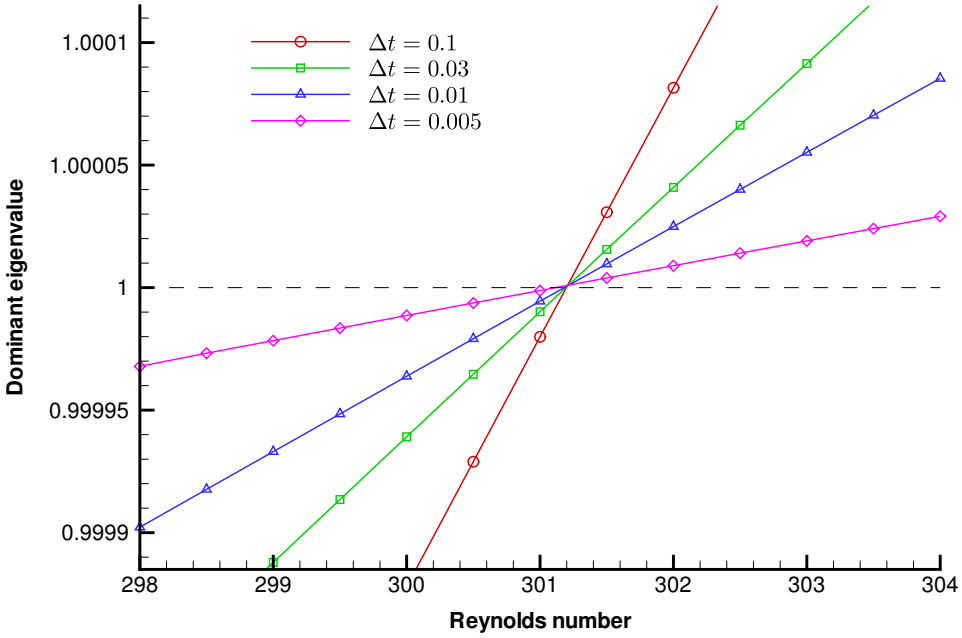

Figure 8.4: Plot of dominant eigenvalue against Reynolds number for the $m = 2$ mode, where the timestep is varied between 0.005 and 0.1. The domain was discretised spatially using a mesh of 50×50 `LinearisedAxisymmetricQTaylorHoodMultiDomainElements`, and a BDF1 timestepper with a non-dimensionalised timestep of 0.005 was employed. The aspect ratio was set to $\Gamma = 1$, and the Reynolds number increased in steps of 0.5.

over the duration of that iteration. If the dominant eigenvector and its corresponding eigenvalue are denoted by $\mathbf{x}_D$ and λ_D respectively, then from

$$\mathcal{B}\,\mathbf{x}_D = \lambda_D\,\mathbf{x}_D \tag{8.35}$$

it is clear that we would also expect the magnitude of λ_D to be larger (in the case of a growing perturbation) if the timestep is increased. This is precisely what we see in figure 8.4.

To complete this validation exercise, we ensured that the computed eigenvectors were resolved by comparing each field carefully at the two different spatial resolutions. Figures 8.5(a) and 8.5(b) show the cosine and sine components respectively of the dominant eigenvector for the $m = 2$ mode at a Reynolds number of 301, for the higher-resolution computations. The problem was discretised spatially using `LinearisedAxisymmetricQTaylorHoodMultiDomainElements` on a uniform mesh containing 50 elements in each direction. A BDF1 timestepping scheme with $\Delta t = 0.01$ was used to

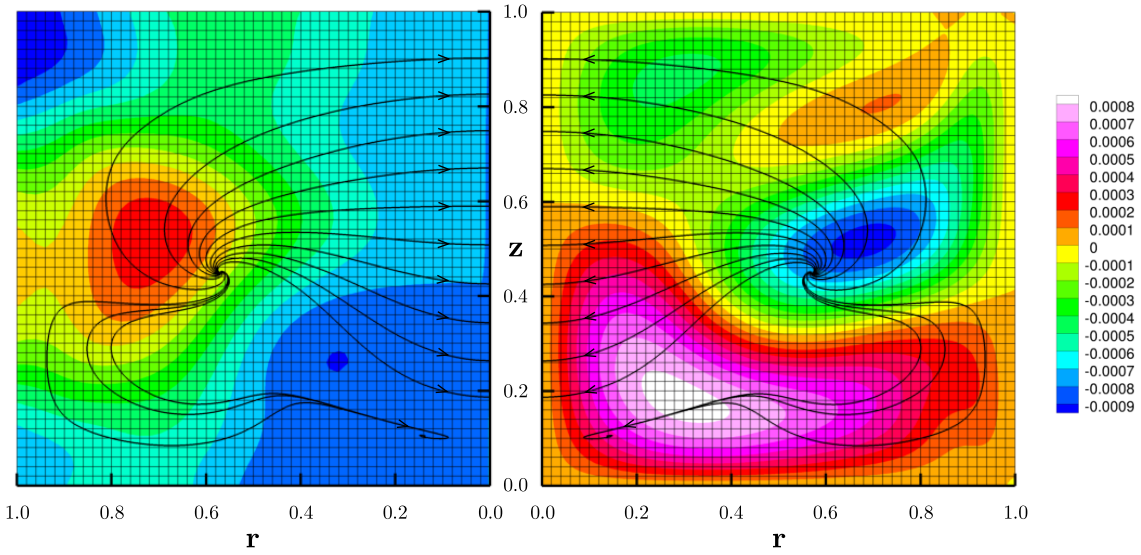

(a) Cosine part

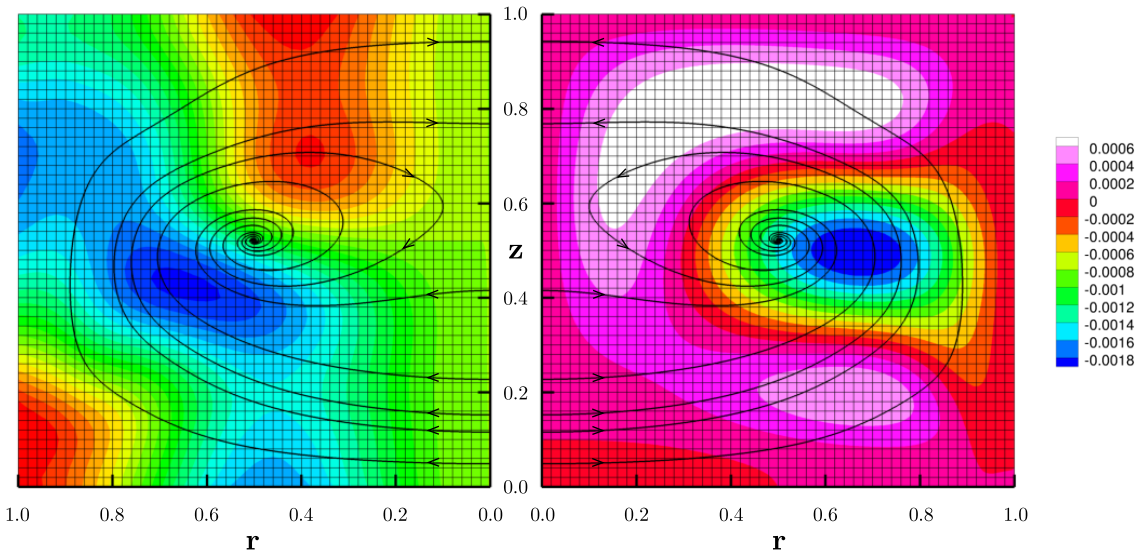

(b) Sine part

Figure 8.5: Plot of the dominant eigenvector for the $m = 2$ mode at Re $= 301$ and $\Gamma = 1$. The domain was discretised spatially using a mesh of 50×50 `Linearised-AxisymmetricQTaylorHoodMultiDomainElements`, and a BDF1 timestepper with a non-dimensionalised timestep of 0.01 was employed. The cosine part of the solution is shown in 8.5(a), and the sine part of the solution is shown in 8.5(b). In both 8.5(a) and 8.5(b) the left- and right-hand plots display colour contours of pressure $P_2(r, z)$ and azimuthal velocity $V_2(r, z)$ respectively, with superimposed streamlines tracking the motion of the in-plane velocity. The legends correspond to the azimuthal velocity contours. On the pressure plots, dark blue and bright red regions correspond to areas of lowest and highest pressure respectively. The cosine component of the pressure ranges from -0.0091 to 0.0443, and the sine component ranges from -0.0227 to 0.0144.

time evolve the equations. In both plots the right-hand side displays colour contours of azimuthal velocity V_2^C and V_2^S at $\theta = 0$, and the left-hand side displays colour contours of pressure P_2^C and P_2^S at $\theta = \pi$. On the pressure plots, dark blue and bright red correspond to the minimum and maximum values of the pressure respectively, whereas the legends to the right of the azimuthal velocity plots describe those contours in terms of the non-dimensional velocity. The streamlines in figure 8.5(a) show the motion of the in-plane velocities U_2^C and W_2^C, and those in 8.5(b) show the motion of their 'sine counterparts' U_2^S and W_2^S. We note that the apparent sources and sinks are due to the fact that the flow is not two-dimensionally divergence-free.

8.1.5 Implementation

The problem discussed above was implemented as a demonstration code in `oomph-lib`, and its source file,

`counter_rotating_disks.cc,`

is located in the

`demo_drivers/axisym_navier_stokes/counter_rotating_disks/`

directory.

8.2 Stability of time-periodic Taylor–Couette flow

Ever since Taylor's investigation into the stability of steady Couette flow in 1923 [Taylor, 1923] there has been considerable research into many different aspects of Taylor–Couette flow. Not until 1962, however, was the effect of modulating the rate of rotation of one or both of the cylinders investigated. Donnelly et al. [1962] performed experiments in which the outer cylinder was at rest while the inner cylinder rotated, and found that modulating the inner cylinder acted to stabilise the flow. In a later numerical study of a similar set up, Carmi and Tustaniwskyj [1981] derived a closed-form analytic solution for the base flow in terms of modified Bessel functions and investigated its stability by performing a Floquet analysis of the linearised perturbation equations. Although they found good agreement in the case of inner cylinder

modulation about a zero mean with experiments [Thompson, 1968], their findings generally opposed the observations of Donnelly et al. [1962] by suggesting that modulation generally acts to destabilise the flow. For the particular case of steady rotation of the inner cylinder and sinusoidal modulation of the outer cylinder about a zero mean, their numerical prediction was directly contradicted by subsequent experiments performed by Walsh and Donnelly for a corresponding system, who observed that the modulation of the outer cylinder acted to stabilise the flow [Walsh and Donnelly, 1988].

This discrepancy motivated the study performed by Murray et al. in their paper *Stabilization of Taylor–Couette flow due to time-periodic outer cylinder oscillation* [Murray et al., 1990], whose numerical linear stability results agree with the experiments of Walsh and Donnelly, except for low frequencies and large modulation amplitudes. As a validation exercise we shall consider the same problem here, in which we have an annular region of incompressible fluid contained between two concentric cylinders which are infinite in the axial direction, as sketched in figure 8.6(a). The inner cylinder has radius R_1 and rotates at a constant angular velocity Ω_1. The outer cylinder has radius R_2 and is driven sinusoidally in time with zero mean rotation, and we define its angular velocity Ω_2 in terms of the angular velocity of the inner cylinder and a forcing frequency ω, so that

$$\Omega_2(t) = \epsilon\,\Omega_1 \cos\omega t. \tag{8.36}$$

8.2.1 The base flow

In the absence of gravitational forces, this problem admits an unsteady, axisymmetric base flow for which the only non-zero component of the velocity is in the azimuthal direction. This velocity field $u_\theta = u_\theta(r,t)$ and the pressure field $p = p(r,t)$ are functions of the radial coordinate and time only, and the base flow is therefore governed by

$$\mathrm{Re}\,\mathrm{St}\,\frac{\partial u_\theta}{\partial t} = \frac{\partial^2 u_\theta}{\partial r^2} + \frac{1}{r}\frac{\partial u_\theta}{\partial r} - \frac{u_\theta}{r^2} \tag{8.37}$$

and

$$\frac{\partial p}{\partial r} = \mathrm{Re}\,\frac{u_\theta^2}{r}. \tag{8.38}$$

We choose the length scale to be the fluid gap width,

$$\mathcal{L} = R_2 - R_1, \tag{8.39}$$

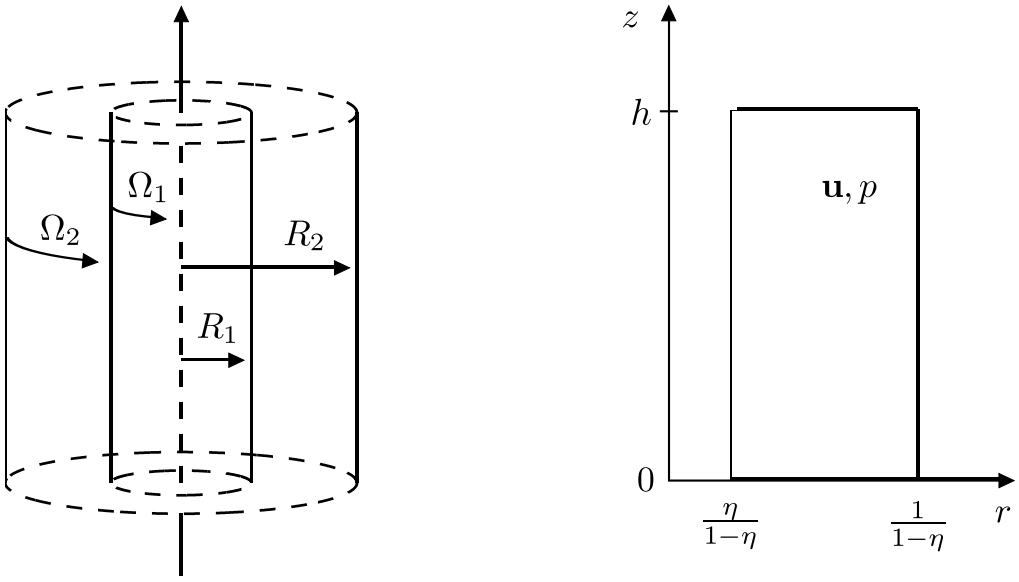

(a) Physical domain

(b) Computational domain

Figure 8.6: Sketch of the time-periodic Taylor–Couette problem. The computational domain represents a radial 'slice' of the physical domain, where the inner and outer solid boundaries are located at $r = \eta/(1-\eta)$ and $r = 1/(1-\eta)$ respectively. The axial extent of the domain has been truncated to an arbitrary height h.

so that the non-dimensional cylinder radii become

$$\frac{R_1}{R_2 - R_1} = \frac{\eta}{1-\eta} \tag{8.40}$$

for the inner cylinder and

$$\frac{R_2}{R_2 - R_1} = \frac{1}{1-\eta} \tag{8.41}$$

for the outer, where $\eta = R_1/R_2$. We will follow Murray et al. by defining the velocity and time scales in terms of the kinematic viscosity ν so that

$$\mathcal{U} = \frac{\nu}{R_2 - R_1} \qquad \text{and} \qquad \mathcal{T} = \frac{(R_2 - R_1)^2}{\nu}, \tag{8.42}$$

and as a result, since the kinematic and dynamic viscosities are related by $\nu = \mu/\rho$, our 'usual' definitions of the Reynolds and Strouhal numbers in the governing equations both evaluate to unity. Using (8.40)–(8.42), however, we find the (non-dimensional) azimuthal velocity boundary condition on the inner cylinder to be

$$u_\theta = \frac{R_1 \Omega_1}{\mathcal{U}} = \left[\frac{\Omega_1 (R_2 - R_1)^2}{\nu}\right] \frac{\eta}{1-\eta}, \tag{8.43}$$

and that on the outer cylinder to be

$$u_\theta = \frac{R_2\Omega_2}{\mathcal{U}} = \epsilon \left[\frac{\Omega_1 (R_2 - R_1)^2}{\nu}\right] \frac{1}{1-\eta} \cos\omega t. \tag{8.44}$$

If we now define a new Reynolds number as

$$\mathrm{Re}^* = \frac{\Omega_1 (R_2 - R_1)^2}{\nu}, \tag{8.45}$$

then the azimuthal velocity boundary conditions on the inner and outer cylinders are given by

$$u_\theta = \mathrm{Re}^* \frac{\eta}{1-\eta} \qquad \text{and} \qquad u_\theta = \epsilon\, \mathrm{Re}^* \frac{1}{1-\eta} \cos\omega t. \tag{8.46}$$

Note that the Reynolds number is now contained within these boundary conditions, rather than appearing in the governing equations. We shall continue to denote this as Re^* to avoid confusion with our 'usual' Re.

Although the problem we are modelling concerns two cylinders of infinite axial extent, we will in practice solve the governing equations in a truncated domain of height h, as sketched in figure 8.6(b). The base flow (u_θ, p) is independent of the axial coordinate z, and the choice of h is therefore arbitrary. In practice, however, its value is restricted by the linear stability problem which will be solved on top of the base flow, and these conditions will be discussed in section 8.2.2. We must ensure that the base flow is translationally invariant in the axial direction, and to be consistant with this we apply the non-penetration condition

$$\frac{\partial u_r}{\partial z} = u_z = 0 \tag{8.47}$$

at the bottom ($z = 0$) and top ($z = h$) boundaries. At the left and right solid boundaries we apply the no-slip condition so that

$$u_r = u_z = 0, \quad u_\theta = \mathrm{Re}^* \frac{\eta}{1-\eta} \quad \text{at} \quad r = \frac{\eta}{1-\eta} \tag{8.48}$$

and

$$u_r = u_z = 0, \quad u_\theta = \epsilon\, \mathrm{Re}^* \frac{1}{1-\eta} \cos\omega t \quad \text{at} \quad r = \frac{1}{1-\eta}. \tag{8.49}$$

This base flow was computed numerically in `oomph-lib` with a mesh containing 32×32 elements, and both Taylor–Hood and Crouzeix–Raviart elements were used for validation purposes. The time-derivatives were discretised using a second-order-accurate BDF scheme with a timestep of $T/40$, where $T = 2\pi/\omega$ is the period of the

flow. The simulation was started impulsively from the initial conditions $u_r = u_z = u_\theta = 0$. A plot of the base solution for an amplitude of $\epsilon = 0.9$, an angular frequency of $\omega = 10.58$ and $\mathrm{Re}^* = 20.96$ is shown in figure 8.7. The ratio of cylinder radii is chosen to be $\eta = 0.88$. Since the solution is independent of the axial coordinate we have simply plotted a 'slice' of the domain, taken at constant z, at each timestep, and for simplicity have normalised the time t over a single period. We note that the solution shown here was deemed to be 'sufficiently periodic' to within the tolerance used for all the computations of this particular problem: the precise details of the measure used to determine this will be discussed in section 8.2.2.

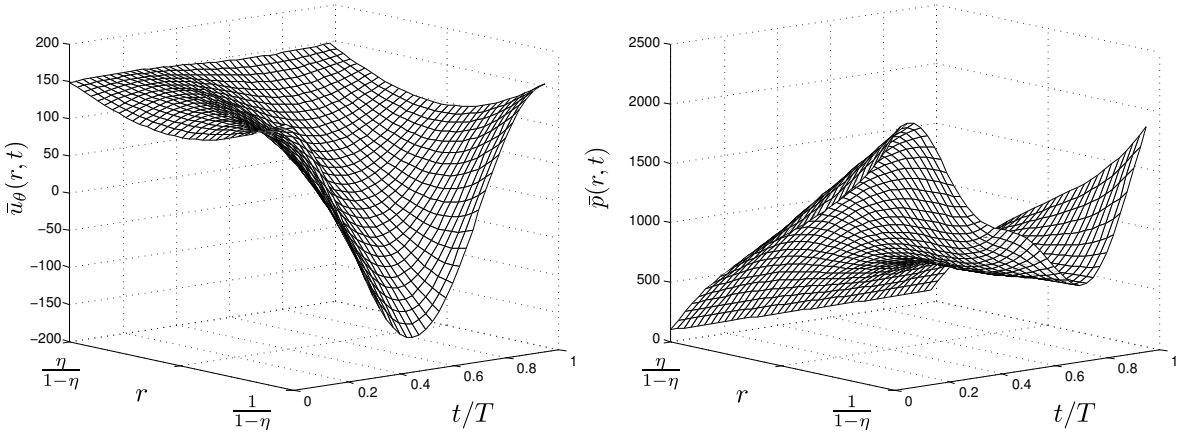

Figure 8.7: Plot of the base flow solution over one period for $\epsilon = 0.9$, $\omega = 10.58$, $\mathrm{Re}^* = 20.96$ and $\eta = 0.88$. The domain was discretised spatially using a mesh of 32×32 `LinearisedAxisymmetricQTaylorHoodMultiDomainElements`, and a BDF2 timestepper with a non-dimensionalised timestep of $2\pi/40\omega$ was employed. The left- and right-hand plots show the azimuthal velocity $\bar{u}_\theta(r,t)$ and pressure $\bar{p}(r,t)$ respectively. The time t has been normalised over one period $T = 2\pi/\omega$.

8.2.2 Perturbation to the base flow

We now wish to investigate the stability of this base solution to axisymmetric perturbations. We shall employ the same technique as was used to analyse the stability of the counter-rotating disks problem (described in section 8.1). We recall that in that example the stability of a given (steady) flow was determined by the dominating eigenvalue of the linear operator corresponding to the action of advancing the perturbation equations from one timestep to the next. Since in this example the base flow

is periodic, we require the dominating eigenvalue of the linear operator corresponding to timestepping the perturbation equations over an *entire period*. The 'perturbation problem' which we wish to solve is governed by the linearised perturbation equations (7.77)–(7.84) formulated in section 7.3. As previously discussed, a significant number of these terms are equal to zero, including all those multiplied by the wavenumber m, and therefore for clarity we shall state these equations again here. The momentum equations which arise through taking the 'cosine' test functions (7.59) are

$$\begin{aligned}\hat{\mathcal{R}}^{[\mathrm{fC}]}_{\mathrm{r}0l} = 2\pi \int_{-1}^{1}\int_{-1}^{1} \Bigg\{ \mathrm{Re}\ \Bigg[& \mathrm{St}\,\bar{r}\frac{\delta U_0^C}{\delta t} + \bar{r}\bar{u}_r\left(\frac{\partial U}{\partial R}\right)_0^C + \bar{r}U_0^C\overline{\frac{\partial u_r}{\partial r}} \\ & + \bar{r}\bar{u}_z\left(\frac{\partial U}{\partial Z}\right)_0^C + \bar{r}W_0^C\overline{\frac{\partial u_r}{\partial z}} - 2\bar{u}_\theta V_0^C \Bigg]\psi_l^{[\mathrm{f}]} \\ & - \left(\bar{r}\frac{\partial \psi_l^{[\mathrm{f}]}}{\partial r} + \psi_l^{[\mathrm{f}]}\right)P_0^C + 2\bar{r}\left(\frac{\partial U}{\partial R}\right)_0^C\frac{\partial \psi_l^{[\mathrm{f}]}}{\partial r} \\ & + \bar{r}\left[\left(\frac{\partial W}{\partial R}\right)_0^C + \left(\frac{\partial U}{\partial Z}\right)_0^C\right]\frac{\partial \psi_l^{[\mathrm{f}]}}{\partial z} + \frac{2}{\bar{r}}U_0^C\psi_l^{[\mathrm{f}]}\Bigg\}\,\bar{\mathcal{J}}_B\,\mathrm{d}s_1\,\mathrm{d}s_2, \end{aligned} \tag{8.50}$$

$$\begin{aligned}\hat{\mathcal{R}}^{[\mathrm{fC}]}_{\mathrm{z}0l} = 2\pi \int_{-1}^{1}\int_{-1}^{1} \Bigg\{ \mathrm{Re}\ \Bigg[& \mathrm{St}\,\bar{r}\frac{\delta W_0^C}{\delta t} + \bar{r}\bar{u}_r\left(\frac{\partial W}{\partial R}\right)_0^C + \bar{r}U_0^C\overline{\frac{\partial u_z}{\partial r}} \\ & + \bar{r}\bar{u}_z\left(\frac{\partial W}{\partial Z}\right)_0^C + \bar{r}W_0^C\overline{\frac{\partial u_z}{\partial z}}\Bigg]\psi_l^{[\mathrm{f}]} \\ & + \bar{r}\left[\left(\frac{\partial W}{\partial R}\right)_0^C + \left(\frac{\partial U}{\partial Z}\right)_0^C\right]\frac{\partial \psi_l^{[\mathrm{f}]}}{\partial r} \\ & + \bar{r}\left[2\left(\frac{\partial W}{\partial Z}\right)_0^C - P_0^C\right]\frac{\partial \psi_l^{[\mathrm{f}]}}{\partial z}\Bigg\}\,\bar{\mathcal{J}}_B\,\mathrm{d}s_1\,\mathrm{d}s_2 \end{aligned} \tag{8.51}$$

and

$$\begin{aligned}\hat{\mathcal{R}}^{[\mathrm{fC}]}_{\theta 0l} = 2\pi \int_{-1}^{1}\int_{-1}^{1} \Bigg\{ \mathrm{Re}\ \Bigg[& \mathrm{St}\,\bar{r}\frac{\delta V_0^C}{\delta t} + \bar{r}\bar{u}_r\left(\frac{\partial V}{\partial R}\right)_0^C + \bar{r}U_0^C\overline{\frac{\partial u_\theta}{\partial r}} + \bar{r}\bar{u}_z\left(\frac{\partial V}{\partial Z}\right)_0^C \\ & + \bar{r}W_0^C\overline{\frac{\partial u_\theta}{\partial z}} + \bar{u}_\theta U_0^C + V_0^C\bar{u}_r\Bigg]\psi_l^{[\mathrm{f}]} \\ & + \left[\bar{r}\left(\frac{\partial V}{\partial R}\right)_0^C - V_0^C\right]\frac{\partial \psi_l^{[\mathrm{f}]}}{\partial r} + \bar{r}\left(\frac{\partial V}{\partial Z}\right)_0^C\frac{\partial \psi_l^{[\mathrm{f}]}}{\partial z} \\ & + \left[\frac{1}{\bar{r}}V_0^C - \left(\frac{\partial V}{\partial R}\right)_0^C\right]\psi_l^{[\mathrm{f}]}\Bigg\}\,\bar{\mathcal{J}}_B\,\mathrm{d}s_1\,\mathrm{d}s_2, \end{aligned} \tag{8.52}$$

and the continuity equation is

$$\hat{\mathcal{R}}^{[\mathrm{pC}]}_{0l} = 2\pi \int_{-1}^{1}\int_{-1}^{1} \left[\bar{r}\left(\frac{\partial U}{\partial R}\right)_0^C + U_0^C + \bar{r}\left(\frac{\partial W}{\partial Z}\right)_0^C \right] \psi_l^{[\mathrm{p}]}\, \bar{\mathcal{J}}_B \, \mathrm{d}s_1 \, \mathrm{d}s_2. \tag{8.53}$$

The 'sine counterparts' that arise through taking the 'sine' test functions (7.60) are

$$\begin{aligned}\hat{\mathcal{R}}^{[\mathrm{fS}]}_{\mathrm{r}0l} = 2\pi \int_{-1}^{1}\int_{-1}^{1} \Bigg\{ \mathrm{Re}\ \Bigg[& \mathrm{St}\,\bar{r}\frac{\delta U_0^S}{\delta t} + \bar{r}\bar{u}_r\left(\frac{\partial U}{\partial R}\right)_0^S + \bar{r}U_0^S\overline{\frac{\partial u_r}{\partial r}} \\ & + \bar{r}\bar{u}_z\left(\frac{\partial U}{\partial Z}\right)_0^S + \bar{r}W_0^S\overline{\frac{\partial u_r}{\partial z}} - 2\bar{u}_\theta V_0^S \Bigg] \psi_l^{[\mathrm{f}]} \\ & - \left(\bar{r}\frac{\partial \psi_l^{[\mathrm{f}]}}{\partial r} + \psi_l^{[\mathrm{f}]}\right) P_0^S + 2\bar{r}\left(\frac{\partial U}{\partial R}\right)_0^S \frac{\partial \psi_l^{[\mathrm{f}]}}{\partial r} \\ & + \bar{r}\left[\left(\frac{\partial W}{\partial R}\right)_0^S + \left(\frac{\partial U}{\partial Z}\right)_0^S\right] \frac{\partial \psi_l^{[\mathrm{f}]}}{\partial z} + \frac{2}{\bar{r}}U_0^S\psi_l^{[\mathrm{f}]} \Bigg\} \bar{\mathcal{J}}_B \, \mathrm{d}s_1 \, \mathrm{d}s_2, \end{aligned} \tag{8.54}$$

$$\begin{aligned}\hat{\mathcal{R}}^{[\mathrm{fS}]}_{\mathrm{z}0l} = 2\pi \int_{-1}^{1}\int_{-1}^{1} \Bigg\{ \mathrm{Re}\ \Bigg[& \mathrm{St}\,\bar{r}\frac{\delta W_0^S}{\delta t} + \bar{r}\bar{u}_r\left(\frac{\partial W}{\partial R}\right)_0^S + \bar{r}U_0^S\overline{\frac{\partial u_z}{\partial r}} \\ & + \bar{r}\bar{u}_z\left(\frac{\partial W}{\partial Z}\right)_0^S + \bar{r}W_0^S\overline{\frac{\partial u_z}{\partial z}} \Bigg] \psi_l^{[\mathrm{f}]} \\ & + \bar{r}\left[\left(\frac{\partial W}{\partial R}\right)_0^S + \left(\frac{\partial U}{\partial Z}\right)_0^S\right] \frac{\partial \psi_l^{[\mathrm{f}]}}{\partial r} \\ & + \bar{r}\left[2\left(\frac{\partial W}{\partial Z}\right)_0^S - P_0^S\right] \frac{\partial \psi_l^{[\mathrm{f}]}}{\partial z} \Bigg\} \bar{\mathcal{J}}_B \, \mathrm{d}s_1 \, \mathrm{d}s_2, \end{aligned} \tag{8.55}$$

$$\begin{aligned}\hat{\mathcal{R}}^{[\mathrm{fS}]}_{\theta 0l} = 2\pi \int_{-1}^{1}\int_{-1}^{1} \Bigg\{ \mathrm{Re}\ \Bigg[& \mathrm{St}\,\bar{r}\frac{\delta V_0^S}{\delta t} + \bar{r}\bar{u}_r\left(\frac{\partial V}{\partial R}\right)_0^S + \bar{r}U_0^S\overline{\frac{\partial u_\theta}{\partial r}} + \bar{r}\bar{u}_z\left(\frac{\partial V}{\partial Z}\right)_0^S \\ & + \bar{r}W_0^S\overline{\frac{\partial u_\theta}{\partial z}} + \bar{u}_\theta U_0^S + V_0^S\bar{u}_r \Bigg] \psi_l^{[\mathrm{f}]} \\ & + \left[\bar{r}\left(\frac{\partial V}{\partial R}\right)_0^S - V_0^S\right] \frac{\partial \psi_l^{[\mathrm{f}]}}{\partial r} + \bar{r}\left(\frac{\partial V}{\partial Z}\right)_0^S \frac{\partial \psi_l^{[\mathrm{f}]}}{\partial z} \\ & + \left[\frac{1}{\bar{r}}V_0^S - \left(\frac{\partial V}{\partial R}\right)_0^S\right] \psi_l^{[\mathrm{f}]} \Bigg\} \bar{\mathcal{J}}_B \, \mathrm{d}s_1 \, \mathrm{d}s_2 \end{aligned} \tag{8.56}$$

and

$$\hat{\mathcal{R}}^{[\mathrm{pS}]}_{0l} = 2\pi \int_{-1}^{1}\int_{-1}^{1} \left[\bar{r}\left(\frac{\partial U}{\partial R}\right)_0^S + U_0^S + \bar{r}\left(\frac{\partial W}{\partial Z}\right)_0^S \right] \psi_l^{[\mathrm{p}]}\, \bar{\mathcal{J}}_B \, \mathrm{d}s_1 \, \mathrm{d}s_2. \tag{8.57}$$

As usual these equations have to be solved in the same domain as the base flow problem, so that r ranges from $\eta/(1-\eta)$ to $1/(1-\eta)$ and z ranges from 0 to h. The

choice of h is based on values quoted by Murray et al.: in their work, they model the domain as infinite in the axial direction, and this allows them to Fourier decompose the perturbation equations in this direction. They then solve the perturbation equations on a one-dimensional mesh and compute the axial wavenumber a as part of the solution. Since our domain is two-dimensional, we require h to be such that an integer number of half-wavelengths can be contained in the axial direction. The simplest choice is to set $h = \pi/a$, where a is taken from the calculations performed by Murray et al. for the particular set of parameters in question.

We note that by setting up the problem in this way we are in fact treating the computational domain as a 'periodic box' designed to fit precisely half a wavelength in the axial direction. Although our choice of h is taken from the calculated values of Murray et al., we acknowledge that these values were informed by the original analysis of G. I. Taylor [Taylor, 1923]. The perturbation equations are subject to the Dirichlet boundary conditions

$$U_0^C = U_0^S = W_0^C = W_0^S = V_0^C = V_0^S = 0 \tag{8.58}$$

on the left and right domain boundaries and the non-penetration conditions

$$\frac{\partial U_0^C}{\partial z} = \frac{\partial U_0^S}{\partial z} = W_0^C = W_0^S = \frac{\partial V_0^C}{\partial z} = \frac{\partial V_0^S}{\partial z} = 0 \tag{8.59}$$

at the upper and lower boundaries. The solution was computed using both `LinearisedAxisymmetricQTaylorHoodMultiDomainElements` and `LinearisedAxisymmetricQCrouzeixRaviartMultiDomainElements`, as discussed in section 7.4, with uniform meshes containing 32×32 elements and a self-starting BDF2 timestepper. The initial condition was identical to that used in the previous validation problem: all six velocity fields were initially prescribed to be smoothly-varying functions of r and z of the form

$$f(r,z) = 4z(z-h)\left(r - \frac{\eta}{1-\eta}\right)\left(r - \frac{1}{1-\eta}\right). \tag{8.60}$$

Having set up the linear problem, the overall stability problem was solved in the following way. For a given Reynolds number, the base flow problem was initialised (as discussed in section 8.2.1) and its degrees of freedom stored as entries of a vector $\mathbf{V}^{(0)}$. The unsteady base solution was then computed over a single period T and its degrees of freedom stored as entries of a vector $\mathbf{V}^{(1)}$. The quantity

$$d^{(1)} = \frac{1}{N_{\text{dof}}}\sqrt{\sum_{i=1}^{N_{\text{dof}}}\left[\left(V_i^{(1)} - V_i^{(0)}\right)^2\right]} \tag{8.61}$$

provides a mesh-independent measure of the difference in the solution at the end of the first period compared to the initial solution. We compared $d^{(1)}$ to a prescribed tolerance, and considered the flow to have settled down to a periodic state if $d^{(1)}$ was less than this value. Otherwise, we computed a second period, constructed $d^{(2)}$ in a similar way and repeated the test. We continued in this way until we were satisfied that we were computing a periodic base solution (to within our prescribed tolerance of 1×10^{-6}), and at this point set up the linear perturbation problem as described above. We then performed the power method, where for every iteration both the base and perturbation equations were timestepped over an entire period T. Once the power method had converged, the resulting dominating eigenvalue was used to determine whether or not the base flow is stable at the Reynolds number in question.

The results given in Murray et al. [Murray et al., 1990] were used as a guide to roughly where we expected the stability thresholds to lie. The actual thresholds were then computed in exactly the same way as described in the counter-rotating disks example (section 8.1.3). First a value of the Reynolds number below the expected threshold was chosen, and the above procedure carried out to determine the stability of the flow. The Reynolds number was then increased slightly, and the procedure performed again, with the initial conditions for the power method taken to be the dominant eigenvector computed for the previous Reynolds number. Once a range of problems at various Reynolds numbers had been solved, the stability threshold was determined by plotting the dominant eigenvalue against Reynolds number. Figure 8.8 shows such a plot for the parameters $\eta = 0.88$, $h = \pi/3.2$, $\epsilon = 0.9$ and $\omega = 10.58$. The two lines correspond to the same set of problems computed at two different spatial resolutions. From this we infer that (to within ± 0.005) the critical Reynolds number at which the flow goes unstable to the $m = 0$ mode is $\mathrm{Re}^* = 20.935$.

8.2.3 Comparison with Murray et al.

The motivation for studying this particular problem was so that the zeroth-mode linear perturbation equations (on stationary meshes) could be validated by comparison against the study of this problem conducted by Murray et al. [Murray et al., 1990]. In this paper the authors decomposed the base flow into the sum of steady and periodic

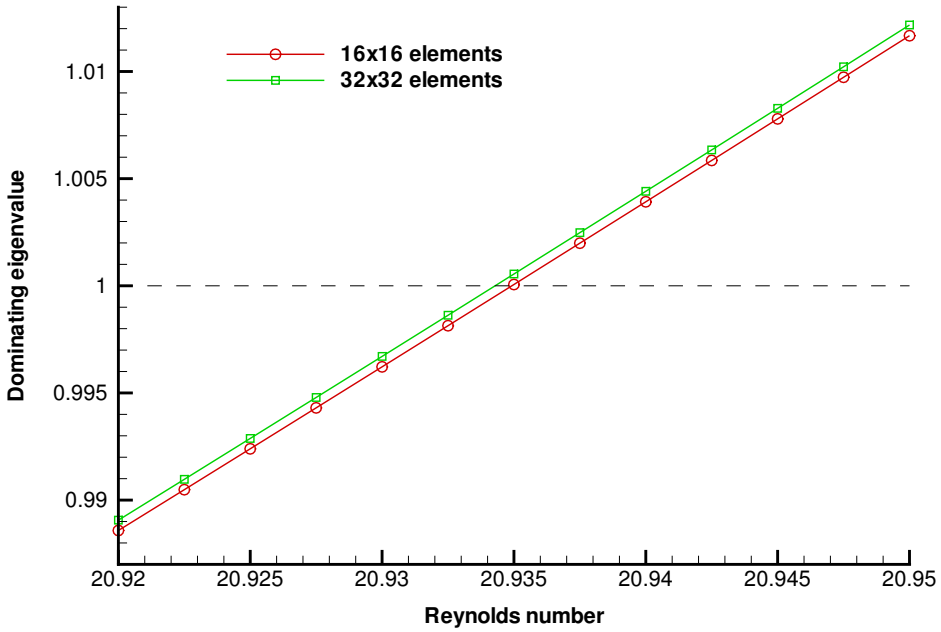

Figure 8.8: Plot of dominant eigenvalue against Reynolds number for the axisymmetric ($m = 0$) mode at two different spatial resolutions, for the parameters $\epsilon = 0.9$, $\omega = 10.58$, $\eta = 0.88$ and $h = \pi/3.2$. The domain was discretised spatially using `LinearisedAxisymmetricQTaylorHoodMultiDomainElements`, and a self-starting BDF2 timestepper with a non-dimensionalised timestep of $2\pi/40\omega$ was employed. The Reynolds number was increased in steps of 0.0025.

components so that the azimuthal velocity is written as

$$\bar{v}(r,t) = V_s(r) + V_p(r,t), \tag{8.62}$$

where the steady part is given analytically by

$$V_s = \frac{\mathrm{Re}^*}{1-\eta^2}\left(\frac{\eta^2}{r\,(1-\eta)^2} - r\,\eta^2\right) \tag{8.63}$$

and the periodic part was determined numerically using the same scheme as the perturbed flow[2]. They then performed a linear stability analysis of the base flow by

[2]We note that throughout this discussion we will adopt Murray et al.'s notation for the three components of the velocity field: hence u, v and w represent the radial, azimuthal and axial components respectively.

writing the field variables in the form

$$\begin{pmatrix} u(r,z,\theta,t) \\ v(r,z,\theta,t) \\ w(r,z,\theta,t) \\ p(r,z,\theta,t) \end{pmatrix} = \begin{pmatrix} 0 \\ \bar{v}(r,t) \\ 0 \\ \bar{p}(r,t) \end{pmatrix} + \begin{pmatrix} \hat{u}(r,t) \\ \hat{v}(r,t) \\ \hat{w}(r,t) \\ \hat{p}(r,t) \end{pmatrix} \exp\left(in\theta + iaz\right), \tag{8.64}$$

where a is the axial wave number and n the azimuthal mode number. They substituted this ansatz into the Navier–Stokes equations to obtain a sixth-order system for the perturbation amplitudes $\hat{u}$, $\hat{v}$, $\hat{w}$ and $\hat{p}$ which is subject to the homogeneous boundary conditions $\hat{u} = \hat{v} = \hat{w} = 0$. The coefficients in the linear problem are periodic, and this motivated the application of Floquet theory, which the authors implemented in two different ways in order to solve the overall stability problem by two distinct approaches. In the first of these the perturbation quantities $\hat{f}(r,t)$ were represented by

$$\hat{f}(r,t) = e^{\sigma t} \sum_{|m| \leq M} f_m(r)\, e^{im\omega t}, \tag{8.65}$$

where σ is a complex growth rate and M is the value of m at which the periodic Fourier series is to be truncated. Substitution of this expansion into the linear system yields a set of coupled boundary value problems in r for the Fourier coefficients $f_m(r)$ in which σ appears as a parameter. This set of problems gives rise to an eigenvalue problem for σ, which the authors solved using the computer code `SUPORT` [Scott and Watts, 1977], choosing a high-order Adams-type timestepping procedure.

The periodic part of the base flow was obtained by assuming a solution of the form

$$V_p(r,t) = \Re\left[V(r)\, e^{i\omega t}\right], \tag{8.66}$$

with appropriate sinusoidal boundary conditions, and substituting this into the governing equations and boundary conditions for the base state to obtain a boundary value problem for $V(r)$. Although $V(r)$, which is complex, has an analytical solution in the form of Kelvin functions, the authors found that it was computationally more efficient to solve for $V(r)$ numerically in the same manner (and at the same time) as the perturbation amplitudes.

Murray et al.'s second approach to solving the stability problem took advantage of the ability to reduce the system of equations for the perturbation amplitudes to a

fourth-order equation for $\hat{u}$ and a second-order equation for $\hat{v}$. A pseudo-spectral technique was then employed by expanding $\hat{u}$ and $\hat{v}$ as a series of Chebyshev polynomials T_n,

$$\hat{u}(r,t) = \sum_{n=0}^{N} u_n(t)\, T_n\big(2\,[r - \eta/(1-\eta)] - 1\big) \tag{8.67}$$

and

$$\hat{v}(r,t) = \sum_{n=0}^{N} v_n(t)\, T_n\big(2\,[r - \eta/(1-\eta)] - 1\big), \tag{8.68}$$

which were required to satisfy the governing equations at specific collocation points. As a result of this discretisation the spatial differential operators in the governing equations are replaced by discrete matrix operators, and the problem becomes a set of coupled ordinary differential algebraic equations in time for the values of $\hat{u}$ and $\hat{v}$ at the collocation points. This system was solved using the computer code `DASSL` [Petzold, 1982], utilising a fifth-order-accurate backward differentiation timestepper. Since in this instance the amplitude of the periodic component of the base flow $V(r)$ was only required at the collocation points, the authors chose to evaluate the Kelvin functions at these points and hence construct V_p according to the analytical solution.

The Floquet analysis in this second approach was carried out by constructing a square fundamental solution matrix of size equal to the number of differential equations, where each column corresponds to a linearly independent solution at the end of one period. The eigenvalues of this matrix are known as Floquet multipliers, from which the complex growth rates are obtained. This approach yields a separate value of σ corresponding to each solution mode, which provides more insight into the relative stability of each mode than the first approach.

Using a combination of these two numerical schemes, Murray et al. performed a range of parameter studies, in part inspired by the experimental results of Walsh and Donnelly [Walsh and Donnelly, 1988]. Only axisymmetric disturbances were considered. For the purposes of validation of the numerical scheme formulated in the current work, we performed a comparison against some of the results quoted by Murray et al. for fixed $\eta = 0.88$ and forcing frequency $\omega = 10.58$. Table 8.2 displays the comparison between the critical Reynolds numbers as determined by Walsh and Donnelly, Murray et al. and the current work, for various values of the modulation amplitude ϵ. We note that Murray et al. convert their definition of the Reynolds number to that used

by Walsh and Donnelly by the relation

$$\widetilde{\mathrm{Re}} = \mathrm{Re}^* \sqrt{\eta/(1-\eta)}, \tag{8.69}$$

and we do the same with the data computed by `oomph-lib`. Two different spatial resolutions were used in these computations: in the first case, both the base flow and the linear perturbation solutions were discretised using the same uniform mesh of 16×16 elements. In the second case, the spatial resolution of both meshes was doubled, and the critical Reynolds number remained unchanged for all values of ϵ. We note that our results agree within 1% to those computed by Murray et al., and within 2.5% to the data collected experimentally by Walsh and Donnelly.

ϵ	0.0	0.3	0.5	0.7	0.9
$\widetilde{\mathrm{Re}}$ (Walsh & Donnelly)	44.5	45.9	47.8	50.8	55.5
$\widetilde{\mathrm{Re}}$ (Murray et al.)	44.5	45.4	47.2	50.5	56.6
$\widetilde{\mathrm{Re}}$ (This work)	44.5	45.4	47.2	50.4	56.7

Table 8.2: Comparison between the critical Reynolds numbers as determined by Walsh and Donnelly, Murray et al. and the current work, for various values of the modulation amplitude ϵ.

In order to ensure that the eigenvectors computed by `oomph-lib` were fully resolved spatially, we compared each field carefully at two different spatial resolutions. Figure 8.9 shows the dominant eigenvector at $\mathrm{Re} = 20.96$ for the higher-resolution computations at four different timesteps over one period. The problem was discretised on a mesh of 32×32 `LinearisedAxisymmetricQTaylorHoodMultiDomainElements`, for the parameters $\epsilon = 0.9$, $\omega = 10.58$, $\eta = 0.88$ and $h = \pi/3.2$. In all four plots 8.9(a)–8.9(d) the right-hand side displays colour contours of azimuthal velocity V_0^C and the left-hand side displays colour contours of pressure P_0^C. On the pressure plots, dark blue and bright red correspond to the minimum and maximum values of the pressure respectively, whereas the legends to the right of the azimuthal velocity plots describe those contours in terms of the non-dimensional velocity. We note that the same contour levels have been used in all figures. The streamlines track the motion of the in-plane velocities U_0^C and W_0^C.

Figure 8.10 plots the time-evolution of a 'slice' (taken at the line $z = 0$) of the radial and azimuthal velocity components of the dominant eigenvector for the same

set of parameters as above. Three complete periods are shown, and we note that when computing the data to produce this figure we suppressed the normalisation of the eigenvector in step (1) of the power method. Because Re $= 20.96$ is very close to (and slightly above) the critical Reynolds number, we note that the dominant eigenvalue is only growing very slightly with each successive period. We can compare this solution to that shown in figure 8.11 for a Reynolds number of 20.50, which is considerably lower than the critical value: in this case, the dominant eigenvector can clearly be seen to be decaying. Figure 8.12 displays the solution for the same problem but at a Reynolds number of 21.50, which is considerably larger than the critical value: here, we observe the dominant eigenvector growing substantially with each successive period, as we would expect.

8.2.4 Implementation

The problem discussed above was implemented as a demonstration code in `oomph-lib`, and its source file,

`time_periodic_taylor_couette.cc,`

is located in the

`demo_drivers/axisym_navier_stokes/time_periodic_taylor_couette/`

directory.

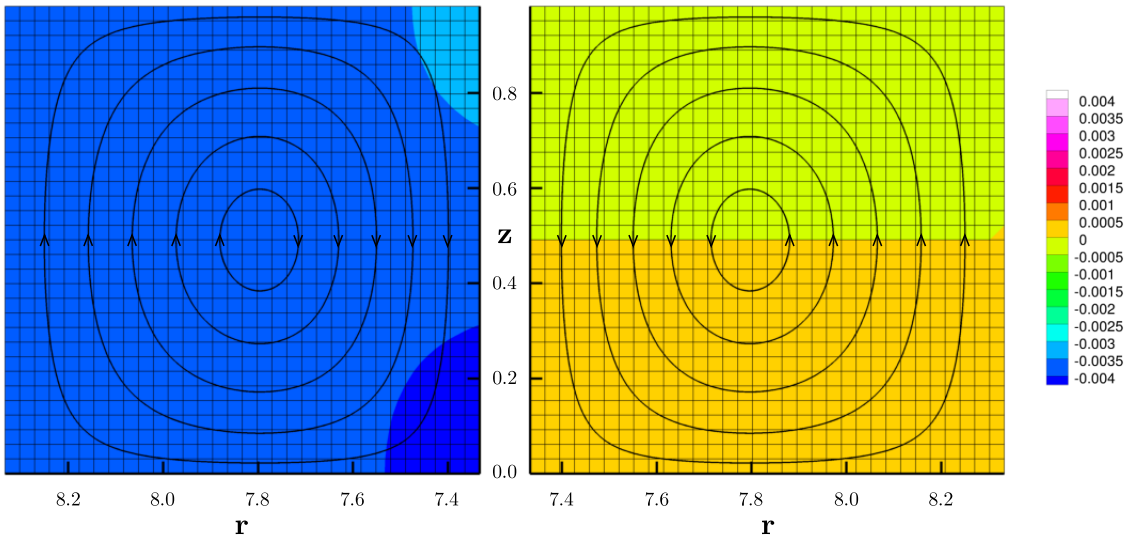

(a) $t = 0.125$

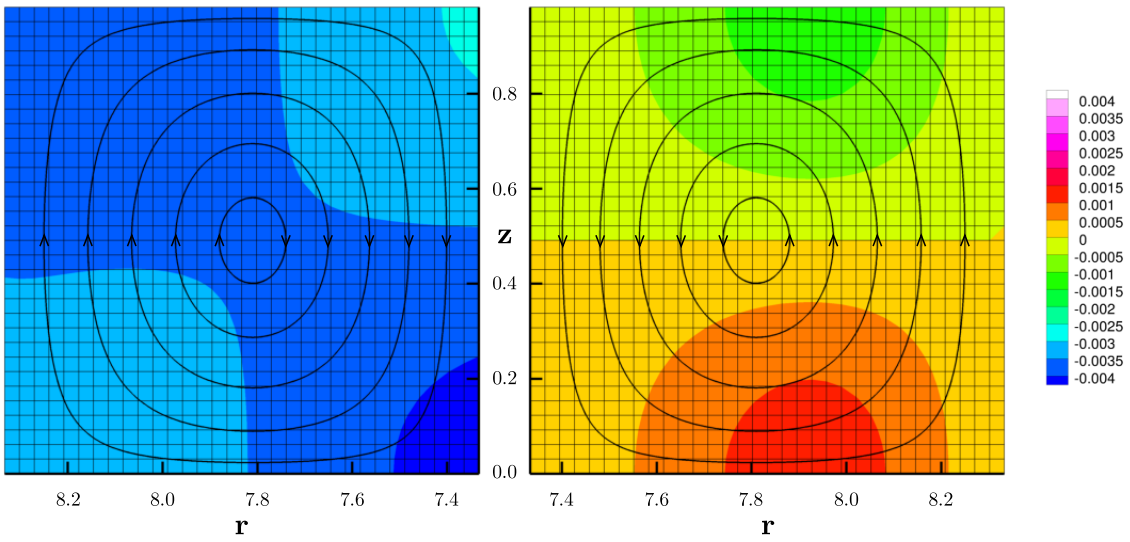

(b) $t = 0.375$

Figure 8.9: Plot of the dominant eigenvector of the axisymmetric ($m = 0$) mode for the parameters $\epsilon = 0.9$, $\omega = 10.58$, Re $= 20.96$, $\eta = 0.88$ and $h = \pi/3.2$, computed on a mesh of 32×32 `LinearisedAxisymmetricQTaylorHoodMultiDomainElements` elements. A self-starting BDF2 timestepper with a non-dimensionalised timestep of $2\pi/40\omega$ has been employed. The solution is shown at four different timesteps over a single period. The right-hand plots display colour contours of azimuthal velocity $V_0^C(r, z)$, as described by the legends to the right of each sub-figure. The left-hand plots display colour contours of the pressure $P_0^C(r, z)$, which vary linearly between the maximum value of 0.0269, shown in bright red, and the minimum value of -0.0269, shown in dark blue, where we have rescaled the pressure so that its mean is zero. On both the left- and right-hand plots, superimposed streamlines track the in-plane velocity.

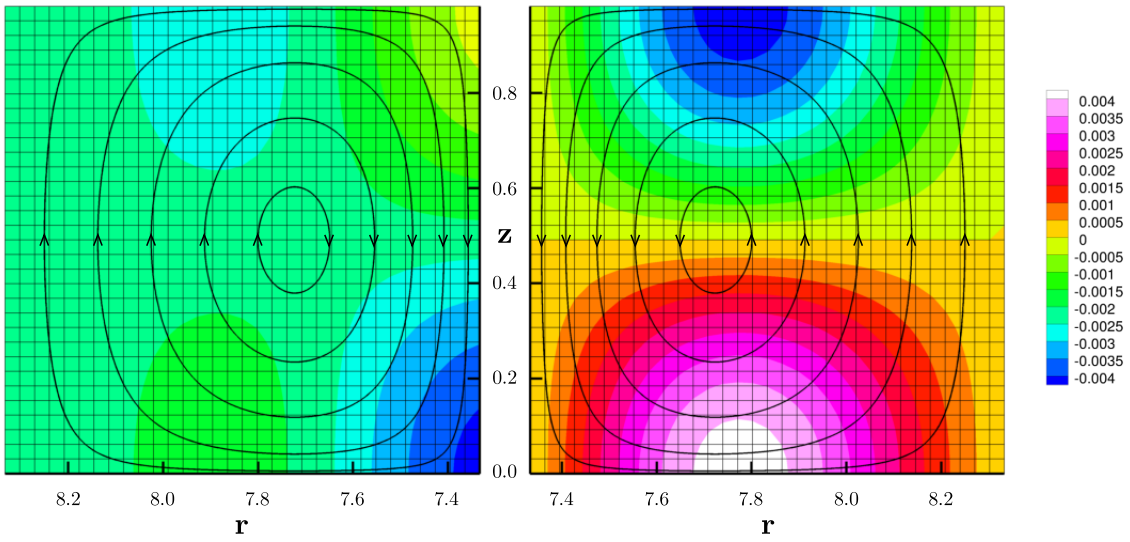

(c) $t = 0.625$

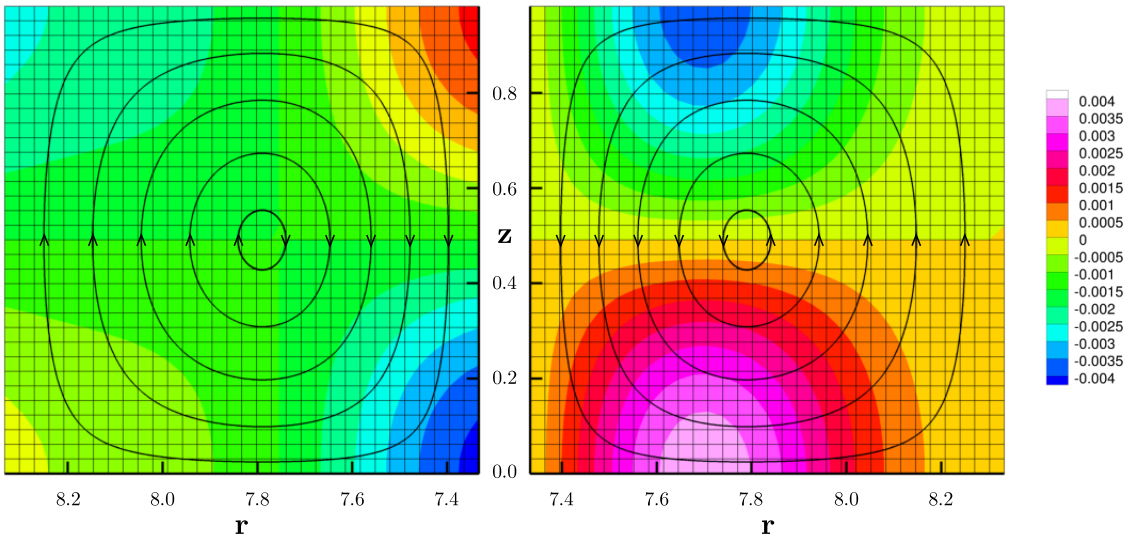

(d) $t = 0.875$

Figure 8.9: Plot of the dominant eigenvector of the axisymmetric ($m = 0$) mode for the parameters $\epsilon = 0.9$, $\omega = 10.58$, Re $= 20.96$, $\eta = 0.88$ and $h = \pi/3.2$, computed on a mesh of 32×32 `LinearisedAxisymmetricQTaylorHoodMultiDomainElements`. A self-starting BDF2 timestepper with a non-dimensionalised timestep of $2\pi/40\omega$ has been employed. The solution is shown at four different timesteps over a single period. The right-hand plots display colour contours of azimuthal velocity $V_0^C(r, z)$, as described by the legends to the right of each sub-figure. The left-hand plots display colour contours of the pressure $P_0^C(r, z)$, which vary linearly between the maximum value of 0.0269, shown in bright red, and the minimum value of -0.0269, shown in dark blue, where we have rescaled the pressure so that its mean is zero. On both the left- and right-hand plots, superimposed streamlines track the in-plane velocity.

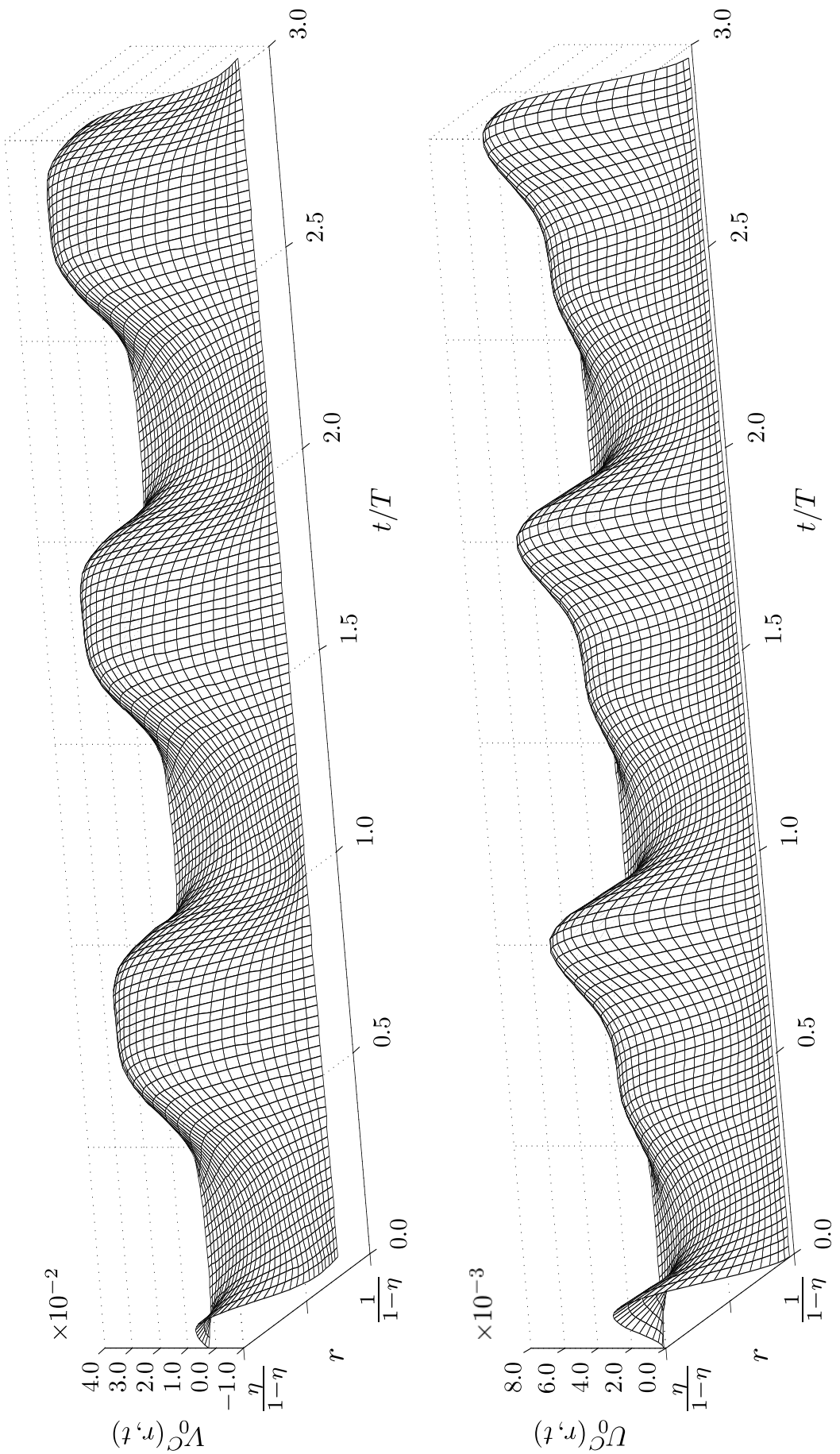

Figure 8.10: Plot of the dominant eigenvector for the parameters $\epsilon = 0.9$, $\omega = 10.58$, $\mathrm{Re} = 20.96$, $\eta = 0.88$ and $h = \pi/3.2$, computed on a mesh of 32×32 `LinearisedAxisymmetricQTaylorHoodMultiDomainElements`. A self-starting BDF2 timestepper with a non-dimensionalised timestep of $2\pi/40\omega$ has been employed. The upper and lower plots display the azimuthal and radial velocities respectively.

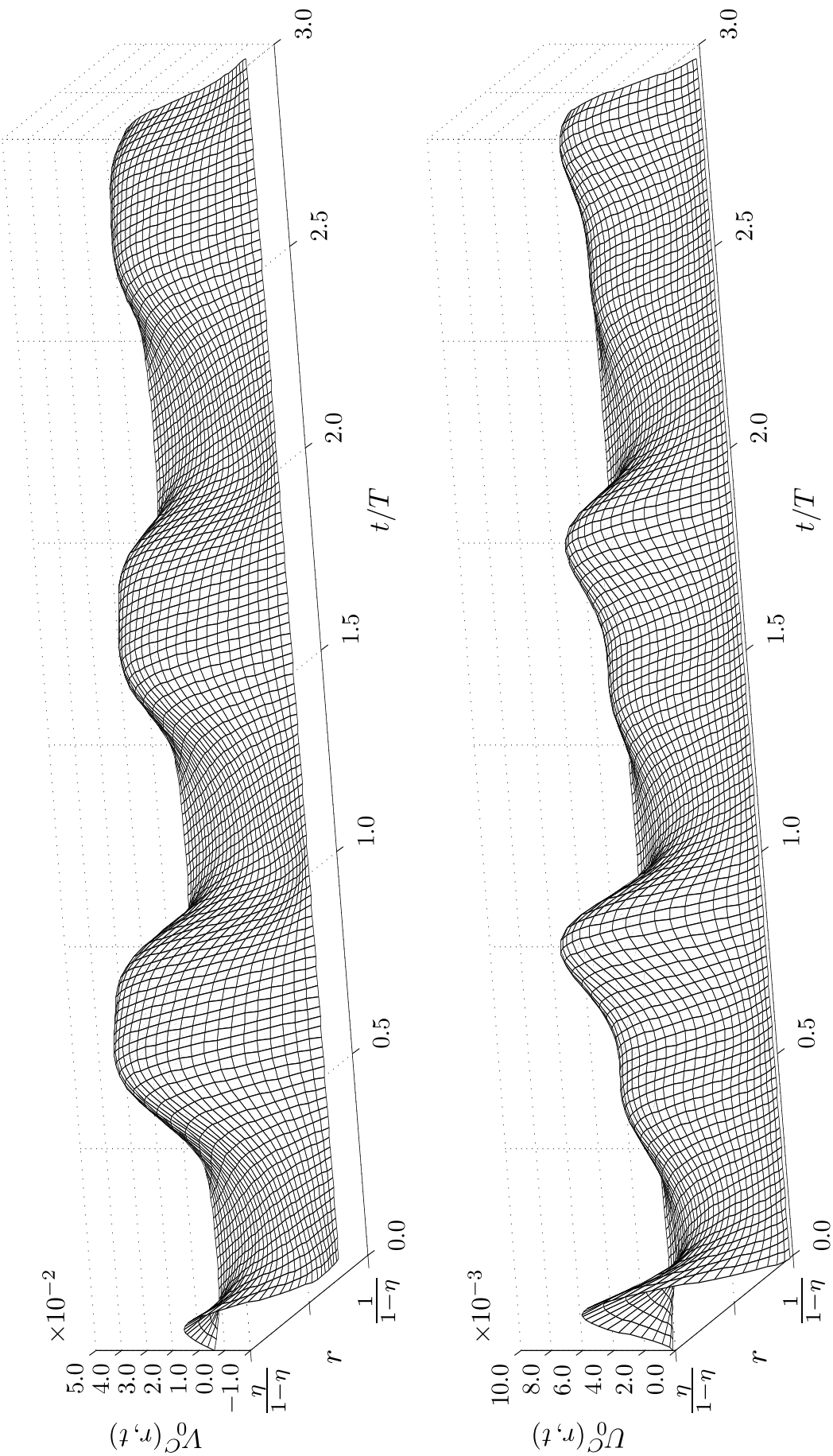

Figure 8.11: Plot of the dominant eigenvector for the parameters $\epsilon = 0.9$, $\omega = 10.58$, $\mathrm{Re} = 20.50$, $\eta = 0.88$ and $h = \pi/3.2$, computed on a mesh of 32×32 `LinearisedAxisymmetricQTaylorHoodMultiDomainElements`. A self-starting BDF2 timestepper with a non-dimensionalised timestep of $2\pi/40\omega$ has been employed. The upper and lower plots display the azimuthal and radial velocities respectively.

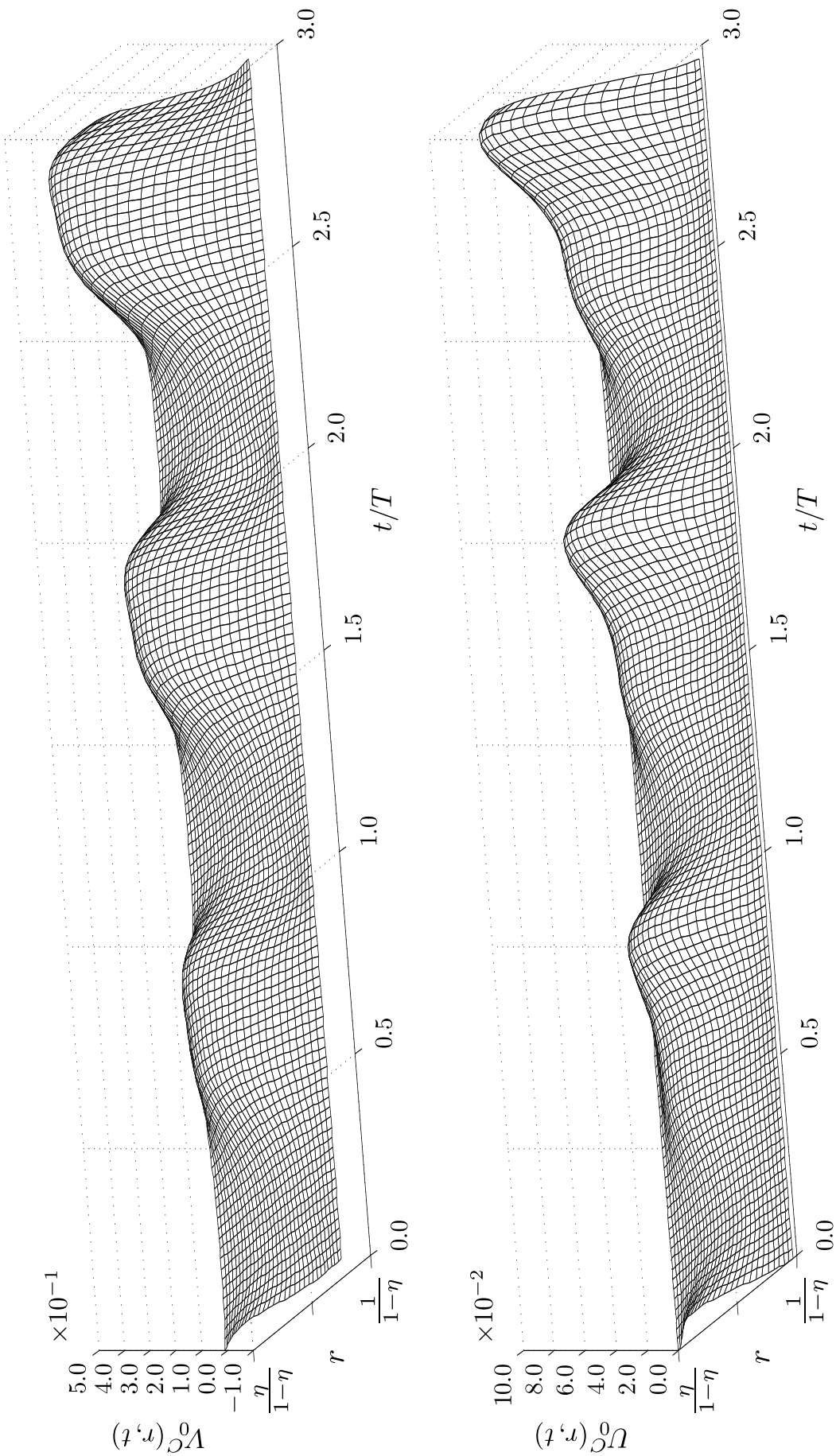

Figure 8.12: Plot of the dominant eigenvector for the parameters $\epsilon = 0.9$, $\omega = 10.58$, $\mathrm{Re} = 21.50$, $\eta = 0.88$ and $h = \pi/3.2$, computed on a mesh of 32×32 `LinearisedAxisymmetricQTaylorHoodMultiDomainElements`. A self-starting BDF2 timestepper with a non-dimensionalised timestep of $2\pi/40\omega$ has been employed. The upper and lower plots display the azimuthal and radial velocities respectively.

Chapter 9

Perturbations to axisymmetric flows: Part two

In this chapter we will continue the discussion of the linearisation of the free surface Navier–Stokes equations in cylindrical coordinates which we began in chapter 7. In that chapter we derived the set of equations which describe a linear, non-axisymmetric perturbation to the bulk axisymmetric equations: here, we will complete the formulation by deriving the free boundary conditions corresponding to a linear, non-axisymmetric perturbation to an otherwise axisymmetric surface.

9.1 Linearisation of the free surface boundary conditions

In section 5.4 we described the boundary conditions which are applied at the interface between two fluids in a general orthogonal coordinate system, and in the following section considered their form in cylindrical polar coordinates if the surface is taken to be axisymmetric. Let us now consider a surface S, again in cylindrical polar coordinates, which is now allowed to vary in the azimuthal direction. As before, we shall parameterise S by $\zeta^1 = \eta$ and $\zeta^2 = \theta$ and establish an explicit connection between the global coordinate system, ξ^i, and the surface coordinates, ζ^α, so that $\xi^1 = R(\zeta^1) = R(\eta)$, $\xi^2 = Z(\zeta^1) = Z(\eta)$ and $\xi^3 = \zeta^2 = \theta$. We can then define the Eulerian position vector

to the surface (at a given time t) to be

$$\mathbf{X}(\eta,\theta) = R(\eta,\theta)\cos\theta\,\mathbf{i} + R(\eta,\theta)\sin\theta\,\mathbf{j} + Z(\eta,\theta)\,\mathbf{k}, \tag{9.1}$$

where $\mathbf{i}$, $\mathbf{j}$ and $\mathbf{k}$ are the Cartesian unit basis vectors as before. Let us now decompose this position vector in the following way,

$$\mathbf{X}(\eta,\theta) = \bar{\mathbf{X}}(\eta) + \epsilon\,\hat{\mathbf{X}}(\eta,\theta), \tag{9.2}$$

where $\epsilon \ll 1$, so that we are considering a small, non-axisymmetric perturbation to an otherwise axisymmetric surface. We note that this is equivalent to performing the decomposition of the global coordinates

$$\begin{aligned} R(\eta,\theta) &= \bar{R}(\eta) + \epsilon\,\hat{R}(\eta,\theta) \quad \text{and} \\ Z(\eta,\theta) &= \bar{Z}(\eta) + \epsilon\,\hat{Z}(\eta,\theta), \end{aligned} \tag{9.3}$$

in exactly the same way as for the bulk equations (equation 7.12 in section 7.1). Substituting (9.3) into (9.1) yields

$$\begin{aligned} \mathbf{X}(\eta,\theta) &= \bar{R}(\eta)\cos\theta\,\mathbf{i} + \bar{R}(\eta)\sin\theta\,\mathbf{j} + \bar{Z}(\eta)\,\mathbf{k} \\ &\quad + \epsilon\left[\hat{R}(\eta,\theta)\cos\theta\,\mathbf{i} + \hat{R}(\eta,\theta)\sin\theta\,\mathbf{j} + \hat{Z}(\eta,\theta)\,\mathbf{k}\right], \end{aligned} \tag{9.4}$$

and it follows from (5.57) that the covariant base vectors of S are given by

$$\begin{aligned} \mathbf{a}_1 &= \frac{\mathrm{d}\bar{R}}{\mathrm{d}\eta}\cos\theta\,\mathbf{i} + \frac{\mathrm{d}\bar{R}}{\mathrm{d}\eta}\sin\theta\,\mathbf{j} + \frac{\mathrm{d}\bar{Z}}{\mathrm{d}\eta}\,\mathbf{k} \\ &\quad + \epsilon\left[\frac{\partial\hat{R}}{\partial\eta}\cos\theta\,\mathbf{i} + \frac{\partial\hat{R}}{\partial\eta}\sin\theta\,\mathbf{j} + \frac{\partial\hat{Z}}{\partial\eta}\,\mathbf{k}\right] \end{aligned} \tag{9.5}$$

and

$$\begin{aligned} \mathbf{a}_2 &= -\bar{R}\,\sin\theta\,\mathbf{i} + \bar{R}\,\cos\theta\,\mathbf{j} \\ &\quad + \epsilon\left[\left(\frac{\partial\hat{R}}{\partial\theta}\cos\theta - \hat{R}\sin\theta\right)\mathbf{i} + \left(\frac{\partial\hat{R}}{\partial\theta}\sin\theta + \hat{R}\cos\theta\right)\mathbf{j} + \frac{\partial\hat{Z}}{\partial\theta}\,\mathbf{k}\right]. \end{aligned} \tag{9.6}$$

The covariant components of the metric surface tensor (5.58) are then given by

$$\begin{aligned} a_{11} &= (\Delta S)^2 + 2\epsilon\left(\frac{\mathrm{d}\bar{R}}{\mathrm{d}\eta}\frac{\partial\hat{R}}{\partial\eta} + \frac{\mathrm{d}\bar{Z}}{\mathrm{d}\eta}\frac{\partial\hat{Z}}{\partial\eta}\right) + \mathrm{O}(\epsilon^2), \\ a_{22} &= \bar{R}^2 + 2\epsilon\bar{R}\hat{R} + \mathrm{O}(\epsilon^2) \end{aligned}$$

and

$$a_{12} = a_{21} = \epsilon\left(\frac{\mathrm{d}\bar{R}}{\mathrm{d}\eta}\frac{\partial\hat{R}}{\partial\theta} + \frac{\mathrm{d}\bar{Z}}{\mathrm{d}\eta}\frac{\partial\hat{Z}}{\partial\theta}\right) + \mathrm{O}(\epsilon^2), \tag{9.7}$$

where

$$(\Delta S)^2 = \left(\frac{\mathrm{d}\bar{R}}{\mathrm{d}\eta}\right)^2 + \left(\frac{\mathrm{d}\bar{Z}}{\mathrm{d}\eta}\right)^2, \tag{9.8}$$

and it follows that its determinant is given by

$$a = \bar{R}^2(\Delta S)^2 + 2\epsilon\bar{R}\left[(\Delta S)^2\hat{R} + \bar{R}\left(\frac{\mathrm{d}\bar{R}}{\mathrm{d}\eta}\frac{\partial\hat{R}}{\partial\eta} + \frac{\mathrm{d}\bar{Z}}{\mathrm{d}\eta}\frac{\partial\hat{Z}}{\partial\eta}\right)\right] + \mathrm{O}(\epsilon^2). \tag{9.9}$$

If we rewrite (9.9) as

$$a = \bar{R}^2(\Delta S)^2\left\{1 + 2\epsilon\left[\frac{\hat{R}}{\bar{R}} + \frac{1}{(\Delta S)^2}\left(\frac{\mathrm{d}\bar{R}}{\mathrm{d}\eta}\frac{\partial\hat{R}}{\partial\eta} + \frac{\mathrm{d}\bar{Z}}{\mathrm{d}\eta}\frac{\partial\hat{Z}}{\partial\eta}\right)\right] + \mathrm{O}(\epsilon^2)\right\} \tag{9.10}$$

then we can use the binomial expansion to evaluate the inverse of a:

$$\frac{1}{a} = \frac{1}{\bar{R}^2(\Delta S)^2} - \frac{2\epsilon}{\bar{R}^2(\Delta S)^2}\left[\frac{\hat{R}}{\bar{R}} + \frac{1}{(\Delta S)^2}\left(\frac{\mathrm{d}\bar{R}}{\mathrm{d}\eta}\frac{\partial\hat{R}}{\partial\eta} + \frac{\mathrm{d}\bar{Z}}{\mathrm{d}\eta}\frac{\partial\hat{Z}}{\partial\eta}\right)\right] + \mathrm{O}(\epsilon^2). \tag{9.11}$$

This allows us to use (5.77) to evaluate the contravariant components of the surface metric tensor,

$$a^{11} = \frac{1}{(\Delta S)^2} - \frac{2\epsilon}{(\Delta S)^4}\left(\frac{\mathrm{d}\bar{R}}{\mathrm{d}\eta}\frac{\partial\hat{R}}{\partial\eta} + \frac{\mathrm{d}\bar{Z}}{\mathrm{d}\eta}\frac{\partial\hat{Z}}{\partial\eta}\right) + \mathrm{O}(\epsilon^2),$$

$$a^{22} = \frac{1}{\bar{R}^2} - \frac{2\epsilon}{\bar{R}^3}\hat{R} + \mathrm{O}(\epsilon^2)$$

and

$$a^{12} = a^{21} = -\frac{\epsilon}{\bar{R}^2(\Delta S)^2}\left(\frac{\mathrm{d}\bar{R}}{\mathrm{d}\eta}\frac{\partial\hat{R}}{\partial\theta} + \frac{\mathrm{d}\bar{Z}}{\mathrm{d}\eta}\frac{\partial\hat{Z}}{\partial\theta}\right) + \mathrm{O}(\epsilon^2), \tag{9.12}$$

and from (5.59) we can now construct the contravariant base vectors of the surface,

$$\begin{aligned}
\mathbf{a}^1 \;=\; & \frac{1}{(\Delta S)^2}\left[\frac{\mathrm{d}\bar{R}}{\mathrm{d}\eta}\cos\theta\,\mathbf{i}+\frac{\mathrm{d}\bar{R}}{\mathrm{d}\eta}\sin\theta\,\mathbf{j}+\frac{\mathrm{d}\bar{Z}}{\mathrm{d}\eta}\,\mathbf{k}\right] \\
& +\frac{\epsilon}{(\Delta S)^4}\left\{\left[\left(\left(\frac{\mathrm{d}\bar{Z}}{\mathrm{d}\eta}\right)^2\frac{\partial\hat{R}}{\partial\eta}-\left(\frac{\mathrm{d}\bar{R}}{\mathrm{d}\eta}\right)^2\frac{\partial\hat{R}}{\partial\eta}-2\frac{\mathrm{d}\bar{R}}{\mathrm{d}\eta}\frac{\mathrm{d}\bar{Z}}{\mathrm{d}\eta}\frac{\partial\hat{Z}}{\partial\eta}\right)\cos\theta\right.\right. \\
& \qquad \left.\left.+\frac{(\Delta S)^2}{\bar{R}}\left(\frac{\mathrm{d}\bar{R}}{\mathrm{d}\eta}\frac{\partial\hat{R}}{\partial\theta}+\frac{\mathrm{d}\bar{Z}}{\mathrm{d}\eta}\frac{\partial\hat{Z}}{\partial\theta}\right)\sin\theta\right]\mathbf{i}\right. \\
& \quad +\left[\left(\left(\frac{\mathrm{d}\bar{Z}}{\mathrm{d}\eta}\right)^2\frac{\partial\hat{R}}{\partial\eta}-\left(\frac{\mathrm{d}\bar{R}}{\mathrm{d}\eta}\right)^2\frac{\partial\hat{R}}{\partial\eta}-2\frac{\mathrm{d}\bar{R}}{\mathrm{d}\eta}\frac{\mathrm{d}\bar{Z}}{\mathrm{d}\eta}\frac{\partial\hat{Z}}{\partial\eta}\right)\sin\theta\right. \\
& \qquad \left.-\frac{(\Delta S)^2}{\bar{R}}\left(\frac{\mathrm{d}\bar{R}}{\mathrm{d}\eta}\frac{\partial\hat{R}}{\partial\theta}+\frac{\mathrm{d}\bar{Z}}{\mathrm{d}\eta}\frac{\partial\hat{Z}}{\partial\theta}\right)\cos\theta\right]\mathbf{j} \\
& \quad \left.+\left[\left(\frac{\mathrm{d}\bar{R}}{\mathrm{d}\eta}\right)^2\frac{\partial\hat{Z}}{\partial\eta}-\left(\frac{\mathrm{d}\bar{Z}}{\mathrm{d}\eta}\right)^2\frac{\partial\hat{Z}}{\partial\eta}-2\frac{\mathrm{d}\bar{R}}{\mathrm{d}\eta}\frac{\mathrm{d}\bar{Z}}{\mathrm{d}\eta}\frac{\partial\hat{R}}{\partial\eta}\right]\mathbf{k}\right\}+\mathrm{O}(\epsilon^2) \qquad (9.13)
\end{aligned}$$

and

$$\begin{aligned}
\mathbf{a}^2 \;=\; & \frac{1}{\bar{R}}\left[-\sin\theta\,\mathbf{i}+\cos\theta\,\mathbf{j}\right] \\
& +\frac{\epsilon}{\bar{R}^2}\left\{\left[\frac{1}{(\Delta S)^2}\frac{\mathrm{d}\bar{Z}}{\mathrm{d}\eta}\left(\frac{\mathrm{d}\bar{Z}}{\mathrm{d}\eta}\frac{\partial\hat{R}}{\partial\theta}-\frac{\mathrm{d}\bar{R}}{\mathrm{d}\eta}\frac{\partial\hat{Z}}{\partial\theta}\right)\cos\theta+\hat{R}\sin\theta\right]\mathbf{i}\right. \\
& \quad +\left[\frac{1}{(\Delta S)^2}\frac{\mathrm{d}\bar{Z}}{\mathrm{d}\eta}\left(\frac{\mathrm{d}\bar{Z}}{\mathrm{d}\eta}\frac{\partial\hat{R}}{\partial\theta}-\frac{\mathrm{d}\bar{R}}{\mathrm{d}\eta}\frac{\partial\hat{Z}}{\partial\theta}\right)\sin\theta-\hat{R}\cos\theta\right]\mathbf{j} \\
& \quad \left.+\frac{1}{(\Delta S)^2}\frac{\mathrm{d}\bar{R}}{\mathrm{d}\eta}\left(\frac{\mathrm{d}\bar{R}}{\mathrm{d}\eta}\frac{\partial\hat{Z}}{\partial\theta}-\frac{\mathrm{d}\bar{Z}}{\mathrm{d}\eta}\frac{\partial\hat{R}}{\partial\theta}\right)\mathbf{k}\right\}+\mathrm{O}(\epsilon^2). \qquad (9.14)
\end{aligned}$$

Recall that, as usual, the global coordinates which parametrise Eulerian space are $\xi^1 = r$, $\xi^2 = z$ and $\xi^3 = \theta$. From (5.90) and (5.93) the global covariant and contravariant basis vectors are therefore

$$\begin{aligned}
\mathbf{g}_1 &= \cos\theta\,\mathbf{i}+\sin\theta\,\mathbf{j}, \\
\mathbf{g}_2 &= \mathbf{k}, \\
\mathbf{g}_3 &= -r\sin\theta\,\mathbf{i}+r\cos\theta\,\mathbf{j} \qquad (9.15)
\end{aligned}$$

and

$$\begin{aligned}
\mathbf{g}^1 &= \cos\theta\,\mathbf{i}+\sin\theta\,\mathbf{j}, \\
\mathbf{g}^2 &= \mathbf{k}, \\
\mathbf{g}^3 &= -\frac{1}{r}\sin\theta\,\mathbf{i}+\frac{1}{r}\cos\theta\,\mathbf{j}. \qquad (9.16)
\end{aligned}$$

We now wish to evaluate these basis vectors at a particular (given) Eulerian position on a surface parametrised by (η, θ), and hence we must decompose the Eulerian coordinates as above (9.3) so that

$$\mathbf{g}_3 \;=\; -\left(\bar{R}+\epsilon\hat{R}\right)\sin\theta\,\mathbf{i}+\left(\bar{R}+\epsilon\hat{R}\right)\cos\theta\,\mathbf{j} \tag{9.17}$$

and

$$\mathbf{g}^3 \;=\; -\left(\frac{1}{\bar{R}}-\epsilon\frac{\hat{R}}{\bar{R}^2}+\mathrm{O}(\epsilon^2)\right)\sin\theta\,\mathbf{i}+\left(\frac{1}{\bar{R}}-\epsilon\frac{\hat{R}}{\bar{R}^2}+\mathrm{O}(\epsilon^2)\right)\cos\theta\,\mathbf{j}. \tag{9.18}$$

The derivatives of the global contravariant base vectors $\mathbf{g}^i$ with respect to the surface coordinates ζ^α are then given by

$$\begin{aligned}
\frac{\partial\mathbf{g}^1}{\partial\eta} \;&=\; \mathbf{0}, & \frac{\partial\mathbf{g}^1}{\partial\theta} \;&=\; -\sin\theta\,\mathbf{i}+\cos\theta\,\mathbf{j},\\
\frac{\partial\mathbf{g}^2}{\partial\eta} \;&=\; \mathbf{0}, & \frac{\partial\mathbf{g}^2}{\partial\theta} \;&=\; \mathbf{0},
\end{aligned} \tag{9.19}$$

$$\frac{\partial\mathbf{g}^3}{\partial\eta} \;=\; \frac{1}{\bar{R}^2}\left[-\frac{\mathrm{d}\bar{R}}{\mathrm{d}\eta}+\epsilon\left(\frac{2\hat{R}}{\bar{R}}\frac{\mathrm{d}\bar{R}}{\mathrm{d}\eta}-\frac{\partial\hat{R}}{\partial\eta}\right)+\mathrm{O}(\epsilon^2)\right]\left(-\sin\theta\,\mathbf{i}+\cos\theta\,\mathbf{j}\right) \tag{9.20}$$

and

$$\begin{aligned}
\frac{\partial\mathbf{g}^3}{\partial\theta} \;=\; &\left[-\frac{1}{\bar{R}}\cos\theta+\frac{\epsilon}{\bar{R}^2}\left(\hat{R}\cos\theta+\frac{\partial\hat{R}}{\partial\theta}\sin\theta\right)+\mathrm{O}(\epsilon^2)\right]\mathbf{i}\\
&+\left[-\frac{1}{\bar{R}}\sin\theta+\frac{\epsilon}{\bar{R}^2}\left(\hat{R}\sin\theta-\frac{\partial\hat{R}}{\partial\theta}\cos\theta\right)+\mathrm{O}(\epsilon^2)\right]\mathbf{j}.
\end{aligned} \tag{9.21}$$

The dynamic condition

From section 5.4 we know that the contributions which are made to the i-th momentum equation by the dynamic boundary condition are given by

$$\begin{aligned}
\mathcal{R}_i^{[\mathrm{f,fs}]} = &-\iint_\Omega p_{\mathrm{ext}}\,n^i\,\phi^{[\mathrm{f}]}\,\mathrm{d}S+\frac{1}{\mathrm{Ca}}\oint_{\partial\Omega} m^i\,\phi^{[\mathrm{f}]}\,\mathrm{d}\lambda-\frac{1}{\mathrm{Ca}}\iint_\Omega \mathbf{a}^\alpha\cdot\frac{\partial\mathbf{g}^i}{\partial\zeta^\alpha}\,\phi^{[\mathrm{f}]}\,\mathrm{d}S\\
&-\frac{1}{\mathrm{Ca}}\iint_\Omega\frac{1}{a}\left[\mathbf{g}^i\cdot\mathbf{a}_1\left(a_{22}\frac{\partial\phi^{[\mathrm{f}]}}{\partial\zeta^1}-a_{21}\frac{\partial\phi^{[\mathrm{f}]}}{\partial\zeta^2}\right)+\mathbf{g}^i\cdot\mathbf{a}_2\left(a_{11}\frac{\partial\phi^{[\mathrm{f}]}}{\partial\zeta^2}-a_{12}\frac{\partial\phi^{[\mathrm{f}]}}{\partial\zeta^1}\right)\right]\mathrm{d}S,
\end{aligned} \tag{9.22}$$

and using (9.7) and (9.11) this becomes

$$\begin{aligned}\mathcal{R}_i^{[\mathrm{f,fs}]} = &- \iint_\Omega p_{\mathrm{ext}}\, n^i\, \phi^{[\mathrm{f}]}\, \mathrm{d}S + \frac{1}{\mathrm{Ca}} \oint_{\partial\Omega} m^i\, \phi^{[\mathrm{f}]}\, \mathrm{d}\lambda - \frac{1}{\mathrm{Ca}} \iint_\Omega \mathbf{a}^\alpha \cdot \frac{\partial \mathbf{g}^i}{\partial \zeta^\alpha}\, \phi^{[\mathrm{f}]}\, \mathrm{d}S \\ &- \frac{1}{\mathrm{Ca}} \iint_\Omega \mathbf{g}^i \cdot \mathbf{a}_1 \left\{ \frac{1}{(\Delta S)^2} \frac{\partial \phi^{[\mathrm{f}]}}{\partial \eta} - \frac{\epsilon}{(\Delta S)^2} \left[\frac{1}{\bar{R}^2} \left(\frac{\mathrm{d}\bar{R}}{\mathrm{d}\eta} \frac{\partial \hat{R}}{\partial \theta} + \frac{\mathrm{d}\bar{Z}}{\mathrm{d}\eta} \frac{\partial \hat{Z}}{\partial \theta} \right) \frac{\partial \phi^{[\mathrm{f}]}}{\partial \theta} \right.\right. \\ &\qquad \left.\left. + \frac{2}{(\Delta S)^2} \left(\frac{\mathrm{d}\bar{R}}{\mathrm{d}\eta} \frac{\partial \hat{R}}{\partial \eta} + \frac{\mathrm{d}\bar{Z}}{\mathrm{d}\eta} \frac{\partial \hat{Z}}{\partial \eta} \right) \frac{\partial \phi^{[\mathrm{f}]}}{\partial \eta} \right] + \mathrm{O}(\epsilon^2) \right\} \mathrm{d}S \\ &- \frac{1}{\mathrm{Ca}} \iint_\Omega \mathbf{g}^i \cdot \mathbf{a}_2 \left\{ \frac{1}{\bar{R}^2} \frac{\partial \phi^{[\mathrm{f}]}}{\partial \theta} - \frac{\epsilon}{\bar{R}^2} \left[2 \frac{\hat{R}}{\bar{R}} \frac{\partial \phi^{[\mathrm{f}]}}{\partial \theta} \right.\right. \\ &\qquad \left.\left. + \frac{1}{(\Delta S)^2} \left(\frac{\mathrm{d}\bar{R}}{\mathrm{d}\eta} \frac{\partial \hat{R}}{\partial \theta} + \frac{\mathrm{d}\bar{Z}}{\mathrm{d}\eta} \frac{\partial \hat{Z}}{\partial \theta} \right) \frac{\partial \phi^{[\mathrm{f}]}}{\partial \eta} \right] + \mathrm{O}(\epsilon^2) \right\} \mathrm{d}S. \end{aligned} \tag{9.23}$$

In order to evaluate this we must first construct the following terms,

$$\begin{aligned} \mathbf{a}^\alpha \cdot \frac{\partial \mathbf{g}^1}{\partial \zeta^\alpha} &= \frac{1}{\bar{R}} - \epsilon \frac{\hat{R}}{\bar{R}^2} + \mathrm{O}(\epsilon^2), \\ \mathbf{a}^\alpha \cdot \frac{\partial \mathbf{g}^2}{\partial \zeta^\alpha} &= 0, \\ \mathbf{a}^\alpha \cdot \frac{\partial \mathbf{g}^3}{\partial \zeta^\alpha} &= \frac{2\epsilon}{\bar{R}^3 (\Delta S)^2} \frac{\mathrm{d}\bar{Z}}{\mathrm{d}\eta} \left(\frac{\mathrm{d}\bar{R}}{\mathrm{d}\eta} \frac{\partial \hat{Z}}{\partial \theta} - \frac{\mathrm{d}\bar{Z}}{\mathrm{d}\eta} \frac{\partial \hat{R}}{\partial \theta} \right) + \mathrm{O}(\epsilon^2), \end{aligned} \tag{9.24}$$

as well as the scalar products of the global contravariant base vectors with the surface covariant base vectors,

$$\begin{aligned} \mathbf{g}^1 \cdot \mathbf{a}_1 &= \frac{\mathrm{d}\bar{R}}{\mathrm{d}\eta} + \epsilon \frac{\partial \hat{R}}{\partial \eta}, & \mathbf{g}^1 \cdot \mathbf{a}_2 &= \epsilon \frac{\partial \hat{R}}{\partial \theta}, \\ \mathbf{g}^2 \cdot \mathbf{a}_1 &= \frac{\mathrm{d}\bar{Z}}{\mathrm{d}\eta} + \epsilon \frac{\partial \hat{Z}}{\partial \eta}, & \mathbf{g}^2 \cdot \mathbf{a}_2 &= \epsilon \frac{\partial \hat{Z}}{\partial \theta}, \\ \mathbf{g}^3 \cdot \mathbf{a}_1 &= 0, & \mathbf{g}^3 \cdot \mathbf{a}_2 &= 1 + \mathrm{O}(\epsilon^2). \end{aligned} \tag{9.25}$$

We can now use (9.24) and (9.25) to consider each component of (9.23) separately:

$$\begin{aligned}\mathcal{R}_{\mathrm{r}}^{[\mathrm{f,fs}]} = &- \iint_\Omega p_{\mathrm{ext}}\, n_r\, \phi^{[\mathrm{f}]}\, \mathrm{d}S - \frac{1}{\mathrm{Ca}} \iint_\Omega \left\{ \frac{1}{\bar{R}} - \epsilon \frac{\hat{R}}{\bar{R}^2} + \mathrm{O}(\epsilon^2) \right\} \phi^{[\mathrm{f}]}\, \mathrm{d}S \\ &- \frac{1}{\mathrm{Ca}} \iint_\Omega \left\{ \frac{1}{(\Delta S)^2} \frac{\mathrm{d}\bar{R}}{\mathrm{d}\eta} \frac{\partial \phi^{[\mathrm{f}]}}{\partial \eta} + \frac{\epsilon}{(\Delta S)^2} \right[\\ &\qquad \frac{1}{(\Delta S)^2} \left(\left(\frac{\mathrm{d}\bar{Z}}{\mathrm{d}\eta} \right)^2 \frac{\partial \hat{R}}{\partial \eta} - \left(\frac{\mathrm{d}\bar{R}}{\mathrm{d}\eta} \right)^2 \frac{\partial \hat{R}}{\partial \eta} - 2 \frac{\mathrm{d}\bar{R}}{\mathrm{d}\eta} \frac{\mathrm{d}\bar{Z}}{\mathrm{d}\eta} \frac{\partial \hat{Z}}{\partial \eta} \right) \frac{\partial \phi^{[\mathrm{f}]}}{\partial \eta} \\ &\qquad + \frac{1}{\bar{R}^2} \frac{\mathrm{d}\bar{Z}}{\mathrm{d}\eta} \left(\frac{\mathrm{d}\bar{Z}}{\mathrm{d}\eta} \frac{\partial \hat{R}}{\partial \theta} - \frac{\mathrm{d}\bar{R}}{\mathrm{d}\eta} \frac{\partial \hat{Z}}{\partial \theta} \right) \frac{\partial \phi^{[\mathrm{f}]}}{\partial \theta} \left.\right] + \mathrm{O}(\epsilon^2) \left.\right\} \mathrm{d}S, \end{aligned} \tag{9.26}$$

$$\mathcal{R}_{\mathrm{z}}^{[\mathrm{f,fs}]} = -\iint_{\Omega} p_{\mathrm{ext}}\, n_z\, \phi^{[\mathrm{f}]}\, \mathrm{d}S - \frac{1}{\mathrm{Ca}} \iint_{\Omega} \left\{ \frac{1}{(\Delta S)^2} \frac{\mathrm{d}\bar{Z}}{\mathrm{d}\eta} \frac{\partial \phi^{[\mathrm{f}]}}{\partial \eta} + \frac{\epsilon}{(\Delta S)^2} \left[\frac{1}{(\Delta S)^2} \left(\left(\frac{\mathrm{d}\bar{R}}{\mathrm{d}\eta} \right)^2 \frac{\partial \hat{Z}}{\partial \eta} - \left(\frac{\mathrm{d}\bar{Z}}{\mathrm{d}\eta} \right)^2 \frac{\partial \hat{Z}}{\partial \eta} - 2 \frac{\mathrm{d}\bar{R}}{\mathrm{d}\eta} \frac{\mathrm{d}\bar{Z}}{\mathrm{d}\eta} \frac{\partial \hat{R}}{\partial \eta} \right) \frac{\partial \phi^{[\mathrm{f}]}}{\partial \eta} + \frac{1}{\bar{R}^2} \frac{\mathrm{d}\bar{R}}{\mathrm{d}\eta} \left(\frac{\mathrm{d}\bar{R}}{\mathrm{d}\eta} \frac{\partial \hat{Z}}{\partial \theta} - \frac{\mathrm{d}\bar{Z}}{\mathrm{d}\eta} \frac{\partial \hat{R}}{\partial \theta} \right) \frac{\partial \phi^{[\mathrm{f}]}}{\partial \theta} \right] + \mathrm{O}(\epsilon^2) \right\} \mathrm{d}S \tag{9.27}$$

and

$$\mathcal{R}_{\theta}^{[\mathrm{f,fs}]} = -\iint_{\Omega} \left(\frac{1}{\bar{R}} - \epsilon \frac{\hat{R}}{\bar{R}^2} + \mathrm{O}(\epsilon^2) \right) p_{\mathrm{ext}}\, n_\theta\, \phi^{[\mathrm{f}]}\, \mathrm{d}S - \frac{1}{\mathrm{Ca}} \iint_{\Omega} \left\{ \frac{2\epsilon}{\bar{R}^3 (\Delta S)^2} \frac{\mathrm{d}\bar{Z}}{\mathrm{d}\eta} \left(\frac{\mathrm{d}\bar{R}}{\mathrm{d}\eta} \frac{\partial \hat{Z}}{\partial \theta} - \frac{\mathrm{d}\bar{Z}}{\mathrm{d}\eta} \frac{\partial \hat{R}}{\partial \theta} \right) + \mathrm{O}(\epsilon^2) \right\} \phi^{[\mathrm{f}]}\, \mathrm{d}S - \frac{1}{\mathrm{Ca}} \iint_{\Omega} \left\{ \frac{1}{\bar{R}^2} \frac{\partial \phi^{[\mathrm{f}]}}{\partial \theta} - \frac{\epsilon}{\bar{R}^2} \left[\frac{1}{(\Delta S)^2} \left(\frac{\mathrm{d}\bar{R}}{\mathrm{d}\eta} \frac{\partial \hat{R}}{\partial \theta} + \frac{\mathrm{d}\bar{Z}}{\mathrm{d}\eta} \frac{\partial \hat{Z}}{\partial \theta} \right) \frac{\partial \phi^{[\mathrm{f}]}}{\partial \eta} + 2 \frac{\hat{R}}{\bar{R}} \frac{\partial \phi^{[\mathrm{f}]}}{\partial \theta} \right] + \mathrm{O}(\epsilon^2) \right\} \mathrm{d}S, \tag{9.28}$$

where we have used (5.108) to write the components of the normal vector $\mathbf{n}$ in terms of the $\mathbf{e}_r$, $\mathbf{e}_z$ and $\mathbf{e}_\theta$ basis defined in (5.26)[1]. If we also consider the position vector to the free surface (9.1) written in terms of this basis,

$$\mathbf{X}(\eta, \theta) = R(\eta, \theta)\, \mathbf{e}_r + Z(\eta, \theta)\, \mathbf{e}_z, \tag{9.29}$$

then we can define a unit tangent vector to the *undeformed* surface in the direction of increasing η as

$$\bar{\mathbf{t}} = \left[\frac{\partial \bar{\mathbf{X}}}{\partial \eta} \cdot \frac{\partial \bar{\mathbf{X}}}{\partial \eta} \right]^{-\frac{1}{2}} \frac{\partial \bar{\mathbf{X}}}{\partial \eta} = \frac{1}{(\Delta S)} \left[\frac{\mathrm{d}\bar{R}}{\mathrm{d}\eta}\, \mathbf{e}_r + \frac{\mathrm{d}\bar{Z}}{\mathrm{d}\eta}\, \mathbf{e}_z \right], \tag{9.30}$$

and therefore the radial and axial components of $\bar{\mathbf{t}}$ are given by

$$\bar{t}_r = \frac{1}{(\Delta S)} \frac{\mathrm{d}\bar{R}}{\mathrm{d}\eta} \qquad \text{and} \qquad \bar{t}_z = \frac{1}{(\Delta S)} \frac{\mathrm{d}\bar{Z}}{\mathrm{d}\eta}. \tag{9.31}$$

At any point on the free boundary Ω a unit vector normal to the surface can be found using

$$\mathbf{n} = \Big[(\mathbf{a}_1 \times \mathbf{a}_2) \cdot (\mathbf{a}_1 \times \mathbf{a}_2) \Big]^{-\frac{1}{2}} (\mathbf{a}_1 \times \mathbf{a}_2)\,. \tag{9.32}$$

[1]From this point forward we will neglect the terms containing integrals over the boundary of the free surface since we will only be considering interfaces with 90^o contact angles.

From (9.5) and (9.6) we have

$$\begin{aligned}\mathbf{a}_1 \times \mathbf{a}_2 \;=\; & \bar{R}\left[-\frac{\mathrm{d}\bar{Z}}{\mathrm{d}\eta}\cos\theta\,\mathbf{i} - \frac{\mathrm{d}\bar{Z}}{\mathrm{d}\eta}\sin\theta\,\mathbf{j} + \frac{\mathrm{d}\bar{R}}{\mathrm{d}\eta}\,\mathbf{k}\right] \\ & + \epsilon\left\{\left[\left(\frac{\mathrm{d}\bar{R}}{\mathrm{d}\eta}\frac{\partial\hat{Z}}{\partial\theta} - \frac{\mathrm{d}\bar{Z}}{\mathrm{d}\eta}\frac{\partial\hat{R}}{\partial\theta}\right)\sin\theta - \left(\bar{R}\frac{\partial\hat{Z}}{\partial\eta} + \hat{R}\frac{\mathrm{d}\bar{Z}}{\mathrm{d}\eta}\right)\cos\theta\right]\mathbf{i}\right. \\ & - \left[\left(\frac{\mathrm{d}\bar{R}}{\mathrm{d}\eta}\frac{\partial\hat{Z}}{\partial\theta} - \frac{\mathrm{d}\bar{Z}}{\mathrm{d}\eta}\frac{\partial\hat{R}}{\partial\theta}\right)\sin\theta + \left(\bar{R}\frac{\partial\hat{Z}}{\partial\eta} + \hat{R}\frac{\mathrm{d}\bar{Z}}{\mathrm{d}\eta}\right)\cos\theta\right]\mathbf{j} \\ & \left. + \left[\bar{R}\frac{\partial\hat{R}}{\partial\eta} + \hat{R}\frac{\mathrm{d}\bar{R}}{\mathrm{d}\eta}\right]\mathbf{k}\right\} + \mathrm{O}(\epsilon^2), \end{aligned} \tag{9.33}$$

and we take the scalar product of (9.33) with itself and apply the binomial expansion to give

$$\begin{aligned}&\Big[(\mathbf{a}_1 \times \mathbf{a}_2)\cdot(\mathbf{a}_1 \times \mathbf{a}_2)\Big]^{-\frac{1}{2}} \\ &\qquad = \frac{1}{\bar{R}\,(\Delta S)}\left\{1 - \epsilon\left[\frac{\hat{R}}{\bar{R}} + \frac{1}{(\Delta S)^2}\left(\frac{\mathrm{d}\bar{R}}{\mathrm{d}\eta}\frac{\partial\hat{R}}{\partial\eta} + \frac{\mathrm{d}\bar{Z}}{\mathrm{d}\eta}\frac{\partial\hat{Z}}{\partial\eta}\right)\right] + \mathrm{O}(\epsilon^2)\right\}. \end{aligned} \tag{9.34}$$

Finally we take the product of (9.33) and (9.34) to obtain

$$\begin{aligned}\mathbf{n} \;=\; & \frac{1}{(\Delta S)}\left[-\frac{\mathrm{d}\bar{Z}}{\mathrm{d}\eta}\cos\theta\,\mathbf{i} - \frac{\mathrm{d}\bar{Z}}{\mathrm{d}\eta}\sin\theta\,\mathbf{j} + \frac{\mathrm{d}\bar{R}}{\mathrm{d}\eta}\,\mathbf{k}\right] \\ & + \frac{\epsilon}{(\Delta S)}\left\{\left[\frac{1}{(\Delta S)^2}\frac{\mathrm{d}\bar{R}}{\mathrm{d}\eta}\left(\frac{\mathrm{d}\bar{Z}}{\mathrm{d}\eta}\frac{\partial\hat{R}}{\partial\eta} - \frac{\mathrm{d}\bar{R}}{\mathrm{d}\eta}\frac{\partial\hat{Z}}{\partial\eta}\right)\cos\theta\right.\right. \\ & \qquad \left. - \frac{1}{\bar{R}}\left(\frac{\mathrm{d}\bar{Z}}{\mathrm{d}\eta}\frac{\partial\hat{R}}{\partial\theta} - \frac{\mathrm{d}\bar{R}}{\mathrm{d}\eta}\frac{\partial\hat{Z}}{\partial\eta}\right)\sin\theta\right]\mathbf{i} \\ & \qquad + \left[\frac{1}{(\Delta S)^2}\frac{\mathrm{d}\bar{R}}{\mathrm{d}\eta}\left(\frac{\mathrm{d}\bar{Z}}{\mathrm{d}\eta}\frac{\partial\hat{R}}{\partial\eta} - \frac{\mathrm{d}\bar{R}}{\mathrm{d}\eta}\frac{\partial\hat{Z}}{\partial\eta}\right)\sin\theta\right. \\ & \qquad \left.\left. + \frac{1}{\bar{R}}\left(\frac{\mathrm{d}\bar{Z}}{\mathrm{d}\eta}\frac{\partial\hat{R}}{\partial\theta} - \frac{\mathrm{d}\bar{R}}{\mathrm{d}\eta}\frac{\partial\hat{Z}}{\partial\eta}\right)\cos\theta\right]\mathbf{j}\right. \\ & \qquad \left. + \frac{1}{(\Delta S)^2}\frac{\mathrm{d}\bar{Z}}{\mathrm{d}\eta}\left(\frac{\mathrm{d}\bar{Z}}{\mathrm{d}\eta}\frac{\partial\hat{R}}{\partial\eta} - \frac{\mathrm{d}\bar{R}}{\mathrm{d}\eta}\frac{\partial\hat{Z}}{\partial\eta}\right)\mathbf{k}\right\} + \mathrm{O}(\epsilon^2). \end{aligned} \tag{9.35}$$

Using (5.26) we can write the components of $\mathbf{n}$ in terms of the $\mathbf{e}_r$, $\mathbf{e}_z$ and $\mathbf{e}_\theta$ basis,

$$\begin{aligned} n_r \;&=\; -\frac{1}{(\Delta S)}\frac{\mathrm{d}\bar{Z}}{\mathrm{d}\eta} + \frac{\epsilon}{(\Delta S)^3}\frac{\mathrm{d}\bar{R}}{\mathrm{d}\eta}\left(\frac{\mathrm{d}\bar{Z}}{\mathrm{d}\eta}\frac{\partial\hat{R}}{\partial\eta} - \frac{\mathrm{d}\bar{R}}{\mathrm{d}\eta}\frac{\partial\hat{Z}}{\partial\eta}\right), \\ n_z \;&=\; \frac{1}{(\Delta S)}\frac{\mathrm{d}\bar{R}}{\mathrm{d}\eta} + \frac{\epsilon}{(\Delta S)^3}\frac{\mathrm{d}\bar{Z}}{\mathrm{d}\eta}\left(\frac{\mathrm{d}\bar{Z}}{\mathrm{d}\eta}\frac{\partial\hat{R}}{\partial\eta} - \frac{\mathrm{d}\bar{R}}{\mathrm{d}\eta}\frac{\partial\hat{Z}}{\partial\eta}\right) \quad \text{and} \\ n_\theta \;&=\; \frac{\epsilon}{\bar{R}\,(\Delta S)}\left(\frac{\mathrm{d}\bar{Z}}{\mathrm{d}\eta}\frac{\partial\hat{R}}{\partial\theta} - \frac{\mathrm{d}\bar{R}}{\mathrm{d}\eta}\frac{\partial\hat{Z}}{\partial\theta}\right), \end{aligned} \tag{9.36}$$

before employing (9.31) to obtain

$$\begin{aligned} n_r &= -\bar{t}_z + \frac{\epsilon}{(\Delta S)}\,\bar{t}_r\left(\bar{t}_z\frac{\partial\hat{R}}{\partial\eta} - \bar{t}_r\frac{\partial\hat{Z}}{\partial\eta}\right), \\ n_z &= \bar{t}_r + \frac{\epsilon}{(\Delta S)}\,\bar{t}_z\left(\bar{t}_z\frac{\partial\hat{R}}{\partial\eta} - \bar{t}_r\frac{\partial\hat{Z}}{\partial\eta}\right) \quad \text{and} \\ n_\theta &= \frac{\epsilon}{\bar{R}}\left(\bar{t}_z\frac{\partial\hat{R}}{\partial\theta} - \bar{t}_r\frac{\partial\hat{Z}}{\partial\theta}\right). \end{aligned} \tag{9.37}$$

We can then use (9.31) and (9.37) to rewrite (9.26)–(9.28) as

$$\begin{aligned} \mathcal{R}_{\mathrm{r}}^{[\mathrm{f,fs}]} = &-\iint_\Omega p_{\mathrm{ext}}\left[-\bar{t}_z + \frac{\epsilon}{(\Delta S)}\,\bar{t}_r\left(\bar{t}_z\frac{\partial\hat{R}}{\partial\eta} - \bar{t}_r\frac{\partial\hat{Z}}{\partial\eta}\right)\right]\phi^{[\mathrm{f}]}\,\mathrm{d}S \\ &-\frac{1}{\mathrm{Ca}}\iint_\Omega\left[\frac{1}{\bar{R}} - \epsilon\frac{\hat{R}}{\bar{R}^2}\right]\phi^{[\mathrm{f}]}\,\mathrm{d}S \\ &-\frac{1}{\mathrm{Ca}}\iint_\Omega\left\{\frac{\bar{t}_r}{(\Delta S)}\frac{\partial\phi^{[\mathrm{f}]}}{\partial\eta} + \epsilon\left[\frac{1}{(\Delta S)^2}\left(\bar{t}_z^2\frac{\partial\hat{R}}{\partial\eta} - \bar{t}_r^2\frac{\partial\hat{R}}{\partial\eta} - 2\bar{t}_r\bar{t}_z\frac{\partial\hat{Z}}{\partial\eta}\right)\frac{\partial\phi^{[\mathrm{f}]}}{\partial\eta}\right.\right. \\ &\qquad\left.\left. + \frac{\bar{t}_z}{\bar{R}^2}\left(\bar{t}_z\frac{\partial\hat{R}}{\partial\theta} - \bar{t}_r\frac{\partial\hat{Z}}{\partial\theta}\right)\frac{\partial\phi^{[\mathrm{f}]}}{\partial\theta}\right]\right\}\mathrm{d}S + \mathrm{O}(\epsilon^2), \end{aligned} \tag{9.38}$$

$$\begin{aligned} \mathcal{R}_{\mathrm{z}}^{[\mathrm{f,fs}]} = &-\iint_\Omega p_{\mathrm{ext}}\left[\bar{t}_r + \frac{\epsilon}{(\Delta S)}\,\bar{t}_z\left(\bar{t}_z\frac{\partial\hat{R}}{\partial\eta} - \bar{t}_r\frac{\partial\hat{Z}}{\partial\eta}\right)\right]\phi^{[\mathrm{f}]}\,\mathrm{d}S \\ &-\frac{1}{\mathrm{Ca}}\iint_\Omega\left\{\frac{\bar{t}_z}{(\Delta S)}\frac{\partial\phi^{[\mathrm{f}]}}{\partial\eta} + \epsilon\left[\frac{1}{(\Delta S)^2}\left(\bar{t}_r^2\frac{\partial\hat{Z}}{\partial\eta} - \bar{t}_z^2\frac{\partial\hat{Z}}{\partial\eta} - 2\bar{t}_r\bar{t}_z\frac{\partial\hat{R}}{\partial\eta}\right)\frac{\partial\phi^{[\mathrm{f}]}}{\partial\eta}\right.\right. \\ &\qquad\left.\left. + \frac{\bar{t}_r}{\bar{R}^2}\left(\bar{t}_r\frac{\partial\hat{Z}}{\partial\theta} - \bar{t}_z\frac{\partial\hat{R}}{\partial\theta}\right)\frac{\partial\phi^{[\mathrm{f}]}}{\partial\theta}\right]\right\}\mathrm{d}S + \mathrm{O}(\epsilon^2) \end{aligned} \tag{9.39}$$

and

$$\begin{aligned} \mathcal{R}_{\theta}^{[\mathrm{f,fs}]} = &-\epsilon\iint_\Omega\frac{p_{\mathrm{ext}}}{\bar{R}^2}\left(\bar{t}_z\frac{\partial\hat{R}}{\partial\theta} - \bar{t}_r\frac{\partial\hat{Z}}{\partial\theta}\right)\phi^{[\mathrm{f}]}\,\mathrm{d}S \\ &-\frac{2\epsilon}{\mathrm{Ca}}\iint_\Omega\frac{\bar{t}_z}{\bar{R}^3}\left(\bar{t}_r\frac{\partial\hat{Z}}{\partial\theta} - \bar{t}_z\frac{\partial\hat{R}}{\partial\theta}\right)\phi^{[\mathrm{f}]}\,\mathrm{d}S \\ &-\frac{1}{\mathrm{Ca}}\iint_\Omega\frac{1}{\bar{R}^2}\left\{\frac{\partial\phi^{[\mathrm{f}]}}{\partial\theta} - \epsilon\left[\frac{1}{(\Delta S)}\left(\bar{t}_r\frac{\partial\hat{R}}{\partial\theta} + \bar{t}_z\frac{\partial\hat{Z}}{\partial\theta}\right)\frac{\partial\phi^{[\mathrm{f}]}}{\partial\eta} + 2\frac{\hat{R}}{\bar{R}}\frac{\partial\phi^{[\mathrm{f}]}}{\partial\theta}\right]\right\}\mathrm{d}S \\ &+\mathrm{O}(\epsilon^2). \end{aligned} \tag{9.40}$$

We note that, as expected, taking just the terms of order one in (9.38)–(9.40) yields the contributions that are made to the momentum equations in the purely axisymmetric case (5.116). From this point onwards we shall consider just the terms of order ϵ since these are the terms which will contribute to the momentum equations in the 'linear perturbation problem' formulated in chapter 7.

We recall that a function $f = f(x, y, z)$ can be integrated over a surface Ω which is parametrised by surface coordinates ζ^1 and ζ^2 in the following manner,

$$\iint_S f(x,y,z)\ \mathrm{d}S = \iint_S f(\mathbf{X}(\zeta^1,\zeta^2))\ |\mathbf{a}_1 \times \mathbf{a}_2|\ \mathrm{d}\zeta^1\,\mathrm{d}\zeta^2, \tag{9.41}$$

and from (9.33) we have

$$|\mathbf{a}_1 \times \mathbf{a}_2| = \bar{R}\,(\Delta S) + \epsilon\left[\hat{R}\,(\Delta S) + \frac{\bar{R}}{(\Delta S)}\left(\frac{\mathrm{d}\bar{R}}{\mathrm{d}\eta}\frac{\partial\hat{R}}{\partial\eta} + \frac{\mathrm{d}\bar{Z}}{\mathrm{d}\eta}\frac{\partial\hat{Z}}{\partial\eta}\right)\right] + \mathrm{O}(\epsilon^2). \tag{9.42}$$

Using (9.41) the terms of order ϵ in (9.38)–(9.40) are therefore

$$\begin{aligned}\hat{\mathcal{R}}_{\mathrm{r}}^{[\mathrm{f,fs}]} = &\iint_\Omega p_{\mathrm{ext}}\left[\bar{t}_z\,(\Delta S)\,\hat{R} + \bar{R}\frac{\partial\hat{Z}}{\partial\eta}\right]\phi^{[\mathrm{f}]}\ \mathrm{d}\eta\,\mathrm{d}\theta \\ &-\frac{1}{\mathrm{Ca}}\iint_\Omega\left\{\left(\bar{t}_r\frac{\partial\hat{R}}{\partial\eta} + \bar{t}_z\frac{\partial\hat{Z}}{\partial\eta}\right)\phi^{[\mathrm{f}]}\right. \\ &\qquad + \left[\bar{t}_r\hat{R} + \frac{\bar{R}}{(\Delta S)}\,\bar{t}_z\left(\bar{t}_z\frac{\partial\hat{R}}{\partial\eta} - \bar{t}_r\frac{\partial\hat{Z}}{\partial\eta}\right)\right]\frac{\partial\phi^{[\mathrm{f}]}}{\partial\eta} \\ &\qquad \left. + \frac{(\Delta S)}{\bar{R}}\,\bar{t}_z\left(\bar{t}_z\frac{\partial\hat{R}}{\partial\theta} - \bar{t}_r\frac{\partial\hat{Z}}{\partial\theta}\right)\frac{\partial\phi^{[\mathrm{f}]}}{\partial\theta}\right\}\mathrm{d}\eta\,\mathrm{d}\theta,\end{aligned} \tag{9.43}$$

$$\begin{aligned}\hat{\mathcal{R}}_{\mathrm{z}}^{[\mathrm{f,fs}]} = &-\iint_\Omega p_{\mathrm{ext}}\left[\bar{t}_r\,(\Delta S)\,\hat{R} + \bar{R}\frac{\partial\hat{R}}{\partial\eta}\right]\phi^{[\mathrm{f}]}\ \mathrm{d}\eta\,\mathrm{d}\theta \\ &-\frac{1}{\mathrm{Ca}}\iint_\Omega\left\{\left[\bar{t}_z\hat{R} + \frac{\bar{R}}{(\Delta S)}\,\bar{t}_r\left(\bar{t}_r\frac{\partial\hat{Z}}{\partial\eta} - \bar{t}_z\frac{\partial\hat{R}}{\partial\eta}\right)\right]\frac{\partial\phi^{[\mathrm{f}]}}{\partial\eta}\right. \\ &\qquad \left. + \frac{(\Delta S)}{\bar{R}}\,\bar{t}_r\left(\bar{t}_r\frac{\partial\hat{Z}}{\partial\theta} - \bar{t}_z\frac{\partial\hat{R}}{\partial\theta}\right)\frac{\partial\phi^{[\mathrm{f}]}}{\partial\theta}\right\}\mathrm{d}\eta\,\mathrm{d}\theta\end{aligned} \tag{9.44}$$

and

$$\begin{aligned}\hat{\mathcal{R}}_{\theta}^{[\mathrm{f,fs}]} = &- \iint_{\Omega} p_{\mathrm{ext}} \frac{(\Delta S)}{\bar{R}} \left(\bar{t}_z \frac{\partial \hat{R}}{\partial \theta} - \bar{t}_r \frac{\partial \hat{Z}}{\partial \theta} \right) \phi^{[\mathrm{f}]} \, \mathrm{d}\eta \, \mathrm{d}\theta \\ &- \frac{1}{\mathrm{Ca}} \iint_{\Omega} \left\{ \frac{2\,(\Delta S)}{\bar{R}^2} \, \bar{t}_z \left(\bar{t}_r \frac{\partial \hat{Z}}{\partial \theta} - \bar{t}_z \frac{\partial \hat{R}}{\partial \theta} \right) \phi^{[\mathrm{f}]} \right. \\ &\qquad - \frac{1}{\bar{R}} \left(\bar{t}_r \frac{\partial \hat{R}}{\partial \theta} + \bar{t}_z \frac{\partial \hat{Z}}{\partial \theta} \right) \frac{\partial \phi^{[\mathrm{f}]}}{\partial \eta} \\ &\qquad \left. + \frac{1}{\bar{R}} \left(\bar{t}_r \frac{\partial \hat{R}}{\partial \eta} + \bar{t}_z \frac{\partial \hat{Z}}{\partial \eta} - (\Delta S) \, \frac{\hat{R}}{\bar{R}} \right) \frac{\partial \phi^{[\mathrm{f}]}}{\partial \theta} \right\} \mathrm{d}\eta \, \mathrm{d}\theta. \end{aligned} \tag{9.45}$$

The kinematic condition

From section 5.4 the weak form of the kinematic boundary condition is given by

$$\mathcal{R}^{[\mathrm{h}]} = \iint_{\Omega} \left(u_i \, n^i - \mathrm{St} \, \frac{\partial X_i}{\partial t} \, n^i \right) \phi^{[\mathrm{f}]} \, \mathrm{d}S, \tag{9.46}$$

where u_i and X_i are the components of the velocity and position vector to the free surface relative to the global contravariant basis. Using (5.117) and (5.108) we can write the components of $\mathbf{u}$, $\mathbf{X}$ and $\mathbf{n}$ in terms of the $\mathbf{e}_r$, $\mathbf{e}_z$ and $\mathbf{e}_\theta$ basis defined in (5.26). From (9.29) we can then write the position vector to the surface at time t,

$$\mathbf{X}(\eta, \theta, t) = R(\eta, \theta, t) \, \mathbf{e}_r + Z(\eta, \theta, t) \, \mathbf{e}_z, \tag{9.47}$$

and (9.46) is therefore given by

$$\mathcal{R}^{[\mathrm{h}]} = \iint_{\Omega} \left[u_r \, n_r + u_z \, n_z + u_\theta \, n_\theta - \mathrm{St} \, \frac{\partial R}{\partial t} \, n_r - \mathrm{St} \, \frac{\partial Z}{\partial t} \, n_z \right] \phi^{[\mathrm{f}]} \, \mathrm{d}S. \tag{9.48}$$

We decompose the velocity components in the usual way (7.11) and use (9.3) to obtain

$$\begin{aligned}\mathcal{R}^{[\mathrm{h}]} = \iint_{\Omega} \left\{ \right. &\bar{u}_r \, n_r + \bar{u}_z \, n_z + \bar{u}_\theta \, n_\theta - \mathrm{St} \, \frac{\partial \bar{R}}{\partial t} \, n_r - \mathrm{St} \, \frac{\partial \bar{Z}}{\partial t} \, n_z \\ &+ \epsilon \left[\hat{u}_r \, n_r + \hat{u}_z \, n_z + \hat{u}_\theta \, n_\theta - \mathrm{St} \, \frac{\partial \hat{R}}{\partial t} \, n_r - \mathrm{St} \, \frac{\partial \hat{Z}}{\partial t} \, n_z \right] \left. \right\} \phi^{[\mathrm{f}]} \, \mathrm{d}S, \end{aligned} \tag{9.49}$$

before employing (9.37) to give

$$\mathcal{R}^{[\mathrm{h}]} = \iint_{\Omega} \Bigg\{ -\bar{u}_r\,\bar{t}_z + \bar{u}_z\,\bar{t}_r + \mathrm{St}\,\frac{\partial \bar{R}}{\partial t}\,\bar{t}_z - \mathrm{St}\,\frac{\partial \bar{Z}}{\partial t}\,\bar{t}_r + \epsilon \Bigg[-\hat{u}_r\,\bar{t}_z + \hat{u}_z\,\bar{t}_r + \mathrm{St}\,\frac{\partial \hat{R}}{\partial t}\,\bar{t}_z - \mathrm{St}\,\frac{\partial \hat{Z}}{\partial t}\,\bar{t}_r + \frac{1}{(\Delta S)} \left(\bar{u}_r\,\bar{t}_r + \bar{u}_z\,\bar{t}_z - \mathrm{St}\,\frac{\partial \bar{R}}{\partial t}\,\bar{t}_r - \mathrm{St}\,\frac{\partial \bar{Z}}{\partial t}\,\bar{t}_z \right) \left(\bar{t}_z \frac{\partial \hat{R}}{\partial \eta} - \bar{t}_r \frac{\partial \hat{Z}}{\partial \eta} \right) + \frac{\bar{u}_\theta}{\bar{R}} \left(\bar{t}_z \frac{\partial \hat{R}}{\partial \theta} - \bar{t}_r \frac{\partial \hat{Z}}{\partial \theta} \right) \Bigg] + \mathrm{O}(\epsilon^2) \Bigg\} \phi^{[\mathrm{f}]}\,\mathrm{d}S. \tag{9.50}$$

We note that taking just the terms of order one in the above expression yields the form of the kinematic boundary condition which was derived in section 5.4 for the purely axisymmetric case (5.121). Using (9.41) and considering only the terms of order ϵ in (9.50) gives

$$\hat{\mathcal{R}}^{[\mathrm{h}]} = \iint_{\Omega} \Bigg\{ (\Delta S) \Bigg[-\bar{t}_z \left(\bar{R}\,\hat{u}_r + \hat{R}\,\bar{u}_r \right) + \bar{t}_r \left(\bar{R}\,\hat{u}_z + \hat{R}\,\bar{u}_z \right) + \mathrm{St}\,\bar{t}_z \left(\bar{R} \frac{\partial \hat{R}}{\partial t} + \hat{R} \frac{\partial \bar{R}}{\partial t} \right) - \mathrm{St}\,\bar{t}_r \left(\bar{R} \frac{\partial \hat{Z}}{\partial t} + \hat{R} \frac{\partial \bar{Z}}{\partial t} \right) + \bar{u}_\theta \left(\bar{t}_z \frac{\partial \hat{R}}{\partial \theta} - \bar{t}_r \frac{\partial \hat{Z}}{\partial \theta} \right) \Bigg] - \bar{R} \left(\bar{u}_r - \mathrm{St}\,\frac{\partial \bar{R}}{\partial t} \right) \frac{\partial \hat{Z}}{\partial \eta} + \bar{R} \left(\bar{u}_z - \mathrm{St}\,\frac{\partial \bar{Z}}{\partial t} \right) \frac{\partial \hat{R}}{\partial \eta} \Bigg\} \phi^{[\mathrm{f}]}\,\mathrm{d}\eta\,\mathrm{d}\theta. \tag{9.51}$$

9.2 Fourier decomposition

The dynamic condition

Let us consider the discretised form of the dynamic boundary terms derived in section 9.1. All variables must now be expressed in terms of the local elemental coordinates (s, θ) rather than the global surface coordinates (η, θ). By use of the chain rule, therefore, the discrete residual equations corresponding to the l-th local test function

are given by

$$\begin{aligned}\hat{\mathcal{R}}^{[\mathrm{f,fs}]}_{\mathrm{r}l} = &\int_0^{2\pi}\int_{-1}^{1} p_{\mathrm{ext}}\left[\bar{t}_z\hat{R}\,\mathcal{J}_S + \bar{R}\frac{\partial\hat{Z}}{\partial s}\right]\phi_l^{[\mathrm{f}]}\,\mathrm{d}s\,\mathrm{d}\theta \\ &-\frac{1}{\mathrm{Ca}}\int_0^{2\pi}\int_{-1}^{1}\left\{\left(\bar{t}_r\frac{\partial\hat{R}}{\partial s}+\bar{t}_z\frac{\partial\hat{Z}}{\partial s}\right)\phi_l^{[\mathrm{f}]}\right. \\ &\qquad+\left[\bar{t}_r\hat{R}+\frac{\bar{R}}{\mathcal{J}_S}\,\bar{t}_z\left(\bar{t}_z\frac{\partial\hat{R}}{\partial s}-\bar{t}_r\frac{\partial\hat{Z}}{\partial s}\right)\right]\frac{\partial\phi_l^{[\mathrm{f}]}}{\partial s} \\ &\qquad\left.+\frac{\mathcal{J}_S}{\bar{R}}\,\bar{t}_z\left(\bar{t}_z\frac{\partial\hat{R}}{\partial\theta}-\bar{t}_r\frac{\partial\hat{Z}}{\partial\theta}\right)\frac{\partial\phi_l^{[\mathrm{f}]}}{\partial\theta}\right\}\mathrm{d}s\,\mathrm{d}\theta, \end{aligned} \tag{9.52}$$

$$\begin{aligned}\hat{\mathcal{R}}^{[\mathrm{f,fs}]}_{\mathrm{z}l} = &-\int_0^{2\pi}\int_{-1}^{1} p_{\mathrm{ext}}\left[\bar{t}_r\hat{R}\,\mathcal{J}_S + \bar{R}\frac{\partial\hat{R}}{\partial s}\right]\phi_l^{[\mathrm{f}]}\,\mathrm{d}s\,\mathrm{d}\theta \\ &-\frac{1}{\mathrm{Ca}}\int_0^{2\pi}\int_{-1}^{1}\left\{\left[\bar{t}_z\hat{R}+\frac{\bar{R}}{\mathcal{J}_S}\,\bar{t}_r\left(\bar{t}_r\frac{\partial\hat{Z}}{\partial s}-\bar{t}_z\frac{\partial\hat{R}}{\partial s}\right)\right]\frac{\partial\phi_l^{[\mathrm{f}]}}{\partial s}\right. \\ &\qquad\left.+\frac{\mathcal{J}_S}{\bar{R}}\,\bar{t}_r\left(\bar{t}_r\frac{\partial\hat{Z}}{\partial\theta}-\bar{t}_z\frac{\partial\hat{R}}{\partial\theta}\right)\frac{\partial\phi_l^{[\mathrm{f}]}}{\partial\theta}\right\}\mathrm{d}s\,\mathrm{d}\theta \end{aligned} \tag{9.53}$$

and

$$\begin{aligned}\hat{\mathcal{R}}^{[\mathrm{f,fs}]}_{\theta l} = &-\int_0^{2\pi}\int_{-1}^{1} p_{\mathrm{ext}}\frac{\mathcal{J}_S}{\bar{R}}\left(\bar{t}_z\frac{\partial\hat{R}}{\partial\theta}-\bar{t}_r\frac{\partial\hat{Z}}{\partial\theta}\right)\phi_l^{[\mathrm{f}]}\,\mathrm{d}s\,\mathrm{d}\theta \\ &-\frac{1}{\mathrm{Ca}}\int_0^{2\pi}\int_{-1}^{1}\left\{\frac{2\mathcal{J}_S}{\bar{R}^2}\,\bar{t}_z\left(\bar{t}_r\frac{\partial\hat{Z}}{\partial\theta}-\bar{t}_z\frac{\partial\hat{R}}{\partial\theta}\right)\phi_l^{[\mathrm{f}]}\right. \\ &\qquad-\frac{1}{\bar{R}}\left(\bar{t}_r\frac{\partial\hat{R}}{\partial\theta}+\bar{t}_z\frac{\partial\hat{Z}}{\partial\theta}\right)\frac{\partial\phi_l^{[\mathrm{f}]}}{\partial s} \\ &\qquad\left.+\frac{1}{\bar{R}}\left(\bar{t}_r\frac{\partial\hat{R}}{\partial s}+\bar{t}_z\frac{\partial\hat{Z}}{\partial s}-\frac{\hat{R}}{\bar{R}}\mathcal{J}_S\right)\frac{\partial\phi_l^{[\mathrm{f}]}}{\partial\theta}\right\}\mathrm{d}s\,\mathrm{d}\theta, \end{aligned} \tag{9.54}$$

where we have defined

$$\mathcal{J}_S = (\Delta S)\,\frac{\mathrm{d}\eta}{\mathrm{d}s}. \tag{9.55}$$

As in section 7.3 we can exploit the periodicity of the problem domain in the azimuthal direction to represent the functions $\hat{R}$ and $\hat{Z}$ as Fourier series expansions,

$$\hat{R}(s,\theta,t) = \sum_{k=0}^{\infty}\left[R_k^C(s,t)\cos k\theta + R_k^S(s,t)\sin k\theta\right] \tag{9.56}$$

and

$$\hat{Z}(s,\theta,t) = \sum_{k=0}^{\infty}\left[Z_k^C(s,t)\cos k\theta + Z_k^S(s,t)\sin k\theta\right]. \tag{9.57}$$

We substitute (9.56) and (9.57) into (9.52)–(9.54) and choose the test function

$$\phi_l^{[\mathrm{f,C}]} = \psi_l^{[\mathrm{f}]}(s)\cos m\theta. \tag{9.58}$$

Performing the integral over θ then yields the contributions to the 'cosine' momentum equations,

$$\begin{aligned}\hat{\mathcal{R}}_{\mathrm{r}ml}^{[\mathrm{fC,fs}]} = \gamma_m\,\pi\int_{-1}^{1} p_{\mathrm{ext}}\left[\bar{t}_z R_m^C\,\mathcal{J}_S + \bar{R}\frac{\partial Z_m^C}{\partial s}\right]\psi_l^{[\mathrm{f}]}\,\mathrm{d}s \\ -\frac{\gamma_m\,\pi}{\mathrm{Ca}}\int_{-1}^{1}\Bigg\{\left(\bar{t}_r\frac{\partial R_m^C}{\partial s}+\bar{t}_z\frac{\partial Z_m^C}{\partial s}\right)\psi_l^{[\mathrm{f}]} \\ +\left[\bar{t}_r R_m^C+\frac{\bar{R}}{\mathcal{J}_S}\,\bar{t}_z\left(\bar{t}_z\frac{\partial R_m^C}{\partial s}-\bar{t}_r\frac{\partial Z_m^C}{\partial s}\right)\right]\frac{\partial\psi_l^{[\mathrm{f}]}}{\partial s} \\ +\frac{m^2\mathcal{J}_S}{\bar{R}}\,\bar{t}_z\left(\bar{t}_z R_m^C-\bar{t}_r Z_m^C\right)\psi_l^{[\mathrm{f}]}\Bigg\}\,\mathrm{d}s,\end{aligned} \tag{9.59}$$

$$\begin{aligned}\hat{\mathcal{R}}_{\mathrm{z}ml}^{[\mathrm{fC,fs}]} = -\gamma_m\,\pi\int_{-1}^{1} p_{\mathrm{ext}}\left[\bar{t}_r R_m^C\,\mathcal{J}_S + \bar{R}\frac{\partial R_m^C}{\partial s}\right]\psi_l^{[\mathrm{f}]}\,\mathrm{d}s \\ -\frac{\gamma_m\,\pi}{\mathrm{Ca}}\int_{-1}^{1}\Bigg\{\left[\bar{t}_z R_m^C+\frac{\bar{R}}{\mathcal{J}_S}\,\bar{t}_r\left(\bar{t}_r\frac{\partial Z_m^C}{\partial s}-\bar{t}_z\frac{\partial R_m^C}{\partial s}\right)\right]\frac{\partial\psi_l^{[\mathrm{f}]}}{\partial s} \\ +\frac{m^2\mathcal{J}_S}{\bar{R}}\,\bar{t}_r\left(\bar{t}_r Z_m^C-\bar{t}_z R_m^C\right)\psi_l^{[\mathrm{f}]}\Bigg\}\,\mathrm{d}s\end{aligned} \tag{9.60}$$

and

$$\begin{aligned}\hat{\mathcal{R}}_{\theta ml}^{[\mathrm{fC,fs}]} = \gamma_m\,\pi\int_{-1}^{1} m\,p_{\mathrm{ext}}\frac{\mathcal{J}_S}{\bar{R}}\left(\bar{t}_r Z_m^S-\bar{t}_z R_m^S\right)\psi_l^{[\mathrm{f}]}\,\mathrm{d}s \\ -\frac{\gamma_m\,\pi}{\mathrm{Ca}}\int_{-1}^{1}\Bigg\{\frac{2m\mathcal{J}_S}{\bar{R}^2}\,\bar{t}_z\left(\bar{t}_r Z_m^S-\bar{t}_z R_m^S\right)\psi_l^{[\mathrm{f}]} \\ -\frac{m}{\bar{R}}\left(\bar{t}_r R_m^S+\bar{t}_z Z_m^S\right)\frac{\partial\psi_l^{[\mathrm{f}]}}{\partial s} \\ -\frac{m}{\bar{R}}\left(\bar{t}_r\frac{\partial R_m^S}{\partial s}+\bar{t}_z\frac{\partial Z_m^S}{\partial s}-\frac{R_m^S}{\bar{R}}\mathcal{J}_S\right)\psi_l^{[\mathrm{f}]}\Bigg\}\,\mathrm{d}s.\end{aligned} \tag{9.61}$$

Next we choose the test function

$$\phi_l^{[\mathrm{f,S}]} = \psi_l^{[\mathrm{f}]}(s)\sin m\theta, \tag{9.62}$$

and again perform the integral over θ to evaluate the contributions to the 'sine' momentum equations,

$$\begin{aligned}\hat{\mathcal{R}}^{[\mathrm{fS,fs}]}_{\mathrm{r}ml} = \gamma_m\,\pi\int_{-1}^{1} p_{\mathrm{ext}}\left[\bar{t}_z R^S_m\,\mathcal{J}_S + \bar{R}\frac{\partial Z^S_m}{\partial s}\right]\psi^{[\mathrm{f}]}_l\;\mathrm{d}s \\ -\frac{\gamma_m\,\pi}{\mathrm{Ca}}\int_{-1}^{1}\Bigg\{\left(\bar{t}_r\frac{\partial R^S_m}{\partial s}+\bar{t}_z\frac{\partial Z^S_m}{\partial s}\right)\psi^{[\mathrm{f}]}_l \\ +\left[\bar{t}_r R^S_m+\frac{\bar{R}}{\mathcal{J}_S}\,\bar{t}_z\left(\bar{t}_z\frac{\partial R^S_m}{\partial s}-\bar{t}_r\frac{\partial Z^S_m}{\partial s}\right)\right]\frac{\partial\psi^{[\mathrm{f}]}_l}{\partial s} \\ +\frac{m^2\mathcal{J}_S}{\bar{R}}\,\bar{t}_z\left(\bar{t}_z R^S_m-\bar{t}_r Z^S_m\right)\psi^{[\mathrm{f}]}_l\Bigg\}\,\mathrm{d}s,\end{aligned} \tag{9.63}$$

$$\begin{aligned}\hat{\mathcal{R}}^{[\mathrm{fS,fs}]}_{\mathrm{z}ml} = -\gamma_m\,\pi\int_{-1}^{1} p_{\mathrm{ext}}\left[\bar{t}_r R^S_m\,\mathcal{J}_S + \bar{R}\frac{\partial R^S_m}{\partial s}\right]\psi^{[\mathrm{f}]}_l\;\mathrm{d}s \\ -\frac{\gamma_m\,\pi}{\mathrm{Ca}}\int_{-1}^{1}\Bigg\{\left[\bar{t}_z R^S_m+\frac{\bar{R}}{\mathcal{J}_S}\,\bar{t}_r\left(\bar{t}_r\frac{\partial Z^S_m}{\partial s}-\bar{t}_z\frac{\partial R^S_m}{\partial s}\right)\right]\frac{\partial\psi^{[\mathrm{f}]}_l}{\partial s} \\ +\frac{m^2\mathcal{J}_S}{\bar{R}}\,\bar{t}_r\left(\bar{t}_r Z^S_m-\bar{t}_z R^S_m\right)\psi^{[\mathrm{f}]}_l\Bigg\}\,\mathrm{d}s\end{aligned} \tag{9.64}$$

and

$$\begin{aligned}\hat{\mathcal{R}}^{[\mathrm{fS,fs}]}_{\theta ml} = \gamma_m\,\pi\int_{-1}^{1} m\,p_{\mathrm{ext}}\frac{\mathcal{J}_S}{\bar{R}}\left(\bar{t}_z R^C_m-\bar{t}_r Z^C_m\right)\psi^{[\mathrm{f}]}_l\;\mathrm{d}s \\ -\frac{\gamma_m\,\pi}{\mathrm{Ca}}\int_{-1}^{1}\Bigg\{\frac{2m\mathcal{J}_S}{\bar{R}^2}\,\bar{t}_z\left(\bar{t}_z R^C_m-\bar{t}_r Z^C_m\right)\psi^{[\mathrm{f}]}_l \\ +\frac{m}{\bar{R}}\left(\bar{t}_r R^C_m+\bar{t}_z Z^C_m\right)\frac{\partial\psi^{[\mathrm{f}]}_l}{\partial s} \\ +\frac{m}{\bar{R}}\left(\bar{t}_r\frac{\partial R^C_m}{\partial s}+\bar{t}_z\frac{\partial Z^C_m}{\partial s}-\frac{R^C_m}{\bar{R}}\mathcal{J}_S\right)\psi^{[\mathrm{f}]}_l\Bigg\}\,\mathrm{d}s.\end{aligned} \tag{9.65}$$

The kinematic condition

Let us now consider the discretised form of the kinematic boundary condition derived in section 9.1,

$$\begin{aligned}\hat{\mathcal{R}}^{[\mathrm{h}]}_l = \int_0^{2\pi}\int_{-1}^{1}\Bigg\{\Bigg[-\bar{t}_z\left(\bar{R}\,\hat{u}_r+\hat{R}\,\bar{u}_r\right)+\bar{t}_r\left(\bar{R}\,\hat{u}_z+\hat{R}\,\bar{u}_z\right) \\ +\mathrm{St}\,\bar{t}_z\left(\bar{R}\frac{\partial\hat{R}}{\partial t}+\hat{R}\frac{\partial\bar{R}}{\partial t}\right)-\mathrm{St}\,\bar{t}_r\left(\bar{R}\frac{\partial\hat{Z}}{\partial t}+\hat{R}\frac{\partial\bar{Z}}{\partial t}\right) \\ +\bar{u}_\theta\left(\bar{t}_z\frac{\partial\hat{R}}{\partial\theta}-\bar{t}_r\frac{\partial\hat{Z}}{\partial\theta}\right)\Bigg]\mathcal{J}_S \\ -\bar{R}\left(\bar{u}_r-\mathrm{St}\,\frac{\partial\bar{R}}{\partial t}\right)\frac{\partial\hat{Z}}{\partial s}+\bar{R}\left(\bar{u}_z-\mathrm{St}\,\frac{\partial\bar{Z}}{\partial t}\right)\frac{\partial\hat{R}}{\partial s}\Bigg\}\phi^{[\mathrm{f}]}_l\;\mathrm{d}s\,\mathrm{d}\theta,\end{aligned} \tag{9.66}$$

where all variables are now expressed in terms of elemental coordinates (s, θ) and $\mathcal{J}_S$ is defined in (9.55). We express $\hat{u}_r$, $\hat{u}_z$ and $\hat{u}_\theta$ as Fourier series expansions as defined in (7.57), and use (9.56) and (9.57). We then make these substitutions in (9.66), choose the test function

$$\phi_l^{[\mathrm{f,C}]} = \psi_l^{[\mathrm{f}]}(s) \cos m\theta \tag{9.67}$$

and integrate with respect to θ to obtain

$$\begin{aligned}\hat{\mathcal{R}}_{ml}^{[\mathrm{hC}]} = \gamma_m \, \pi \int_{-1}^{1} \Bigg\{ \Bigg[& - \bar{t}_z \left(\bar{R} \, U_m^C + \bar{u}_r \, R_m^C \right) + \bar{t}_r \left(\bar{R} \, W_m^C + \bar{u}_z \, R_m^C \right) \\ & + \mathrm{St} \, \bar{t}_z \left(\bar{R} \frac{\partial R_m^C}{\partial t} + \frac{\partial \bar{R}}{\partial t} R_m^C \right) - \mathrm{St} \, \bar{t}_r \left(\bar{R} \frac{\partial Z_m^C}{\partial t} + \frac{\partial \bar{Z}}{\partial t} R_m^C \right) \\ & + m \, \bar{u}_\theta \left(\bar{t}_z \, R_m^S - \bar{t}_r \, Z_m^S \right) \Bigg] \mathcal{J}_S \\ & - \bar{R} \left(\bar{u}_r - \mathrm{St} \frac{\partial \bar{R}}{\partial t} \right) \frac{\partial Z_m^C}{\partial s} + \bar{R} \left(\bar{u}_z - \mathrm{St} \frac{\partial \bar{Z}}{\partial t} \right) \frac{\partial R_m^C}{\partial s} \Bigg\} \psi_l^{[\mathrm{f}]} \, \mathrm{d}s. \end{aligned} \tag{9.68}$$

Choosing the test function in (9.66) to be

$$\phi_l^{[\mathrm{f,S}]} = \psi_l^{[\mathrm{f}]}(s) \sin m\theta \tag{9.69}$$

and again integrating with respect to θ yields

$$\begin{aligned}\hat{\mathcal{R}}_{ml}^{[\mathrm{hS}]} = \gamma_m \, \pi \int_{-1}^{1} \Bigg\{ \Bigg[& - \bar{t}_z \left(\bar{R} \, U_m^S + \bar{u}_r \, R_m^S \right) + \bar{t}_r \left(\bar{R} \, W_m^S + \bar{u}_z \, R_m^S \right) \\ & + \mathrm{St} \, \bar{t}_z \left(\bar{R} \frac{\partial R_m^S}{\partial t} + \frac{\partial \bar{R}}{\partial t} R_m^S \right) - \mathrm{St} \, \bar{t}_r \left(\bar{R} \frac{\partial Z_m^S}{\partial t} + \frac{\partial \bar{Z}}{\partial t} R_m^S \right) \\ & - m \, \bar{u}_\theta \left(\bar{t}_z \, R_m^C - \bar{t}_r \, Z_m^C \right) \Bigg] \mathcal{J}_S \\ & - \bar{R} \left(\bar{u}_r - \mathrm{St} \frac{\partial \bar{R}}{\partial t} \right) \frac{\partial Z_m^S}{\partial s} + \bar{R} \left(\bar{u}_z - \mathrm{St} \frac{\partial \bar{Z}}{\partial t} \right) \frac{\partial R_m^S}{\partial s} \Bigg\} \psi_l^{[\mathrm{f}]} \, \mathrm{d}s. \end{aligned} \tag{9.70}$$

9.3 Implementation

We implemented equations (9.59)–(9.61), (9.63)–(9.65), (9.68) and (9.70) in the `get_residual(...)` and `get_jacobian(...)` functions of a newly-developed `Linearised-AxisymmetricFluidInterfaceElement` class, which directly inherits from `FaceElement`.

In a directly analogous fashion to the elements used to compute the interfacial boundary conditions in the base flow, the additional functionality that is specific to the chosen node-strategy is added via two derived classes: `ElasticLinearisedAxisymmetricFluidInterfaceElement` and `PerturbedSpineLinearisedAxisymmetricFluidInterfaceElement`.

The coupling between the perturbation and base flow problems is performed using the 'multi-domain' approach, which we described in section 7.4 and applied to two single-phase problems in chapter 8. In chapter 10 we will be discussing the application of the equations formulated in chapter 7 and the current chapter to the numerical simulation of two-phase flows, where the solutions to both the base flow and perturbation problems are computed on meshes that deform in response to the position of the interface in the *base flow* problem. We recall from section 7.3 that in our general (three–dimensional) formulation of the linear problem the perturbed nodal positions in the radial and axial directions are given (for arbitrary azimuthal mode m) by

$$r(s_1, s_2, \theta, t) = \bar{r}(s_1, s_2, t) + R_m^C(s_1, s_2, t)\cos m\theta + R_m^S(s_1, s_2, t)\sin m\theta \tag{9.71}$$

and

$$z(s_1, s_2, \theta, t) = \bar{z}(s_1, s_2, t) + Z_m^C(s_1, s_2, t)\cos m\theta + Z_m^S(s_1, s_2, t)\sin m\theta. \tag{9.72}$$

In (9.71) and (9.72) the quantities $\bar{r}$ and $\bar{z}$ correspond to the base flow nodal positions, which are by construction also the physical positions at which the nodes in the linear problem are located. The perturbations to these 'base' nodal positions are then represented by the four fields R_m^C, R_m^S, Z_m^C and Z_m^S, which are discretised in the usual way. The discrete unknowns corresponding to the values of these fields at any given node are represented by additional nodal values, which are then updated accordingly by the chosen node-update strategy. If a pseudo-solid approach is employed these unknowns are computed directly (using the equations of elasticity) as part of the solution to the overall problem. If the method of spines is used, these nodal values become 'enslaved' variables that are updated algebraically. We will use this latter method in both the problems considered in the following chapter. Moreover, we will assume that the interface is only ever perturbed in an axial direction and that we can therefore express

this perturbation $\hat{\mathbf{X}}$ at a given time t as

$$\hat{\mathbf{X}}(r,\theta) = \sum_{m=0}^{\infty} \Big[H_m^C(r)\cos m\theta + H_m^S(r)\sin m\theta \Big]\,\mathbf{e}_z, \tag{9.73}$$

where $H_m^C(r)$ and $H_m^S(r)$ are unknowns which need to be determined as part of the solution. They are discretised in the usual way,

$$\begin{aligned} H_m^C(s) &= \sum_{j=1}^{N_{\text{node}}} \widehat{(H_m^C)}_j\, \psi_j^{[\text{f}]}(s), \\ H_m^S(s) &= \sum_{j=1}^{N_{\text{node}}} \widehat{(H_m^S)}_j\, \psi_j^{[\text{f}]}(s), \end{aligned} \tag{9.74}$$

where s is the local coordinate that parametrises the free surface and $\psi^{[\text{f}]}$ are the same shape functions as those used to interpolate the velocity degrees of freedom.

Having discretised $H_m^C(r)$ and $H_m^S(r)$ we now construct the mesh of the linear problem such that its N_{node} nodes are distributed along N_{spine} spines which are oriented so that they are parallel to the z-axis, in exactly the same way as in the base flow problem. As before, each node j is located at a fixed fraction w_j along a particular spine $\hat{s}_j$. Each of these so-called 'perturbed spines' is associated with a corresponding 'base' spine $\bar{s}_j$ in the base flow problem, and we note that this construction requires us to have the same number of nodes in the radial direction in both problems. The perturbed spines differ from those in the base problem by each storing two values for their 'heights', corresponding to the unknown coefficients $\widehat{(H_m^C)}_{\hat{s}}$ and $\widehat{(H_m^S)}_{\hat{s}}$ ($\hat{s} = 1, \ldots, N_{\text{spine}}$). These coefficients are determined by solving the two kinematic conditions at the interface, which from (9.68) and (9.70) are given by

$$\begin{aligned} \hat{\mathcal{R}}_{ml}^{[\text{hC}]} = \gamma_m\,\pi \int_{-1}^{1} \Bigg\{ \Bigg[&- t_z \bar{R}\, U_m^C + t_r \bar{R}\, W_m^C - \text{St}\, t_r \bar{R} \frac{\partial H_m^C}{\partial t} - m\, t_r\, \bar{u}_\theta\, H_m^S \Bigg] \mathcal{J}_S \\ &- \bar{R} \left(\bar{u}_r - \text{St}\, \frac{\partial \bar{R}}{\partial t} \right) \frac{\partial H_m^C}{\partial s} \Bigg\} \psi_l^{[\text{f}]}\, \mathrm{d}s \end{aligned} \tag{9.75}$$

and

$$\begin{aligned} \hat{\mathcal{R}}_{ml}^{[\text{hS}]} = \gamma_m\,\pi \int_{-1}^{1} \Bigg\{ \Bigg[&- t_z \bar{R}\, U_m^S + t_r \bar{R}\, W_m^S - \text{St}\, t_r \bar{R} \frac{\partial H_m^S}{\partial t} + m\, t_r\, \bar{u}_\theta\, H_m^C \Bigg] \mathcal{J}_S \\ &- \bar{R} \left(\bar{u}_r - \text{St}\, \frac{\partial \bar{R}}{\partial t} \right) \frac{\partial H_m^S}{\partial s} \Bigg\} \psi_l^{[\text{f}]}\, \mathrm{d}s. \end{aligned} \tag{9.76}$$

With this machinery in place, the process of updating the bulk nodal positions (in the linear problem) involves two steps. Firstly, the actual Eulerian positions of the

nodes, X_{ij}, are updated so that the position of the interface is the same as in the base flow problem. Since the nodes will only ever move in the axial direction this is achieved by prescribing

$$X_{2j} = w_j \, H_{\bar{s}_j}, \tag{9.77}$$

where $H_{\bar{s}_j}$ is the 'height' of the base spine corresponding to the perturbed spine that node j is associated with[2]. Secondly, the perturbations to the nodal perturbations in the axial direction are updated by directly prescribing their nodal values via

$$\widehat{(Z_m^C)}_j = w_j \, \widehat{(H_m^C)}_{\hat{s}_j} \tag{9.78}$$

and

$$\widehat{(Z_m^S)}_j = w_j \, \widehat{(H_m^S)}_{\hat{s}_j}. \tag{9.79}$$

We note that, as in the base problem, the use of this 'sparse' node-update procedure is advantageous from a computational perspective since the nodal values $\widehat{(Z_m^C)}_j$ and $\widehat{(Z_m^S)}_j$ are merely enslaved variables which are updated algebraically, rather than additional degrees of freedom in the problem. Since we only allow the nodes to move vertically, the nodal values corresponding to radial perturbations of the nodal positions are set to zero everywhere.

Equations (9.75) and (9.76) are implemented in the `get_residual(...)` and `get_jacobian(...)` functions of the `PerturbedSpineLinearisedAxisymmetricFluidInterfaceElement` class. These functions overload those defined in the base class, and we therefore have to re-implement the contributions to the momentum equations that arise from the dynamic boundary conditions, (9.59)–(9.61) and (9.63)–(9.65). In this

[2]Note that in this context we take j to represent the j-th global node, as opposed to the j-th local node inside any particular element.

(more specific) implementation, these contributions are given by

$$\hat{\mathcal{R}}^{[\mathrm{fC,fs}]}_{\mathrm{r}ml} = \gamma_m \,\pi \int_{-1}^{1} p_{\mathrm{ext}} \bar{R} \frac{\partial H^C_m}{\partial s} \psi^{[\mathrm{f}]}_l \,\mathrm{d}s - \frac{\gamma_m \,\pi}{\mathrm{Ca}} \int_{-1}^{1} \bar{t}_z \left[\frac{\partial H^C_m}{\partial s} \psi^{[\mathrm{f}]}_l - \frac{\bar{R}}{\mathcal{J}_S} \bar{t}_r \frac{\partial H^C_m}{\partial s} \frac{\partial \psi^{[\mathrm{f}]}_l}{\partial s} - \frac{m^2 \mathcal{J}_S}{\bar{R}} \bar{t}_r \, H^C_m \psi^{[\mathrm{f}]}_l \right] \mathrm{d}s, \quad (9.80)$$

$$\hat{\mathcal{R}}^{[\mathrm{fC,fs}]}_{\mathrm{z}ml} = - \frac{\gamma_m \,\pi}{\mathrm{Ca}} \int_{-1}^{1} \bar{t}_r^2 \left[\frac{\bar{R}}{\mathcal{J}_S} \frac{\partial H^C_m}{\partial s} \frac{\partial \psi^{[\mathrm{f}]}_l}{\partial s} + \frac{m^2 \mathcal{J}_S}{\bar{R}} H^C_m \, \psi^{[\mathrm{f}]}_l \right] \mathrm{d}s, \quad (9.81)$$

$$\hat{\mathcal{R}}^{[\mathrm{fC,fs}]}_{\theta ml} = \gamma_m \,\pi \, m \int_{-1}^{1} p_{\mathrm{ext}} \frac{\mathcal{J}_S}{\bar{R}} \bar{t}_r \, H^S_m \, \psi^{[\mathrm{f}]}_l \,\mathrm{d}s - \frac{\gamma_m \,\pi \, m}{\mathrm{Ca}} \int_{-1}^{1} \frac{\bar{t}_z}{\bar{R}} \left[\frac{2\mathcal{J}_S}{\bar{R}} \bar{t}_r \, H^S_m \, \psi^{[\mathrm{f}]}_l - H^S_m \frac{\partial \psi^{[\mathrm{f}]}_l}{\partial s} - \frac{\partial H^S_m}{\partial s} \psi^{[\mathrm{f}]}_l \right] \mathrm{d}s, \quad (9.82)$$

$$\hat{\mathcal{R}}^{[\mathrm{fS,fs}]}_{\mathrm{r}ml} = \gamma_m \,\pi \int_{-1}^{1} p_{\mathrm{ext}} \bar{R} \frac{\partial H^S_m}{\partial s} \psi^{[\mathrm{f}]}_l \,\mathrm{d}s - \frac{\gamma_m \,\pi}{\mathrm{Ca}} \int_{-1}^{1} \bar{t}_z \left[\frac{\partial H^S_m}{\partial s} \psi^{[\mathrm{f}]}_l - \frac{\bar{R}}{\mathcal{J}_S} \bar{t}_r \frac{\partial H^S_m}{\partial s} \frac{\partial \psi^{[\mathrm{f}]}_l}{\partial s} - \frac{m^2 \mathcal{J}_S}{\bar{R}} \bar{t}_r \, H^S_m \psi^{[\mathrm{f}]}_l \right] \mathrm{d}s, \quad (9.83)$$

$$\hat{\mathcal{R}}^{[\mathrm{fS,fs}]}_{\mathrm{z}ml} = - \frac{\gamma_m \,\pi}{\mathrm{Ca}} \int_{-1}^{1} \bar{t}_r^2 \left[\frac{\bar{R}}{\mathcal{J}_S} \frac{\partial H^S_m}{\partial s} \frac{\partial \psi^{[\mathrm{f}]}_l}{\partial s} + \frac{m^2 \mathcal{J}_S}{\bar{R}} H^S_m \, \psi^{[\mathrm{f}]}_l \right] \mathrm{d}s \qquad \text{and} \quad (9.84)$$

$$\hat{\mathcal{R}}^{[\mathrm{fS,fs}]}_{\theta ml} = - \gamma_m \,\pi \, m \int_{-1}^{1} p_{\mathrm{ext}} \frac{\mathcal{J}_S}{\bar{R}} \bar{t}_r \, H^C_m \, \psi^{[\mathrm{f}]}_l \,\mathrm{d}s - \frac{\gamma_m \,\pi \, m}{\mathrm{Ca}} \int_{-1}^{1} \frac{\bar{t}_z}{\bar{R}} \left[- \frac{2\mathcal{J}_S}{\bar{R}} \bar{t}_r \, H^C_m \, \psi^{[\mathrm{f}]}_l + H^C_m \frac{\partial \psi^{[\mathrm{f}]}_l}{\partial s} + \frac{\partial H^C_m}{\partial s} \psi^{[\mathrm{f}]}_l \right] \mathrm{d}s. \quad (9.85)$$

Following the structure of the 'standard' spines implementation, we developed a 'perturbed spine' class hierarchy. The actual perturbed spines themselves are defined in the `PerturbedSpine` class, and the `PerturbedSpineElement<BULK_ELEMENT>` takes an existing element as a template parameter and adds the necessary functionality to allow the element to be updated using perturbed spines.

Chapter 10

Applications to two-phase flows

In chapter 7 we derived the equations which describe a linear, non-axisymmetric perturbation to an axisymmetric flow governed by the Navier–Stokes equations in a cylindrical coordinate system. In the previous chapter we then extended this formulation by deriving the corresponding free boundary conditions. This extended formulation allows us to study linear perturbations to arbitrary axisymmetric two-phase flows in cylindrical geometries. We shall illustrate the use of these equations by applying them to two problems. In the first of these, we revisit the example described in section 6.2. We solve this (fully-axisymmetric) problem using the decomposition described in chapters 7 and 9 in order to demonstrate the methodology, and compare the results to those obtained previously using the single, fully-nonlinear code. The second problem concerns the time-evolution of non-axisymmetric modes in a two-phase flow in which a non-axisymmetric interface is allowed to relax under the influence of surface tension and gravitational forces.

10.1 Axisymmetric perturbations to an axisymmetric base flow

We consider the problem sketched in figure 10.1, in which two immiscible, incompressible viscous fluids are contained within a cylindrical vessel. The physical problem is exactly the same as that discussed in section 6.2 of this work: The governing equations have to be solved in the domain $r \in [0, 1]$, $z \in [0, 2]$, with gravity acting in the negative

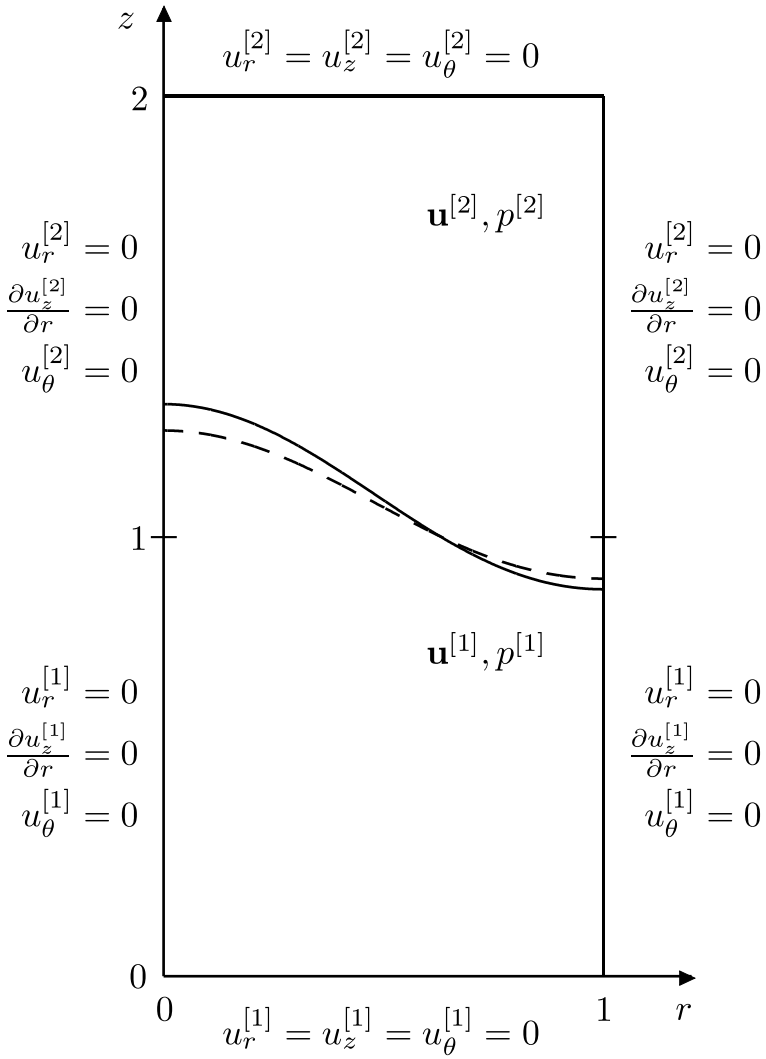

Figure 10.1: Sketch of an axisymmetric two layer interface problem which has been decomposed into two problems: a base flow and a perturbation to this base flow. The dashed line corresponds to the position of the interface in the base flow, while the solid line represents the 'actual' interface position, which can be obtained by combining the base flow position with the perturbation to that position (as described in equation 10.2).

z direction. The axis of the cylindrical container is located at $r = 0$ where we apply the symmetry condition $u_r = u_\theta = 0$. This condition is also applied at the 'slippery' outer wall ($r = 1$), as before. We apply the no-slip condition $u_r = u_z = u_\theta = 0$ at the top and bottom solid boundaries ($z = 0$ and $z = 2$). The interface is located at $\mathbf{X}$ and is subject to the usual kinematic and dynamic boundary conditions (6.3 and 6.4). At time $t = 0$ the interface is deformed so that

$$\mathbf{X}(r) = r\,\mathbf{e}_r + [1.0 + \epsilon J_0(kr)]\;\mathbf{e}_z, \tag{10.1}$$

where the wavenumber k is constrained to be a zero of $J_1(k)$ as discussed in section 6.1.

We are revisiting this example in order to solve the problem using the system of decomposed governing equations and boundary conditions formulated in chapters 7 and 9 respectively. Using this scheme, we decompose the position vector to the surface in the manner described in section 9.1,

$$\mathbf{X}(r) = \bar{\mathbf{X}}(r) + \epsilon\,\hat{\mathbf{X}}(r), \tag{10.2}$$

where $\epsilon \ll 1$, which can be thought of as a small (linear) axisymmetric perturbation to an axisymmetric base flow. The governing equations of the base flow are the usual axisymmetric Navier–Stokes equations

$$R_\rho^{[\beta]}\mathrm{Re}\left[\mathrm{St}\,\frac{\partial \bar{u}_r^{[\beta]}}{\partial t} + \bar{u}_r^{[\beta]}\frac{\partial \bar{u}_r^{[\beta]}}{\partial r} - \frac{\bar{u}_\theta^{[\beta]2}}{r} + \bar{u}_z^{[\beta]}\frac{\partial \bar{u}_r^{[\beta]}}{\partial z}\right] = -\frac{\partial \bar{p}^{[\beta]}}{\partial r} + R_\mu^{[\beta]}\left[\frac{\partial^2 \bar{u}_r^{[\beta]}}{\partial r^2} + \frac{1}{r}\frac{\partial \bar{u}_r^{[\beta]}}{\partial r} - \frac{\bar{u}_r^{[\beta]}}{r^2} + \frac{\partial^2 \bar{u}_r^{[\beta]}}{\partial z^2}\right],$$

$$R_\rho^{[\beta]}\mathrm{Re}\left[\mathrm{St}\,\frac{\partial \bar{u}_z^{[\beta]}}{\partial t} + \bar{u}_r^{[\beta]}\frac{\partial \bar{u}_z^{[\beta]}}{\partial r} + \bar{u}_z^{[\beta]}\frac{\partial \bar{u}_z^{[\beta]}}{\partial z}\right] = -\frac{\partial \bar{p}^{[\beta]}}{\partial z} - R_\rho^{[\beta]}\frac{\mathrm{Re}}{\mathrm{Fr}} + R_\mu^{[\beta]}\left[\frac{\partial^2 \bar{u}_z^{[\beta]}}{\partial r^2} + \frac{1}{r}\frac{\partial \bar{u}_z^{[\beta]}}{\partial r} + \frac{\partial^2 \bar{u}_z^{[\beta]}}{\partial z^2}\right],$$

$$R_\rho^{[\beta]}\mathrm{Re}\left[\mathrm{St}\,\frac{\partial \bar{u}_\theta^{[\beta]}}{\partial t} + \bar{u}_r^{[\beta]}\frac{\partial \bar{u}_\theta^{[\beta]}}{\partial r} + \frac{\bar{u}_r^{[\beta]}\bar{u}_\theta^{[\beta]}}{r} + \bar{u}_z^{[\beta]}\frac{\partial \bar{u}_\theta^{[\beta]}}{\partial z}\right] = R_\mu^{[\beta]}\left[\frac{\partial^2 \bar{u}_\theta^{[\beta]}}{\partial r^2} + \frac{1}{r}\frac{\partial \bar{u}_\theta^{[\beta]}}{\partial r} - \frac{\bar{u}_\theta^{[\beta]}}{r^2} + \frac{\partial^2 \bar{u}_\theta^{[\beta]}}{\partial z^2}\right] \tag{10.3}$$

and

$$\frac{\partial \bar{u}_r^{[\beta]}}{\partial r} + \frac{\bar{u}_r^{[\beta]}}{r} + \frac{\partial \bar{u}_z^{[\beta]}}{\partial z} = 0, \tag{10.4}$$

where $\beta = 1, 2$ labels the lower and upper fluids respectively. These equations are subject to

$$\begin{aligned} \bar{u}_r^{[1]} = \bar{u}_z^{[1]} = \bar{u}_\theta^{[1]} = 0 \qquad & \text{at} \quad z = 0, \\ \bar{u}_r^{[2]} = \bar{u}_z^{[2]} = \bar{u}_\theta^{[2]} = 0 \qquad & \text{at} \quad z = 2, \\ \bar{u}_r^{[\beta]} = \bar{u}_z^{[\beta]} = 0 \qquad & \text{at} \quad r = 0 \ \text{ and } \ r = 1, \end{aligned} \tag{10.5}$$

and the initial shape of the interface is defined by

$$\bar{\mathbf{X}}(r) = r\,\mathbf{e}_r + [1.0 + a_{\mathrm{B}} J_0(kr)]\ \mathbf{e}_z, \tag{10.6}$$

where a_{B} represents the amplitude of the deflection away from the equilibrium position at $z = 1$. On top of this base flow we solve a linear axisymmetric perturbation problem subject to

$$\begin{aligned} \hat{u}_r^{[1]} = \hat{u}_z^{[1]} = \hat{u}_\theta^{[1]} = 0 \qquad & \text{at} \quad z = 0, \\ \hat{u}_r^{[2]} = \hat{u}_z^{[2]} = \hat{u}_\theta^{[2]} = 0 \qquad & \text{at} \quad z = 2, \\ \hat{u}_r^{[\beta]} = \hat{u}_z^{[\beta]} = 0 \qquad & \text{at} \quad r = 0 \ \text{ and } \ r = 1 \end{aligned} \tag{10.7}$$

and an initial interface deflection of

$$\hat{\mathbf{X}}(r) = r\,\mathbf{e}_r + a_{\mathrm{P}} J_0(kr)\,\mathbf{e}_z, \tag{10.8}$$

where we require $a_{\mathrm{P}} \ll a_{\mathrm{B}}$ in order for the decomposition (10.2) to be valid.

The solutions to these coupled problems were computed on identical meshes containing 50 elements in the radial direction and 100 elements in the axial direction, using a spine node-update strategy as discussed in section 9.3. Crouzeix–Raviart elements and their linearised counterparts were used for the base and perturbation problems respectively, with initial conditions corresponding to an impulsive start from zero initial velocity. The time-derivatives were discretised using a second-order-accurate BDF scheme with a (non-dimensionalised) timestep of 0.025. Figure 10.2 displays a time-trace of the height of the interface at the symmetry axis for the parameters Re $= 51.3$, St $= 0.2$, Fr $= 0.04$ and Ca $= 5.0$. The density and viscosity ratios

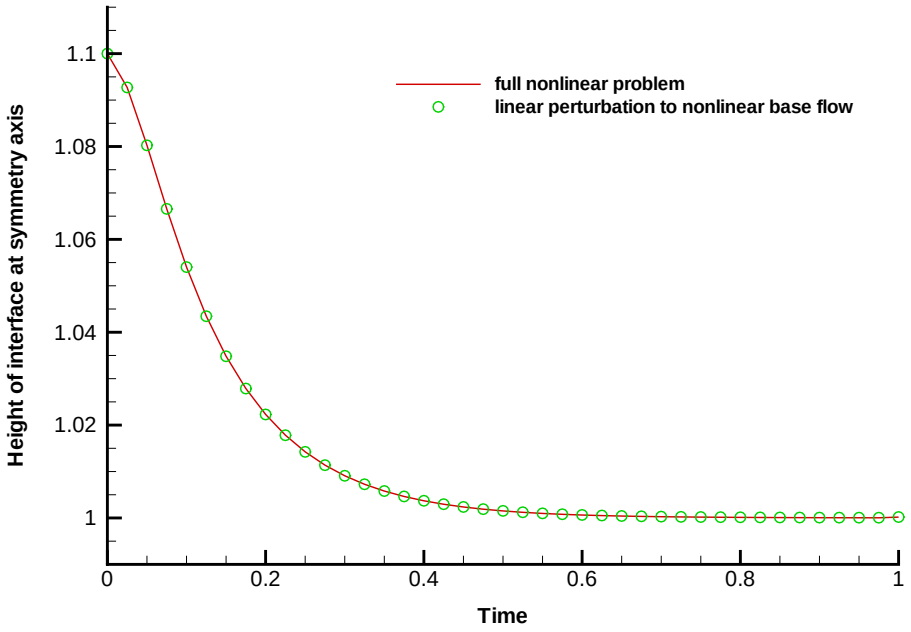

Figure 10.2: Time-trace of the height of the interface at $r = 0$ for the parameters Re $= 51.3$, St $= 0.2$, Fr $= 0.04$, Ca $= 5.0$, $R_\rho = 0.529$ and $R_\mu = 52.9$. The solid line represents the solution of the fully-nonlinear problem described in section 6.2, computed using a mesh of 50×100 Crouzeix–Raviart elements and an initial deflection amplitude of $\epsilon = 0.1$. We compare this to the solution of the decomposed problem described in the current section, computed using a base state mesh of 50×100 Crouzeix–Raviart elements and a perturbed state mesh of 50×100 `LinearisedAxisymmetricQCrouzeixRaviartMultiDomainElements`, with initial deflection amplitudes of $a_{\mathrm{B}} = 0.09$ and $a_{\mathrm{P}} = 0.01$. All problems employed a second-order BDF scheme with a non-dimensional timestep of 0.025.

were set to $R_\rho = 0.529$ and $R_\mu = 52.9$, and the amplitudes of the initial interface deflections were chosen to be $a_{\mathrm{B}} = 0.09$ and $a_{\mathrm{P}} = 0.01$. The actual position of the interface is recovered using (10.2), and is shown as points in figure 10.2. The solid line is the computed solution for the same parameters (and the same spatial and temporal discretisation) using the fully-nonlinear code described in section 6.2, with an initial amplitude of deflection of $\epsilon = 0.1$. We note that the two time-traces display excellent agreement. Figure 10.3 shows snapshots at various timesteps of the radial profile of the interface as it relaxes towards the equilibrium position. The thick, dashed lines correspond to the combined interface position computed using the decomposed problem described above, while the thin, continuous lines display the reference solution computed using the fully-nonlinear code. We note that these solutions again display

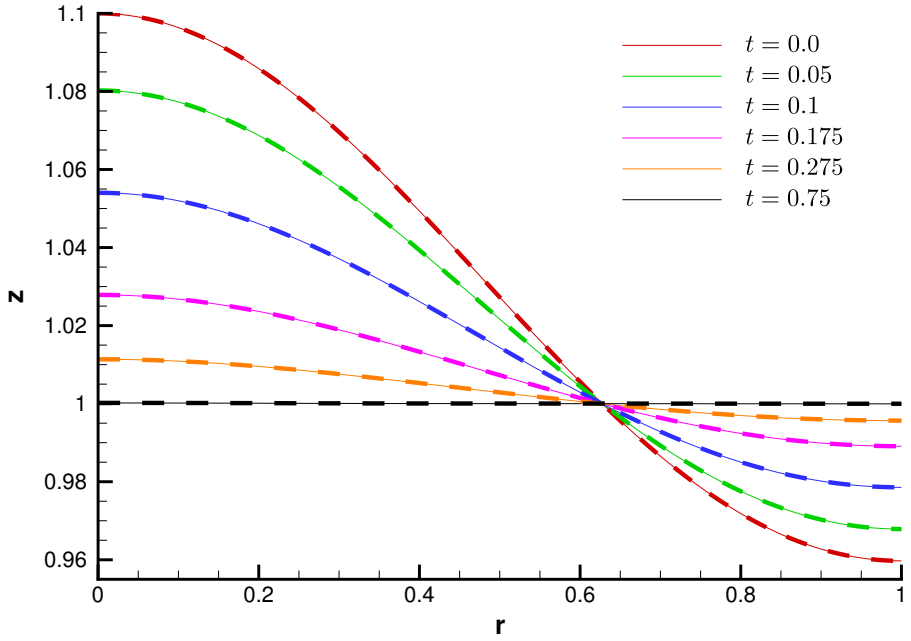

Figure 10.3: Plot of the radial profile of the interface at various timesteps for the parameters Re $= 51.3$, St $= 0.2$, Fr $= 0.04$, Ca $= 5.0$, $R_\rho = 0.529$ and $R_\mu = 52.9$. The thick, dashed lines represent the solution computed using the decomposed problem described in the current section, computed using a base state mesh of 50×100 Crouzeix–Raviart elements and a perturbed state mesh of 50×100 `LinearisedAxisymmetricQCrouzeixRaviartMultiDomainElements`, with initial deflection amplitudes of $a_{\mathrm{B}} = 0.09$ and $a_{\mathrm{P}} = 0.01$. The thin, continuous lines represent the corresponding solution computed using the fully-nonlinear code described in section 6.2, which employed a mesh of 50×100 Crouzeix–Raviart elements and an initial deflection amplitude of $\epsilon = 0.1$. All problems were discretised temporally using a second-order BDF scheme with a non-dimensional timestep of 0.025.

excellent point-wise agreement.

10.2 Non-axisymmetric perturbations

We now consider the same problem as in section 10.1, but restrict ourselves to the case in which the base flow is prescribed to be the steady solution

$$\bar{u}_r^{[\beta]} = \bar{u}_z^{[\beta]} = \bar{u}_\theta^{[\beta]} = 0, \qquad \bar{p}^{[1]} = -\frac{\mathrm{Re}}{\mathrm{Fr}} z, \qquad \bar{p}^{[2]} = -\frac{\mathrm{Re}}{\mathrm{Fr}} \left[R_\rho^{[2]} (z-1) + 1 \right], \quad (10.9)$$

and the (unperturbed) position of the interface is the plane $z = 1$. We wish to investigate the effect of perturbing the interface by an arbitrary, non-axisymmetric function $f(r, \theta)$, and allowing it to relax under the influence of gravity and capillary

forces. We note that this is another extension of the problem studied in section 6.2, in which we simulated the relaxation of the axisymmetric ($m = 0$) mode only. In this case, however, the governing equations are the linearised perturbation equations (7.77)–(7.84) and the interface conditions are the linearised dynamic (9.59)–(9.65) and kinematic (9.75 and 9.76) conditions. The governing equations are subject to the no-slip condition at the upper and lower (solid) boundaries,

$$\begin{aligned} U_m^{C[1]} = U_m^{S[1]} = W_m^{C[1]} = W_m^{S[1]} = V_m^{C[1]} = V_m^{S[1]} = 0 \qquad \text{at} \quad z = 0, \\ U_m^{C[2]} = U_m^{S[2]} = W_m^{C[2]} = W_m^{S[2]} = V_m^{C[2]} = V_m^{S[2]} = 0 \qquad \text{at} \quad z = 2, \end{aligned} \tag{10.10}$$

and the usual 'slippery wall' conditions at the outer boundary,

$$U_m^{C[\beta]} = U_m^{S[\beta]} = \frac{\partial W_m^{C[\beta]}}{\partial r} = \frac{\partial W_m^{S[\beta]}}{\partial r} = V_m^{C[\beta]} = V_m^{S[\beta]} = 0 \quad \text{at} \quad r = 1. \tag{10.11}$$

The boundary conditions at the symmetry axis differ depending on the azimuthal mode number m. In all modes the surface must meet the symmetry boundary at 90^o. In all modes with $m > 0$ the interface height is restricted to be zero at $r = 0$, otherwise modulation by $\cos m\theta$ and $\sin m\theta$ would lead to a discontinuity. Furthermore, in odd-numbered modes we do not have the usual non penetration condition at $r = 0$: it is physically allowable for fluid to have finite radial and azimuthal velocity at the symmetry axis. Consequently, the boundary conditions at the symmetry axis are

$$U_0^{C[\beta]} = U_0^{S[\beta]} = \frac{\partial W_0^{C[\beta]}}{\partial r} = \frac{\partial W_0^{S[\beta]}}{\partial r} = V_0^{C[\beta]} = V_0^{S[\beta]} = 0 \qquad \text{at} \quad r = 0 \tag{10.12}$$

for the axisymmetric ($m = 0$) mode,

$$\frac{\partial U_m^{C[\beta]}}{\partial r} = \frac{\partial U_m^{S[\beta]}}{\partial r} = W_m^{C[\beta]} = W_m^{S[\beta]} = \frac{\partial V_m^{C[\beta]}}{\partial r} = \frac{\partial V_m^{S[\beta]}}{\partial r} = 0 \qquad \text{at} \quad r = 0 \tag{10.13}$$

for odd m and

$$U_m^{C[\beta]} = U_m^{S[\beta]} = W_m^{C[\beta]} = W_m^{S[\beta]} = V_m^{C[\beta]} = V_m^{S[\beta]} = 0 \qquad \text{at} \quad r = 0 \tag{10.14}$$

for even, non-zero m.

The initial perturbation to the interface was chosen to be

$$\hat{\mathbf{X}}(r, \theta) = \epsilon \left\{ J_0(kr) + \sum_{m=1}^{\infty} \frac{1}{2} \Big[\big(1 - \cos(2\pi r)\big) \big(\cos m\theta + \sin m\theta \big) \Big] \right\} \tag{10.15}$$

with k equal to the first (non-zero) root of $J_1(k)$, which is approximately 3.8317. The solution was computed on a uniform mesh containing 20×40 `Linearised-AxisymmetricQCrouzeixRaviartMultiDomainElements` in the radial and axial directions respectively. The simulation was started impulsively from zero initial velocity, and the time-derivatives were discretised using the usual second-order-accurate BDF scheme with a timestep of 0.05. The red (solid) line in figure 10.4 displays a time-trace of the height of the interface at the symmetry axis for the parameters $\mathrm{Re} = 50.0$, $\mathrm{St} = 1.0$, $\mathrm{Fr} = 1.0$, $\mathrm{Ca} = 1.0$, $R_\mu = 0.1$ and $R_\rho = 1.0$ for the axisymmetric ($m = 0$) mode. The initial perturbation amplitude was chosen to be $\epsilon = 0.01$, and we note that this time-trace agrees with that computed using the fully-nonlinear code in section 6.2, as we would expect. Since both fluids are of the same density, the only restoring force in this simulation is that of surface tension, and this acts to revert the interface to its undeformed state. As it settles down to its equilibrium position we see the usual oscillation of the interface, which is damped as the energy in the system is dissipated through viscous forces.

Let us now consider the effect of setting the density ratio to 0.1, so that the upper fluid is ten times less dense than the bottom fluid. When the density ratio is reduced, the upper fluid has less mass and as a consequence the inertia of the overall system is reduced. Since there has been no change in the viscosity of the system, the ratio of viscous forces to inertial forces has increased and this causes the frequency of the oscillations to increase. Additionally, we now include the restoring force of gravitational acceleration: this increases the damping of the oscillations and results in the equilibrium position of the interface being approached more rapidly. Both of these effects can be seen in the time-trace for this simulation, which is shown as the green (dashed) line in figure 10.4.

The blue (dot-dashed) line in this figure plots the time-trace for the same problem, but this time with the density ratio set to 2.0. In this case the system is no longer stably stratified, since the upper fluid has twice the density of the lower fluid. The inertia of the system as a whole has increased relative to the overall viscosity, and as a result the oscillations are of lower frequency than either of the previous two cases. However, the major consequence of an unstably stratified system is that the gravitational acceleration is no longer a restoring force, but acts against the force

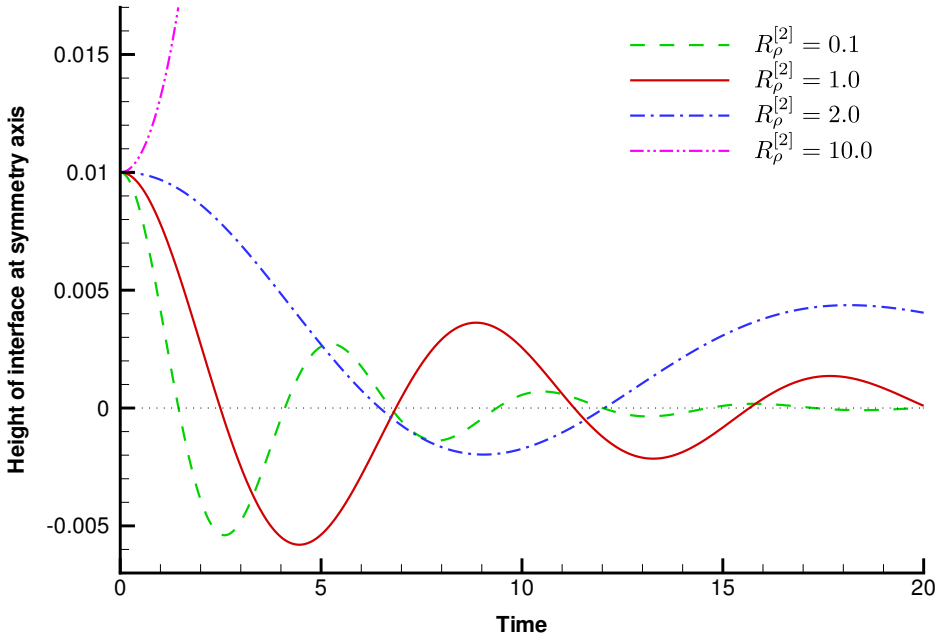

Figure 10.4: Time-trace of the height of the interface at the symmetry axis for the axisymmetric ($m = 0$) mode for the parameters Re $= 50.0$, St $= 1.0$, Fr $= 1.0$, Ca $= 1.0$, $R_\mu = 0.1$ and an initial perturbation amplitude of $\epsilon = 0.01$. The four lines correspond to four different values of the density ratio. The domain was discretised spatially using a mesh of 20×40 `LinearisedAxisymmetricQCrouzeixRaviart-MultiDomainElements`, and a second-order BDF timestepping scheme with a non-dimensional timestep of 0.05 was employed.

provided by surface tension in an attempt to destabilise the interface. From figure 10.4 it can be seen that at this set of parameters the capillary force is still sufficiently strong for this axisymmetric mode to remain stable, but the growth rate of the oscillations is larger than in the neutral density case. As we continue to increase the density of the upper fluid we will eventually reach a point when the force of gravitational acceleration causes the perturbation to grow, as can be seen in the purple (double-dot-dashed) line representing the time-trace of the interface height for a system with $R_\rho = 10.0$.

Figure 10.5 displays the time-traces of the next six azimuthal modes for the same four cases discussed above. Because all of the non-axisymmetric modes are required to be zero at the symmetry axis, we choose to take the trace the height of the interface at the point $r = 0.5$, which corresponds to the point in the domain at which the deformation is greatest in the initial configuration (10.15). We note that the structure of the non-axisymmetric Navier–Stokes equations is such that the system of governing

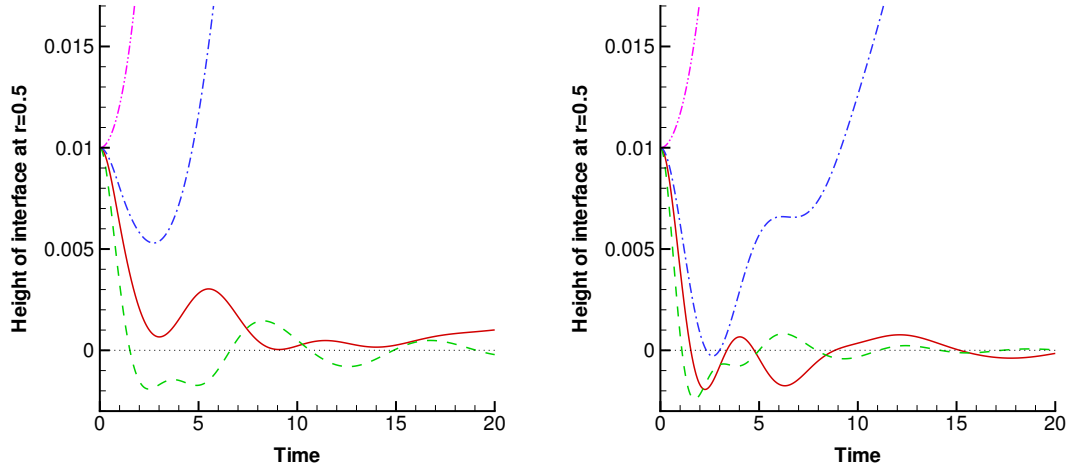

(a) $m = 1$

(b) $m = 2$

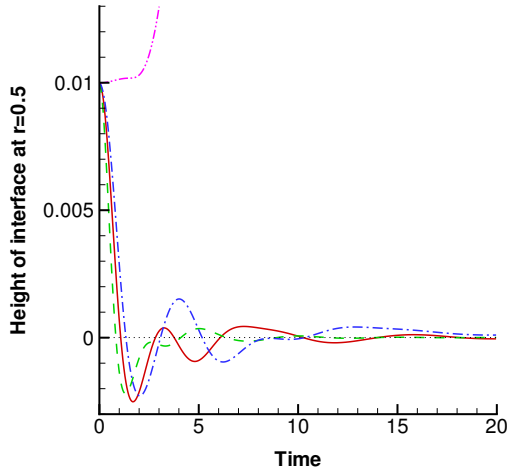

(c) $m = 3$

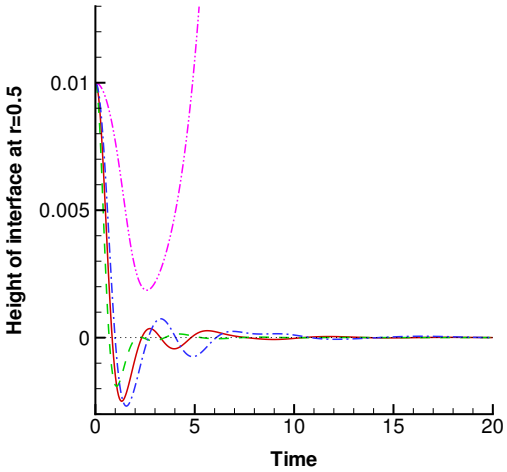

(d) $m = 4$

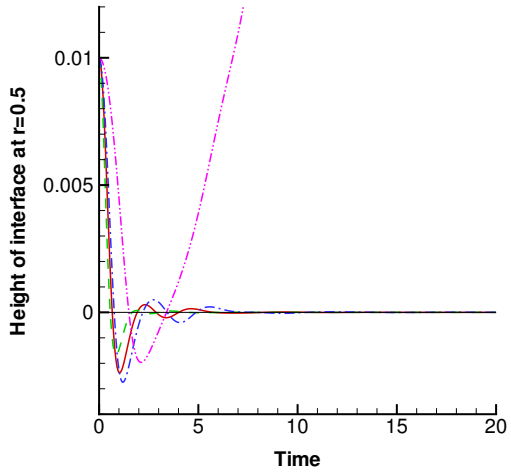

(e) $m = 5$

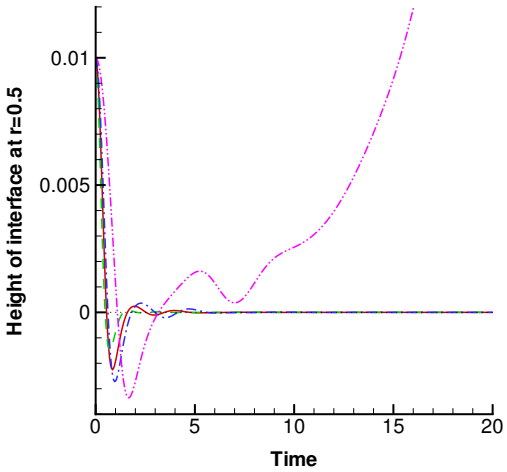

(f) $m = 6$

Figure 10.5: Time-traces of the height of the interface at $r = 0.5$ for modes 1–6 for the parameters Re $= 50.0$, St $= 1.0$, Fr $= 1.0$, Ca $= 1.0$ and $R_\mu = 0.1$. The four lines correspond to four different values of the density ratio. The problem was discretised using 20×40 `LinearisedAxisymmetricQCrouzeixRaviartMultiDomainElements`, and a BDF2 scheme with non-dimensional timestep of 0.05.

equations and boundary conditions cannot be separated in an analogous manner to the axisymmetric case, and therefore we are unable to set the initial conditions such that we only excite one eigenmode of the system for these higher modes. Consequently the resulting time-traces (10.5(a))–(10.5(f)) display superpositions of multiple eigenmodes, and each of these will oscillate with its own frequency and decay at its own rate. As we continue to time-evolve the equations we will eventually be left with the single eigenmode which decays least quickly, but in most cases the amplitude of the perturbation is sufficiently small by the time this has happened that it is impossible to see at the scales presented in figure 10.5. We note that, in general, the oscillation frequency increases and the growth rate decreases as the mode number is increased: this is the expected behaviour since the curvature of the interface increases with increasing mode number.

We will conclude the discussion of these results by presenting the velocity and pressure fields for the $m = 3$ mode of the neutral density ($R_\rho = 1.0$) case at five different timesteps. Figure 10.6 displays the time-trace of the interface height at $r = 0.5$ for this mode, and we have marked on the five points at which we will present 'snapshots' of the solution. These points have been chosen because they *roughly* span one period of the oscillation.

Figure 10.7 shows plots of the velocity and pressure fields for the parameters Re $=$ 50.0, St $= 1.0$, Fr $= 1.0$, Ca $= 1.0$, $R_\rho = 1.0$ and $R_\mu = 0.1$. The flow fields are three-dimensional, and we present contours of azimuthal velocity $V_3(r, z)$ in the plane $\theta = 0$ and contours of pressure $P_3(r, z)$ in the plane $\theta = 2\pi/3$. These particular 'slices' have been chosen since in both cases $\sin(3\theta) = 0$ and $\cos(3\theta) = 1$, and hence the solution is given simply by the cosine components of the fields, $V_3^C(r, z)$ and $P_3^C(r, z)$. We note, however, that because the initial conditions for both the sine and cosine parts of the solution are identical (see equation 10.15), the 'cosine solutions' $V_3^C(r, z)$ and $P_3^C(r, z)$ at $\theta = 0$ and $\theta = 2\pi/3$ are identical to their sine counterparts $V_3^S(r, z)$ and $P_3^S(r, z)$ in the $\theta = \pi/6$ and $\theta = 5\pi/6$ planes respectively. Legends for the contours are displayed next to each figure and we note that the same contour levels have been used in all figures.

Recall that the solutions of the linear problem are computed on meshes which deform in response to the motion of the interface in the *base flow*. Since in this case

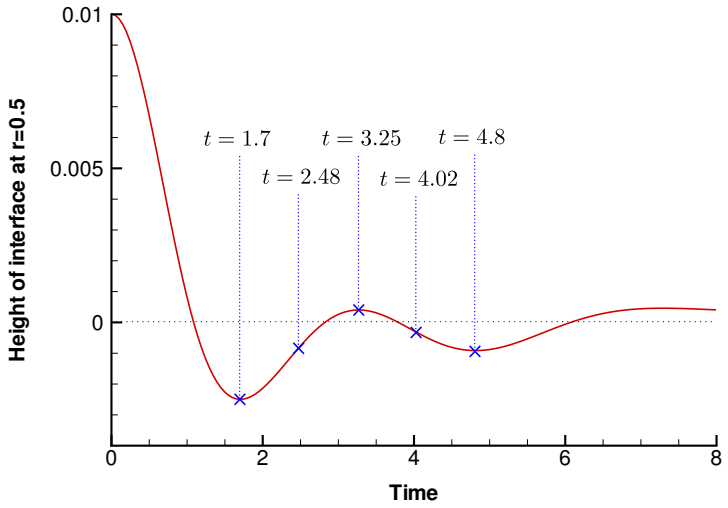

Figure 10.6: Time-trace of the height of the interface at $r = 0.5$ for the $m = 3$ mode for the parameters Re $= 50.0$, St $= 1.0$, Fr $= 1.0$, Ca $= 1.0$, $R_\rho = 1.0$ and $R_\mu = 0.1$. The problem was discretised using 20×40 `LinearisedAxisymmetricQCrouzeixRaviart-MultiDomainElements`, and a BDF2 scheme with non-dimensional timestep of 0.05. The five points represent the timesteps at which 'snapshots' of the solution will be displayed.

the base state has been set up so that the interface is in its equilibrium position, we note that the meshes in figure 10.7 are perfectly uniform. The bold line halfway up each plot denotes the position of the interface in the base flow, and the perturbation to this 'base position' is then displayed as a surface plot above the cylindrical domain. We have scaled up the axial coordinate on these surface plots so that the shape of the surface can more clearly be seen, and have used the same scaling across figures 10.7(a)–10.7(e). The motion of this surface can be inferred from the velocity vectors, which track the in-plane velocity $U_3^C(r, z)$ and $W_3^C(r, z)$. We note that the apparent sources and sinks in these in-plane fields appear because the solution is not two-dimensionally divergence-free.

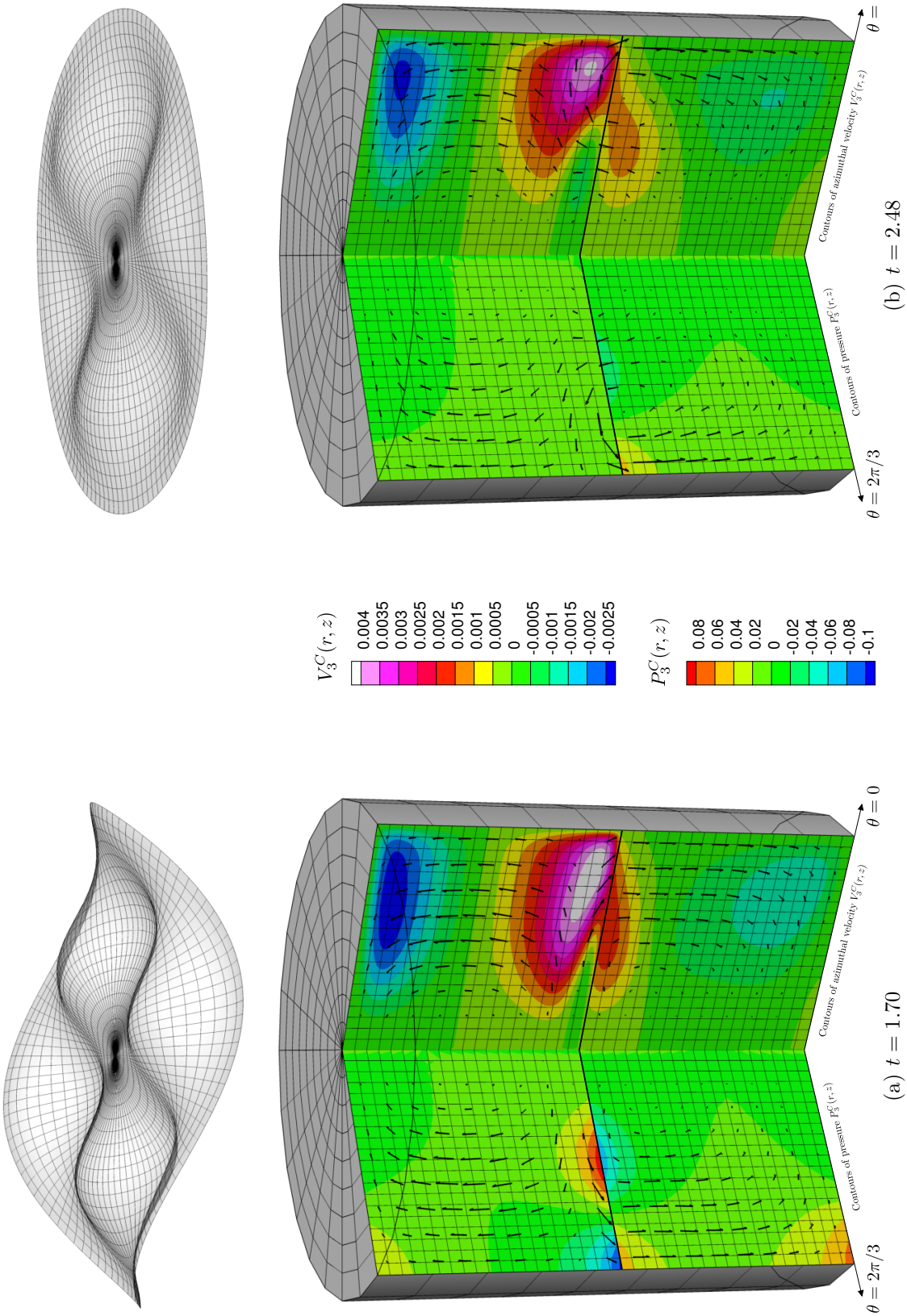

Figure 10.7: Flow fields and interface perturbation for the $m = 3$ mode for $\mathrm{Re} = 50.0$, $\mathrm{St} = 1.0$, $\mathrm{Fr} = 1.0$, $\mathrm{Ca} = 1.0$, $R_\rho = 1.0$ and $R_\mu = 0.1$.

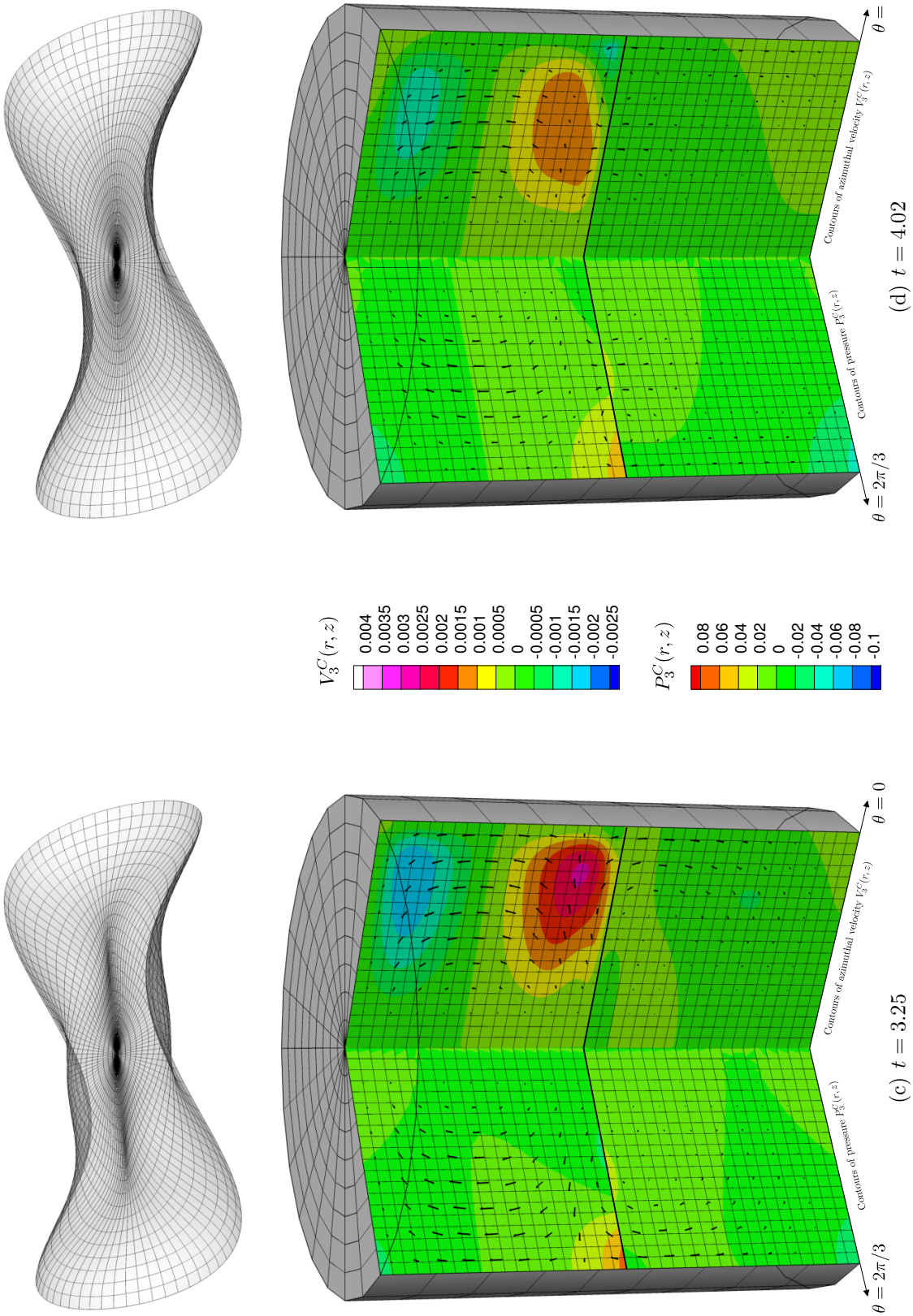

Figure 10.7: Flow fields and interface perturbation for the $m = 3$ mode for $\mathrm{Re} = 50.0$, $\mathrm{St} = 1.0$, $\mathrm{Fr} = 1.0$, $\mathrm{Ca} = 1.0$, $R_\rho = 1.0$ and $R_\mu = 0.1$.

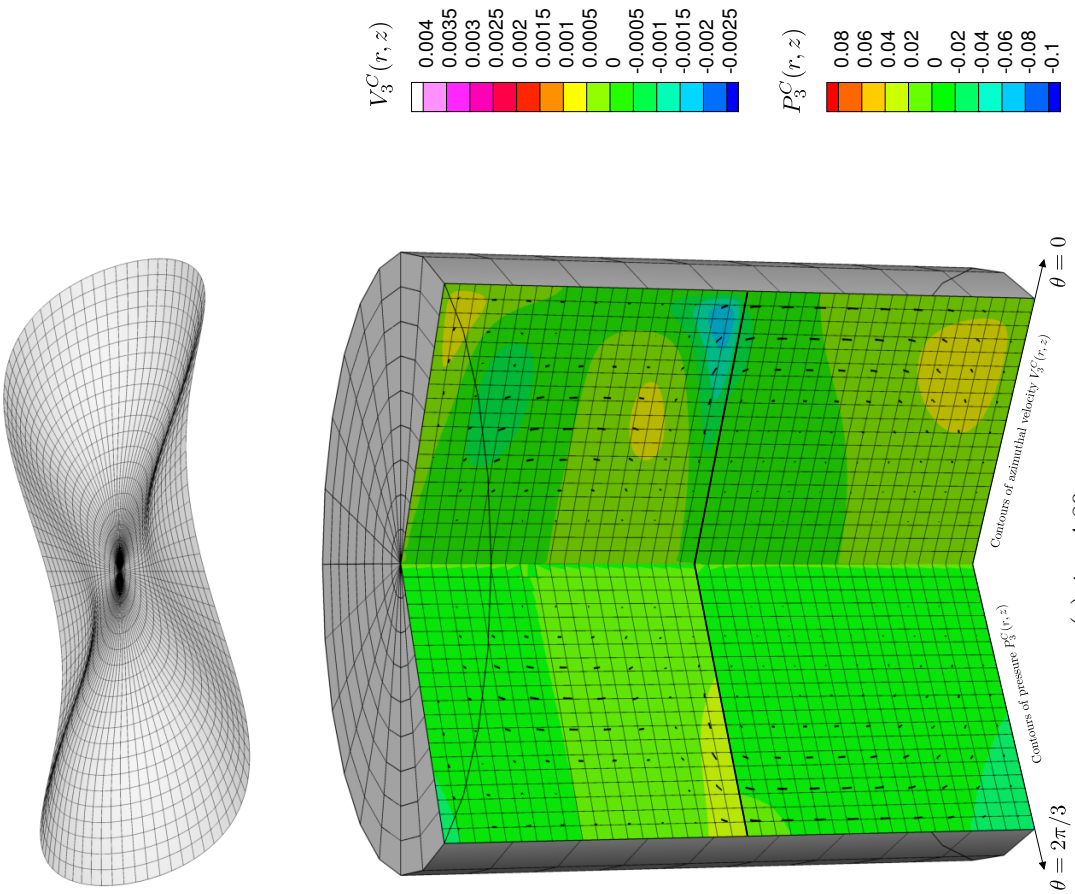

(e) $t = 4.80$

Figure 10.7: Flow fields and interface perturbation for the $m = 3$ mode for $\mathrm{Re} = 50.0$, $\mathrm{St} = 1.0$, $\mathrm{Fr} = 1.0$, $\mathrm{Ca} = 1.0$, $R_\rho = 1.0$ and $R_\mu = 0.1$.

Chapter 11

Conclusions and outlook

In this thesis we presented the finite element formulation of the equations governing

(i) time-dependent, non-linear, axisymmetric two-phase flows, and

(ii) the evolution of linear, non-axisymmetric perturbations to such flows.

This formulation was implemented within `oomph-lib` in such a way that problems (i) and (ii) above can be solved as separate `Problem` objects, with the one-way coupling between them facilitated by `oomph-lib`'s multi-domain functionality. The newly-developed methodology was carefully validated by comparison against linear analyses (where possible) and existing numerical results generated using different techniques.

Two different approaches to the problem of updating the bulk nodal positions in response to the motion of a free surface were developed. The first of these was based on the method of spines, and we augmented `oomph-lib`'s existing spine functionality to allow the computation of perturbations to 'base' nodal positions which are themselves determined using this method. Spine-based node-update strategies are computationally inexpensive but do not (currently) allow for spatial refineability, and therefore we also designed all of our equation classes to accomodate the updating of the bulk nodal positions using a pseudo-solid approach. Although this meshing strategy is far more computationally expensive, the implementation of refineable versions of the `LinearisedAxisymmetricQTaylorHoodMultiDomainElement` and `Linearised-AxisymmetricQCrouzeixRaviartMultiDomainElement` classes (which were developed as part of this project) enables these elements to benefit from `oomph-lib`'s general refineable element framework and error estimation routines. In addition, domains which

are discretised using this pseudo-solid meshing strategy do not suffer from the restriction of requiring the interface shape to remain 'one-to-one': in principle, 'any' interface shape can be accommodated, although in practice there will come a point at which the individual elements are sufficiently deformed that the mesh is no longer adequate. The use of `oomph-lib`'s 're-meshing' functionality, however, will (in principle) allow the indefinite time-evolution of an arbitrary deformation to be computed, including scenarios where there is a complete 'overturning' of the interface.

When developing this general perturbation framework, great care was taken to ensure that the newly-written classes were designed in such a way that they provided clean and intuitive interfaces to the rest of the library. Wherever possible, the inheritance structure of any newly-developed functionality was designed to 'mirror' that of existing classes, with the aims of maximising user friendliness and overall 'transparency' of the library's data structures. The same philosophy was applied to the documentation that was written as a part of this project. In this way the functionality developed during this project can be easily combined with existing `oomph-lib` functionality to solve highly-complex problems within a robust overall framework. In addition, the inclusion of this code within a library of this type makes it straightforward to develop the methodology implemented here further at a later date should additional, more specific functionality be required.

The `oomph-lib` source code is freely available from

`http://www.oomph-lib.org,`

which contains instructions for the installation and customisation of the library, as well as links to the extensive range of documentation. The functionality that we have added to `oomph-lib` can be used to solve, in principle, 'any' arbitrary single- or two-phase problem involving the time-evolution of a linear perturbation to an otherwise axisymmetric base flow. The wide range of problems which can now be solved include (but are certainly not limited to) those discussed in chapter 1 of the current work. It is hoped that, with further development of this and other areas of the library, users will utilise (and build on) this core framework to solve an increasingly complex and diverse range of single- and multi-physics problems. Examples of problems which can be studied using this framework include the onset of instability in the experiment first proposed by Shyh and Munson, in which a growing non-axisymmetric disturbance is observed

when a cylindrical vessel containing two fluids is oscillated sinusoidally with period T about its axis of rotational symmetry [Shyh and Munson, 1986], as well as problems involving Plateau–Rayleigh-type instabilities in viscous jets, such as those studied by [Ponstein, 1959] and Meyer and Weihs [1987], and related problems involving annular coatings of viscous fluid on wires or on the insides of tubes. When combined with a solid mechanics framework (such as those already present within `oomph-lib`), this methodology could also be used to investigate the stability of various fluid-structure interaction problems, which has much relevance to the study of biological flows: for example, the work of Halpern and Grotberg on airway closure, in which they consider instabilities which arise in liquid-lined flexible tubes [Halpern and Grotberg, 1992].

Bibliography

P. R. Amestoy, I. S. Duff, and J. Y. L'Excellent. Multifrontal parallel distributed symmetric and unsymmetric solvers. *Computer Methods in Applied Mechanics and Engineering*, 184(24):501 – 520, 2000.

Z. Bai, J. Demmel, J. Dongarra, A. Ruhe, and H. van der Vorst. *Templates for the solution of algebraic eigenvalue problems: a practical guide*. Society for Industrial and Applied Mathematics, Philadelphia, PA, USA, 2000.

G. K. Batchelor. Note on a class of solutions of the navier-stokes equations representing steady rotationally-symmetric flow. *The Quarterly Journal of Mechanics and Applied Mathematics*, 4(1):29–41, 1951.

G. K. Batchelor and A. E. Gill. Analysis of the stability of axisymmetric jets. *Journal of Fluid Mechanics*, 14:529–551, 12 1962.

G. K. Batchelor and J. M. Nitsche. Instability of stratified fluid in a vertical cylinder. *Journal of Fluid Mechanics*, 252:419–448, 7 1993.

S. Carmi and J. I. Tustaniwskyj. Stability of modulated finite-gap cylindrical couette flow: linear theory. *Journal of Fluid Mechanics*, 108:19–42, 7 1981. ISSN 1469-7645. doi: 10.1017/S0022112081001961.

A. Davey and P. G. Drazin. The stability of poiseuille flow in a pipe. *Journal of Fluid Mechanics*, 36:209–218, 4 1969. ISSN 1469-7645.

J. W. Demmel, S. C. Eisenstat, J. R. Gilbert, X. S. Li, and J. W. H. Liu. A supernodal approach to sparse partial pivoting. *SIAM J. Matrix Analysis and Applications*, 20 (3):720–755, 1999.

J. Donea, S. Guiliani, and J. P. Halleux. An arbitrary Lagrangian-Eulerian finite-element method for transient dynamic fluid structure interactions. *Computer Methods in Applied Mechanics and Engineering*, 33:689–723, 1982.

R. J. Donnelly, F. Reif, and H. Suhl. Enhancement of hydrodynamic stability by modulation. *Phys. Rev. Lett.*, 9:363–365, Nov 1962. doi: 10.1103/PhysRevLett.9.363.

P. G. Drazin and W. H. Reid. *Hydrodynamic Stability.* Cambridge Mathematical Library. Cambridge University Press, 2004.

R. D. Falgout and U. M. Yang. HYPRE: a library of high performance preconditioners. In *Preconditioners, Lecture Notes in Computer Science*, pages 632–641, 2002.

A. Y. Gelfgat, P. Z. Bar-Yoseph, and A. Solan. Three-dimensional instability of axisymmetric flow in a rotating lid-cylinder enclosure. *Journal of Fluid Mechanics*, 438:363–377, 7 2001.

S. L. Goren. The instability of an annular thread of fluid. *Journal of Fluid Mechanics*, 12:309–319, 2 1962. ISSN 1469-7645. doi: 10.1017/S002211206200021X.

H. Görtler. Instabilitaumt laminarer grenzchichten an konkaven wänden gegenber gewissen dreidimensionalen störungen. *ZAMM*, 21:250–52, 1940.

A. E. Green and W. Zerna. *Theoretical Elasticity.* Clarendon Press, 1954.

P. M. Gresho and R. L. Sani. *Incompressible flow and the finite element method. Volume Two: Isothermal laminar flow.* John Wiley and Sons, Ltd., Chichester, 2000.

D. Halpern and J. B. Grotberg. Fluid-elastic instabilities of liquid-lined flexible tubes. *Journal of Fluid Mechanics*, 244:615–632, 1992.

M. Heil and A. L. Hazel. `oomph-lib` – an object-oriented multi-physics finite-element library. In M. Schäfer and H.-J. Bungartz, editors, *Fluid-Structure Interaction*, pages 19–49. Springer, 2006. `oomph-lib` is available as open-source software at `http://www.oomph-lib.org`.

M. Heroux, R. Bartlett, V. Howle, R. Hoekstra, J. Hu, T. Kolda, R. Lehoucq, K. Long, R. Pawlowski, E. Phipps, A. Salinger, H. Thornquist, R. Tuminaro, J. Willenbring, and A. Williams. An overview of trilinos. Technical Report SAND2003-2927, Sandia National Laboratories, 2003.

R. E. Hewitt and A. L. Hazel. Midplane-symmetry breaking in the flow between two counter-rotating disks. *Journal of Engineering Mathematics*, 57(3):273–288, 2007.

HSL2004. A collection of Fortran codes for large scale scientific computation, 2004. `http://www.cse.clrc.ac.uk/nag/hsl/hsl.shtml`.

S. F. Kistler and L. E. Scriven. Coating flows. In J.R.A. Pearson and S.M. Richardson, editors, *Computational Analysis of Polymer Processing*, pages 243–299. Springer Netherlands, 1983.

L. P. Lebedev and M. J. Cloud. *Tensor analysis*. World Scientific, New Jersey, London, Singapore, Hong Kong, 2003.

R. B. Lehoucq, D. C. Sorensen, and C. Yang. *ARPACK Users' Guide: Solution of Large-scale Eigenvalue Problems with Implicitly Restarted Arnoldi Methods*. Software, Environments, Tools. SIAM, 1998.

J. Meyer and D. Weihs. Capillary instability of an annular liquid jet. *Journal of Fluid Mechanics*, 179:531–545, 6 1987. ISSN 1469-7645. doi: 10.1017/S0022112087001642.

T. Mullin. Experimental studies of transition to turbulence in a pipe. *Annual Review of Fluid Mechanics*, 43(1):1–24, 2011.

B. T. Murray, G. B. McFadden, and S. R. Coriell. Stabilization of taylor–couette flow due to time-periodic outer cylinder oscillation. *Physics of Fluids A: Fluid Dynamics*, 2:2147, 1990.

C. Nore, M. Tartar, O. Daube, and L. S. Tuckerman. Survey of instability thresholds of flow between exactly counter-rotating disks. *Journal of Fluid Mechanics*, 511: 45–65, 2004.

H. Oertel and L. Prandtl. *Prandtl's Essentials of Fluid Mechanics*. Applied mathematical sciences. Springer, 2004.

P. L. O'Sullivan and K. S. Breuer. Transient growth in circular pipe flow. i. linear disturbances. *Physics of Fluids (1994-present)*, 6(11):3643–3651, 1994. doi: http://dx.doi.org/10.1063/1.868421.

R. L. Panton. *Incompressible Flow*. John Wiley and Sons, Inc., 2005.

L. E. Payne and W. H. Pell. The stokes flow problem for a class of axially symmetric bodies. *Journal of Fluid Mechanics*, 7:529–549, 4 1960.

L. R. Petzold. Description of DASSL: A differential/algebraic system solver. Technical report, Sandia National Labs., Livermore, CA (USA), 1982.

J. A. F. Plateau. *Statique expérimentale et théorique des liquides soumis aux seules forces moléculaires*. Number v. 1 in Statique expérimentale et théorique des liquides soumis aux seules forces moléculaires. Gauthier-Villars, 1873.

J. Ponstein. Instability of rotating cylindrical jets. *Applied Scientific Research, Section A*, 8(1):425–456, 1959. ISSN 0365-7132. doi: 10.1007/BF00411768.

William H. Press, Saul A. Teukolsky, William T. Vetterling, and Brian P. Flannery. *Numerical Recipes 3rd Edition: The Art of Scientific Computing*. Cambridge University Press, 3rd edition, 2007.

Lord Rayleigh. On the instability of jets. *Proceedings of the London Mathematical Society*, s1-10(1):4–13, 1878.

Lord Rayleigh. Investigation of the Character of the Equilibrium of an Incompressible Heavy Fluid of Variable Density. *Proc. London Math. Soc.*, 14:170–177, 1883.

O. Reynolds. An experimental investigation of the circumstances which determine whether the motion of water shall be direct or sinuous, and of the law of resistance in parallel channels. *Proceedings of the royal society of London*, 35(224-226):84–99, 1883.

K. F. Riley, M. P. Hobson, and S. J. Bence. *Mathematical Methods for Physics and Engineering: A Comprehensive Guide*. Cambridge University Press, 2002.

W. S. Saric. Görtler vortices. *Annual Review of Fluid Mechanics*, 26(1):379–409, 1994.

P. J. Schmid and D. S. Henningson. Optimal energy density growth in hagen–poiseuille flow. *Journal of Fluid Mechanics*, 277:197–225, 10 1994. ISSN 1469-7645. doi: 10.1017/S0022112094002739.

M. R. Scott and H. A. Watts. Computational solution of linear two-point boundary value problems via orthonormalization. *SIAM Journal on Numerical Analysis*, 14 (1):40–70, 1977.

C. K. Shyh and B. R. Munson. Interfacial instability of an oscillating shear layer. *Journal of Fluids Engineering*, 108:89–92, Mar 1986.

J. Stewart. *Calculus (Stewart)*. Brooks/Cole, Cengage Learning, 2012.

G. I. Taylor. Stability of a viscous liquid contained between two rotating cylinders. *Philosophical Transactions of the Royal Society of London. Series A, Containing Papers of a Mathematical or Physical Character*, 223:pp. 289–343, 1923.

R. Thompson. PhD thesis, Department of Meteorology, Massachusetts Institute of Technology, 1968.

S. Tomotika. On the instability of a cylindrical thread of a viscous liquid surrounded by another viscous fluid. *Proceedings of the Royal Society of London. Series A, Mathematical and Physical Sciences*, 150(870):322–337, 1935.

D. J. Tritton. *Physical Fluid Dynamics*. Oxford Science Publications. Clarendon Press, 1988.

T. J. Walsh and R. J. Donnelly. Taylor-couette flow with periodically corotated and counterrotated cylinders. *Phys. Rev. Lett.*, 60:700–703, Feb 1988.

C. E. Weatherburn. *Differential Geometry of Three Dimensions*. Number v. 1 in Differential Geometry of Three Dimensions. Cambridge University Press, 1955.

C. Weber. Zum zerfall eines flssigkeitsstrahles, 1931.

P. J. Zandbergen and D. Dijkstra. Von Karman swirling flows. *Annual Review of Fluid Mechanics*, 19(1):465–491, 1987.

O. C. Zienkiewicz and J. Z. Zhu. The superconvergent patch recovery and a posteriori error estimates. part 1: The recovery technique. *International Journal for Numerical Methods in Engineering*, 33(7):1331–1364, 1992a.

O. C. Zienkiewicz and J. Z. Zhu. The superconvergent patch recovery and a posteriori error estimates. part 2: Error estimates and adaptivity. *International Journal for Numerical Methods in Engineering*, 33(7):1365–1382, 1992b.